JOURNAL OF BIOLOGICAL REGULATORS & HOMEOSTATIC AGENTS
Volume 28, No. 3, July - September, 2014

CONTENTS

JOURNAL OF BIOLOGICAL REGULATORS & HOMEOSTATIC AGENTS Vol. 28, no. 3, 357-366 (2014)

EDITORIAL

NONLINEAR QUANTUM PHENOMENA AND BIOPHYSICAL ASPECTS OF COMPLEXITY RELATED TO HEALTH AND DISEASE

L. BRIZHIK[1,2] and A. FOLETTI[3,4]

[1]Department of Nonlinear Condensed Matter Physics, Bogolyubov Institute for Theoretical Physics, Kyiv, Ukraine; [2]Wessex Institute of Technology, Ashurst, Southampton, UK; [3]Department of Innovative Technologies, University of Applied Sciences of Southern Switzerland-SUPSI, Switzerland; [4]Institute of Translational Pharmacology, CNR, Rome, Italy

Received August 28, 2013 – Accepted June 17, 2014

In this paper we discuss living systems as a non-linear self-interacting phenomenon, stabilized by the non-linear interaction between matter and self-created electromagnetic field. Such electromagnetic field can arise, in particular, as the radiation from electrosolitons which mediate the charge transport along macromolecules in metabolic redox processes. The non-linear nature of solitons results in an effective mechanism and leads to the synchronization of redox processes. It allows intra- and inter-cellular communication and long-range coherence in the system. One peculiar property of solitons is the resonant effect of external weak stimuli on their dynamics, which can explain the mechanism of low-intensity (non-thermal) electromagnetic therapies. We also discuss the stabilizing role of noise and spatial symmetry breaking in living organisms as open dissipative structures far from equilibrium, and health/disease states as the corresponding attractors of the system in the multi-parametric phase diagram. The essential role of electromagnetic potentials in self-regulation and self-healing processes is analyzed, based on the long-range matter-field interaction and fast information transfer, provided by the electromagnetic potentials.

In the present paper, based on Quantum Physics and Physics of open nonlinear dissipative systems, we discuss living systems as a non-linear self-interacting phenomenon, which can be stabilized by the non-linear interaction between matter and self-created electromagnetic field. In particular, such non-linear self-interacting mechanism may follow from the theory of molecular solitons, as discussed below. We address our paper to a broad, interdisciplinary audience and therefore, avoid using mathematical equations to make reading easier, redirecting the interested reader to the original papers where detailed mathematical and physical descriptions can be found.

Hereunder we mention briefly some of the properties of living systems which cannot be described according to linear models of closed systems. One of the main arguments is that the metabolism of living organisms is possible only under the permanent exchange with surrounding energy, matter and information. Therefore, such systems should inevitably be described according to the theory of non-linear open dissipative systems.

Even at the cellular level we see a complex and

Key words: non-linearity, complexity, solitons, endogenous electromagnetic field, electrosolitons, coherence, resonance, system information therapy, attractor, health, disease, allostasis

Mailing address: Dr Larissa Brizhik,
Bogolyubov Institute for Theoretical Physics,
Metrolohichna Str., 14b,
Kyiv 03680, Ukraine
Tel.: +380 44 5213152
Fax: +380 44 5265998
e-mail: brizhik@bitp.kiev.ua

0393-974X (2014)

hierarchic structure in which all sub-units are mutually inter-connected (1). Every cellular sub-unit is complex and manifests collective properties, like a crystal is different from the atoms from which it is built, because of the role of its 'collective' arrangement. How can a complex biological organism function in the most reliable way under permanently changing surrounding conditions? In a living organism, millions of biochemical reactions occur per second, each of which must take place at a given location, specific time, and proper rate, which are necessary to support the metabolism within the interval of its stability. Cell proliferation is a good example of this type of strict balance. What mechanism regulates such balance, what tool controls the metabolism, and what mechanism supports the local biochemical reactions in remote areas that respond to the global needs of an organism? In other words, what is the mechanism converting short-range biochemical interactions into long-range ones that provide support to an organism's metabolism as a whole? A possible physical answer is 'an endogenous field is the control tool'. If this is the case, the nature and origin of such field need to be defined as does the mechanism of interaction between this field and matter. How do this mutually interacting (hence, self-interacting, hence, non-linear) field and matter support the dynamic stability of the living organism and what are the quasi-stationary states of such a system?

It is worth recalling that 'linear' systems are theoretical models. Such linearizations are often forced to make a physical and mathematical description of a system possible, according to current knowledge. In many cases linearization is enough to describe some properties of a system. Up to the XX century, all physics was physics of linear systems. However, since it is an approximation model, linearization sometimes is not enough. In many cases, like those mentioned above, we must describe systems as essentially non-linear, which allow us to derive completely new properties of the system under study. The impressive success of physics and mathematics of non-linear systems in the XX-XXI centuries has allowed scientists not only to theoretically study numerous nonlinear phenomena in physics and biology, but also to apply non-linear systems to technologies, from microelectronics to information transfer technologies.

In the following sections, we will show that non-linear concepts provide us, at least, qualitative, and sometimes also quantitative, answers to scientific problems. One of the essential notions of the non-linear physics and mathematics is the notion of a 'soliton', defined as a localized solution of non-linear wave equations, which is stable under interaction with other solitons and with respect to the influence of external perturbations.

Molecular solitons

It is a well established fact that the metabolism of living systems is supported by the energy released in the hydrolysis of adenosinethriphosphate (ATP) molecules into adenosinediphosphate molecules at the final step of a long chain of biochemical reactions (1). According to the optical spectra of polypeptides, for cases of, e.g., protein synthesis, this energy is stored in the form of the so-called AMID-I excitation (mainly the excitation of the double carbon-oxygen bond C=O) of the nearest peptide group, which is the group of chemically bond HNCO atoms of the macromolecule in the vicinity of the chemical reaction. It is also well known that all metabolic processes are accompanied by the transport of charges (electrons and protons) released in redox processes, such as photosynthesis and animal intracellular respiration (1). In the 1960s-70s, a central scientific problem was the identification of mechanisms by which the tiny amount of energy released in the hydrolysis of ATP be transferred from the place where the chemical reaction took place to the place where the energy is utilized for the metabolism, at physiological temperatures - a problem known as 'crisis in bio-energetics' (2). A similar question is how can electrons propagate from a donor to acceptor macromolecule in the Krebbs cycle's electron transport chain during redox processes. No linear physical model can explain the efficiency of ATP hydrolysis energy transfer or electron transport on macroscopic distances at physiological temperatures.

A.S. Davydov has shown that such processes can be facilitated by polypeptide macromolecules in the cell (2). Polypeptides and other macromolecules, such as DNA, enzymes, as well as clusters of water molecules structured around bio-macromolecules (3), have a regular crystal-like structure, stabilized by hydrogen bonds, which are formed between

peptide groups, between peptide groups and nearest water molecules, or between water molecules within the cell. Such hydrogen bonds are relatively soft, in comparison with chemical bonds. It has been shown analytically and numerically (2) that the account of the periodicity of the structure and its flexibility, described as an electron-lattice interaction, leads to self-trapping of the AMID-I excitation or an electron (below we call electron, hole, proton, molecular excitation in a macromolecule 'a quasi-particle') in a soliton state. The wave-function of a quasi-particle in a soliton state is

$$\Psi_s = \frac{1}{2}\ Sech(g(R-Vt)/a)e^{ikR-i\Phi(t)} \qquad (1)$$

Where R is the coordinate along the molecular chain, a is the lattice constant, g is the dimensionless electron-lattice coupling constant, V is the velocity of the propagation of the soliton, k and $\Phi(t)$ are its wave-vector and phase, respectively. From Eq.(1) we see, that the quasi-particle is localized in the chain within the finite area of the width $l_s=2\pi a/g$, determined by the strength of the coupling between the electron and chain deformation. It follows from Eq. (1) that a soliton propagates coherently along the chain with the average velocity V. Thus, a soliton created on one end of the chain, will reach the other end of the chain with probability equal to 1 within the time $\tau = L/V$. Here $L=Na$ is the length of the chain, consisting of N subunits (peptide groups in a polypeptide chain).

In such a soliton state the total energy of the system, E_{tot} which includes the energy of the quasi-particle and the energy of the deformation of a molecular chain, is:

$$E_{tot} = E_0 - 2J - \frac{1}{2}Jg^2 \qquad (2)$$

From Eq. (2) we see that this energy is lower than the energy of a chain with a free quasi-particle, $E_f=E_0 - 2J$. Here E_0 is the energy of the electron level on an isolated peptide group (or unit cell in the case of water molecule chain, DNA, etc.), J is the electron exchange interaction energy, determined by the overlap of the electron wave-functions on the neighbouring peptide groups in a polypepdide chain, and the binding energy of the soliton is

$$E_s = -Jg^2/4$$

Such solitons are exceptionally stable not only because of their lower energy, but also because they do not emit linear 'sound waves', since they can move with a subsonic velocity only, i.e. there is practically no energy dissipation. Therefore, macromolecules facilitate energy transfer (and in a similar way charge transport) via the soliton mechanism and make such transport possible to occur on large distances, up to hundreds of angstroms (2). As we have mentioned above, this is due to the interaction of quasi-particles (electrons, holes, protons, molecular excitations like AMID-I excitation, etc.) with local deformation of macromolecules induced by these quasi-particles. This interaction leads to self-trapping of quasi-particles in nonlinear soliton-like states, usually called 'molecular solitons' for neutral quasi-particles, and 'electrosolitons' for charged particles (2). Below we will use the term 'soliton' in its general meaning.

There is experimental evidence of the non-linear nature of AMID-I excitations, their exceptionally large life-time in macromolecules has been measured using laser spectroscopy (2). Unfortunately, up to now there is no direct experimental evidence of the role of solitons in redox processes. Nevertheless, the theory of molecular solitons can explain various properties of charge transport chain in redox processes (2), which in our opinion justifies further studies of the soliton concept.

Such non-linear soliton-like states possess very peculiar features, which make them different from linear electron states, i.e., free electron, proton, hole, etc. Some of these properties are exceptionally large life-time, dynamical stability and coherent propagation along macromolecules. Large life-time and stability are the result of the non-linear nature of soliton formation which, as described above, arises from the electron self-trapping in the potential well created by the quasi-particle itself in the form of local deformation of the macromolecule (2). As a result, solitons are described by systems of non-linear equations, in which self-induced non-linearity compensates the dispersion of a quasi-particle, which

means that solitons behave like stable quantum quasi-particles. It is important to note that soliton solutions (and, hence, solitons' exceptional stability) cannot be obtained when linearization is applied, in no order of the theory of perturbations.

Endogenous electromagnetic field and coherence

It follows from theoretical study (4) that propagating along macromolecules, solitons expire periodicity of the macromolecule in the form of the periodical Peierls-Nabarro potential relief with the period equal to the lattice period of the macromolecule

$$U_{PN}=U_0\sin\left(2\pi\frac{R}{a}\right) \tag{3}$$

Here U_0 is the height of the potential relief, determined by the width of the localization of the soliton. This leads to oscillations of soliton velocity with the frequency of the main harmonic of oscillations, ω_0, proportional to the average soliton velocity,

$$\omega_0 = 2\pi\frac{R_0}{a} \tag{4}$$

as it is shown analytically and numerically in (4). The average soliton velocity, that provides electron transport in redox process, is determined by the intensity of the redox process itself.

Such oscillating type of soliton propagation means that solitons, moving from a site to a site, periodically accelerate and decelerate. The non-zero time derivative of the velocity of a charged particle, according to Maxwell equations, results in the emission of the electromagnetic field. Solution of the corresponding Maxwell equations for a soliton shows that this field has an electromagnetic radiation component (5), which decreases slowly with distance, slower than the decrease of the electric and magnetic fields. The frequency of the main harmonic of the soliton eigen-radiation, ω_{rad}, is equal to the frequency of the main harmonic of oscillations of the soliton velocity ω_0, given in Eq. (2):

$$\omega_{rad}=\omega_0, \tag{5}$$

i.e., it is determined by the rate of redox processes. Moreover, this type of radiation is the one electric dipoles emit (5). Thus, according to the soliton concept the self-induced soliton radiation is physiologically relevant as it is determined by the metabolism of the corresponding system reflecting different hierarchical levels of the organism ranging from microscopic components up to macroscopic ones.

Solitons in different macromolecules exchange, among them, their individual electromagnetic radiation: each soliton moves in the radiation field created by all other solitons. The solution of the corresponding equations shows that, moving in this common radiation field, solitons attain equal velocities. In other words, the field synchronizes their dynamics (5). This means, according to Eqs. (4)-(5), that the eigen electromagnetic field leads to a synchronization of frequencies of soliton radiation and gives rise to the appearance of system coherence: solitons move with the same velocities and emit radiation with equal frequencies, i.e., they move with the same rhythm, in tune with each other, coherently. As a result of such soliton coherence, the total intensity of the radiation in the system, I_r, is proportional to the square of the total number of solitons, N^2, - a relationship known as the 'laser effect'. This radiation field is much stronger than a field created by particles moving with different velocities, non-coherently. In the latter case, the intensity is proportional to the number of particles, N. In a macroscopic organism the number of solitons N (i.e., electrons, that are released in the redox processes per unit of time) is a macroscopic number, and the difference between $I_r \propto N^2$ and $I \propto N$ is huge. Therefore, such a coherent radiation field can be strong enough to provide a long-range order and fulfill the role of controlling the metabolism of an organism (5-8). Therefore, charged solitons play the role of hypothetic coherent dipoles which emit macroscopic coherent electromagnetic radiation,

as it has been suggested by Herbert Fröhlich (6). We can expect a very complicated structure of this endogenous electromagnetic field, because it is determined by electrosolitons and their bound states, bisolitons, in different bio-macromolecules and in different tissues and organs. It has various frequency components arising from oscillations of biological membranes and other polar structures, in particular, microtubules, coherent domains of extracellular and intracellular water (2, 5, 7). This field should also have a complex polarization structure because the helical structure of macromolecules determines polarization of the electrosoliton self-induced radiation. It must have a complex geometrical structure determined by the optical properties and geometry of various tissues and organs as well as the whole body.

On the other hand, the electromagnetic field in the organism can be partly self-trapped, forming a pattern of waveguides similar to electromagnetic waveguides in non-linear optical systems (8). This makes such a macroscopic structure stable on a large scale, able to reinstall a long-range order in cells, organs, tissues and systems after the appearance of a local disorder, for instance, due to a disease. This can constitute one of the mechanisms of self-healing through self-regulation and self-regeneration potential.

Taking into account the electromagnetic properties of electrosolitons described above, we can suggest a hypothesis, that non-linear interaction of self-induced electromagnetic radiation and matter (brain) can result in partial self-trapping of the total electromagnetic radiation in the brain. This opens the possibility that appearance of consciousness arises from dynamic metabolic processes and collective coherent complex dynamics of self-interacting matter and corresponding field. In spite of the self-trapping, i.e., localization, the field incorporates the whole organism, and is a collective state of the integral global electromagnetic field mirroring all its enfolded features. It is a kind of electromagnetic vector entrapping the specificities of each single individual at each single time.

We are far from calculating this structure in detail, but we can rely on qualitative analysis, based on modern quantum physics and quantum electrodynamics, as well as on data of the evidence-based medicine and Eastern medicine and on the experimental measurements of endogenous electromagnetic fields (9-11). Such complex non-linear quantum approach suggests a holistic description of the health-disease state of an organism and of the life phenomenon.

We hypothesize that in a living organism the whole hierarchy of 'selves' can arise, from a microscopic self-trapped electron to a macroscopic self-induced field, to a self-arising consciousness, to formation of psychic ego ("self"), to self-formed/self-sustained collective ego. Through electromagnetic radiation, namely through vector-potential, a fast macroscopic long-range interaction can be attained not only between cells, organs, tissues, but also between different organisms (8) by mean of the resonance phenomenon, which we name bio-resonance when involving living structures. Thus, coherence is manifested at all levels of the organization of living matter from synchronization of redox processes at a cellular level up to coherence of individual consciousness and psyche, to formation of societies through a 'collective consciousness' as arising from the collective self-interacting coherent electromagnetic field, formed by the fields of individuals. The principles of feedback and coherence are necessary conditions for successful functioning of individuals and societies. Indeed, 'coherence' as manifested in the form of self-agreement, happiness, emotional balance, inner and external sense of coherence, sense of meaning, agreement with the nearest surrounding (family, friends, colleagues, environment), with the whole society and nature, is a necessary health condition. We know intuitively the role of music, poetry, arts, nature on well-being. Exploring further the concept of coherence, we can say that they 'induce' (or at least increase) a coherence of the corresponding audio, visual, tactile and kinesthetic systems of an individual, and in a resonant way they can increase or even induce self-agreement and appearance of a more general coherence, and can lead to self-healing via activation of the self-regulation processes.

Some biophysical aspects of complexity related to health and disease

From the point of view of the theory of complex dissipative structures (12), health and disease can be represented as quasi-stationary local minima of the corresponding organism in its complex multi-parametric phase space, and, thus, can represent

the corresponding quasi-stationary attractors for the state of the organism, each corresponding to its local energy minimum in the potential energy profile. Appearance of a disease in the organism is not only a manifestation of a corresponding organ dysfunction, genome disruption, or metabolism imbalance (metabolism being defined as the self-regulation dynamic between anabolic and catabolic phases aimed to keep allostasis), but is also - and perhaps mainly - an attempt of the organism to cope with sudden or long-lasting stressor(s), inherited or attained due to certain reasons, like external negative effects or intrinsic malfunctioning (bad diet, lack of vitamins, improper physical activity, nerve stress, psychic and/or emotional tension, etc.). Therefore, one can conclude that 'killing' a disease is not the solution of the problem at all. It can even enhance the problem, mapping it on a higher level, and can cause a new disease(s) due to the inter-connection of all processes, organs and systems in the organism according to systems biology and systems medicine viewpoint (13-15). Examples are abundant in medicine: side effects of drugs, allergic reactions, increase of drug-resistance, post-operative complications, are only a few that could be mentioned. In contrast, the main aim should be to understand and treat not only the symptoms, namely the effect, but rather also the causes, namely the meaning, of the disease. In this framework, the disease is an attempt to keep health aimed to maintenance of allostasis. Thus, the disease bears within itself the solution for the organism to regain health. It has to be considered as the solution that the organism provides to preserve its own life within the adaptive dynamic. Health and disease, as quasi-stationary, allostatic time-space condition involving different levels, such as cells, organs, tissues, systems, functions or the whole organism, can be considered as attractors. Being so interconnected with each other, 'health' and 'disease' are both necessary to sustain the living organism. Somehow, we need diseases to restore health leading, through increase of resilience, to a feed-forward toward salutogenesis, a stronger health attractor. In turn, we need a 'health attractor' to restore diseases and the process goes on endlessly yielding personal evolution. A very different situation is seen when the disease becomes chronic and leads to a feed-forward, through progressive defiance, toward pathogenesis, a stronger 'disease attractor'. Therefore, health-disease dynamics could be represented by a bifurcation behavior in which one path could lead to a stronger health attractor and the other one could lead to a stronger disease attractor: the first one is useful to improve personal evolution while the second one is detrimental, but both are essential parts of any complex, nonlinear and evolutionary-based life process .

Power of weakness

Weak external stimuli do not cause stress on the organism, instead they can cause a relatively weak feedback. This can be one of the reasons why therapies, based on weak external stimuli, do not cause treatment rejection. Among such therapies are ultra-weak resonant electromagnetic therapy; System Information Therapy (the two are based on external and endogenous signals, respectively), ultra-low frequency electric dynamical stimulation, homeopathy, even such weak stimuli like just phase-shifted eigen-factor treatments (phase-shifted eigen-electromagnetic field, urine therapy, own-blood injections, etc.). Rather than responding to these stimuli as if they were intrusions that demand a defence reaction of the organism, they are incorporated into the hierarchy of physiological processes, which can result in mobilization of self-training and self-healing processes in the organism (6). Moreover, synergetics of such 'friendly' weak stimuli treatments can be very important, again due to the inter-connection of processes and organs, and due to their complexity and non-linearity.

Weak (low intensity) low frequency stimuli can be converted through the biochemical/physiological processes into signals of frequencies equal or higher than biologically relevant frequencies, which then can be integrated into the morphogenetic (endogenous) electromagnetic field (16) in the most natural way, and thus, most efficient way, without negative impact on health. High frequency stimuli can be integrated provided their frequencies are in a strict resonance with the frequencies present in the endogenous electromagnetic field. Through an endogenous electromagnetic field, short-range interactions can be converted into long-range interactions, thus, they can provide a dynamical order to the whole organism. This applies first of all

to the whole range of biochemical reactions which, spatially distributed on a macroscopic scale (all over the organism), occur in a necessary spatial location at a very precise rate under the instantaneously varying conditions. This applies also to the well-coordinated functioning of all organs and systems of the organism to maintain its quasi-stable (allostatic) functioning and interaction with the surrounding. Indeed, it has been proven that electromagnetic signals in the extremely low frequency range are able to transfer specific information pattern to living cells triggering stem cells differentiation, epithelial cell and neuronal cell differentiation (17), as well as human neuroblastoma cell differentiation toward a normal cell type by electronically transferring the molecular signals of retinoic acid even when mediated by the aqueous system constituting cell culture medium (see (18) and references therein). Little is known about the physical mechanisms of such biological effects, but their resonant non-thermal character indicates their non-linear origin. Molecular solitons can be one of the possible potential mediators, acting on one of the lowest levels of the biological hierarchy through their involvement in energy and charge transport processes. Namely, in the non-linear states, electrons (solitons) have non-thermal resonant sensitivity to the electromagnetic external signals, according to theoretical studies (8), unlike conventional electrons in 'linear' models.

For successful results with weak stimuli treatment, stimuli have to be delivered to the organism at proper conditions depending on their nature. For instance, ultra-weak electromagnetic microwave resonant treatment requires a choice of proper resonances and delivery of these signals to the corresponding disease biological active zones with high level of localization accuracy due to a very short signal wavelength (few millimeters). In the case of weak low-frequency stimuli, these conditions are again proper frequency and power of the signal, but the area of the delivery of the signal can be less confined due to a bigger signal wavelength. Often it is noticed that treatments with weak stimuli are more successful when acting not only on the zone of the direct projection of the problem (disease), but also on the corresponding symmetric zone in the case of symmetric organs. In many cases of acute disease, acting on a remote biologically active zone turns out to be more successful than on the zone of direct projection. A possible explanation according to the concept of self-interacting eigen-field and matter could be that the healthy organ (zone) responds more actively to the stimuli, than the ill organ (zone). This response generates a local radiation field, which, via the mechanism discussed above, induces a long-range coherent signal that induces healing of the remote ill organ (zone). Following this concept, it can also be explained why in the case of a regime chosen less properly, there are no negative effects: the healthy organ does not react to such stimuli due to the exceptional stability of a non-linear system in a soliton-type state through the adaptation and allostasis (capability to maintain stability through dynamic changes) mechanism, thus preventing negative response (changes) both of the healthy and ill organs (zones). In order to settle as carefully as possible the parameters of carrying and modulating waves as well as the intensity of the magnetic field and duration of treatment to be delivered, it is useful and effective, for instance, the procedure patented by Omura as "o-ring bi-digital resonance test" (19).

Temporal and spatial symmetry breaking and role of noise

Living systems are complex open systems which can exist providing permanent exchange with energy, matter and information within the system and with the surrounding environment is possible at the proper rate. According to physics, any type of process is governed not by energy but by free energy, $F=E-T\Delta S$, determined as the difference between the energy (E) and product of temperature (T) and difference of entropies of the corresponding initial and final states (ΔS). In living systems, entropy decreases locally, but not globally. As discussed above, in a living system a non-local electromagnetic field can be self-created and its dynamically induced vector-potential can be a source of negentropy of living matter, determining the arrow of time from the past to the future (20).

In this respect, it is necessary to note also the essential role of noise in complex systems and living organisms (12). Noise arises from a nonzero temperature at which the metabolism of any living organism is possible, moreover, such temperature ranges within finite temperature interval, limited both from below

and from above, unlike a white noise. It arises also from a dissipative nature of life and its openness and its global nature due to interrelatedness. Such noise in living matter is not a side product of the corresponding processes as one could expect from a mechanical point of view, but is a source of energy and information to restore and maintain complex non-linear dynamics in a way, similar to stochastic resonance. Pure rhythm is a property of a 'dead' matter, some level of noise always accompanies heart rhythm, brain functioning, according to the corresponding electrocardiograms and encephalograms that have, therefore, typical chaotic and not random dynamics. Even cellular structures, organs, tissues and the whole body possess breaking of spatial symmetry (asymmetry) and have a fractal structure. Of course, the extent of asymmetry and noise/signal ratio has to be very small, most probably, there are corresponding critical values of these parameters, true life windows above which energy balance and coherence get destroyed, disease potential increases and a phase transition from healthy to ill state can take place. And, vice versa, decreasing the asymmetry extent and/or noise/signal ration via treatment, we can expect improvement of health. Indeed, a relationship between the presence of the allostatic load and fluctuating asymmetry (i.e., asymmetric activation of symmetric group of muscles due to a loose of coherence into the inter-hemispheric synchrony at the brain level) is known (20-23). Human beings develop fluctuating asymmetry in response to environmental stress. The expression of the total amount of the different efforts they are involved while surviving and evolving, keeping and improving allostasis, through lots of adaptive response at once is described as allostatic load. It is well established that the brain is the key organ in coping with stress and in keeping allostasis through activation of self-regulation and self-recovery properties of the organism (25). The Systems Information Therapy approach operating in the extremely low frequency range of the electromagnetic signals by means of a resonance effect, in a large group of patients showed complete disappearance or significant decrease of fluctuating asymmetry (26). According to (26) disappearance of fluctuating asymmetry could be a marker of a disappearance or at least of a not negligible decrease of the excess of the allostatic load of the examined subject. It has been reported that reduction of allostatic load contribute to a global reduction of morbidity and mortality contributing to a successful aging (27) therefore the possibility of periodical management and relief of allostatic load by mean of Systems Information Therapy protocols could disclose a relevant integrative perspective in preventive medicine as well as in personalized medicine (28, 29).

Breaking of temporal and spatial symmetry and the self-interactive nature of living systems at all levels of matter organization opens a possibility for an active work with the least need of external energy. Living organisms are the most efficient energy and information 'processors' in nature, which is one of the reasons of life's stability as a global phenomenon. In particular, we refer to a ratchet phenomenon - an appearance of the oriented drift velocity in a non-linear system under the action of an unbiased periodical force, i.e., periodical force with zero mean-value. In particular, it has been shown in (30) that such a ratchet dynamics of solitons can take place in macromolecules under the effects of membrane oscillating potentials and is thermally enhanced. This reduces the amount of energy required for charge transport, and, hence, required to sustain redox processes and therefore, the entire metabolism.

Conclusions and discussion: from feedback through feedforward to the future

The self-interactive nature of living systems at all levels of matter organization and intrinsically breaking of temporal and spatial symmetry of all macromolecules, organs, and systems, opens a possibility for an active work with the least use of external energy. Living organisms are the most efficient energy and information 'processors' in nature, which is one of the reasons of life's stability as a global phenomenon. One of the mechanisms of such efficiency occurs through the ratchet phenomenon. This phenomenon is an appearance of the oriented drift (appearance of the directed velocity) in a non-linear system under the action of an unbiased periodical force, i.e., periodical force with zero mean-value. In particular, it has been shown in (30) that solitons in macromolecules attain such a ratchet dynamics in the presence of the unbiased electromagnetic field, and that such ratchet dynamics is thermally enhanced: at certain temperatures, the

drift of solitons is higher than at zero temperature, the critical values of the intensity of the field and period of oscillations are much lower than at zero temperature, etc. In a cell membrane oscillating potentials can play the role of the 'external field'. This reduces the amount of energy required for charge transport, i.e., required to sustain redox processes and therefore, the whole metabolism. Thermal enhancement of ratchet dynamics is one of the examples showing the important role of temperature in living systems. While in most conventional physical systems temperature is the source of disorder and energy loss, in non-linear systems temperature and noise can be the source of restoring the order (energy, signal, etc.).

Finally, we stress an essential role for healthy life of a global aim of an individual and even of a society. If indeed self-interaction of electromagnetic field and matter takes place in living organisms, we can expect that the 'quality of thoughts' (which are determined by frequency patterns of brain activity), incorporated into the field-matter interaction, can determine the state of health through functioning of the corresponding organs. We can also intuitively understand the role of dreams and aims not only as life plans, but also as control tools for quality of life. This is highly coherent with the central role the brain plays in allostasis (18). Such aims can play a role of 'remote attractors' which mobilize vital forces to reach the aim. This, in turn, can enhance eigen-coherence through the self-interaction mechanism between the eigen-field and matter (brain) and thus, can support necessary conditions for health. Thus, the eigen-induced electromagnetic vector-potential can act as a driving force to reach the aim and as a control tool for health. On the contrary, the loss of a remote aim, like loss of the attractor, can reduce the coherence and can even break the connection of an individual with the universe and lead to the loss of his/her life motivation. In other words, through the change of an electromagnetic pattern, an absence of a global aim and connection with the universe changes the status of consciousness and psyche, which in its turn through the change of redox processes and change of the metabolism, can break self-regulated functioning of organs and systems, which negatively affects the physiological state of the whole organism. This can further block self-maintaining of the long-range coherence of the organism, which diminishes vital forces and results in a progression of the disease.

In spite of the fact that the present paper has a rather speculative character, we think it sheds new light on some of the aspects of the complex phenomenon of life and health. Its main ideas are based on the theory of non-linear open dissipative systems and the role of non-linear interaction of matter and eigen-created electromagnetic field. To conclude, we point out that in a non-linear self-interacting system of a molecular chain an electron self-trapped in a soliton state, solitons form the potential barrier for their own propagation (see Eq. (3)). Similarly, we can say: 'We create our problems ourselves'. Want to be healthy, be healthy! Cope with negative thoughts, don't live in your past, live for the future, work hard to be happy and you will be healthy. Break ego, be in a unison with the nature, and the nature will reward you enhancing evolution of your higher self.

ACKNOWLEDGEMENTS

The authors warmly acknowledge stimulating discussions with E. Del Giudice (deceased) and Prof. J. Pokorny (Prague, Czech Republic). We also thank Colin Egan for careful reading and improving the text of the paper. One of the authors, LSB, acknowledges stimulating discussions with Dr. Wabe Heringa and expresses her gratitude to the organizers of the Second International Symposium "Biophysical Aspects of Complexity in Health and Disease" (Lugano, Switzerland, May 18-19, 2012) for stimulating working atmosphere and financial travel support.

REFERENCES

1. Lehninger AL. Biochemistry. Worth Publishers Inc., New York; 1972.
2. Davydov AS. Solitons in Molecular Systems (2nd ed.), Reidel, Dordrecht; 1985.
3. Pollack GH. Water, energy and life: Fresh views from the water's edge. Int J Des Nat Ecodyn 2010; 5:27-9.
4. Brizhik L, Cruzeiro-Hansson L, Eremko A, Olkhovska Yu. Soliton dynamics and Peierls-Nabarro barrier in a discrete molecular chain. Phys Rev B 2000; 61:1129-41.
5. Brizhik L, Eremko A. Nonlinear model of the origin of endogenous alternating electromagnetic fields and

self regulation of metabolic processes in biosystems. Electromagn Biol Med 2003; 22:31-9.
6. Fröhlich H, editor. Biological coherence in response to external stimuli. Berlin: Springer Verlag; 1988.
7. Del Giudice E, De Ninno A, Fleischmann M, Mengoli G, Milani M, Talpo G, Vitiello G. Coherent quantum electrodynamics in living matter. Electromagn Biol and Med 2006; 25:522-30.
8. Brizhik LS, Del Giudice E, Maric-Oehler W, Popp F-A, Schlebusch K-P. On the dynamics of self-organization in living organisms. Electromagn Biol Med 2009; 28:28-40.
9. Pohl HA. Oscillating fields about growing cells. Proceedings of the International Symposium on Quantum Biology and Quantum Pharmacology. Int J Quant Chem 1980; 18(S):411-31.
10. Pokorný J, Hašek J, Jelínek F. Endogenous electric field and organization of living matter. Electromagn Biol Med 2005; 24:185-97.
11. Montagnier L, Aissa J, Ferris S, Montagnier J-L, Lavallée C. Electromagnetic signals are produced by aqueous nanostructures derived from bacterial DNA sequences. Interdiscip Sci 2009; 1:81-90.
12. Prigogine I, Nicolis G. Self-Organisation in Non-Equilibrium System, From Dissipative Structures to Order Through Fluctuations. New York, Wiley, 1977.
13. Cornish-Bowden A, Cárdenas ML. System biology may work when we learn to understand the parts in terms of the whole. Biochem Soc Trans 2005; 33(pt3):516-9.
14. Carlson RJ. Holism and reductionism as perspective in medicine and patient care. West J Med 1979; 131:466-70.
15. Ahn A C, Tewari M, Poon C-S, Phillips RS. The clinical applications of a system approach. PLoS Medicine 2006; 3:e209.
16. Levin M. The wisdom of the body: future techniques and approaches to morphogenetic fields in regenerative medicine, developmental biology and cancer. Regen Med 2011; 6:667-73.
17. Foletti A, Ledda M, De Carlo F, Grimaldi S, Lisi A. Calcium ion cyclotron resonance (ICR), 7.0 Hz, 9.2 microT magnetic field exposure initiate differentiation of pituitary corticotrope-derivated AtT20 D16V cells. Electromagn Biol Med 2010; 29(3):63-71.
18. Foletti A, Ledda M, D'Emilia E, Grimaldi S, Lisi A. experimental finding on the electromagnetic information transfer of specific molecular signals mediated through aqueous system on two human cellular Models. J Altern Complement Med 2012; 18(3):258-61.
19. Omura Y. New simple early diagnostic methods using Omura's "Bi-Digital O-Ring Dysfuntion Localization Method" and acupuncture organ representation points, and their applications to the "drug & food compatibility test" for individual organs and to auricular diagnosis of internal organs—part I.", Acupunct Electrother Res 1981; 6:239-54.
20. Tiezzi E. Steps Toward an Evolutionary Physics. Billerica, MA: WIT Press, 2005.
21. Parson PA. Fluctuating asymmetry: an epigenetic measurement of stress. Biol Rev Camb Philos Soc 1990; 65(2):131-45.
22. Livshits G, Kobyliansky E. Fluctuating asymmetry as a possible measure of developmental homeostasis in human: a review. Hum Biol 1991; 63:441-66.
23. Kowner R. Psychological perspective on human developmental stability and fluctuating asymmetry: sources applications and implications. Br J Psychol 2001; 92:447-69.
24. Al-Elisa E, Egan D, Wassersung R. Fluctuating asymmetry and low back pain. Evolution and Human Behaviour 2004; 25:31-7.
25. McEwen BS, Gianaros PJ. Central role of the brain in stress and adaptation: links to socioeconomic status, health, and disease. Ann NY Acad Sci 2010; 1186:190-222.
26. Foletti A, Grimaldi S. Systems Information Therapy and the central role of the brain in allostasis. J Phys: Conference Series 2011; 329:012027.
27. Seeman TE, McEwen BS, Rowe JW, Singer BH. Allostatic load as a marker of cumulative biological risk: MacArthur studies of successful aging. Proc Nat Acad Sci USA 2001; 98:4770-5.
28. Henney AM. The promise and challenge of personalized medicine: aging populations, complex diseases, and unmet medical need. Croat Med J 2012; 53:207-10.
29. Foletti A, Grimaldi S, Lisi A, Ledda M, Liboff AR. Bioelectromagnetic medicine: The role of resonance signaling. Electromagn Biol Med 2013; 32:484-99.
30. Brizhik L, Eremko A, Piette B, Zakrzewski W. Thermal enhancement and stochastic resonance of polaron ratchet. Phys Rev B 2014; 89(6-1):062905.

JOURNAL OF BIOLOGICAL REGULATORS & HOMEOSTATIC AGENTS Vol. 28, no. 3, 367-375 (2014)

EDITORIAL

CENTRAL PRECOCIOUS PUBERTY: FROM PHYSIOPATHOLOGICAL MECHANISMS TO TREATMENT

V. CHIRICO[1] , A. LACQUANITI[2,3], V. SALPIETRO[1], M. BUEMI[2], C. SALPIETRO[1] and T. ARRIGO[1]

[1]Department of Pediatric Sciences, University of Messina, Messina, Italy; [2]Department of Internal Medicine, University of Messina, Messina, Italy; [3]Department of Internal Medicine, Mediterranean Institute for Transplantation and Advanced Specialized Therapies, ISMETT, University of Pittsburgh Medical Center, Palermo, Italy

Received June 10, 2013 – Accepted July 28, 2014

Puberty is a complex, coordinated biological process with multiple levels of regulations. The timing of puberty varies greatly in children and it is influenced by environmental, endocrine and genetic factors. Precocious puberty (PP) is an important issue, affecting between 1 in 5.000-10.000 children. The physiopathological mechanism is still unknown. From an etiological point of view, PP may be subdivided into gonadotropin-releasing hormone (GnRH) -dependent and independent causes. GnRH-dependent PP, often called central precocious puberty (CPP), is based on hypothalamic-pituitary-gonadal axis activation associated with progressive pubertal development, accelerated growth rate and advancement of skeletal age. Conversely, peripheral precocious puberty (PPP) is related to sex steroid exposure, independently of hypothalamic–pituitary–gonadal (HPG) axis activation. Kisspeptins play a central role in the modulation of GnRH secretion with peripheral factors that influence the timing of puberty, such as adipokines and endocrine disrupting chemicals. Moreover, PP could be related to genetic disorders, involving pivotal genes of the HPG axis. The standard test used to verify HPG activity is the gonadotropin response to administered GnRH analogs. We describe the physiopathological mechanisms of PP and its clinical implications, analysing diagnostic flow-chart and new potential biomarkers that could reveal PP. An update of the current literature was also carried out regarding the recent novelty for treatment.

Precocious puberty (PP) affects between 1 in 5.000-10.000 children, with health and psychosocial consequences, in relation to peers and reduced final height (1). Furthermore, this condition has been associated with long-term adverse outcomes, such as an increased risk of adult obesity, type 2 diabetes and breast cancer (2).

A debate among pediatric endocrinologists concerning the necessity of revision of the age limit for what is considered PP requiring further diagnostic evaluation is still open due to the decline in the lower age limit of normality at pubertal onset (3).

Establishing the diagnosis of PP requires documenting pubertal physical findings and measuring luteinizing hormone (LH) concentration, which is the key biochemical assessment of pubertal status. When these first level tests are suggestive of PP, a stimulation test with gonadotropin-releasing hormone (GnRH) should be performed to assess the degree of activation of the hypothalamic–pituitary–

Key words: precocious puberty, obesity, GnRH analogue, biomarkers, kisspeptin, endocrine disrupting chemicals

Mailing address: Prof. Carmelo Salpietro,
Department of Pediatrics,
University Hospital "G. Martino",
Via Consolare Valeria, 1
98100 Messina, Italy
Tel.: +39 0902213114 Fax: +39 090.2213115
e-mail: cdsalpietro@unime.it

0393-974X (2014)

gonadal (HPG) axis.

Moreover, these analyses, associated with radiological assessments, allow the clinicians to distinguish between central and peripheral forms of PP. In recent years, potential new peptides have been evaluated, such as inhibin and kisspeptin. This editorial focuses on pathophysiological mechanisms underlying PP and new available biomarkers. Moreover, an update of the current literature on recent novelties for the treatment of PP has been carried out.

MECHANISMS AND RISK FACTORS

Normal pubertal development is caused by the increasing pulsatile activity of the GnRH pulse generator which leads to the maturation of LH and follicle stimulating hormone (FSH) secretion and subsequently to the maturation of gonads and their activity. For the initiation of puberty, a functioning GnRH neuronal network and pulsatile GnRH secretion are critical prerequisites. Two mechanisms are responsible for the central control of pulsatile GnRH secretion: a tonic inhibitory restraint and excitatory inputs to GnRH neurons. Novel regulators of GnRH secretion have been found to be essential for normal pubertal development. In particular, a G-protein-coupled receptor gene called GPR54 and a family of neuropeptides encoded by the Kiss1 gene named kisspeptins, play a key role in the physiological mechanisms of puberty (4).

A number of clinical conditions offer clues regarding the influence on environmental factors, such as nutrition and body size, on puberty. In particular, a relationship between body mass index and timing of pubertal onset in

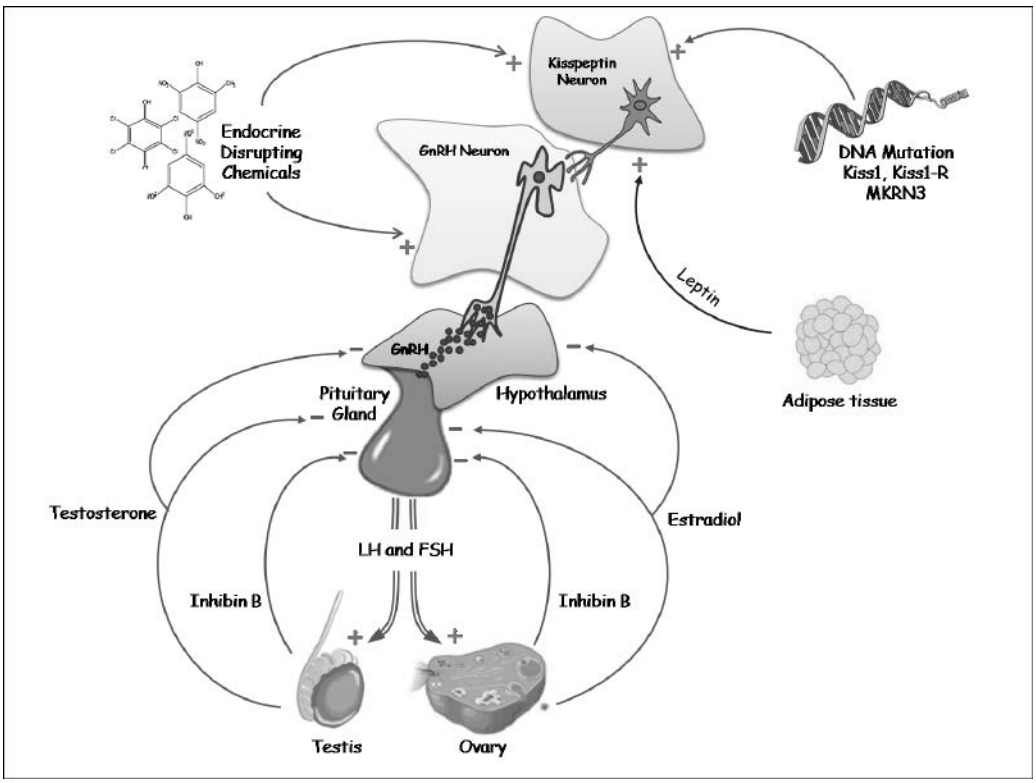

Fig. 1. *GnRH neurons, which receive trans-synaptic and glial inputs, release GnRH to the hypophysial portal blood system, starting the pulsatile secretion of gonadotropins, LH and FSH, that stimulate the maturation and regulate the function of the gonads. Estradiol and testosterone, secreted by gonads, exert a negative feedback to hypothalamus and pituitary to regulate GnRH secretion. The same action is determined by inhibin B, which negatively regulates FSH and LH secretion. The hypothalamus-pituitary-gonad axis is influenced by peripheral regulators. In particular, high levels of adipokines, such as leptin, often observed in obese children, promotes the GnRH release through kisspeptin neurons stimulation. Similarly, endocrine disrupting chemicals could represent important triggers to puberty beginning. The lack of inhibitors of GnRH system, as observed in genetic disorders involving kisspeptin, its receptor or the makorin ring finger 3 gene, represent another mechanism of precocious puberty. GnRH: gonadotropin-releasing hormone; LH: Luteinizing Hormone; FSH: Follicle Stimulating Hormone*

girls has been revealed (5, 6).

A central role is played by the adipose tissue which is responsible for an amplified androgen conversion to estrogens, through an aromatase action and an increased insulin resistance, leading to enhanced bioavailability of sex steroids. The link between peripheral adipose tissues and central nervous system is based on adipokines and gastrointestinal peptides, such as leptin, which communicate the energy store status and the adequate starting time for the energy-intensive process of pubertal development. However, there are other important determinants of puberty. Recent studies support the hypothesis that certain stressful psychosocial factors in infancy and childhood may lead to earlier pubertal maturation (7).

Moreover, exposure to endocrine disrupting chemicals (EDCs), such as pythoestrogens, are other possible candidates that may influence the endogenous endocrine milieu, and therefore potentially affect maturation of the reproductive system. A wide variety of synthetic EDCs has been recognized by environmental agencies, including pesticides, pollutants and substances used in plastic manufacturing, whereas natural EDCs could be found in several nutrients.

They influence puberty through their estrogenic, anti-estrogenic, androgenic, anti-androgenic effects or through their direct effects on GnRH. In fact, it was demonstrated that EDCs may act in the brain by stimulating hypothalamic neurons, thereby releasing kisspeptin and causing earlier onset of puberty (8).

Moreover, central PP has also been associated to genetic factors. Several genes have been identified in the complex network of inhibitory, stimulatory, and permissive neuroendocrine factors involved in the control of puberty onset. Mutations in the gene encoding kisspeptin-1 (KISS1) and in the gene encoding its receptor (KISS1R) have been associated with central precocious puberty (9). It was demonstrated that the deficiency of the makorin ring finger 3 (MKRN3) gene, located on long arm of chromosome 15, causes familial central PP in humans (10). Fig. 1 summarizes the main mechanisms involved in the physiopathological process of the central precocious puberty.

PRECOCIOUS PUBERTY ASSESSMENT

A combination of clinical signs, bone age, pelvic echography in girls, and hormonal data are required to diagnose PP and make a judgment concerning progression and prognosis. It is important to differentiate between central PP (CPP) and peripheral types of PP (PPP) because of the differences in differential diagnosis and the fundamentally treatment options. A CPP is defined as organic when it is associated with a lesion of the central nervous system (hamartoma, hydrocephalus, infection) (11, 12), whereas an idiopathic form is diagnosed when the neuroradiological evaluation shows no lesion. The frequency of organic and idiopathic CPP varies according to the subject's sex; idiopathic CPP rarely occurs in boys, but accounts for 70–80% of CPP cases in girls. On the other hand, a PPP is due to an increase of sex steroids with no evidence of activation of the hypothalamic-pituitary-gonadal (HPG) axis. It could be secondary to either genetic disorders or very heterogeneous acquired diseases, such as adrenal, gonadal and surrenal tumor, congenital adrenal hyperplasia (13). Table I highlights differential characteristics between the two forms of PP.

Clinical evaluation

PP is classically defined as the development of secondary sexual characteristics before the age of 8 years in girls (presenting with Tanner stage B2) and before 9 years in boys (Tanner G2 and/or testicular volume $\geq$ 4 ml) (14). In addition to pubic hair, the clinical evaluation of male genital and female breast development is the standard method to monitor pubertal development, since it identifies the progression of secondary sexual characteristics (15).

The method proposed by Marshall and Tanner is the most commonly used for this purpose, describing the main changes in external sexual characteristics that occur during the period before (stage 1) and after puberty (stage 5) (16).

Furthermore, the onset of puberty is accompanied by an acceleration of linear growth and bone maturation. As a result, bone age will always be advanced compared to chronological age and statural age of the child, with premature closure of the epiphyseal cartilage of conjugation.

Laboratory tests

Timely diagnosis and careful clinical assessment remains pivotal to successful PP management. To demonstrate the early activation of HPG axis in children with pubertal development, the gold standard for laboratory confirmation of CPP is the maximal

Table I. *Etiological classification of precocious puberty.*

Gonadotropin dependent (Central PP)	
CNS Lesions • Hypothalamic hamartoma • Tumours: optic glioma, germ cell tumour, astrocytoma • Congenital malformations: arachnoid cyst, hydrocephalus, neural tube defect • Acquired: head trauma, cranial irradiation, infection, perinatal asphyxia	
Non-CNS Lesion • Idiopathic • Activating KISS1 gene and GPR54 • Endocrine disruptor exposure; excess endogenous steroids (e.g. CAH)	
Gonadotropin independent (Peripheral PP)	
Male	Female
Congenital	*Congenital*
Activating LH receptor mutation (testotoxicosis) Congenital Adrenal hyperplasia DAX1 gene mutation	GNAs gene activating somatic mutation (McCune–Albright syndrome)
Acquired	*Acquired*
Leydig cell tumour, granulosa cell tumour hCG secreting tumours Exogenous sex steroids	Ovarian Cyst / Tumor Surrenal Tumor Exogenous sex steroids
Long-standing, untreated primary hypothyroidism	

PP: precocious puberty; CNS: central nervous system; KISS1: Kisspeptin-1;GPR54: G protein-coupled receptor 54; CAH: Congenital Adrenal Hyperplasia; LH: luteinizing hormone; hCG: human chorionic gonadotropin

LH level after GnRH stimulation. However, this test is inconvenient for patients and labor-intensive for clinicians as well as being expensive to carry out. Hence, there has been an effort to find measures that can substitute or simplify this method. Even though the basal concentration of LH and the subcutaneous GnRH analogue stimulation test are suggested as alternatives, none of these are sufficient to substitute as a gold standard.

GnRH agonist stimulation test

The key endocrine investigation is to determine LH and FSH response to acute GnRH stimulation in order to distinguish between central and non-central (peripheral) forms of PP. For decades, GnRH testing has been the standard dynamic test to assess pubertal disorders in children. More recently, leuprolide acetate (LA) stimulation test and other GnRH agonists (GnRHa) have been employed. A potential advantage of GnRHa versus GnRH is that the former compounds elicit prolonged stimulation of gonadotropin secretion and these hormones, in turn, stimulate sex hormone secretion by the gonads. However, despite substantial evidence indicating that a single stimulated gonadotropin sample is informative, many centres continue to obtain multiple samples during LA stimulation test, leading to longer test duration, higher costs, and greater

inconvenience to patients (17).

Inhibin B levels

In the past decade, measurements of serum inhibin, produced by granulosa cells in small antral follicles under the influence of FSH, and anti-Mullerian hormone have provided useful tools for clinical investigation in gonadal disorders, including pubertal development diseases. It was revealed that, in girls with CPP, inhibin B levels were in accordance with the clinical stage of maturation, whereas in boys with delayed puberty. Furthermore, inhibin B levels were very low in congenital defects of the gonadotropin-releasing hormone-FSH-testis axis, but they were normal or intermediate in constitutional delayed puberty (18).

Determining inhibin B levels together with FSH levels is a considerable help for diagnosing disorders of pubertal development, but further studies are needed.

Kisspeptin levels

Kisspeptins act directly and indirectly on GnRH neurons to modulate GnRH secretion. Kisspeptin levels were significantly higher in girls with CPP than in pre-pubertal girls, and were positively correlated with FSH and LH peak levels after GnRH stimulation, demonstrating that it could serve as a marker for diagnosis and follow-up of CPP and representing a valuable parameter for monitoring treatment efficacy (19).

Metabolomic approach

A metabolomic approach was also assessed to identify metabolite urinary markers in PP subjects. Jia detected an altered urinary metabolic signature in PP girls, revealing several key metabolic systems involvement, such as up-regulated catecholamine and serotonin metabolic pathways (20). Moreover, Jang demonstrated that urine metabolomics provided several potential metabolic clues for PP mechanism, revealing abnormal metabolism of amino acid, especially aromatic amino acid, with a close correlation with CPP pathogenesis (21).

These urinary metabolite markers could

Table II. *Diagnostic tools to detect precocious puberty.*

	Precocious Puberty
Clinical history	• Family history (suggest a genetic condition) • Prior CNS insults (trauma, radiation, meningitis, tumors) • Psychological evaluation (disruptive behaviour, male aggression, emotionally labile, depression)
Clinical Assessment	• Features of puberty (present or not, duration, progression rate) • Height and weight • Secondary sex characteristics • Bone maturation • Café-au-lait spots, goiter, bone deformity
Laboratory tests	• LH and FSH levels • GnRH stimulation test • Hormonal evaluation (estradiol, prolactin, hCG, hCG/testosterone) • Inhibin and kisspeptin levels
Radiological exams	• X-ray (evaluating bone age) • Pelvic ultrasound for internal genitalia / ovaries • Ultrasound or CT adrenals • MRI/CT hypothalamus or pituitary glands

CNS: central nervous system; LH: Luteinizing Hormone; FSH: Follicle Stimulating Hormone; GnRH: gonadotropin-releasing hormone; hCG: human chorionic gonadotropin; CT: computed tomography; MRI: magnetic resonance imaging

Table III. *Management and outcomes of precocious puberty therapy.*

Indications to treat children with precocious puberty				
• Clear diagnostic criteria for precocious puberty • Pubertal LH level after GnRH stimulation and LH/FSH ratio after GnRH stimulation above diagnostic limit • Rapid pubertal development (progression from one pubertal stage to the next ina markedly shorter period of time than normal) • Abnormal height potential (final height prediction < 3rd centile or < target height range or height for bone age < -2 SD) • Loss of height potential during follow up (Δ bone age more than Δ statural age) • Psychological / behaviour reasons related to precocious development of secondary sex characteristics				
Outcomes of precocious puberty therapy				
• Prevention of psychological and social alterations • Regression of sexual characters • Block of sexual maturation • Slow bone maturation • Improvement of definitive stature • Prevention of early initiation of sexual life • Risk prevention of sexual abuse				
Choices available for the treatment of precocious puberty				
	Rapid Acting	Monthly Depot	3-mo Depot	12-mo Implant
Dosing	3-4 times daily or every day	Every 28 days	Every 90 days	Every year
Advantage	Quick on/off	Dosing and efficacy well studied	Fewer injections and fewer compliance concerns	No injections needed
Disadvantage	Multiple daily doses needed with poor compliance	Painful injections and suboptimal compliance	Painful injections	Surgical procedure for insertion and removal

GnRH: gonadotropin-releasing hormone; LH: luteinizing hormone; FSH: follicle-stimulating hormone

provide a potential alternative diagnostic and stratification approach for the clinical management of PP, but further studies are needed to confirm these preliminary data.

Instrumental methods

Different studies evaluated the role of pelvic sonography in the diagnosis of PP in girls, highlighting that an increase in uterine and ovarian measurements could represent an early and sensitive sign of PP (22) Thus, pelvic ultrasound, a non invasive, inexpensive and reliable tool, may give a complementary indication to the GnRH test for the distinction between isolated premature thelarche and early-stage PP.

Brain MRI is always indicated for boys with isolated CPP, to search for a lesion, but its usefulness for girls is debated. The age of children may represent a valid cut off, considering that girls with PP development of central origin before 8 years of age

should continue to be examined by a brain MRI. Also BMI, advanced bone age, LH and FSH peaks, have been proposed as factors which may identify girls at high risk of organic CPP (23). Table II summarizes clinical, laboratoristic and radiological tests required to obtain a correct diagnosis of CPP.

PRECOCIOUS PUBERTY TREATMENT

GnRHa therapy

GnRHa therapy is the only choice of treatment in patients with PP. The main aim of PP treatment is to minimise any loss of final adult height, prevent the progression of secondary sexual characteristics and promote psychological well-being. However, GnRHa therapy is not indicated for every patient with PP because there is not always evidence of pubertal responsiveness to GnRH or any apparent impairment of height potential or significantly advanced bone age (24). Several preparations of GnRHa are currently available, including leuprorelin, triptorelin and goserelin, which are available as monthly and three-monthly depot preparations.

Although GnRHa treatment has a proven track record in terms of efficacy and safety for the treatment of CPP, the requirement for intermittent injections is inherently unpopular in a pediatric population. Thus, the histrelin implant represents a potentially appealing and novel mode of delivery, resulting in a continuous diffusion (25). Table III synthesizes the available therapeutic choices to treat central precocious puberty.

Effects of GnRHa treatment

More than 20 years of experience with GnRHa treatment in CPP has provided important data on outcome regarding final height (FH), body mass index (BMI), bone mineral density (BMD) and reproduction.

Final height

Significant impairment of FH in untreated CPP has dominated the rationale for intervening with GnRHa treatment. The use of a long-acting GnRHa can initially induce gonadotropin secretion followed by pituitary desensitization and suppression of puberty. By this mechanism, GnRHa contributes to higher adult height (26). However, there are no systemic randomized controlled trials analysing the effects of long-acting GnRHa therapy on FH.

The FH increment, with respect to predicted height, can range from 3 to 10 cm, although realistically, a height gain of 4–6 cm is usual after at least 3–4 years of GnRHa treatment in girls with CPP. Arrigo et al. underlined that height gain from GnRHa therapy onset until FH attainment is generally rather limited (on average 2.9 cm) in girls with idiopathic CPP. FH is also significantly conditioned by both target height and treatment duration (27). Outcome data for FH are even less established for boys in whom the incidence of PP is lower than in girls. An analysis of FH from 11 studies showed a remarkably varied mean height gain of 1.8 to 15.0 cm (28)

Body mass index

Many of the past studies concerning the auxological effect of treatment with GnRHa in CPP have focused on final height outcomes, and less attention has been paid to the body weight changes.

Published data have demonstrated an increase in BMI during treatment with GnRHa, (29) whereas other reports suggested a reduction of BMI under gonadotropin-suppressive therapy or a weight excess not significantly related to GnRH agonist treatment (30).

Bone mineral density

The effect of GnRHa therapy for PP on BMD is unclear and data are controversial. Girls with PP have lower BMD for chronological age and increased bone reasorption markers, with an improvement observed during the first year of therapy with GnRHa (31) On the other hand, Hong et al. demonstrated that three-year treatment with GnRHa in CPP patients did not impair bone maturation (32).

Reproductive potential and ovulatory dysfunction

There are no adverse effects in the longer term to reproductive potential, with a reactivation of gonadal function after treatment cessation. Moreover, no increased risk of ovulatory dysfunction associated with hirsutism or polycystic ovary syndrome has been observed (24).

Side effects

GnRH agonists are generally well tolerated in

children and adolescents. In patients with a history of local reaction to GnRH, particularly those with a history of atopy, it may be appropriate to perform skin testing before proceeding with therapy. Systemic hypersensitivity reactions to GnRHa are a rare but important side effect of therapy. GnRHa are synthetic analogues of GnRH that inhibit FSH and LH hormone and have histamine- releasing activity. Local hypersensitivity to depot leuprolide injection, consisting of erythema and, less commonly, sterile abscess, occurs in up to 5% of children who receive this agent. Antibody formation against the GnRH agonist peptides has been a postulated cause for sterile abscess formation (33).

CONCLUSIONS

The key endocrine investigation is to determine the LH and FSH response to acute GnRH stimulation. Ultrasound examination could serve as a complementary tool and, consequently, for the early initiation of appropriate treatment. The treatment goals are prevention of early menarche and early sexual activity, the halting or regression of secondary sex characteristics, normalization of height velocity and deceleration of bone maturation.

Precocious puberty can be a troubling time for children and their parents, but fortunately there is medical treatment to stop further physical pubertal development, and there are several forms of support strategies available.

REFERENCES

1. Partsch JC, Heger S, Sippell WG. Management and outcome of central precocious puberty. Clinical Endocrinology 2002; 56:129-48.
2. Franceschi R, Gaudino R, Marcolongo A, Gallo MC, Rossi L, Antoniazzi F, Tatò L. Prevalence of polycystic ovary syndrome in young women who had idiopathic central precocious puberty. Fertil Steril 2010; 93:1185-91.
3. Sørensen K, Mouritsen A, Aksglaede L, Hagen CP, Mogensen SS, Juul A. Recent secular trends in pubertal timing: implications for evaluation and diagnosis of precocious puberty. Horm Res Paediatr 2012; 77:137-45.
4. Popa SM, Clifton DK, Steiner RA. The role of kisspeptins and GPR54 in the neuroendocrine regulation of reproduction. Annu Rev Physiol 2008; 70:213-38.
5. Biro FM, Greenspan LC, Galvez MP. Puberty in Girls of the 21st Century J Pediatr Adolesc Gynecol 2012; 25:289-94.
6. Chirico V, Cannavò S, Lacquaniti A, et al. Prolactin in obese children: a bridge between inflammation and metabolic-endocrine dysfunction. Clin Endocrinol (Oxf) 2013; 79:537-44.
7. Bogaert AF. Age at puberty and father absence in a national probability sample. J Adolesc 2005; 28:541-6.
8. Losa-Ward SM1, Todd KL, McCaffrey KA, Tsutsui K, Patisaul HB. Disrupted organization of RFamide pathways in the hypothalamus is associated with advanced puberty in female rats neonatally exposed to bisphenol A. Biol Reprod 2012; 87:28.
9. Silveira LG, Noel SD, Silveira-Neto AP, et al. Mutations of the KISS1 gene in disorders of puberty. J Clin Endocrinol Metab. 2010; 95:2276-80.
10. Abreu AP, Dauber A, Macedo DB, et al. Central precocious puberty caused by mutations in the imprinted gene MKRN3. N Engl J Med 2013; 368:2467-75.
11. Salpietro V, Mankad K, Kinali M, et al. Pediatric idiopathic intracranial hypertension and the underlying endocrine-metabolic dysfunction: a pilot study. J Pediatr Endocrinol Metab 2014; 27:107-15.
12. Salpietro V, Polizzi A, Bertè LF, et al. Idiopathic intracranial hypertension: a unifying neuroendocrine hypothesis through the adrenal-brain axis. Neuro Endocrinol Lett 2012; 33:569-73.
13. Trivin C, Couto-Silva AC, Sainte-Rose C, Chemaitilly W, Kalifa C, Doz F, Zerah M, Brauner R. Presentation and evolution of organic central precocious puberty according to the type of CNS lesion. Clin Endocrinol (Oxf) 2006; 65:239-45.
14. Carel JC, Eugster EA, Rogol A, et al. Consensus statement on the use of gonadotropin-releasing hormone analogs in children. Pediatrics 2009; 123:e752-62
15. Tinggaard J1, Mieritz MG, Sørensen K, Mouritsen A, Hagen CP, Aksglaede L, Wohlfahrt-Veje C, Juul A. The physiology and timing of male puberty. Curr Opin Endocrinol Diabetes Obes 2012; 19:197-203.

16. Marshall WA, Tanner JM. Variations in the pattern of pubertal changes in boys. Arch Dis Child 1970; 45:13-22.
17. Demirbilek H, Alikasifoglu A, Gonc E, Ozon A, Kandemir N. Assessment of gonadotropin suppression in girls treated with GnRH analogue for central precocious puberty: validity of single luteinizing hormone measurement after leuprolide acetate injection. Clin Endocrinol (Oxf) 2012; 76:126-30.
18. Crofton PM, Evans AE, Groome NP, Taylor MR, Holland CV, Kelnar CJ. Dimeric inhibins in girls from birth to adulthood: relationship with age, pubertal stage, FSH and oestradiol. Clin Endocrinol (Oxf) 2002; 56:223-30.
19. de Vries L, Shtaif B, Phillip M, Gat-Yablonski G. Kisspeptin serum levels in girls with central precocious puberty. Clin Endocrinol (Oxf) 2009; 71:524-8.
20. Qi Y, Li P, Zhang Y, et al. Urinary metabolita markers of precocious puberty. Mol Cell Proteomics 2012; 11:M111.
21. Yang L, Tang K, Qi Y, Ye H, Chen W, Zhang Y, Cao Z. Potential metabolic mechanism of girls' central precocious puberty: a network analysis on urine metabonomics data. BMC Syst Biol 2012; 6:S19.
22. Eksioglu AS, Yilmaz S, Cetinkaya S, Cinar G, Yildiz YT, Aycan Z. Value of pelvic sonography in the diagnosis of various forms of precocious puberty in girls. J Clin Ultrasound 2013; 41:84-93.
23. Chemaitilly W, Trivin C, Adan L, Gall V, Sainte-Rose C, Brauner R. Central precocious puberty: clinical and laboratory features. Clin Endocrinol (Oxf) 2001; 54:289-94.
24. Magiakou MA, Manousaki D, Papadaki M, et al. The efficacy and safety of gonadotropin-releasing hormone analog treatment in childhood and adolescence: a single center, long-term follow-up study. J Clin Endocrinol Metab 2010; 95:109-17.
25. Eugster EA, Clarke W, Kletter GB, et al. Efficacy and safety of histrelin subdermal implant in children with central precocious puberty: a multicenter trial. J Clin Endocrinol Metab 2007; 92:1697-704.
26. Antoniazzi F, Arrigo T, Cisternino M, et al. End results in central precocious puberty with GnRH analog treatment: the data of the Italian Study Group for Physiopathology of Puberty. J Pediatr Endocrinol Metabol 2000; 13:773-80.
27. Arrigo T, Cisternino M, Galluzzi F, et al. Analysis of the factors affecting auxological response to GnRH agonist treatment and final height outcome in girls with idiopathic central precocious puberty. Eur J Endocrinol1999; 141:140-44.
28. Bertelloni S, Mul D. Treatment of central precocious puberty by GnRH analogs: long-term outcome in men. Asian J Androl 2008; 10:525-34.
29. Lee SJ, Yang EM, Seo JY, Kim CJ. Effects of gonadotropin-releasing hormone agonist therapy on body mass index and height in girls with central precocious puberty. Chonnam Med J 2012; 48:27-31.
30. Arrigo T, De Luca F, Antoniazzi F, Galluzzi F, Segni M, Rosano M, Messina MF, Lombardo F. Reduction of baseline body mass index under gonadotropin-suppressive therapy in girls with idiopathic precocious puberty. Eur J Endocrinol 2004; 150:533-37.
31. Assa A, Weiss M, Aharoni D, Mor A, Rachmiel M, Bistritzer T. Evaluation of bone density in girls with precocious and early puberty during treatment with GnRH agonist. J Pediatr Endocrinol Metab 2011; 24:505-10.
32. Park HK, Lee HS, Ko JH, Hwang IT, Lim JS, Hwang JS. The effect of gonadotrophin-releasing hormone agonist treatment over 3 years on bone mineral density and body composition in girls with central precocious puberty. Clin Endocrinol 2012; 77:743-48.
33. Daskivich TJ, Oh WK. Failure of gonadotropin-releasing hormone agonists with and without sterile abscess formation at depot sites: Insight into mechanisms? Urology 2006; 67:e15-7.

JOURNAL OF BIOLOGICAL REGULATORS & HOMEOSTATIC AGENTS Vol. 28, no. 3, 377-380 (2014)

EDITORIAL

RELATIONSHIP BETWEEN SEROTONIN AND MAST CELLS: INHIBITORY EFFECT OF ANTI-SEROTONIN

S.K. KRITAS[1], A. SAGGINI[2], G. CERULLI[3], A. CARAFFA[4], P. ANTINOLFI[4], A. PANTALONE[5], M. ROSATI[6], M. TEI[3], A. SPEZIALI[3], R. SAGGINI[7] and P. CONTI[8]

[1]Department of Microbiology and Infectious Diseases, School of Veterinary Medicine, Aristotle University of Thessaloniki, Macedonia, Greece; [2]Department of Dermatology, University of Rome Tor Vergata, Rome, Italy; [3]Nicola's Foundation, Onlus, Arezzo, Italy; [4]Orthopedic Division, University of Perugia, Perugia, Italy; [5]Orthopedic Division, University of Chieti-Pescara, Chieti, Italy; [6]Gynecology Clinic, Pescara Hospital, Pescara, Italy; [7]Department of Neurosciences and Imaging, Faculty of Medicine and Surgery, G. d'Annunzio University Chieti-Pescara, Chieti, Italy; [8]Immunology Division, Medical School, University of Chieti-Pescara, Chieti, Italy

Received August 2, 2014 – Accepted September 26, 2014

Serotonin (5-HT) is an important neurotransmitter that acts in both central and peripheral nervous system, and has an impact on cell proliferation, migration and apoptosis. 5HT exerts its effects via several receptors. Treatment with anti-5-HT receptors diminish the severity of contact allergy in experimental animals, an effect mediated by mast cells; while an agonist reduces the stress level and relieves pruritus in patients with atopic dermatitis. Mast cells are important for both innate and adaptive immunity and they are activated by cross-linking of FcεRI molecules, which are involved in the binding of multivalent antigens to the attached IgE molecules, resulting in a variety of responses including the immediate release of potent inflammatory mediators. Serotonin is present in murine mucosal mast cells and some authors reported that human mast cells may also contain serotonin, especially in subjects with mastocytosis. Here we report the interrelationship between mast cells, serotonin and its receptor inhibitor.

It has been nearly 70 years since Rapport, Green and Page isolated and identified serotonin.

Serotonin. In 1952 Blaschko found that the natural substrate for tryptophane decarboxilase was 5-hydroxytryptophan, and the following year 5-hydroxytryptophan decarboxylase, the enzyme that generates serotonin, was isolated. For many years there has been much interest in the mechanisms of release of biogenic amines such as serotonin.

Serotonin 5-HT is first converted to 5-hydroxyindoleacetaldehyde and then to 5-hydroxyindoleacetic acid as a result of the action of an aldehyde dehydrogenase. Oxidative deamination by monoamine oxidase is the chief mechanism of serotonin degradation. Brain homogenates *in vitro* and brain *in vivo* are able to hydroxylate tryptophan and serotonin synthesis which can only be greatly reduced at the level of 5-hydroxylation of the amino acid, and its degradation can be slowed by amine oxidase inhibitors (1). 5-HT can be released from nerve cells by a Ca^{++}-mediated mechanism involving vesicles or by the reverse action of 5-HT transporter

Key words: serotonin, 5-HT, mast cells, inflammation, brain, immunity

Mailing address:
Spyridon K. Kritas, DVM, PhD, Dipl. ECPHM Associate Professor,
Department of Microbiology and Infectious Diseases,
School of Veterinary Medicine, Aristotle University of Thessaloniki,
54124 Thessaloniki, Macedonia, Greece
Tel./Fax: +30 2310 999940
e-mail: skritas@vet.auth.gr

0393-974X (2014)

(2).

Serotonin (5-HT) is one of the key neuro-transmitters that acts in both central and peripheral nervous system, has an impact on cell proliferation, migration and apoptosis and exerts its effects via several receptors (3). Seven families of 5-HT receptors have been identified to date in mammals, 5-HT_1 through 5-HT_7, each including distinct receptor subtypes (4). 5-HT_3 receptors are ligand-gated ion channels mediating fast depolarization. All the other 5-HT receptors are G protein-coupled receptors: 5-HT_1 and 5-HT_5 receptors inhibit adenylate cyclase, 5-HT_4, 5-HT_6 and 5-HT_7 receptors stimulate adenylate cyclase, whereas the 5-HT_2 receptor family is positively linked to phospholipase C (5). Intra-derma injection of serotonin provokes pruritus in human skin, an effect that can be relieved by an antagonist of 5-HT3R which is used in the treatment of pruritus associated with malignant disease (6). Histamine and 5-HT induce itch upon intradermal injection, however, serotonin is much weaker than histamine in provoking pruritus (7). Pruritus was selectively inhibited by the treatment with an H4R antagonist in a Th2 cell-mediated mouse skin inflammation model that mimics several features of atopic dermatitis (7).

Treatment with anti-5-HT1AR diminishes the severity of contact allergy in experimental animals, an effect mediated by mast cells; while an agonist of this same receptor reduces the stress level and relieves pruritus in patients with atopic dermatitis, a disease also mediated by mast cells (8). Agonists of 5-HT2AR reduce the severity of contact allergic reactions in experimental animal model; while anti-5-HT2R inhibits allergic contact dermatitis in humans. Receptor activation (5-HT1AR) in the brain reduces inflammation mediated by caspase-3 and therefore by IL-1 beta, an effect involving PLC, and dependent on ERK, MAPK and PKC. Serotonin has a role in inflammatory response and its receptors. 5-HT_{1A} receptor-positive mast cells, 5-HT_{2A} receptor and serotonin reuptake transporter-positive may be a target for inflammatory diseases mediated by 5-HT. T lymphocytes may be targets for therapy with serotonergic drugs in several diseases involving 5-HT (9).

5-HT_7 receptor mRNA is highly expressed in thalamus, hypothalamus, amygdala and hippocampus and can be detected in many CNS areas (10). Pharmacological blockade of 5-HT_7 receptors has antiepileptic and anxiolytic effects, while pharmacological activation of 5-HT_7 receptors reduce REM sleep and cause hypothermia. Systemic administration of 5-HT_7 receptor agonists affect circadian rhythms and body temperature (11)as well as improving learning.

Mast cells. Mast cells posses high-affinity IgE receptors (FcεRI) and are ubiquitous, predominantly localized in mucosal and connective tissues and distributed along blood vessels (12). Abundant evidence indicates that mast cells play a key role in inflammation, and their products modulate inflammatory mediator production (13). Mast cells can be activated by antigens, cytokines, growth factors, and hormones, leading to differential release of distinct mediators without degranulation (14). Serotonin is present in murine mucosal mast cells in the lamina propria and some authors reported that human mast cells may also contain serotonin, especially in subjects with mastocytosis (15). In connective tissue formation there is an accumulation of mast cells believed to produce important ground substance components including serotonin which mediates the connective tissue repair and regeneration. Mast cell degranulation and serotonin mediate local vascular injury with edema formation and inflammation. A variety of substances provokes release of serotonin from mast cells, among them 48/80, LPS, propamidine, toluidine blue, polymyxin B, morphine, egg white, etc.; while allicine, luteolin, ninhydrin, flavonoids and dinitrophenol inhibit serotonin release (16).

Many of the biological effects of mast cell activation are mediated by biogenic amines, such as serotonin, which are stored in and released from cytoplasmic granules. In human mast cells the only mediator of this class that is present in significant quantities is histamine, while in mouse and other rodents serotonin is very important, similarly to or more than histamine.

Neuronal growth factor, cytokines, and other compounds are capable of enhancing the synthesis of 5-HT from L-tryptophan. It is generally accepted that serotonin and its derivatives in the nervous system function quite differently from that in the rest of the body and that little of the somatic

serotonin penetrates the brain. 5-HT is synthesized by epidermal melanocytes, platelets, mast cells and other inflammatory cells. Serotonin is present in the gastrointestinal tract and platelets where it is involved in peristalsis, coagulation and regulation of the circulation (17). It has been reported that rodent mast cells produce 5-HT, but human mast cells have not yet been fully examined (17).

Therefore, serotonin mediates sleep–wakefulness cycles, mood, emotional and food behaviors, and thermoregulation, and in pathophysiological conditions may provoke secretomotor activity and initiate nausea, pain, inflammation and pruritus. It is also involved in atopic dermatitis, inflammation, chronic stress, psoriasis, eczema, allergy, migraine, nerve-gut dysfunction, hyperalgesia, urticaria, cancer and has a contracting effect on smooth muscle.

5-HTT is an anti-receptor which down-regulates 5-HT3R expression, and has been used in the treatment of some inflammatory and malignant skin diseases. The injection of 5-HT in experimental animal model enhances c-fos-like immunoreactivity which is present in rat brain and is involved in antidepressant-like action (18). 5-HT1AR agonists may activate NF-kB which is involved in the survival and proliferation of T and B cells.

The use of 5-HT receptor antagonists inhibit the agonist activity induced by some stimulators such as substance P, or neurotransmitters, in mast cells and may have an anti-inflammatory action.

It has been reported that some cannabimimetic fatty acid derivatives which are useful for the alleviation of asthma and are weak ligands either for CB1 or CB2 receptors, have anti-inflammatory activity (19).

Many clinical and experimental reports suggest the possibility that anti-inflammatory effects of selective serotonin reuptake inhibitors in atopic dermatitis patients might be at least partly due to their suppressive effect on T cells. In humans, serotonin receptors and serotonin transporter protein are expressed on several cells including mast cells, T cells, natural killer cells, Langerhans cells, and sensory nerve endings. It is still questionable whether serotonergic drugs exert the immunosuppressive effects via serotonin receptor or serotonin transporter. Bupropion, a selective serotonin re-uptake inhibitor antidepressant, with unique pharmacological profile, has also an anti-inflammatory effect (20).

Mast cells, melanocytes and platelets, by producing a variety of chemotactic factors, participate in the activation of immune cells and initiate delayed-type hypersensitivity (21). However, in the skin the major source of serotonin are platelets.

Pro-inflammatory cytokines/chemokines are known to alter the metabolism and release of 5-HT in the central nervous system by rapidly regulating neuronal 5-HTT activity via p38 MAPK-linked pathways (22). Chemokines have chemotactic properties on inflammatory cells and other cell types. RANTES, MCP-1 and belong to the C-C class of chemokine supergene family and play a role in regulating Th-cell cytokine production and leukocyte trafficking. RANTES and MCP-1 are mediators of acute inflammatory responses and play a fundamental role in histamine and serotonin generation and cell function in mast cells (23). Since MCP-1 and Rantes are chemoattractant for mast cells and play a role in their degranulation it is likely that these chemokines are involved in the generation and release of serotonin *in vitro* and in clinical trials.

Nerve growth factor (NGF), which is a diffusible protein playing a crucial role in several organ functions and is a target-derived pro-survival factor for sensory and sympathetic neurons derived from ganglia, stimulates release of 5-HT by mast cells in the rat peritoneum and is widely recognized as an important factor responsible for the survival and maintenance of the phenotype of specific subsets of peripheral neurons and basal forebrain cholinergic nuclei during development and maturation.

Further studies in this area should be conducted to confirm the findings described in this article and elucidate the precise mechanism of

Table I. *The pathway for the synthesis of serotonin from tryptophan.*

L-Tryptophan→L-triptophan-5-monooxygenase (Tryptophanhydroxylase)→5-Hydroxy-L-Tryptophan→5-Hydroxytryptophan decarboxylase (Aromatic L-amino acid decarboxylase)→SEROTONIN (5-HT).

neuroimmunological interaction between mast cells and serotonin generation and release.

REFERENCES

1. Neckameyer WS, Coleman CM, Eadie S, Goodwin SF. Compartmentalization of neuronal and peripheral serotonin synthesis in Drosophila melanogaster. Genes Brain Behav 2007; 6(8):756-69.
2. Yao Y, Bergold PJ, Penington NJ. Acute Ca(2+)-dependent desensitization of 5-HT(1A) receptors is mediated by activation of protein kinase A (PKA) in rat serotonergic neurons. Neuroscience 2010; 169(1):87-97.
3. Sommer C. Is serotonin hyperalgesic or analgesic? Curr Pain Headache Rep 2006; 10(2):101-6.
4. Lanfumey L, Hamon M. 5-HT1 receptors. Curr Drug Targets CNS Neurol Disord 2004; 3(1):1-10.
5. Rodríguez D, Brea J, Loza MI, Carlsson J. Structure-based discovery of selective serotonin 5-HT(1B) receptor ligands. Structure 2014; 22(8):1140-51.
6. Nishida K, Takechi K, Akiyama T, Carstens MI, Carstens E. Scratching inhibits serotonin-evoked responses of rat dorsal horn neurons in a site- and state-dependent manner. Neuroscience 2013; 250:275-81.
7. Hägermark O. Peripheral and central mediators of itch. Skin Pharmacol 1992; 5(1):1-8.
8. Walford HH, Zuraw BL. Current update on cellular and molecular mechanisms of hereditary angioedema. Ann Allergy Asthma Immunol 2014; 112(5):413-8.
9. Thorslund K, Nordlind K. Serotonergic drugs--a possible role in the treatment of psoriasis? Drug News Perspect 2007; 20(8):521-5.
10. Ballaz SJ, Akil H, Watson SJ. Analysis of 5-HT6 and 5-HT7 receptor gene expression in rats showing differences in novelty-seeking behavior. Neuroscience 2007; 147(2):428-38.
11. Adriani W, Travaglini D, Lacivita E, Saso L, Leopoldo M, Laviola G. Modulatory effects of two novel agonists for serotonin receptor 7 on emotion, motivation and circadian rhythm profiles in mice. Neuropharmacology 2012; 62(2):833-42.
12. Kritas SK, Saggini A, Varvara G, et al. Impact of mast cells on the skin. Int J Immunopathol Pharmacol 2013; 26(4):855-9.
13. Kritas SK, Saggini A, Varvara G, et al. Mast cell involvement in rheumatoid arthritis. J Biol Regul Homeost Agents 2013; 27(3):655-60.
14. Kritas SK, Saggini A, Varvara G, et al. impact of mast cells in rejection of allografts. Eur J Inflamm. Vol. 11, no. 3, 609-614 (2013).
15. Metcalfe DD. Mast cell mediators with emphasis on intestinal mast cells. Ann Allergy 1984; 53(6 Pt 2):563-75.
16. Shaik-Dasthagirisaheb YB, Varvara G, Murmura G, et al. Inhibitor effect of antioxidant flavonoids quercitin, and capsaicin in mast cell inflammation. Eur J Inflamm 2013; 11:353-57.
17. Foley S, Garsed K, Singh G, et al. Impaired uptake of serotonin by platelets from patients with irritable bowel syndrome correlates with duodenal immune activation. Gastroenterology 2011; 140(5):1434-43.
18. Kawahara R, Soeda F, Kawaura K, Honda S, Miki R, Noguchi T, Shirasaki T, Takahama K. Effect of tipepidine with novel antidepressant-like action on c-fos-like protein expression in rat brain. Brain Res 2013; 1513:135-42.
19. Di Marzo V, Melck D, De Petrocellis L, Bisogno T. Cannabimimetic fatty acid derivatives in cancer and inflammation. Prostaglandins Other Lipid Mediat 2000; 61(1-2):43-61.
20. Tan EK, Grattan CE. Drug-induced urticaria. Expert Opin Drug Saf 2004; 3(5):471-84.
21. Kritas SK, Saggini A, Cerulli G, et al. Corticotropin-releasing hormone, microglia and mental disorders. Int J Immunopathol Pharmacol 2014; 27(2):163-7.
22. Katafuchi T, Kondo T, Take S, Yoshimura M. Enhanced expression of brain interferon-alpha and serotonin transporter in immunologically induced fatigue in rats. Eur J Neurosci 2005; 22(11):2817-26.
23. Kritas SK, Saggini A, Cerulli G, et al. Asthma and mast cell biology. Eur J Inflamm 2014; 12:261-265.

COLLAGEN IMPLANTS IN EXPERIMENTAL TENDON INJURY IN RABBITS: A CLINICAL, ULTRA-STRUCTURAL AND BIOMECHANICAL INVESTIGATION

A. MOSHIRI[1], A. ORYAN[2], A. MEIMANDIPARIZI[1] and N. MAFFULLI[3,4]

[1]Division of Surgery and Radiology, Department of Clinical Sciences, School of Veterinary Medicine, Shiraz University, Shiraz, Iran; [2]Department of Pathology, School of Veterinary Medicine, Shiraz University, Shiraz, Iran; [3]Centre for Sport and Exercise Medicine, Barts and the London School of Medicine and Dentistry, University of London, Queen Mary, United Kingdom; [4]Department of Musculoskeletal Medicine and Surgery, University of Salerno School of Medicine and Surgery, Salerno, Italy

Received November 12, 2012 – Accepted May 14, 2014

This study investigated the effects of hybridized micro and nano structured collagen implants on tendon healing in an experimental tendon injury in rabbits. Fifty mature male New Zealand white rabbits were randomly divided into two groups of treated and control. Two cm of the left Achilles tendon were discarded. In the treated group, a 3-dimensional (3D) collagen implant was engineered and implanted in the defect area. No implant was used in the control group. At day 120 after injury, the Achilles tendon of the animals were ultrasonographically (days 0-120 after injury) and radiographically (day 120 after injury) examined, and the animals were euthanized. The tendons were dissected and used for gross pathological, histopathological, ultra-structural and biomechanical investigations. Application of the collagen implant significantly increased the diameter of the newly regenerated tissue in the defect area compared to the control tendons. Treatment also significantly increased the echogenicity and homogeneity of the injured area, the diameter of the collagen fibrils and fibers, maturity of the tenoblasts, number of tenocytes, collagen density, alignment, ultimate and yield load, stiffness, stress and modulus of elasticity. The collagen implants were almost totally absorbed 120 days after surgery. No inflammatory reaction or tissue degeneration or necrosis was evident in the treated tendons compared to the control ones. 3D collagen implants produced a newly regenerated tendinous tissue at the defect area that was morphologically and biomechanically superior to the control group. This collagen implant was biocompatible and biodegradable with high bio-safety in rabbits.

Surgical reconstruction of large Achilles tendon defects is technically demanding, and may fail to improve the function of the injured limb (1-3). Tendon grafts are an option, but autografts may produce donor site morbidity, and allo- and xenografts have serious limitations including availability, disease transmission and rejection (3, 4). Tissue engineering is an option (5, 6). Different scaffolds are used to reconstruct such defects (1, 7, 8). An ideal scaffold for tendon healing should be biodegradable, biocompatible; it should promote tenoconduction, tenoinduction, tenogenesis and should have tenoincorporative properties with

Keywords: tendon, healing, implant, collagen, biomechanic, scanning electron microscopy

Mailing address:
Prof. Nicola Maffulli MD, MS, PhD, FRCP, FRCS(Orth), FFSEM;
Centre for Sports and Exercise Medicine,
Mile End Hospital, 275 Bancroft Road,
London E1 4DG, England
Tel.: +44 20 8223 8839 Fax: +44 20 8223 8930
e-mail: n.maffulli@qmul.ac.uk

0393-974X (2014)

the neotenon (3, 5). To date, none of the available scaffolds have all these characteristics (5). The choice of biomaterial and the structure of the construct are two key steps for designing a proper tissue engineered scaffold for tendon regeneration and repair (3, 5). To produce a suitable scaffold aiming to mimic the native tendon, collagen could be a suitable biomaterial (5, 8). Collagen has optimum biocompatibility, biodegradability and bioactivity (7, 8). In addition, most of the tendon is composed of collagen type I which is polymerized as fibrils, fibers, fiber bundles and fascicles (9, 10). Therefore, a suitable tissue engineered based scaffold should mimic the structure of the native tendon so that it should be composed of aligned fibrils and fibers (3). Two techniques are used to produce fibrillar scaffolds, namely gelation and electrospinning (11, 12). Gelation, a traditional method, produces large fibers; by electrospinning, it is possible to produce nano-sized collagen fibrils (11, 12). Gel system is a cost effective way to produce tissue engineered scaffolds (3). However, in the gel system, controlling the alignment and size of the fibers during polymerization is difficult (12). Moreover, such constructs have low biomechanical properties, which makes them not useful for tendon tissue engineering purposes (5). In electrospinning of different biomaterials, the degree of fiber alignment and size is easily controllable (11, 12). However, electrospinning is an expensive technology which reduces its application (12). Combining gelation and electrospinning of collagen type I molecules, a novel three-dimensional scaffold could be produced consisting of both aligned collagen fibrils and fibers.

We produced a tissue engineered based three-dimensional collagen scaffold by a combination of gel system and electrospinning technologies to closely mimic the native tendon environment for tissue ingrowth. The effectiveness of such construct in a large tendon defect model was tested on rabbits. We hypothesized that collagen scaffold may have beneficial roles in cellular migration, proliferation, alignment and matrix production. This may improve the morphology and function of injured tendons.

MATERIALS AND METHODS

Study design

Fifty skeletally-mature male White New Zealand rabbits 12 to 14 months old and 3.15±0.15 kg body mass were randomly assigned to treated (n=25) and control (n=25) groups. The left Achilles tendon of each animal in both groups was designated as the injured tendon (n=25 tendons in each group), and the right normal contra-lateral tendon (NCT) was left intact (n=25 tendons in each group). The rabbits were housed in individual standard rabbit cages and maintained on standard rabbit diet (pellet) with no limitation of access to food or water. The left Achilles tendons of the treated group [injured treated tendons (ITTs)] were compared with the right NCTs and with the injured control tendons (ICTs), 120 days after injury.

Preparation of collagens implants

Collagen type I was extracted from bovine tendons, and its purity confirmed by SDS/PAGE (11). The acid solubilized collagen molecules were electrospun on a dual plate device to produce large and aligned electrospun collagen fibers (12). After electrospinning, the acid-solubilized bovine tendon type I collagen molecules were mixed with electrospun collagen fibers and polymerized in an incubator at 4°C for 48 h to produce a three-dimensional collagen gel. The collagens were aligned under 12 Tesla magnetic fields (CRETA, Grenoble) during polymerization (13). The collagen composite was cut into several pieces of the same size and shape as the rabbit's Achilles apparatus. The collagen composites were cross-linked after suspension in iso-osmolar 0.1% riboflavin solution, using UV (wavelength of 365 nm) irradiation (14). The final product was repeatedly washed with distilled water, and received 100 Gray g-radiation and was suspended in ethanol 96% to produce and maintain its sterility until surgery (Fig. 1A). The morphology of the scaffolds were studied by scanning electron microscopy and the presence of highly aligned collagen fibers was confirmed in the scaffold (Fig. 1 B-D). Sterility and low endotoxin content of the scaffold was confirmed by microbiological and Limulus amebocyte lysate tests, respectively (15).

Premedication and anesthesia

The animals were premedicated and anesthetized by intramuscular administration of 1 mg/kg Acepromazine maleate and a combination of 15 mg/kg Ketamine and 0.05 mg/kg Xylazin hydrochloride, respectively (All from, Alfasan Co. Woerden, Netherlands) (16-18).

Injury induction and surgical reconstruction

Under aseptic conditions, a longitudinal skin incision was made over the Achilles tendon complex. Then, 2 cm of the Achilles tendon with the covering paratenon were completely excised by transverse incisions. The defect was reconstructed using double strand modified Kessler core

pattern (PDS 0-4, Ethicon, INC.1997, J&J, USA). This aligned the tendon extremities, and produced a 2 cm gap between the tendon ends. For insertion of the implants in the tendon gap, a double strand suture was passed through the longitudinal axis of the implants. The subcutaneous tissue and skin over the lesion were closed routinely (Fig. 1 E-G). Postoperative analgesia with fentanyl (Matrifen, Roskilde, DK) patch was provided for 3 days.

Contrast radiography

Non-ionized iodinated contrast medium (0.5 mL) was injected subcutaneously over the lesion under ultrasonography guidance. The animals were left alone after injection for 10 minutes to relax, and allow for the iodinated contrast medium to distribute subcutaneously over the tendon. Lateral radiographs from both legs of each rabbit were taken.

Ultrasonography

At weekly intervals, transverse and longitudinal ultrasonographic images from the injured and normal tendons were provided via a 12 MHz linear probe (Siemens SLR-400, Berlin, Germany; Echowave 3.23 software) (19). Echogenicity, homogeneity and peritendinous adhesions were scored (Table I).

Ethics and euthanasia

The animals were euthanised 120 days after tendon injury. The animals were anesthetized by IM injection of 15 mg/kg Ketamine, 2 mg/kg Xylazine, and 1 mg/kg Acepromazine (Alfasan Co, Woerden, Netherlands). Euthanasia was provided by intra-cardiac injection of 1 mg/kg Gallamine triethiodide (Specia Co., Paris, France) (20). The study was approved by the local Ethics Committee of our faculty.

Sample collection

Five animals of each group were used for contrast radiography. For ultrasonography, the left and right Achilles tendons of the animals were studied (n=20 left and n=20 right in each group). After euthanasia, the injured and the contralateral tendons were dissected and assessed for gross pathology (n=20 left and n=20 right for each group). In each group, the samples were randomly divided into two equal subgroups. Subgroup 1 was used for biomechanical testing, and subgroup 2 was used for histopathology and scanning electron microscopy (SEM). The tendons in subgroup 2 were divided longitudinally into two parts. Part A was used for histopathology, and part B for SEM.

Gross pathology

Each injured tendon (n=20 for each group) and NCT (n=20 for each group) was carefully evaluated for color changes, adhesion to the surrounding tissues, and any other abnormalities (21). Hyperemia and peritendinous adhesions were scored (Table I). The transverse diameter of the injured area was measured using a digital caliper.

Histopathological and histomorphometric analyses

In each group, a longitudinal tendon sample from the injured area (n=10) and normal contralateral tendons (n=10) were used for histopathological and histomorphometric analyses. After fixation in 10% neutral buffered formalin, the samples were washed, dehydrated, cleared, embedded in paraffin wax, longitudinally sectioned at 4–5 μm in thickness, stained with hematoxylin and eosin, and examined by light microscopy (Olympus, Tokyo, Japan). The pictures were then recorded by a digital camera (Sony T-700, Tokyo, Japan) and transferred to a software (Adobe Photoshop CS-5, Ca, USA) for digital analysis. Five photomicrographs obtained from each tissue section (n=5) of each tendon sample (n=10 in each group) were used for histopathological analysis (a total of 250 histopathologic fields). Total cellularity, immature tenoblasts, mature tenoblasts, tenocytes, neutrophils, lymphocytes, macrophages, plasma cells and blood vessels of the tendon proper were counted (magnification ×200) (22). Collagen mass density was analyzed by computer software (Image J, NIH, Ca, USA), and reported as percentage (19). The colors of the photomicrographs were converted into individual diagrams based on their color type, and the area of the diagrams was measured to determine collagen density (19). Alignment, tissue maturity and perivascular edema were scored (Table I).

Scanning electron microscopy

In each group, the tendon samples (n=10 L; n=10 R) were fixed in 2.5% cold glutaraldehyde in a 0.1M cacodylate buffer, pH 7.2. The samples were dehydrated in graded ethanol, dried by Hexa-methyl-disalysin (TAAB Co., London, UK), and then gold coated on Cupper mount. Different magnifications of ×50 to ×30,000 were used to analyze the SEM characteristics of the implants and tendon samples. The tendon surface and also the orientation, diameter and differentiation of the collagen fibrils and fibers together with their density were then analyzed.

Biomechanical testing

The tendons were mounted between the two cryoclamps. The biomechanical tests were performed using a tensile testing machine (Instron® Tensile Testing Machine, London, UK). Each tendon was loaded by elongating it at a displacement rate of 10 $mm \cdot s^{-1}$ until a 50% decrease in load was detected. Load and crosshead

displacement data were recorded at 1500 Hz, and load-deformation and stress-strain curves were generated for each specimen using TestWorks 4 software (SUME Systems Corporation). The ultimate load, yield load, stiffness, ultimate strain, maximum stress and modulus of elasticity of the samples were determined (18, 22).

Statistical analysis

The measured values of the injured tendons of each group (left leg) were compared with the measured values of their normal contra-lateral tendons (right legs) of the same group using paired sample *t*-test. The measured values of the right and left tendons of the treated animals were compared with those of the right and left tendons of the control animals using the independent sample *t*-test. The results were expressed as mean ± standard deviation. The Mann-Whitney U test was used to analyze the scored values and the results were reported as mean (min-max). Statistics were performed using the computer software SPSS version 19 (SPSS Inc. Chicago, IL, USA). Differences of $p<0.05$ were considered significant.

Inter tester and intra tester reliability

The investigators who undertook the measurements and analyses of the results were unaware of the experimental design and grouping details. Each evaluation and measurement was performed in triplicate and the mean of the measured values were reported. For ultrasonographic and radiographic evaluations, three veterinary radiologists evaluated the tendons and reported their results. For gross pathologic, histopathologic and SEM evaluations, three expert healing pathologists evaluated samples and reported their results. No significant differences were seen between the results of the individuals ($P>0.05$).

RESULTS

Contrast radiography

The contrast medium (CM) completely covered the injured treated tendons (ITTs), and at 120 days post injury (DPI) no sign of gap formation was evident in the injured area. The CM covered the proximal and distal parts of the injured control tendons (ICTs), but the gap was not covered with the CM, and a radiolucent space was seen instead of the radio-opaque area in these tendons. The CM partially filled the gap in the ICTs, and showed the shape of the tendon in both proximal and distal parts of the defect. The diameter of the lesions in the ITTs was similar to normal tendon, but the diameter of the ICTs was significantly lower than both the ITTs and normal tendons (Fig. 2).

Ultrasonography

The diameter of the ITTs was significantly higher than the ICTs (2.95±0.24 *vs* 1.96±0.16, $P=0.001$). The ITT scores were significantly greater for echogenicity [2(1-2) *vs* 2(2-3), $P=0.048$], homogeneity [1.5(1-2) *vs* 3(2-3), $P=0.021$], and peritendinous adhesion [2(1-3) *vs* (3(2-3), $P=0.039$] compared to the ICTs at 120 DPI.

A different pattern of echogenicity through the length of the ICTs was seen at ultrasonography: hyper-echogenicity, hypo-echogenicity and dyshomogeneity were seen. The hyper-echogenic areas corresponded to the intact portion of the tendons, and the hypo-echogenic area corresponded to the injured part of the control tendons. This pattern was not evident in the ITTs. In general, the appearance of the ITTs was superior to that of the ICTs, but the ITTs still showed hypo-echogenicity compared to the normal contralateral tendons (NCTs). Compared to the ICTs, the ITTs showed no echogenicity around the tendon, suggesting lower peritendinous adhesion formation around the tendon (Fig. 3).

Gross pathology

The ITT scores were significantly greater for peritendinous adhesion [2(1-3) *vs* 3(2-3), $P=0.048$] and hyperemia [2(1-2) *vs* 2.5(2-3), $P=0.046$] compared to the ICTs. The diameter of the ITTs was significantly greater than the ICTs (2.86±0.33mm *vs* 1.75±0.23mm, $P=0.001$). Generally, the ICTs showed adhesion to the surrounding structures, and it was hard to distinguish between the regenerated part of the tendon and the peritendinous adhesions. The regenerated tissue in the injured area was a transparent loose areolar connective tissue. Unlike the ICTs, the ITTs showed a dense and organized structure almost indistinguishable from their normal contralateral tendons, and were easily dissected and removed from the surrounding fascia. In the ICTs, the tendon edges were not covered or filled with the newly regenerated connective tissue. In the ITTs, the tendon edges were completely replaced with a new tendinous structure, and the continuity between the edges was diagnostic. No remnant of the suture material was seen in either group, but in most

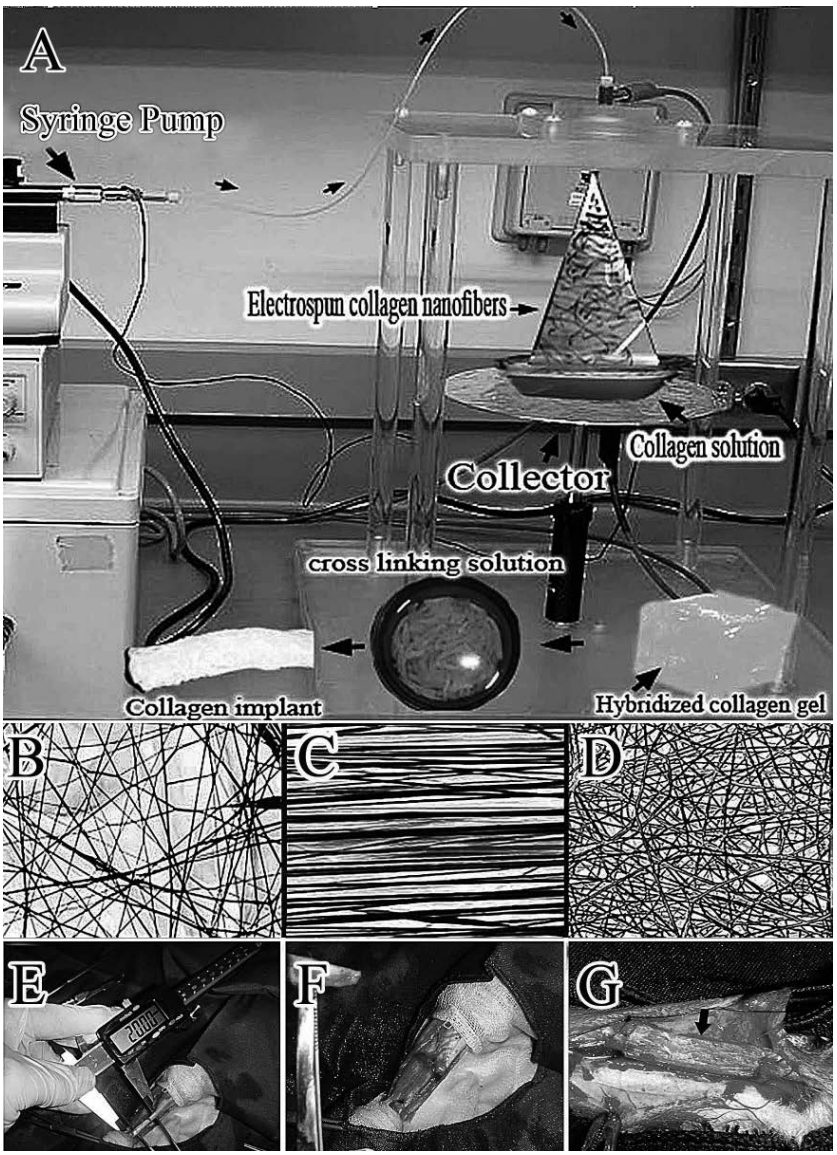

Fig. 1. ***A)*** *A syringe pump was filled with type I collagen solution, obtained from bovine Achilles tendon. The collagen molecules were pumped into the electrically charged needle of the electro-spinning device and aligned along the direction of the – (negative) and + (positive) poles of the high voltage transformator on the collector. After electrospinning, the acid-solubilized bovine tendon type I collagen molecules were mixed with the electrospun collagen fibers and polymerized at 4°C for 48 h to produce a tridimensional collagen gel. The collagens were aligned under 12 Tesla magnetic fields during polymerization. The collagen implants were cut into several pieces of the same size and shape as the rabbit's Achilles tendon apparatus. The collagen composites were cross-linked after suspension in iso-osmolar 0.1% riboflavin solution, using UV irradiation. The collagen implant was left to dry at room temperature to remove the chemical solvents. Then, it was repeatedly washed with distilled water, received 100 Gray g-radiation and suspended in ethanol 96% to produce and maintain its sterility until surgery.* ***B)*** *SEM, Randomized collagen microfibers formed in a regular collagen solution.* ***C)*** *SEM, Electrospun collagen nanofibers aligned through the direction of the – and + poles of the high voltage supplier.* ***D)*** *SEM, the final structure of the hybridized bioimplant after combining the randomized jelly structure with electrospun collagen nanofibers.* ***E*** *and* ***F)*** *Two cm of the left Achilles tendon of the rabbits were cut and discarded, and a 2 cm tendon gap was produced, and then maintained by a modified Kessler suture.* ***G)*** *The collagen implant was implanted in the defect area in the treated group. No prosthesis was used in the control group. A 2-cm gap was produced in the tendon, and left alone.*

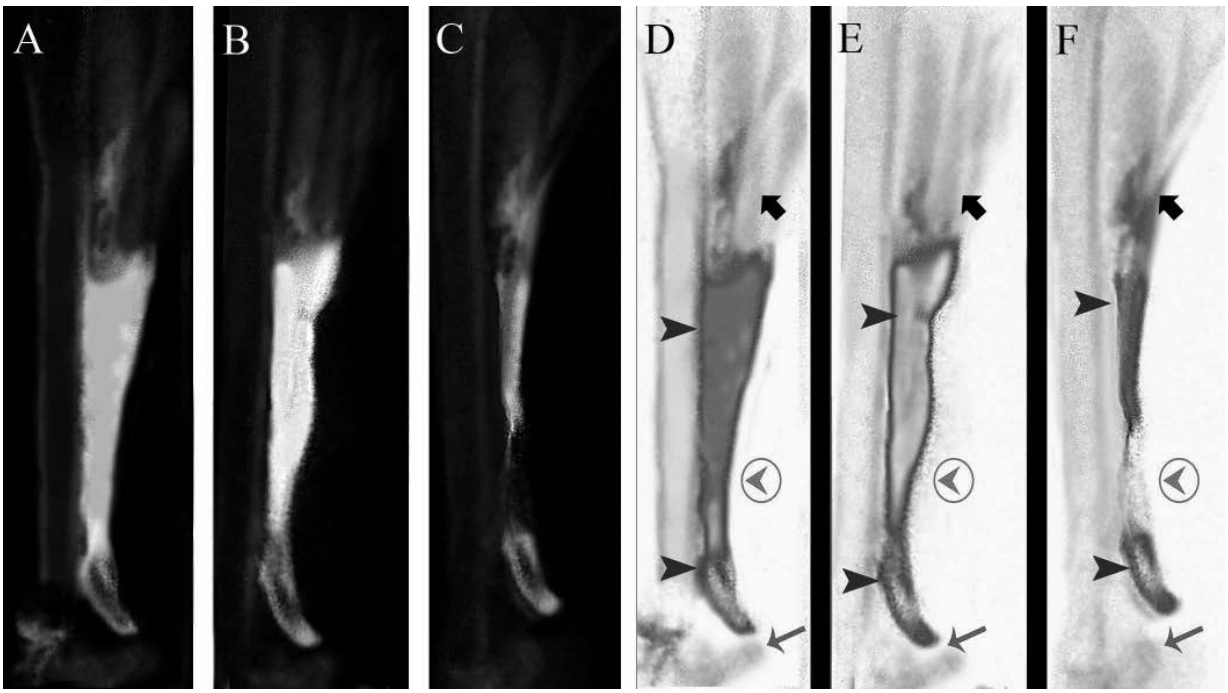

Fig. 2. *Positive contrast radiography of the injured treated (**A**), intact (**B**) and injured control legs (**C**) of the animals, 120 days after injury. **D, E, F**) Inverted pictures of the positive contrast radiographs (A, B, C). Based on the radiographical reports, the collagen implant was absorbed and substituted with a newly regenerated fibrous connective tissue with similar opacity of the normal tendon after 120 days of tendon injury [(A and D (treated) vs B and E (normal tendon)]. The gap was fully filled with this newly regenerated fibrous connective tissue. In the control tendons (C and F), the gap was not fully filled with the newly regenerated soft tissue and the contrast material was not able to cover the gap area. The gap was present even after 120 days of tendon injury. The arrow heads show upper and lower limits of the Achilles tendons. The circular arrow head show the injured area. The thick arrows show the Gastrocnemius Soleus muscle at the upper end of the rabbits Achilles tendon, and the thin arrows show the calcaneal tuberosity at the lower end of the rabbits Achilles tendon.*

instances the surface of the ICTs, unlike the ITTs, was hyperemic (Fig. 4).

Histopathological findings

Compared to the ICTs, inflammation in the ITTs was lower, and the mesenchymal cells were more mature. No tissue reaction was seen in the ITTs at 120 DPI, and most of the collagen prosthesis was absorbed and substituted with newly regenerated tendinous tissue. The remnant of the collagen implant was present as islands of collagens in the center of the tendon proper, and acted as a micro-scaffold to align the newly regenerated collagen fibers. The crimp pattern was restored, and there were few peritendinous adhesions. Neither necrosis nor degeneration were seen at histopathology, and the remnant of the suture material was seen at the proximal and distal parts of the injured area.

The vascular distribution was improved and the immature vessels were degenerated, but the large vessels were well organized at the periphery of the tendon proper. The tenoblasts and tenocytes were aligned parallel with the collagen fibers in a longitudinal direction.

On the other hand, areas of degeneration and necrosis were seen in the ICTs, and numerous immature blood vessels, surrounded by perivascular edema, were present in these lesions. Many mononuclear inflammatory cells were still present in the lesions, and the mesenchymal cells were immature. The collagen fibers showed a low density, were disorganized, and most of the lesions were

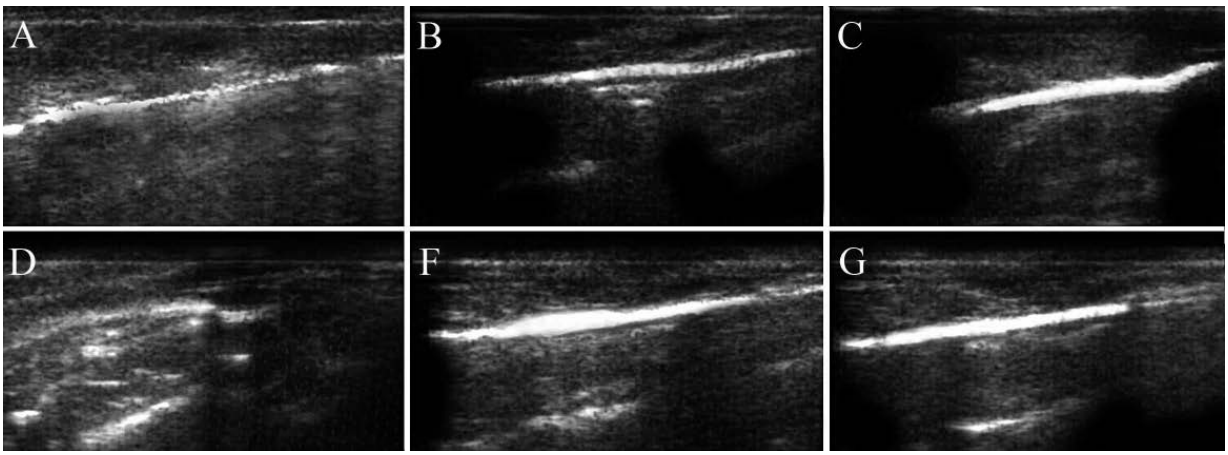

Fig. 3. *Plain ultrasonography of the rabbits Achilles tendon, 120 days after injury. The echogenicity of the injured area of the injured control tendon (**A** and **D**) is low, and the injured area shows an amputated view. The tendinous structure in the defect area is not organized in this group (D). Peritendinous adhesions are also seen in the periphery of the injured area with lower echogenicity than the tendinous structure (A). The echogenicity of the injured area is not homogenous (A and D). In the injured tendons treated with collagen implant (**B** and **F**), no amputated view is seen in the injured area and the defect is filled with the newly regenerated fibrous connective tissue in a similar patterns to normal tendon (**C** and **G**). But the echogenicity of the injured treated tendons is still slightly lower than the normal tissue. The peritendinous adhesions are not diagnostic in these tendons, and the diameter of the newly regenerated tissue is larger than the injured area of the control tendon.*

filled with edema, lipid vacuoles and small blood vessels. The characteristic nature of the regenerated tissue was similar to the surrounding fascia, and did not appear as a tendon proper (Fig. 5).

Total cellularity, total tenoblasts and immature tenoblasts in the ITTs significantly decreased compared to the ICTs, at 120 DPI (P=0.001 for all) (Table II). There were no significant differences in the number of mature tenoblasts between the injured areas of either group at this stage (P=0.972). However, the ITTs showed a significantly higher number of tenocytes compared to the ICTs (P=0.001). No significant differences were seen in the number of neutrophils and plasma cells in the lesions of either group (P=0.789, P=0.428, respectively). Lymphocyte and macrophage infiltration were significantly lower in the ITTs compared to the ICTs (P=0.001). The ITTs showed significantly lower total vascularity compared to the ICTs (P=0.001). They also showed significantly lower number of small- and medium-sized blood vessels compared to the ICTs (P=0.001, P=0.006, respectively), but there were no significant differences in the number of the large vessels between the two groups (P=0.622).

The diameter of the mature tenoblasts showed no significant differences between the lesions of either group (P=0.089). However, the transverse diameter of the immature tenoblasts and tenocytes were significantly lower in the ITTs compared to the ICTs (P=0.001 for both). The diameter of the small-, medium- and large-sized blood vessels were significantly higher in the ITTs compared to the ICTs (P=0.001 for all). Cell density and background density (the density of non-collagenic and non-cellular parts of the tendon) of the ITTs were significantly lower than the ICTs (P=0.001 for both), but the collagen density was significantly higher in the ITTs compared to the ICTs (P=0.001).

Compared to the ICTs, the crimp pattern of the ITTs was improved, but the differences were not statistically significant (P=0.121). The ITT scores were significantly greater for tissue alignment, perivascular edema and peritendinous adhesions compared to the ICTs (P=0.049, P=0.001, P=0.001, respectively).

Scanning electron microscopy

The diameter of the collagen fibrils of the ITTs

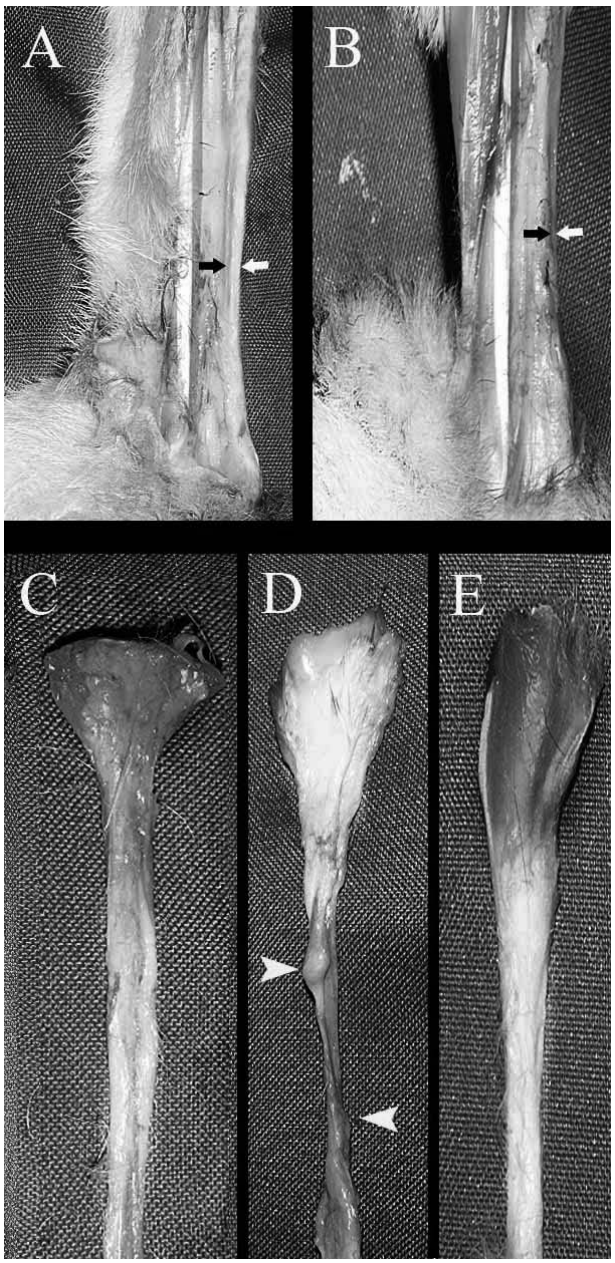

Fig. 4. *Gross pathology of the injured tendons, 120 days after injury.* ***A*** *(treated) and* ***B*** *(control) show the left leg of the rabbits. The arrows show the superficial and deep limit surface of the Achilles tendon of rabbits.* ***C*** *(treated)* ***D*** *(control) and* ***E*** *(normal) show dissected Achilles tendons of the rabbits. The distance between the cutting edges of a control tendon is indicated by arrow heads. The newly regenerated soft fibrous connective tissue filled the gap area of the treated group. This dense fibrous connective tissue is organized and connected the cut edges of the injured tendons after 120 days of tendon injury in the treated group. No remnant of the collagen implant is seen grossly at the injured area, and the degree of peritendinous adhesions is low in these tendons (A, C). The diameter of the injured area of the control group is lower than the treated tendons. The cut edges of the injured control tendons are still present (See arrow heads,* ***D****) in the injured area and a loose areolar connective tissue with a characteristic hyperemia is present in the gap area. This newly regenerated soft tissue is far behind the normal tendinous tissue and has characteristics similar to subcutaneous fascia (B and D). Muscular fibrosis and atrophy is seen in the gastrocnemius muscle of the injured control legs (D). These fibrotic changes are not seen in the treated and normal legs (C and E).*

was significantly greater than the ICTs (P=0.001), but the diameter of the collagen fibers between the two groups was not significantly different (P=0.089) (Table III). The ITTs showed a well-organized collagen structure: the fibers and fiber bundles were completely developed. In the ICTs, the fiber bundles and fibers were still at their initial stage of differentiation. Unlike the ICTs, the collagen fibrils and fibers of the ITTs were oriented and aligned along the direction of major stress. Neither alignment nor crimp pattern was diagnostic in the ICTs. The ITTs showed a significantly higher percentage of collagen density and a lower percentage and number of cell density at ultrastructural level (P=0.001 for all). The tenoblasts of the ITTs were mature and cigar-shaped, exhibited lower diameter and were aligned parallel to collagen fibers and fiber bundles. The cellular structure of the ICTs was immature and disorganized throughout the disorganized collagen fibrils and immature fibers. The fiber bundles in the ICTs were not properly formed, the crimp pattern was not detectable, and the collagen fibrils were disorganized and haphazardly distributed (Fig. 6).

Biomechanical findings

The ITTs showed significantly higher ultimate load, yield load, stiffness, maximum stress and modulus of elasticity and lower ultimate strain and yield strain compared to the ICTs (P=0.001

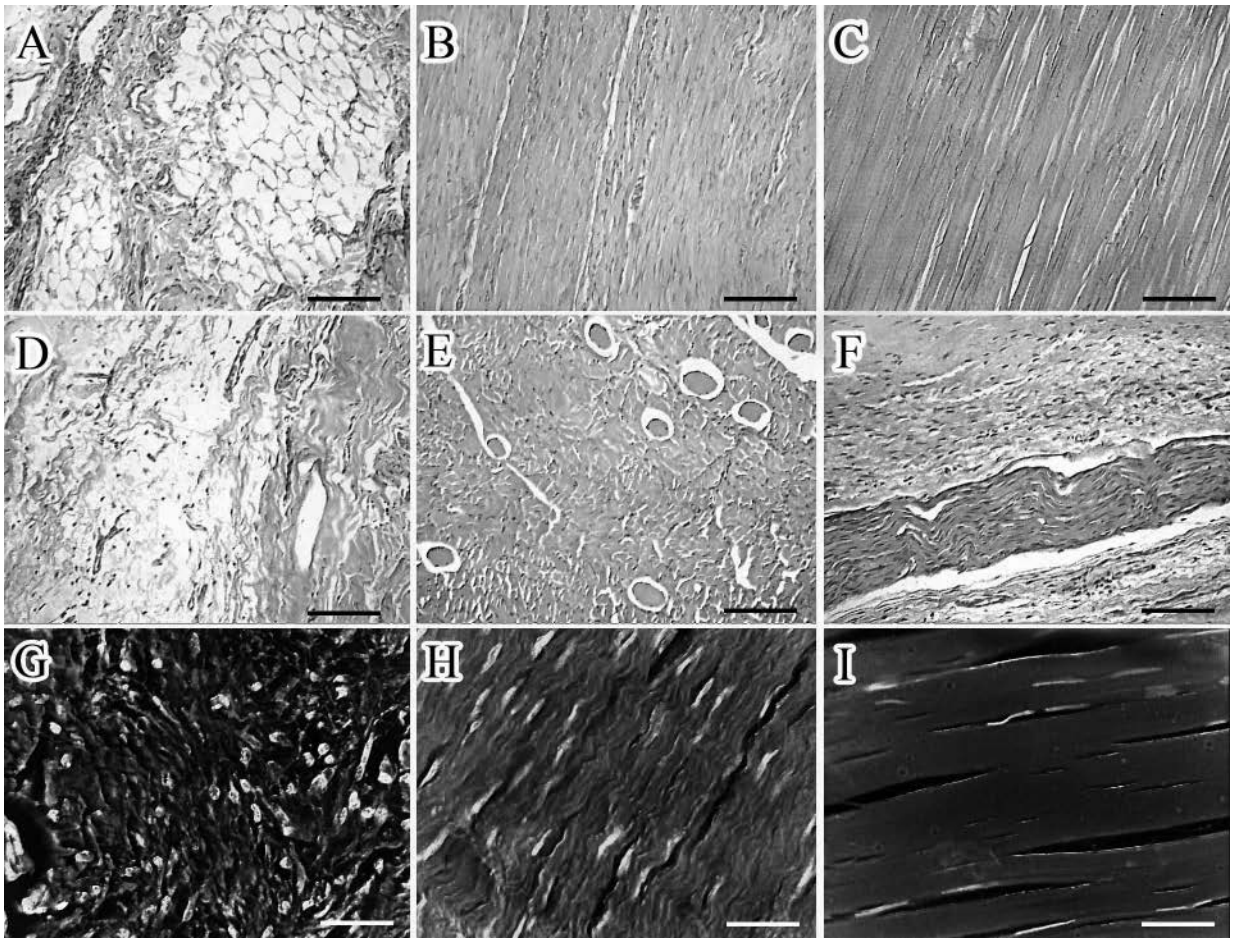

Fig. 5. *Histopathological findings of the injured tendons, 120 days after injury. The newly regenerated soft connective tissue is seen in the injured area of the injured control tendons (**A**, **D**, **G**). Large amounts of adipose tissue and numerous immature blood vessels are seen in this section (A and D). No tendinous structure is formed in the defect area of this tendon. Collagen density is low and unorganized. No tissue maturity is seen at the defect area. The tenoblasts are mostly immature and are aligned in a circular pattern (G). The collagen mass density in the defect area of the injured treated tendons is greatly improved and the collagen fibers are aligned along the longitudinal axis of the tendon (**B**). In the cross section (**E**) and longitudinal section (**F**) of the injured treated tendons, the remnants of the collagen implant are seen as small islands. The newly regenerated collagen fibers are aligned along the direction of the collagen implant, gastrocnemius muscle and the calcaneal tuberosity. These remnants of the collagen implants acted as a scaffold for the newly regenerated collagen fibers and had a major role in their alignment and maturity. Mature tenoblasts and tenocytes are aligned along the direction of the highly matured collagen fibers (**H**). In the normal tendon, the number of cells is low and the cells are mostly tenocytes (**I**). Collagen mass density is high and the collagen fibers are highly matured and aligned along the direction of the stress transmitted from the gastrocnemius muscle to calcaneal tuberosity (C). A-F are stained by H&E. Scale bar=50 μm. G-I are inverted pictures of the H&E stained sections. Scale bar=12.5 μm.*

for all) (Table IV). Although the biomechanical characteristics of the ITTs were significantly higher than the ICTs, the biomechanical properties of the injured tendons of both groups were still significantly lower than their NCTs (P<0.05). Hence, the ultimate load, yield load, stiffness, maximum stress and modulus of elasticity were significantly lower, and the ultimate strain and yield strain were significantly higher than their NCTs (P=0.001 for all). There were no significant differences between the ultimate load,

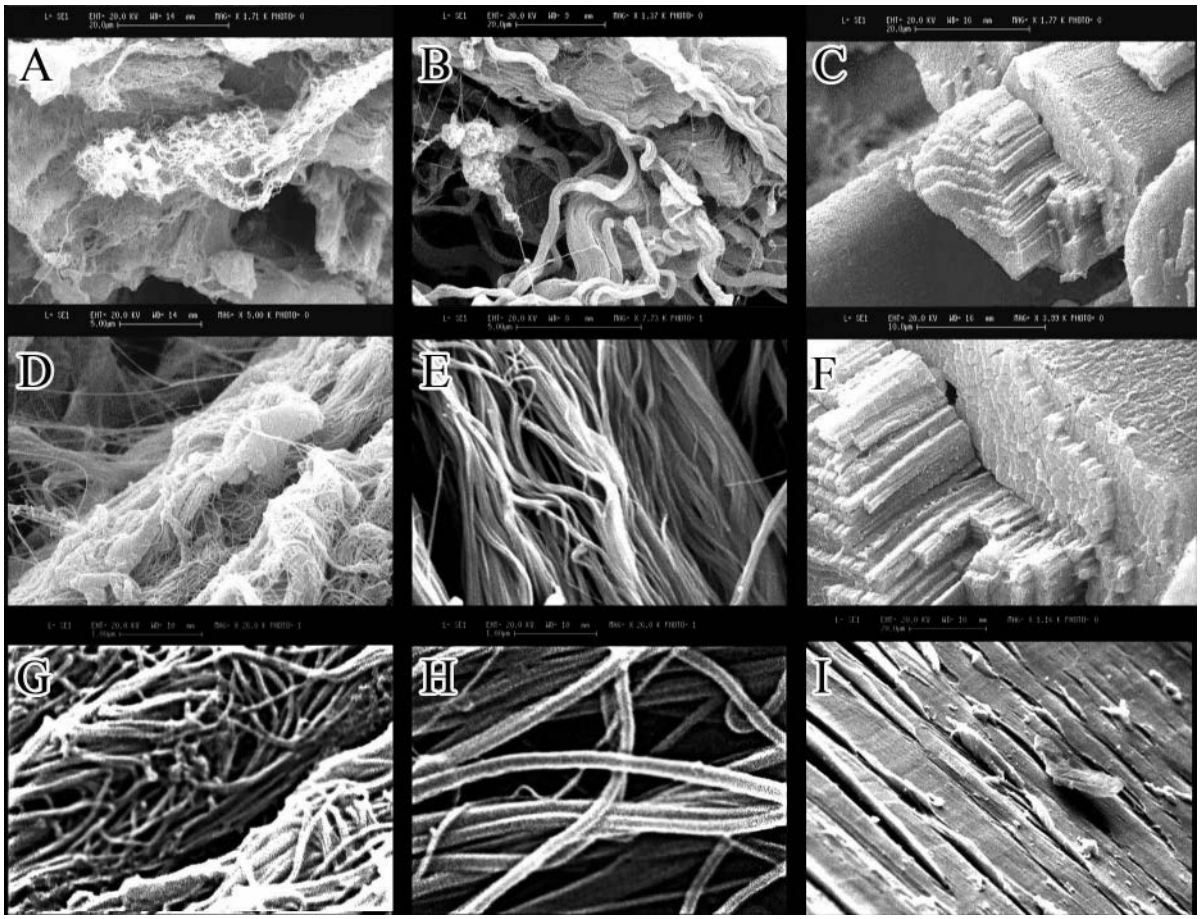

Fig. 6. *SEM, 120 days after injury. **A**, **D** and **G**) Injured control tendons at different magnification (×1.7, 5, 26K respectively). The immature collagen fibrils are randomly arranged and failed to produce fibers or fiber bundles (A). The collagen fibrils are not organized and are immature, and are unimodally distributed. Their diameters are small (D and G). **B**, **E**, **H**) The injured treated tendons. The fiber bundles (B), fibers (E) and fibrils (H) are formed and are unidirectionally aligned. Such differentiation in the hierarchical structure of the collagen is not seen in the injured control area (A and D). Although various levels of the collagenic structures of the injured treated area are completely differentiated after 120 days of injury, the diameter of the collagen fibers and fiber bundles is far behind that of the normal tendon (**C** and **F**). In normal tendon, the fiber bundles are highly mature (C), and are composed of small fibers (C and F). These fibers are highly impacted in these bundles, and they are also composed of highly aligned collagen fibrils (C and F). **I**) A longitudinal section of the normal tendon. The collagen fibers are highly aligned and the mature tenoblasts and tenocytes are laid along the longitudinal direction of the collagen fibers. Magnification for B,E and H are 1.4, 7.7 and 26 and for C, F and I are 1.7,4 and 1.16K, respectively.*

yield load, stiffness, stress, ultimate strain, yield strain and modulus of elasticity of the NCTs of the treated and control groups (P>0.05).

DISCUSSION

Implantation of the three-dimensional collagen implant in a rabbit tendon defect model significantly increased the biomechanical performance of the injured tendons compared to the natural ability of the healing response. Perhaps, the first explanation is the ability of the collagen implant to maintain continuity between the tendon stumps. This characteristic, together with the chemo-attractive characteristic of the collagen molecules, possibly increased the rate of cell migration from the tendon ends and the peritendinous tissues to the injured area.

The first step in tendon healing is the inflammatory

Table I. *Scoring criteria used to define the ultrasonographic, gross and histopathological findings.*

	A) Ultrasonographical features of the injured tendons		
SCORE	**1. Echogenicity**	**2. Hyperechogenic area/hypoechogenic area of the tendons (homogeneity)**	**3. Transverse movement of the tendon (Index for peritendinous adhesion)**
0	normal echogenicity	smooth (homogenous) echogenicity	freely movement
1	slightly hyper-echoic	non-smooth (heterogeneous) echogenicity (mild)	movable in one direction (left or right)
2	Hyper-echoic	non-smooth echogenicity (moderate)	movable in one direction with force (left or right)
3	Hypo-echoic	Amputated view or non-smooth echogenicity (severe)	fixed or non-movable
	B) Gross pathologic features of the injured tendons		
SCORE	**1. Peritendinous adhesion**	**2. Hyperemia**	**Status**
0	No adhesion	no hyperemia, shiny glistening surface appearance	normal
1	tendon was easily detached from the surrounding tissues by blunt dissection	only in the paratenon	mild
2	for detachment from the surrounding tissues, tendon needed little sharp dissection	it was extended to the tendon proper but it was not severe in nature	moderate
3	for detachment from the surrounding tissues, tendon needed completely sharp dissection	it was extensively extended to the tendon proper and made its appearance more pink and dark	severe
	C) Histopathologic features of the injured tendons		
SCORE	**1. Alignment**	**2. Perivascular edema**	**Status**
0	most of the collagen fibers were longitudinally oriented in only one direction and the tenoblasts and tenocytes were laid longitudinally along their orientation	No edema	normal
1	collagen fibers were longitudinally oriented in one direction pattern but there were few areas of unorganized collagen fibers in the field	presence of edema just around small blood vessels	mild
2	collagen fibers were not longitudinally oriented and the irregular orientation pattern was predominant	Presence of edema around small and medium sized blood vessels	moderate
3	there was no obvious pattern and the collagen fibers were disorganized	Presence of edema around all types of vessels	severe
SCORE	**3. Crimp pattern**		**Status**
0	Crimp pattern was present		normal
1	Crimp pattern was not present		Far behind normal

stage, when inflammatory cells infiltrate into the injured area (3, 9). Collagen molecules attract inflammatory cells (23, 24). The presence of the collagenous material in the wound could initiate inflammation and increase tissue reaction (24, 25). The inflammatory cells possibly migrate during the first stage of tendon healing to degrade the collagen implant (8, 23). This results in increasing inflammation, possibly because of the phagocytosis activity of the neutrophils (10). These cells should be more numerous than in the control tendons in the earlier stages of tendon healing.

Inflammation plays a key role in tendon healing, and without inflammation tendon healing would not continue in an effective fashion (3, 9). However, this was not evident in our experimental set-up because our evaluation time was 120 days after surgical application of collagen implants, and we would therefore have missed this stage. We indirectly followed the inflammatory cells in the later stages of tendon healing. In the earlier stages of inflammation, numerous neutrophils and macrophages initiate the healing process and facilitate fibroplasia (10, 18). In the second phase, the fibroplasia stage, immature

Table II. *Histopathological findings of the injured treated and injured control tendons, 120 days post injury and surgical reconstruction (Quantitative assessments).*

	Injured control tendons (left Achilles tendon)	**Injured tendons treated with collagen implant (left Achilles tendon)**	
	Mean and Standard Deviation	Mean and Standard Deviation	*P Value*
Total cellularity	443.11 ± 16.37	289.17 ± 8.36	0.001*
Total fibroblasts and fibrocytes	322.14 ± 15.19	222.48 ± 9.68	0.001*
Immature fibroblasts (tenoblasts)	167.48 ± 12.11	68.73 ± 6.37	0.001*
Mature fibroblasts (tenoblasts)	121.44 ± 11.34	122.91 ± 3.84	0.972
Fibrocyte (tenocyte)	22.01 ± 2.53	33.31 ± 2.69	0.001*
Neutrophils	1.09 ± 0.69	0.97 ± 0.63	0.789
Lymphocytes	63.51 ± 5.6	39.63 ± 5.2	0.001*
Plasma cells	2.56 ± 1.12	1.15 ± 0.87	0.428
Macrophages	33.22 ± 5.67	22.44 ± 2.64	0.001*
Number of vessels (total)	32.87 ± 6.26	16.9 ± 3.28	0.001*
Number of small vessels	17.29 ± 2.24	10.16 ± 0.98	0.001*
Number of medium vessels	6.83 ± 0.75	4.72 ± 0.65	0.006*
Number of large vessels	4.74 ± 1.65	3.1 ± 0.93	0.622
Diameter of immature fibroblasts (μm)	7.82 ± 1.13	5.49 ± 0.33	0.001*
Diameter of mature fibroblasts (μm)	3.31 ± 0.39	2.79 ± 0.36	0.089
Diameter of fibrocytes (μm)	1.52 ± 0.08	1.24 ± 0.05	0.001*
Diameter of small vessels (μm)	15.24 ± 0.97	21.6 ± 1.93	0.001*
Diameter of medium vessels (μm)	42.57 ± 1.85	50.48 ± 1.65	0.001*
Diameter of large vessels (μm)	81.62 ± 4.31	101.04 ± 3.57	0.001*
Percentage of collagen density	23.52 ± 4.03	62.38 ± 3.02	0.001*
Percentage of cell density	19.86 ± 1.65	10.62 ± 1.36	0.001*
Percentage of background density	48.46 ± 2.9	32.9 ± 2.84	0.001*
Semi-quantitative scored values			
Crimp pattern	$0.75^{Mean} \pm 0.44^{Sd}$	0.6 ± 0.5	0.121
	1^{Median} $(0\text{-}1)^{Min\text{-}Max}$	1 (0-1)	
Collagen fibers' alignment	2.55 ± 0.51	1.65 ± 0.48	0.049*
	3 (2-3)	2 (1-2)	
Perivascular edema	2.8 ± 0.41	1.6 ± 0.5	0.001*
	3 (2-3)	2 (2-3)	
Peritendinous adhesion	2.75 ± 0.44	1.75 ± 0.44	0.001*
	3 (2-3)	2 (1-2)	

*Histopathologic fields: n=5. Histopathologic sections: n=5. Tendon samples: n=10. Total picture for each group: n=250. Independent sample t-test was used to compare the significant differences between the left injured legs of the treated groups and control groups. Significant differences were determined at confidence interval of 95% and P<0.05. For semi-quantitative analysis (scoring system) non-parametric Mann Whitney U test was used to define the significant differences between groups (P<0.05). Quantitative data are reported as a Mean ± standard deviation and scored values are reported as Mean ± standard deviation and they are also reported as median (minimum-maximum). The significant p value is indicated with * in the tables. The results are in triplicate.*

Table III. *SEM. Ultra-structural findings of the injured treated and injured control tendons; 120 days post injury and surgical reconstruction (Quantitative assessments).*

	Injured control tendons (left Achilles)	**Injured treated tendons (left Achilles tendon)**	
	Mean and Standard Deviation	Mean and Standard Deviation	*P Value*
Diameter of collagen the fibrils (nm)	39.2 ± 5.02	61.92 ± 3.92	*0.001**
Diameter of the collagen fibers (nm)	525.14 ± 10.75	546.45 ± 15.96	*0.089*
Diameter of the fiber bundles (nm)	Not developed	2864.75 ± 330.34	*0.001**
Diameter of the fascicles (nm)	Not developed	Not developed	
Number of the cells	195.71 ± 9.75	75.72 ± 5.57	*0.001**
Density of the collagen fibrils (%)	47.03 ± 4.88	65.76 ± 3.9	*0.001**
Cell density (%)	17.06 ± 1.25	9.97 ± 1.64	*0.001**

*SEM pictures: n=5. SEM sections: n=5. Tendon samples: n=10. Total picture for each group: n=250. Independent sample T-test was used to compare the significant differences between the left injured legs of the treated groups and control groups. Significant differences were determined at confidence interval of 95% and P<0.05. The significant p value is indicated with **.*

Table IV. *Biomechanical findings of the injured treated and injured control tendons, 120 days post injury and surgical reconstruction (Quantitative assessments).*

		Left Achilles	*Left Achilles*	*Right Achilles*	*Right Achilles*			
Variable	**Unit**	**Injured Control Tendons (1)**	**Injured Treat -ed tendons (2)**	**Normal Tendons of the control group (3)**	**Normal Tendons of the Treated Group (4)**	**P Value (1 vs 2)**	**P Value (2 vs 4)**	**P Value (3 vs 4)**
Ultimate load	*Newton (N)*	41.42 ± 5.77	118.91 ± 16.07	344.07 ± 39.15	349.32 ± 33.09	*0.001**	*0.001**	*0.924*
Yield load	*(N)*	29.73 ± 6.65	99.03 ± 15.12	298.92 ± 28.86	303.19 ± 26.79	*0.001**	*0.001**	*0.694*
Stiffness	*(N)/mm*	11.7 ± 2.01	59.21 ± 5.06	211.79 ± 28.59	203.32 ± 19.31	*0.001**	*0.001**	*0.915*
Strain	%	20.44 ± 2.81	13.4 ± 0.88	10.91 ± 0.45	10.62 ± 0.78	*0.001**	*0.001**	*0.802*
Yield strain	%	17.38 ± 2.33	10.99 ± 1.05	8.24 ± 0.33	7.97 ± 0.38	*0.001**	*0.001**	*0.577*
Maximum stress	*(N)/mm2*	11 ± 1.39	18.54 ± 2.32	32.62 ± 4.05	33.31 ± 3.44	*0.001**	*0.001**	*0.976*
Modulus of elasticity	*(N)/mm2*	0.53 ± 0.1	1.38 ± 0.23	2.99 ± 0.38	3.15 ± 0.46	*0.001**	*0.001**	*0.898*

*Independent sample t-test was used to compare the significant differences between the left injured legs of the treated groups and control groups. Significant differences were determined at confidence interval of 95% and P<0.05. The significant p value is indicated with * in the tables.*

fibroblasts are predominant (9). Macrophages, lymphocytes and plasma cells are also highly infiltrated in this newly regenerated granulation tissue (3). However, the number of neutrophils has substantially reduced (9).

The ITTs showed significantly less inflammatory cells such as neutrophils, macrophages, and especially lymphocytes at 120 DPI, compared to the ICTs, suggesting that the inflammatory stage in the ITTs had passed faster than in the ICTs. In addition, compared to the ICTs, the ITTs showed better differentiation, alignment and maturation of the newly regenerated collagen fibrils, fibers and fiber bundles. The significantly lower cellularity and improved tenoblast maturity demonstrated that the ITTs were probably in the maturation stage of tendon healing (3, 9). Moreover, the imaging results and the gross pathological appearance of the ITTs were almost

comparable to the intact tendons at 120 DPI. On the other hand, the morphologic characteristics of the ICTs showed that the healing process, although not in the inflammatory stage, did not match with further stages of tendon healing (10, 17). This suggests that the healing process was not properly initiated and did not continue in an effective manner. The high degree of inflammatory cell infiltrate together with the presence of disorganized immature collagen fibrils, degenerative changes, and several immature blood vessels observed in the ICTs suggests that the unassisted injured tendon defect failed to produce tendinous tissue, so that a loose areolar connective tissue, far from a normal tendinous tissue, was formed in the ICTs.

One of the most clinically relevant issues after tendon injury is the development of peritendinous adhesion (26). Prolonged inflammation increases peritendinous adhesions, as continuous inflammation initiates a longer fibroplasia phase so that fibroblasts migrate and release their collagen constituents at different directions of the lesion (3, 9). In normal healing, the epitenon and paratenon are damaged, and the fibroblasts are free to migrate and proliferate in all directions (20). The proliferation phase is more severe and prolonged if the blood vessels are damaged because more fibrin is deposited in the lesion (21). The fibrin clot in the injured area acts as a scaffold for fibroblasts and produces more peritendinous adhesions (3).

In the present experiment, the ITTs showed significantly lower amounts of peritendinous adhesions around the injured area. Two different mechanisms could be proposed for this finding. The first is the ability of collagen to initiate and increase inflammation (23, 24, 27). Based on these morphological results, it should be highlighted that the collagen implant did not prolong the inflammation but possibly increased its quality and rate. By increasing infiltration of the inflammatory cells, the fibrin clot is degraded and absorbed faster than with lower inflammatory response (3, 9, 18). The second mechanism could result from attraction of the fibroblasts by the collagen implant and migration of these cells in the direction of the implant fibers (8, 23). Collagen is a potent chemo-attractant for fibroblasts *in vivo*, and this accelerates repair of the damaged tissue (8). By this mechanism, tenoblast proliferation is more beneficial, because the implanted collagen is not laid outside the injured area, and the newly regenerated collagen fibers are more compact and aligned in the direction of the collagen fibers of the implant. Thus, this tissue engineering manipulation reduces peritendinous adhesion. Ambulation on the injured leg could improve the alignment of the collagen along the stress line in the longitudinal axis of the tendon (10). It has been shown that disorganized collagen scaffold interferes with fibroblast mediated deposition of organized extracellular matrix *in vitro* (28).

Enhanced alignment improves the maturity of the collagen fibrils and fibers, and stress on the injured tendons could facilitate the merging of the small collagen fibrils and increase their tolerance against tensile strength and weight (18, 22). By increasing the diameter of the collagen fibrils, the biomechanical performance of the injured tendon is also increased (9, 16, 17).

Another explanation for the effectiveness of collagen implant on the biomechanical performance of the regenerated tissue was the bio- and cyto-compatibility and biodegradability of the three-dimensional collagen implant. These characteristics are important in the improved structural organization and biomechanical properties of the ITTs demonstrated in the present study. At 120 DPI, the collagen implant was almost fully absorbed, and only some small islands of the implant were evident in the center of the construct. The tenocytes and tenoblasts infiltrated through these parts of the collagen implant and aligned in the direction of the collagen fibers of the collagen implant. In addition, the newly regenerated collagen fibers were aligned around them in the same direction. In an experimental tendon injury in rabbits, the preserved large diameter collagen fibrils in the injured tendons treated with hyaluronic acid acted as scaffolds for the newly regenerated collagen fibrils (19). These newly regenerated collagen fibrils showed greater transverse diameter at ultrastructural level compared to the controls (19). The three-dimensional collagen implants were able to increase the biomechanical performance of the regenerated tissue.

Although the xenogenous-based collagen implant may have a role in increasing inflammation, no evidence of rejection at the injured area of the treated tendons was seen at 120 DPI. The results of the present study are in accordance with those by

Allman et al. (27), who showed that implantation of porcine extracellular matrix in mice initiated an immune response consistent with a remodeling reaction rather than rejection.

The major merit of the collagen implant is that, unlike tendon xenografts, there is no need for immunosuppression and, because the implant integrates with the newly regenerated tissue and is eventually completely absorbed, it bestows its characteristics on the new tendon but does not remain part of it, as is the case with some other prostheses (29). For example, Nishimoto et al. (30) found that after implantation of a poly-L-lactic acid based prosthesis in a ligament defect model in rabbits, despite excellent biomechanical properties of the repaired area, the implant was not degraded and no new tissue had replaced the scaffold after 16 weeks. Sato et al. (1) investigated several different synthetic-based artificial tendons (e.g. polylactic acid), the mechanical properties of which declined over 26 weeks, but were not replaced by new ligaments. In contrast with these findings, and in line with ours, Gigante et al. (8), using a highly aligned bilamellar membrane of type I purified equine collagen in a multi-lamellar conformation to augment a patellar tendon defect model in rabbits, found that the scaffold was incorporated with the native tendon. In addition, Enea et al. (7), working with a patellar tendon defect in a sheep model and using an experimental protocol similar to ours, but with a different type of collagen implant, found that it was incorporated into the repaired tissue after 3-6 months.

This study has some limitations. A major limitation was that the short-term effect of the collagen implant on tendon healing was not investigated. This was because we were not sure about the effectiveness of the collagen implant on large tendon defect models in rabbits. Therefore, we decided to let the healing process progress, and investigate only the final outcome. Another limitation is the methods of observation. For example, we did not use ELISA tests to define the pro-inflammatory cytokines and matrix metalloproteinases. Perhaps, further biochemical studies combined with the results of the present study in future investigations will enable to describe in greater details the mechanism of action of the collagen implants on tendon healing *in vivo*.

In conclusion, the hybridized nano-micro-structured three-dimensional collagen implant produced a newly regenerated tendinous tissue that was morphologically and biomechanically close to intact tendons after 120 days of injury in a large tendon defect model. This type of collagen implant was not rejected, was biodegradable and biocompatible, and was well tolerated *in vivo*. Application of such collagen implant may have some value in the clinical setting. However, studies on different species and clinical trials are needed to confirm the results of the present study.

ACKNOWLEDGEMENTS

The authors would like to thank the authorities of Shiraz University and the Iranian National Science Foundation (INSF) for their financial support (Grant number: 87020247). The kind assistance of Dr N. Golestani from the Department of Clinical Sciences, Mr. L. Shirvani, Mr. G. Yousefi, Mr. M. Zareh from the Department of Pathobiology, School of Veterinary Medicine and Mr A. Solhpour from the Department of Materials Sciences, Faculty of Engineering, Shiraz University, Shiraz, Iran is highly appreciated and acknowledged.

REFERENCES

1. Sato M, Maeda M, Kurosawa H, Inoue Y, Yamauchi Y, Iwase H. Reconstruction of rabbit Achilles tendon with three bioabsorbable materials: histological and biomechanical studies. J Orthop Sci 2000; 5:256-67.
2. Park YS, Sung KS. Surgical reconstruction of chronic Achilles tendon ruptures using various methods. Orthopedics 2012; 35:e213-e18.
3. Moshiri A, Oryan A. tendon and ligament tissue engineering, healing and regenerative medicine. J Sports Med Doping Stud 2013; 3:126.
4. Yang M, Wang Z, Li Y, Guo B. Bilateral cadaveric Achilles tendon graft in reconstruction after tendon tumor resection. J Foot Ankle Surg 2013; 52:103-6.
5. Chen J, Xu J, Wang A, Zheng M. Scaffolds for tendon and ligament repair: review of the efficacy of commercial products. Expert Rev Med Devices 2009; 6:61-73.
6. Maffulli N, Longo UG, Loppini M. New options in the management of tendinopathy. Open Access J

Sports Med 2010; 1:29-37.
7. Enea D, Gwynne J, Kew S, et al. Collagen fibre implant for tendon and ligament biological augmentation. *In vivo* study in an ovine model. Knee Surg Sports Traumatol Arthrosc 2013; 21:1783-93.
8. Gigante A, Busilacchi A, Lonzi B, Cecconi S, Manzotti S, Renghini C, Giuliani A, Mattioli-Belmonte M. Purified collagen I oriented membrane for tendon repair: An *ex vivo* morphological study. J Orthop Res 2013; 31:738-45.
9. Sharma P, Maffulli N. Tendon injury and tendinopathy: healing and repair, J Bone Joint Surg Am 2005; 87:187-202.
10. Sharma P, Maffulli N. Biology of tendon injury: healing, modeling and remodeling. J Musculoskelet Neuronal Interact 2006; 6:181-90.
11. Foltran I, Foresti E, Parma B, Sabatino P, Roveri N. Novel biologically inspired collagen nanofibers reconstituted by electrospinning method. Macromol Symp 2008; 269:111-18.
12. Wray LS, Orwin EJ. Recreating the microenvironment of the native cornea for tissue engineering applications. Tissue Eng Part A 2009; 15:1463-72.
13. Dubey N, Letourneau PC, Tranquillo RT. Neuronal contact guidance in magnetically aligned fibrin gels: effect of variation in gel mechano-structural properties. Biomaterials 2001; 22:1065-75.
14. McCall AS, Kraft S, Edelhauser HF, et al. Mechanisms of corneal tissue cross-linking in response to treatment with topical riboflavin and long-wavelength ultraviolet radiation (UVA). Invest Ophthalmol Vis Sci 2010; 51:129-38.
15. Siritientong T, Srichana T, Aramwit P. The effect of sterilization methods on the physical properties of silk sericin scaffolds. AAPS Pharm Sci Tech 2011; 12:771-81.
16. Moshiri A, Oryan A. Structural and functional modulation of early healing of full-thickness superficial digital flexor tendon rupture in rabbits by repeated subcutaneous administration of exogenous human recombinant basic fibroblast growth factor. J Foot Ankle Surg 2011; 50:654-62.
17. Oryan A, Moshiri A. A long term study on the role of exogenous human recombinant basic fibroblast growth factor on the superficial digital flexor tendon healing in rabbits. J Musculoskelet Neuronal Interact 2011; 11:185-95.
18. Oryan A, Moshiri A, Meimandiparizi AH. Effects of sodium-hyaluronate and glucosamine-chondroitin sulfate on remodeling stage of tenotomized superficial digital flexor tendon in rabbits: a clinical, histopathological, ultrastructural, and biomechanical study. Connect Tissue Res 2011; 52:329-39.
19. Oryan A, Moshiri A, Meimandiparizi AH, Raayat Jahromi A. Repeated administration of exogenous Sodium-hyaluronate improved tendon healing in an *in vivo* transection model. J Tissue Viability 2012; 21:88-102.
20. Oryan A, Moshiri A, Meimandiparizi AH. Short and long term healing of the experimentally transverse sectioned tendon in rabbits. Sports Med Arthrosc Rehabil Ther Technol 2012; 4:14.
21. Oryan A, Moshiri A, Raayat AR. Novel application of Theranekron® enhanced the structural and functional performance of the tenotomized tendon in rabbits. Cells Tissues Organs 2012; 196:442-55.
22. Oryan A, Moshiri A. Recombinant fibroblast growth protein enhances healing ability of experimentally induced tendon injury *in vivo*. J Tissue Eng Reg Med 2014; 8(6):421-31.
23. Postlethwaite AE, Seyer JM, Kang AH. Chemotactic attraction of human fibroblasts to type I, II, and III collagens and collagen-derived peptides. Proc Natl Acad Sci USA 1978; 75:871-5.
24. Anselme K, Bacques C, Charriere G, Hartmann DJ, Herbage D, Garrone R. Tissue reaction to subcutaneous implantation of a collagen sponge. A histological, ultrastructural, and immunological study. J Biomed Mater Res 1990; 24:689-703.
25. Badylak SF. Xenogeneic extracellular matrix as a scaffold for tissue reconstruction. Transpl Immunol 2004; 12:367-77.
26. Khanna A, Friel M, Gougoulias N, Longo UG, Maffulli N. Prevention of adhesions in surgery of the flexor tendons of the hand: what is the evidence? Br Med Bull 2009; 90:85-109.
27. Allman AJ, McPherson TB, Badylak SF, Merrill LC, Kallakury B, Sheehan C, Raeder RH, Metzger DW. Xenogeneic extracellular matrix grafts elicit a TH2-restricted immune response. Transplantation 2001; 71:1631-40.
28. Saeidi N, Guo X, Hutcheon AE, et al. Disorganized

collagen scaffold interferes with fibroblast mediated deposition of organized extracellular matrix *in vitro*. Biotechnol Bioeng 2012; 109:2683-98.

29. Veillette CJ, Cunningham KD, Hart DA, Fritzler MJ, Frank CB. Localization and characterization of porcine patellar tendon xenograft antigens in a rabbit model of medial collateral ligament replacement. Transplantation 1998; 27; 65:486-93.
30. Nishimoto H, Kokubu T, Inui A, et al. Ligament regeneration using an absorbable stent-shaped poly-L-lactic acid scaffold in a rabbit model. Int Orthop 2012; 36:2379-86.

SERUM GLYCOPEPTIDOLIPID CORE IgA ANTIBODY LEVELS IN PATIENTS WITH CHEST COMPUTED TOMOGRAPHY FEATURES OF *MYCOBACTERIUM AVIUM-INTRACELLULARE* COMPLEX PULMONARY DISEASE

Y. SHIMIZU[1,4], A. TAKISE[1], H. MORITA[2], Y. HOSOMI[3], N. KASAHARA[1], T. KAWATA[1], T. HORIE[1], Y. ISHII[4] and M. YAMADA[5]

[1]Department of Respiratory Medicine, [2]Department of Diagnostic Radiology, [3]Department of Laboratory Medicine, Maebashi Red Cross Hospital, Maebashi, Gunma Japan; [4]Department of Pulmonary Medicine and Clinical Immunology, Dokkyo Medical University School of Medicine, Mibu, Tochigi, Japan; [5]Department of Medicine and Molecular Science, Gunma University Graduate School of Medicine, Gunma, Japan

Received September 27, 2013 – Accepted July 10, 2014

Measurement of serum glycopeptidolipid core IgA antibody (GPL antibody) was recently reported to show a high sensitivity and specificity for diagnosing *Mycobacterium avium-intracellulare* complex (MAC) pulmonary disease (MAC-PD), but its clinical value has not been confirmed. This study aims to evaluate the seropositive rate in patients with suspected MAC-PD based on chest computed tomography (CT), and to examine whether GPL antibody reflects the extent of lung involvement on CT or the number of bacteria in sputum, retrospectively. Among 66 patients with suspected MAC-PD on CT, 36 patients were negative for MAC by culture and 30 were positive. Sputum grades of MAC were evaluated by fluorochrome microscopy of sputum smears. The lungs were divided into six regions to assess the extent of disease. Serum levels of GPL antibody were measured with an enzyme immunoassay (cut-off value >0.7 U/ml). The GPL antibody positive rate was 19.4% among patients who were negative for MAC by culture versus 73.3% among culture–positive patients. The serum level of GPL antibody was significantly correlated with the sputum smear grade (r=0.43, p<0.05) and was also correlated with the number of lung regions showing MAC-PD features on CT (r=0.43, p<0.05). Some MAC-PD patients may have CT features of MAC with positive level of GPL antibody, although the diagnosis cannot be confirmed by culture. GPL antibody levels reflect the pulmonary burden of MAC, as assessed from the sputum smear grade and number of involved regions on chest CT.

Infection with *Mycobacterium avium – intracellulare* complex (MAC) is the most common non-tuberculous mycobacterial pulmonary disease (NTM-PD) (1-3). In addition to clinical and radiographic features, examination of sputum, samples, bronchial washings, or tissue biopsy samples has been used for the diagnosis of MAC-PD. Isolation of non-tuberculous mycobacteria (NTM) by culture and subsequent testing with specific DNA probes for *M. avium* and *M. intracellulare* are

Key-words: Mycobacterium avium, *mycobacterium intracellulare*, *computed tomography, glycopeptidolipid core IgA antibody, serodiagnosis*

Mailing address: Yasuo Shimizu, M.D., Ph.D.
Department of Pulmonary Medicine and Clinical Immunology, Dokkyo Medical University School of Medicine, 880 Kitakobayashi, Mibu, Tochigi 321-0293, Japan
Tel.: +81 282 87 2151 Fax: +81 282 86 5080
e-mail: yasuo-s@dokkyomed.ac.jp

0393-974X (2014)

generally performed. However, it is not always easy to obtain sputum samples or bronchial washings, and recovery of NTM from clinical samples can sometimes be difficult. Although the 2007 American Thoracic Society (ATS)/Infectious Disease Society of America (IDSA) guidelines simplified the diagnosis of NTM-PD, there are some patients who do not fit these diagnostic criteria (2, 4). Therefore, it has been hoped that novel diagnostic tools for NTM will be developed.

The glycopeptidolipid (GPL) core is a common structure of GPL antigen, which is a major cell surface antigen of MAC that is not present on *M. tuberculosis* or *M. Kansasii* (5, 6). Recently, measurement of the serum level of IgA antibody specific for the GPL core (GPL antibody) has been reported to be a useful diagnostic tool for MAC-PD and for differentiating MAC from pulmonary tuberculosis (TB) and *M. Kansasii* infection (7-9). When GPL antibody was measured by enzyme immunoassay, its level was higher in MAC-PD patients who had larger nodular lesions (10-30 mm) compared with patients who had smaller nodular lesions (<10 mm), and its level showed a weak correlation with the number of involved segments on CT when the lungs were divided into 18 segments (7). The sensitivity of GPL antibody for MAC-PD was 84.3% and the specificity was 100% when a cut-off value > 0.7 U/ml was employed. Analysis of the relation between antibody levels and the features of MAC on chest radiographs showed that the GPL antibody level was higher in the nodular bronchiectatic type than in the fibrocavity subtype (8). Furthermore, the usefulness of serodiagnosis with GPL antibody was reported in the United States, although high antibody levels were also found in patients with infection caused by *M. abscessus* and *M. fortuitum* (9).

The present study was performed to further investigate the usefulness of serodiagnosis with GPL antibody in clinical practice. From the findings on plain chest X-ray films, MAC-PD is divided into two types (nodular bronchiectatic and fibrocavity) according to the ATS/IDSA statement, but chest CT scanning is usually performed as well (2). In the present study, the serum level of GPL antibody was measured in patients who were suspected to have MAC-PD from chest CT findings, which have not previously been assessed in comparison with GPL antibody. The diagnostic sensitivity of this antibody was also examined in MAC-PD patients who met the diagnostic criteria for NTM according to ATS/IDSA (2), as well as in MAC-PD patients who did not meet all of the criteria. Furthermore, whether GPL antibody reflects the burden of infection was investigated by comparing the antibody level with the number of lung regions showing lesions on chest CT, and with the number of bacteria in sputum samples on microscopic examination.

MATERIALS AND METHODS

Subjects

This study investigated 66 patients who attended Maebashi Red Cross Hospital between June 2012 and June 2013, retrospectively. Patients receiving anticancer agents, steroids, or immuno suppressive agents were excluded. Patients with suspected MAC-PD based on chest CT findings were enrolled. TB was excluded by the polymerase chain reaction (PCR), by enzyme immunoassay for TB of colonies grown from samples, or by the interferon-g release assay of peripheral blood (QuantiFERON®-TB Gold, Japan BCG Laboratory, Tokyo, Japan; or T-spot® TB, Oxford Immunotec, Oxford, UK). Treatment of sputum samples for culture of mycobacteria and isolation of DNA from sputum or bronchial washings for PCR were performed as described previously (10).

Patients were divided into two groups. Group A was composed of 36 patients with features of MAC-PD on chest CT who were negative for MAC by culture, smear, and PCR. Group B was composed of 30 patients with features of MAC-PD on chest CT who had at least one positive culture and were positive for MAC by PCR. The final diagnosis of MAC species of *M. avium, M. intracellulare, or M. avium-intracellulare complex* was carried out by PCR. Group B was further divided into two subgroups. Patients who met the diagnostic criteria for NTM in the ATS/IDSA statement were classified as having definite MAC-PD (2). This subgroup met the following microbiological criteria: i) positive cultures from at least two separate sputum samples and ii) positive culture from at least one sample of bronchial washings (lavage fluid). The patients who did not meet these criteria were classified as having probable MAC-PD and this subgroup had only one positive sputum culture. The present study was conducted according to the guidelines of the Declaration of Helsinki and all patients gave informed consent.

CT findings and smear grade

All patients underwent chest CT, and were suspected

as having MAC-PD based on the findings. The CT features of MAC-PD were classified according to previous studies with addition of the hypersensitivity type: i) bronchiectasis; ii) cavitation; iii) centrilobular nodules (defined as multiple, well-circumscribed areas of increased attenuation around the terminal or respiratory bronchioles, with the majority of the nodules being about 5 mm in size); iv) consolidation; v) larger nodules (>10 mm); and vi) hypersensitivity. The hypersensitivity type is MAC hypersensitivity pneumonitis associated with exposure to MAC (11-13). The CT scans were assessed by two physicians and one radiologist. On chest CT, the lungs were divided into six regions: right upper lobe (RUL), right middle lobe (RML), right lower lobe (RLL), left upper lobe (LUL), lingula (Lg), and left lower lobe (LLL). Smears were graded by microscopy with fluorochrome staining from 1+ (1-9 organisms per 10 high-power fields) to 4+ (>90 organisms per high-power field) according to the ATS/IDSA statement (2, 14).

Measurement of serum GPL core IgA antibody

Measurement of serum GPL antibody levels was performed by enzyme immunoassay according to the manufacturer's instructions (Tauns Laboratory Inc., Shizuoka, Japan). The cut-off value was set at 0.7 U/ml, and levels > 0.7 U/ml were defined as positive, as reported previously (8).

Statistical analysis

Results are expressed as the mean ± SD. The significance of differences between two groups was calculated by the Mann-Whitney U-test. Correlations were assessed with Spearman's rank correlation coefficient analysis. The GPL antibody levels in lobes were compared using the Kruskal-Wallis test and Dunn's multiple comparison test as a post-hoc analysis. Statistical significance was accepted at $*p<0.05$.

RESULTS

The characteristics of group A (n=36) and group B (n=30) are shown in Table I. There were no significant differences in age, body mass index (BMI), and smoking history (pack-years). In group A, bronchial lavage was carried out for 6/36 and 1 of the 6 patients was positive for serum GPL antibody. In group B, 5/30 patients underwent bronchial lavage and 3 of the 5 patients were positive for GPL antibody. Among the mycobacterial species isolated, *M. avium - intracellulare complex* was most frequent in group B.

The main CT finding suggestive of MAC-PD was bronchiectasis in group A *versus* centrilobular changes in group B. Cavitation was more frequent in group B compared with group A (Fig. 1). GPL antibody was positive in 7/36 patients (19.4%) from group A and 22/30 patients (73.3%) from group B (using a cut-off value >0.7 U/ml).

The serum level of GPL antibody was significantly higher in group B (5.4±6.4) than in group A (0.8±1.9) ($*p=0.0002$, Fig. 2). When group B was further divided into patients with definite MAC (n=23) and patients with probable MAC (n=7), the serum level of GPL antibody was higher in the definite MAC subgroup (6.4±6.8) than the probable MAC

Table I. *Characteristics of the patients.*

Group	A	B
n	36	30
Age, years	68.3(11.8)	71.7(10.9)
M/F	17/19	15/15
BMI	21.0(3.7)	19.8(3.6)
smoking history, pack years	10.2(16.1)	15.3(21.2)
cur, ex-, never	2, 16, 18	0, 16, 14
MAC species		
M. avium		10
M. Intracellulare		5
M. avium and intracellulare		15

Patients of group A were MAC-PD suspected by CT, but negative for MAC by sputum smear, PCR and culture. Patients of group B were MAC-PD suspected by CT, and positive culture for MAC. Smoking history was shown current (cur), ex-, and never smoker. Parameters are shown as mean (±SD).

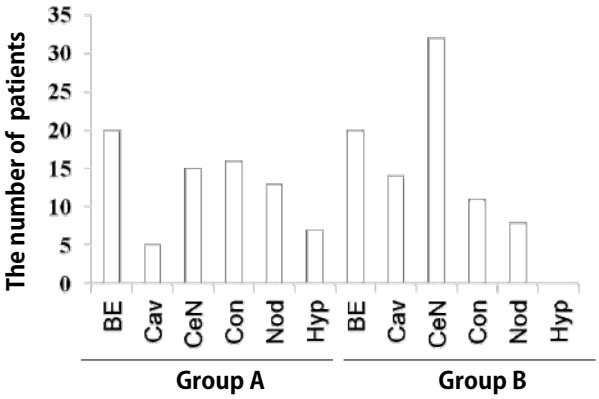

Fig. 1. *The number of patients with each chest CT feature of MAC pulmonary disease (MAC-PD) in group A (MAC-PD suspected by CT, but negative for MAC by sputum smear, PCR, and culture) and group B (MAC-PD suspected by CT and positive culture for MAC). BE: bronchiectasis; Cav: cavitation; Cen: centrilobular nodules; Con: consolidation; Nod: nodules; hypersensitivity.*

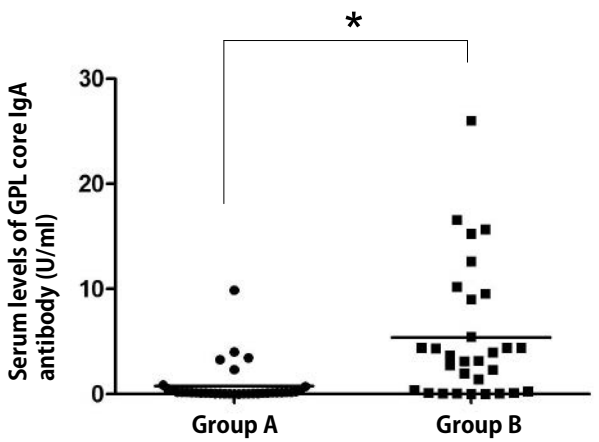

Fig. 2. *Serum levels of GPL antibody in group A (MAC-PD suspected, but negative for MAC by sputum smear, PCR, and culture) and group B (MAC-PD suspected by CT and positive culture for MAC). The antibody level was significantly higher in group B than in group A (*p=0.0002). Horizontal bars indicate mean GPL antibody levels in each group.*

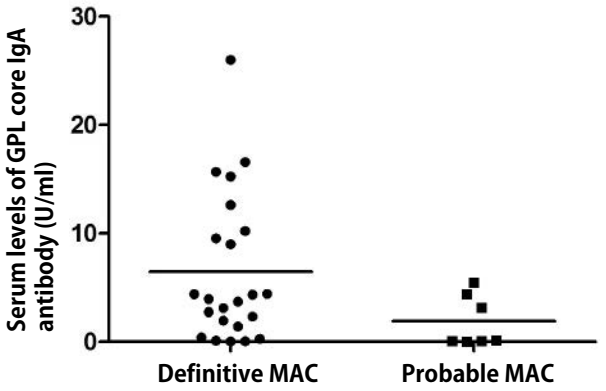

Fig. 3. *Serum levels of GPL antibody in group B patients with definite MAC-PD (23 patients meeting the criteria for MAC-PD in the ATS/IDSA statement) and group B patients with probable MAC-PD (7 patients not meeting the criteria for MAC-PD in the ATS/IDSA statement). The GPL antibody level was higher in the definite subgroup than in the probable subgroup (p=0.09) but was not statistically significant. Horizontal bars indicate mean GPL antibody levels in each group. Statistical significance: *p<0.05.*

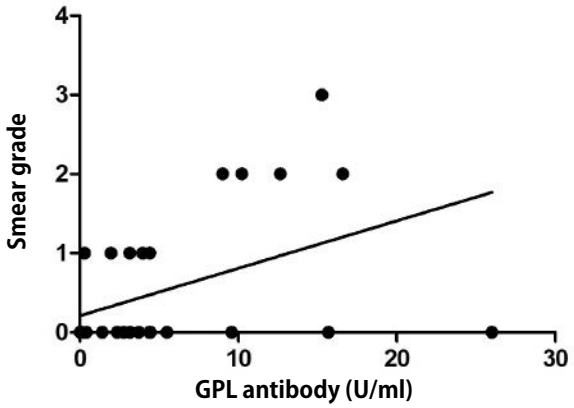

Fig. 4. *Correlation between the serum level of GPL antibody and the sputum smear grade determined by microscopy in group B. Five patients who underwent bronchial lavage had grade 0 sputum smears. There was a significant positive correlation between the serum level of GPL antibody and the sputum smear grade (r=0.43, *p=0.02).*

subgroup (1.9±2.4) (p=0.091, Fig. 3). In the definite MAC subgroup, 17/23 patients were positive for GPL antibody, and the sensitivity of this antibody for MAC-PD was 73.9% (cut-off value >0.7 U/ml). In the probable MAC subgroup, 3/7 (42.9 %) patients were positive for GPL antibody.

In group B, the serum level of GPL antibody was significantly correlated with the sputum smear

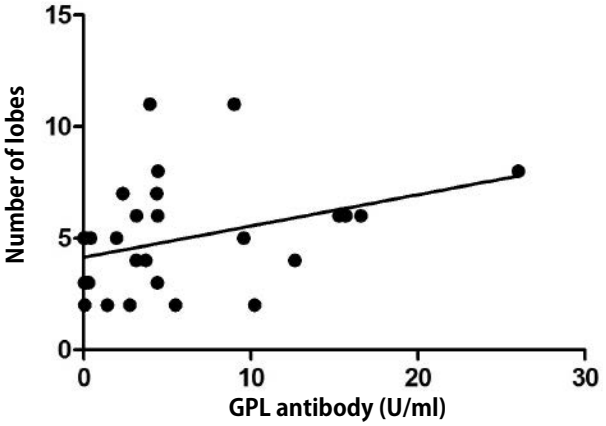

Fig. 5. *Correlation between the serum level of GPL antibody and the number of lung regions with features of MAC-PD on chest CT in group B. The lungs were divided into the following 6 regions: right upper lobe (RUL), right middle lobe (RML), right lower lobe (RLL), left upper lobe (LUL), lingula (Lg), and left lower lobe (LLL). There was a significant positive correlation between the serum level of GPL antibody and the number of lung regions showing features of MAC-PD on chest CT scans (r=0.43, *p=0.02).*

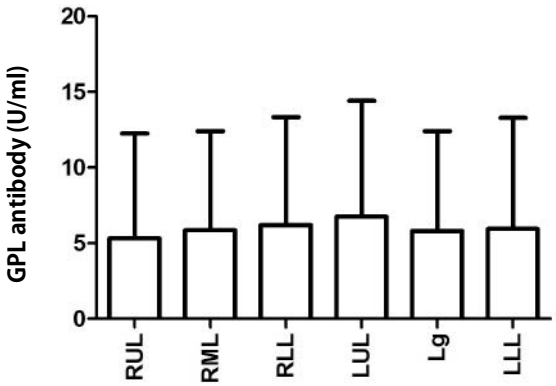

Fig. 6. *Comparison of GPL antibody levels of each lobe in group B. The lungs were divided into RUL, RML, RLL, LUL, Lg, and LLL. There were no statistically significant differences between the lobes of the serum levels of GPL antibody.*

grade (r=0.43, *p=0.02, Fig. 4). In group B, five patients underwent bronchial lavage. Before lavage, the sputum smear grade of these 5 patients was 0, so the smear grade was set as 0 when assessing its correlation with GPL antibody levels. In group B, the serum level of GPL antibody was correlated with the number of lung regions showing features of MAC-PD (r=0.43, *p=0.02, Fig. 5). GPL antibody levels were not statistically different between lobes (Fig. 6).

DISCUSSION

There are many pulmonary diseases with similar chest CT findings to MAC, including TB, diffuse panbronchiolitis, chronic obstructive pulmonary disease, sarcoidosis, interstitial pneumonia, and sometimes hypersensitivity pneumonitis (2), so it is not easy to distinguish MAC-PD from other conditions. A previous study showed that chest CT findings were related to the pathological features of MAC-PD (11).

Based on this previous report on the chest CT findings of MAC (11), the present study investigated serodiagnosis with GPL antibody in patients who had suspected MAC-PD by chest CT, but were negative for MAC by sputum smear, PCR, and culture (group A). As a result, GPL antibody was positive in 19.4% (using a cut-off value > 0.7 U/ml). It was reported that only 10 out of 100 patients who showed positive cultures for MAC were diagnosed as having MAC-PD with broncciectasis (15). GPL antibody has been proven to show a high sensitivity (84.3%) and high specificity (100%) for MAC-PD, and serodiagnosis was reported to be useful for distinguishing among MAC-PD, MAC contamination, pulmonary TB, other lung diseases, and healthy subjects (8). A considerable number of MAC-PD patients in group A showed negative culture of sputum or bronchial washings in the present study. Bronchiectasis was most frequent in group A, and MAC infection has been reported to promote the development of bronchiectasis (11, 16). Patients who are positive for GPL antibody but negative for MAC by culture need to be observed carefully, and performing further examinations such as bronchial lavage is recommended. Although GPL antibody shows a high sensitivity and specificity for MAC-PD, it has been reported that antibody levels are also high in patients with *M. abscessus* and *M. fortuitum* infection or immuno-competence (9, 17, 18). Identification of the correct species is important (19), emphasizing the need to make efforts to obtain samples and perform culture.

The present study showed that the GPL antibody level was significantly higher in culture-positive

group B than in culture-negative group A. When group B was further divided into definite MAC-PD and probable MAC-PD, the GPL antibody level was higher in the definitive MAC-PD subgroup than in the probable MAC-PD subgroup. Patients with definite MAC had positive culture results from at least two separate sputum samples or positive results from at least one sample of bronchial washings. Therefore, definite MAC-PD patients could be considered as those who were able to expectorate micro-organisms in the sputum. In contrast, probable MAC-PD patients could be considered to be those who were unable to expectorate enough sputum. The correlation between the volume of expectorated sputum and the serum level of GPL antibody was examined in group B (definite MAC-PD + probable MAC-PD combined), revealing that serum GPL antibody levels were significantly correlated with the microscopic sputum smear grade. Since the bacterial burden in clinical specimens is considered to reflect the number of bacteria seen on microscopic examination (2), GPL antibody possibly reflects the burden of MAC infecting the lungs.

In the present study, the lungs were divided into six regions (RUL, RML, RLL, LUL, Lg, and LLL) for assessing chest CT scans, which is a simple method to adopt for routine use. The serum level of GPL antibody in culture-positive group B was significantly correlated with the number of lung regions showing features of MAC-PD, however the levels were not different between lobes. This suggests that GPL antibody may reflect the extent of spread of MAC-PD, in addition to the burden of infection evaluated by sputum smear grade. Supporting this hypothesis, it has been reported that the GPL antibody level is correlated with the number of affected lung segments on chest CT (when the lungs are divided into 18 segments) and it has been suggested that further comparison of antibody levels with radiographic findings is warranted (7-9).

Some MAC-PD patients cannot expectorate enough sputum for examination, or have difficulty with bronchial washing as observed in this study. Therefore MAC contamination could not exclude probable MAC-PD in the present study. Diagnosis of NTM disease remains complicated. A skin test employing both *M. avium* sensitin and purified protein derivative from *M. tuberculosis* has been reported to be useful for distinguishing MAC from TB, and this dual skin test was also reported to be useful for avoiding misdiagnosis of latent TB (20, 21). Therefore, further diagnostic methods for MAC-PD need to be developed.

In conclusion, some patients who have chest CT findings consistent with MAC-PD are negative for MAC by culture and other patients with positive chest CT findings have insufficient positive culture results to fit the diagnostic criteria (2). Since measurement of serum GPL antibody show a high specificity for MAC-PD, a positive antibody test supports the diagnosis of this disease. The level of GPL antibody was shown to reflect the burden and spread of MAC infection in the lungs, but whether this antibody indicates the progression of MAC-PD or the response to treatment remains unknown. A recent study revealed that progressive lung disease due to MAC is associated with specific VNTR genotypes (22). Whether the GPL antibody level reflects the progression of MAC-PD in association with specific VNTR genotypes also needs to be investigated further.

ACKNOWLEDGEMENTS

The authors thank Shingaku Kaneko and the staff of the Department of Laboratory Medicine of Maebashi Red Cross Hospital for their assistance with culture and PCR testing.

REFERENCES

1. Wickremasinghe M, Ozerovitch LJ, Davies G, Wodehouse T, Chadwick M, Abdallah S, Shah P, Wilson R. Non-tuberculous mycobacteria in patients with bronchiectasis. Thorax 2005; 60:1045-51.
2. Griffith DE, Aksamit T, Brown-Elliott BA, et al. An official ATS/IDSA statement: diagnosis, treatment, and prevention of nontuberculous mycobacterial diseases. Am J Respir Crit Care Med 2007; 175:367-416.
3. Glassroth J. Pulmonary disease due to nontuberculous mycobacteria. Chest 2008; 133:243-51.
4. Chae DR, Kim YI, Kee SJ, et al. The impact of the 2007 ATS/IDSA diagnostic criteria for nontuberculous mycobacterial disease on the

diagnosis of nontuberculous mycobacterial lung disease. Respiration 2011; 82:124-29.
5. Brennan PJ, Nikaido H. The envelope of mycobacteria. Annu Rev Biochem 1995; 64:29-63.
6. Aspinall GO, Chatterjee D, Brennan PJ. The variable surface glycolipids of mycobacteria: structures, synthesis of epitopes, and biological properties. Adv Carbohydr Chem Biochem 1995; 51:169-242.
7. Kitada S, Nishiuchi Y, Hiraga T, et al. **S**erological test and chest computed tomography findings in patients with *Mycobacterium avium* complex lung disease. Eur Respir J 2007; 29:1217-23
8. Kitada S, Kobayashi K, Ichiyama S, et al. Serodiagnosis of *Mycobacterium avium*-complex pulmonary disease using an enzyme immunoassay kit. Am J Respir Crit Care Med 2008; 177:793-97.
9. Kitada S, Levin A, Hiserote M, Harbeck RJ, Czaja CA, Huitt G, Kasperbauer SH, Daley CL. Serodiagnosis of *Mycobacterium avium complex* pulmonary disease in the United States. Eur Respir J 2013; 42:454-460.
10. Shimizu Y, Dobashi K, Yoshikawa Y, et al. Five-antituberculosis Drug-resistance Genes Detection Using Array System. J Clin Biochem Nutr 2008; 42:228-34.
11. Fujita J, Ohtsuki Y, Suemitsu I, et al. Pathological and radiological changes in resected lung specimens in *Mycobacterium avium intracellulare* complex disease. Eur Respir J 1999; 13:535-40.
12. Marras TK, Wallace RJ Jr, Koth LL, Stulbarg MS, Cowl CT, Daley CL. Hypersensitivity pneumonitis reaction to *Mycobacterium avium* in household water. Chest 2005; 127:664-71.
13. Kanno K, Akai M, Kato T, Tada T, Watanabe K, Shiozaki K, Hase M. Hypersensitivity pneumonitis-like disease caused by exposure to *Mycobacterium avium* complex in bathtub water at home: a case report. Kekkaku 2012; 87:403-07.
14. Pfyffer GE, Brown-Elliott BA, Wallace RJ Jr. *Mycobacterium*: general characteristics, isolation and staining procedures, 8th ed. P.R. Murray, ed. ASM Press. Washington, DC, 2003; p532–59.
15. Swensen SJ, Hartman TE, Williams DE. Computed tomographic diagnosis of *Mycobacterium avium-intracellulare* complex in patients with bronchiectasis. Chest 1994; 105:49-52.
16. Obayashi Y, Fujita J, Suemitsu I, Kamei T, Nii M, Takahara J. Successive follow-up of chest computed tomography in patients with *Mycobacterium avium-intracellulare* complex. Respir Med 1999; 93:11-5.
17. Jeong BH, Kim SY, Jeon K, Lee SY, Shin SJ, Koh WJ. Serodiagnosis of *Mycobacterium avium* complex and *Mycobacterium abscessus* complex pulmonary disease using IgA antibodies to glycopeptidolipid core antigen. J Clin Microbiol 2013; 51:2747-9
18. Shu CC, Ato M, Wang JT, et al. Sero-diagnosis of Mycobacterium avium complex lung disease using serum immunoglobulin A antibody against glycopeptidolipid antigen in Taiwan. PLoS One 2013; 8:e80473.
19. van Ingen J. Diagnosis of nontuberculous mycobacterial infections. Semin Respir Crit Care Med 2013; 34:103-9.
20. von Reyn CF, Williams DE, Horsburgh CR Jr, Jaeger AS, Marsh BJ, Haslov K, Magnusson M. Dual skin testing with Mycobacterium avium sensitin and purified protein derivative to discriminate pulmonary disease due to *M. avium* complex from pulmonary disease due to *Mycobacterium tuberculosis*. J Infect Dis 1998; 177:730-6.
21. Larson EM, O'Donnell M, Chamblee S, Jaeger AS, Marsh BJ, Haslov K, Magnusson M. Dual skin tests with *Mycobacterium avium* sensitin and PPD to detect misdiagnosis of latent tuberculosis infection. Int J Tuberc Lung Dis 2011; 15:1504-9.
22. Kikuchi T, Watanabe A, Gomi K, et al. Association between mycobacterial genotypes and disease progression in *Mycobacterium avium* pulmonary infection. Thorax 2009; 64:901-7.

DYNAMIC CHANGES IN DNA METHYLATION STATUS IN PERIPHERAL BLOOD MONONUCLEAR CELLS FOLLOWING AN ACUTE BOUT OF EXERCISE: POTENTIAL IMPACT OF EXERCISE-INDUCED ELEVATIONS IN INTERLEUKIN-6 CONCENTRATION

P.J. ROBSON-ANSLEY[1,2], A. SAINI[3], C. TOMS[1], L. ANSLEY[1], I.H. WALSHE[4], M.A. NIMMO[5] and J.A. CURTIN[6]

[1]Faculty of Health and Life Sciences, Northumbria University, Newcastle-upon-Tyne, UK; [2]Department of Physiological Sciences, Stellenbosch University, South Africa; [3]Department of Physiology and Pharmacology, Karolinska Institutet, Sweden; [4]School of Sport, University of Stirling, Stirling, UK; [5]School of Sport, Exercise and Health, Loughborough, UK; [6]The University of Manchester, Manchester Academic Health Science Centre, University Hospital of South Manchester NHS Foundation Trust, Manchester, UK

Received October 10, 2013 – Accepted May 12, 2014

The aim of the present study was to examine the relationship between interleukin (IL)-6 concentrations and DNA methylation in the peripheral blood mononuclear cells (PBMCs) of trained runners after a bout of prolonged, strenuous exercise. Eight healthy trained males completed a treadmill run at 60% vVO_{2max} for 120 min followed by a 5-km time trial in a fasted condition. Whole blood samples were taken prior to, immediately before and 24 h following exercise. From these samples, PBMCs were isolated for analysis and plasma IL-6 concentrations were measured. The methylation status of DNA extracted from PBMCs was analysed using the Illumina 27k methylation beadchip platform. Global DNA methylation status was unaltered immediately and up to 24 hours following a bout of prolonged exercise in comparison to pre-exercise. Despite no change in global DNA methylation, plasma IL-6 concentrations were significantly related to the DNA methylation status of 11 genes. Our study demonstrates that the methylome is stable, while discovering a novel link between exercise-induced increases in circulating IL-6 and the DNA methylation status of 11 individual genes. Based on our preliminary findings, the mechanisms by which changes in plasma IL-6 concentrations and DNA methylation in response to exercise interact require further study.

The molecular mechanisms involved in the physiological adaptation to exercise are not fully understood. Adaptation is predominantly driven by changes in gene expression, which may be governed by exercise-induced modifications to the epigenome (1). Epigenetics is the study of phenotypic or gene expression patterns heritable through cell division that are independent of changes in the underlying DNA sequence (2). Epigenetics has also been defined more broadly as the dynamic regulation of gene expression by sequence-independent mechanisms, including changes in DNA methylation and histone

Key words: DNA methylation, exercise, interleukin-6

Mailing address: Prof. Paula Robson-Ansley,
Faculty of Health and Life Sciences,
Northumbria University,
Newcastle-upon-Tyne,
NE1 8ST, UK
Tel.: +44 191 224 7774
e-mail: paula.ansley@northumbria.ac.uk

0393-974X (2014)

DISCLOSURE: ALL AUTHORS REPORT NO CONFLICTS OF INTEREST RELEVANT TO THIS ARTICLE.

modifications (3) that also include acetylation, ubiquitination, sumoylation and phosphorylation, all of which play central roles in silencing or activating gene expression. The present study will focus specifically on DNA methylation.

DNA methylation and transcriptional regulation

DNA methylation preferentially occurs at the C5 position of cytosines in the CG motif, forming 5'-methylcytosines that account for approximately 1% in the mammalian genome (4). In eukaryotes the presence of methylated cytosines in a gene's promoter is associated with transcriptional repression. Thus, hypermethylation of a gene's promoter CpG region acts to silence gene expression; hypomethylation of a gene's promoter CpG region on the other hand is associated with transcriptional activation (5). In addition to changes in promoter methylation, DNA methylation can repress gene expression by blocking the binding of transcription factors to enhancers. Several transcription factors can bind to a particular sequence of unmethylated DNA but cannot bind to that DNA if one of its cytosines is methylated; methylated cytosines can recruit the binding of proteins that regulate histone activity.

Whilst the epigenome is tightly regulated, studies have demonstrated that DNA methylation in both human and animal tissue can be perturbed by environmental stimuli including exercise (6). Indeed, a single exercise session has been shown to affect DNA methylation status in muscle tissue that results in gene expression changes, providing evidence for a dynamic role of DNA methylation in gene expression regulation (6). Specifically, Barrès and co-workers (6) showed that exercise could demethylate the promotor regions of genes associated with metabolic signalling such as *PGC-1α, PPAR-δ* and *PDK4*. Findings indicated that the amount of demethylation correlated with the intensity of the exercise, with individuals who had cycled with higher intensity showing the greatest gene demethylation and transcriptional activation.

It is known that exercise will elevate circulating levels of the pro-inflammatory cytokine interleukin-6 (IL-6) to a magnitude increase – depending on duration and intensity – of 100-fold over baseline (7). Previous research has shown that abnormal DNA methylation patterns are associated with chronic inflammation and altered expression of the DNA methyl transferase gene (DNMT1) with chronic exposure of cells to inflammatory mediators such as the cytokine IL-6 (8). In contrast to chronic inflammation, exercise induces an acute and transient stress to the human body. Presently, DNA methylation changes associated with acute exercise-induced elevations in IL-6 is unknown. Interleukin-6 is a pleiotropic cytokine with a wide range of biological activities (9, 10), such as support of erythropoeisis, regulation of immune system responses and generation of acute phase reactions (11) as well as having a metabolic role inducing counterregulatory hormones (12). The aim of this study was to characterise DNA methylation profile in peripheral blood mononuclear cells (PBMC) following a bout of prolonged exercise using a genome-wide approach and to evaluate the relationship between plasma IL-6 concentrations and individual gene methylation status.

MATERIALS AND METHODS

Recruitment and ethics

Eight endurance-trained males were recruited and provided written informed consent to take part in the study. All participants were free from any symptoms of illness for at least four weeks prior to, and until completion of the study. None were taking anti-inflammatory pharmaceuticals or vitamin supplements or any other medications.

Exclusion criteria included any chronic medical condition and a history of any condition resulting in a prolonged period (greater than six months) of fatigue. The study and the informed consent procedure was approved by the Northumbria University Faculty of Health and Life Sciences research ethics committee and was performed in accordance with national and international frameworks (13, 14).

Preliminary testing

Prior to completion of the main trials, participants' maximal oxygen uptake (VO_{2max}) and running velocity at VO_{2max}(vVO_{2max}) were obtained on a motorised treadmill (hp Cosmos Pulsar, Germany). Initial treadmill speed was set at 12 km•h^{-1} on a 1% gradient, and increased by 1 km•h^{-1} every three minutes until volitional exhaustion. Expired gas was measured throughout via an online breath-by-breath analyser (Cortex meta analyser 3B, Germany), and heart rate was measured during the last thirty seconds of each stage via short range telemetry (Polar RS400,

Finland) The test was considered maximal if a minimum of two of the following were fulfilled; a change in VO_2 less than 2 mL•kg^{-1}•min^{-1} across the last two stages; a minimum respiratory exchange ratio of 1.15 and a heart rate greater than 90% age predicted maximum (calculated as 220-age).

Experimental trials

To control for nutritional status, participants were asked to keep a food diary for the 24-hour period prior to their first main trial and then repeat the same food intake the day before the resting sample. Participants were instructed to abstain from exercise, alcohol and caffeine for the twenty-four hour period preceding each trial and until the final blood sample was collected the following day. On the day of the main trials, participants arrived at the laboratory at 09:00 after a twelve-hour fast during which they could consume water *ad libitum*. They were asked to empty their bladder after which their height and body mass were obtained. They were then seated for a period of ten to fifteen minutes, when a blood sample was obtained from an antecubital vein into vacutainers (PRE). Following this, participants underwent a protocol known to induce moderate elevations in circulating IL-6 concentration (15). This consisted of a two-hour run at 60% VO_{2max} interspersed with sprints at 90% VO_{2max} for the last thirty seconds of every ten minutes. On completion of the endurance run participants then completed a 5-km time trial after which a second blood sample was obtained (POST). A final blood sample was obtained the following morning, after a twelve hour fast (POST24). Laboratory environmental conditions throughout the study were 20.0±1.4°C and 38±6% relative humidity**.**

Plasma IL-6 analysis

At each blood sampling point, blood was collected in a K3EDTA coated vacutainer that was immediately centrigued for 10 min and aspirated. The supernatant was stored at -80°C until later analysis. Plasma IL-6 concentration was measured in duplicate using a commercially available high-sensitivity ELISA (R & D systems, Abingdon, UK).

Peripheral blood mononuclear cell (PBMC) sample preparation

PBMCs were isolated from blood collected in heparin tubes. DNA was extracted from the PBMCs using QIAamp® DNA Mini kit (Qiagen, Hilden, Germany) as per the manufacturer's instructions. Since the assay determines the proportion of methylated cytosine in bisulfite-converted DNA, our DNA samples were bisulfite converted prior to analysis. One ug of DNA was bisulfite-converted (EZ-96 DNA Methylation-Gold Kit™; Zymo, Orange, USA). Bi-sulfite treatment of DNA samples converts unmethylatedcytosines to uracils, whereas methylated cytosines are protected and remain cytosine. The original methylation status is subsequently established by determining whether a base at a given locus was converted to a uracil.

llumina® Infinium® Methylation Assay

Quantitative measurements of DNA methylation were determined for 27,578 CpG dinucleotides spanning 14,475 designable RefSeq genes by an Illumina approved service provider as per the manufacturer's instructions. The CpG sites were chosen by Illumina to include the promoter, 5', and 3' region of genes. In addition, CpGs sites were chosen to cover CpG islands and shores, CpG sites outside of CpG islands, as well as Disease-associated regions identified through genome wide association studies. Bisulfite-treated whole genome amplified DNA was hybridised to locus-specific DNA oligomers linked to individual bead types representing each CpG locus – the methylated (C) and the unmethylated (T). The resulting DNA methylation beta values were continuous variables between 0 and 1, representing the ratio of the intensity of the methylated bead type to the combined locus intensity.

Data analysis

Cytokine data are presented as mean ± S.D. Data was analysed using SPSS version 19. To examine the sphericity of the data, Mauchly's test of sphericity was used, with a Greenhouse-Geisser correction applied for any violations. To examine whether there was a significant increase in plasma IL-6, a one-way repeated analysis of covariance was conducted, with a Bonferroni adjustment where necessary. The accepted level of statistical significance was set at $p \leq 0.05$.

Quality control and analysis of the methylation data was conducted using the R statistical software platform and BioConductor suite of packages. Each CpG site was assessed to determine whether methylation was altered by a bout of exercise immediately and 24 hours post exercise. The analysis was carried out using LIMMA on a CpG-site by CpG-site basis, adjusting for CHIP to account for any batch effects. Multiple testing was adjusted for using the Benjamini-Hochberg method. The Database for Annotation, Visualization and Integrated Discovery (DAVID) v6.7 was used to identify enriched Kyoto Encyclopedia of Genes and Genomes (KEGG) pathways (16). In addition, Ingenuity pathway analysis (IPA; www.ingenuity.com; a curated database of the relationships between genes obtained from published articles, and genetic and expression data repositories) was used to identify biological pathways common to genes with altered methylation ($p<0.001$, before adjusting for

multiple testing) immediately and 24 hours post exercise. Pathways common to genes whose methylation status was associated with circulating IL-6 were looked for. IPA determined whether the associated CpG sites were significantly enriched in a specific biological function or network by assessing direct or indirect interactions. Significance was assigned if right-tailed Fisher's exact test p-value <0.05.

RESULTS

All subjects completed the exercise trial with mean (±S.D.) age 25±4 years, height 180±5 cm, weight 77±9.8 kg and VO_{2max} 53±6 mL•kg^{-1}•min^{-1}. During the two-hour run, mean exercise intensity was 70±5% of VO_{2max} while mean heart rate was 154±9 beats•min^{-1} and rating of perceived exertion was 11±2 during the pre-load. The time trial was completed in a mean time of 1541±315 s, mean heart rate during the time trial was 173±14 beats•min^{-1} and rating of perceived exertion was 16±1.

There was a significant elevation in plasma IL-6 levels immediately following the bout of prolonged exercise, which returned to baseline by 24-h post-exercise ($F=30.190$, $p\leq0.05$) (Fig. 1). A bout of prolonged exercise did not alter the methylation status of any CpG site immediately post-exercise nor 24 h post-exercise ($p>0.05$, after adjusting for multiple testing). Mild degrees of fluctuation in global methylation status were observed with exercise but after adjusting for multiple testing these effects were not statistically significant (Fig. 2, A and B). Interestingly, there was more fluctuation immediately post exercise than 24 hours post exercise (Fig. 2, A and B). Immediately post exercise, 53 CpG sites had altered methylation (unadjusted $p=0.001$), however none were significant after adjusting for multiple testing. We used DAVID to identify enriched KEGG pathways among these genes and found none, indicating that this variation may either be false positives or perhaps random fluctuation. No individual CpG site differed 24 hours after exercise (unadjusted $p<0.001$).

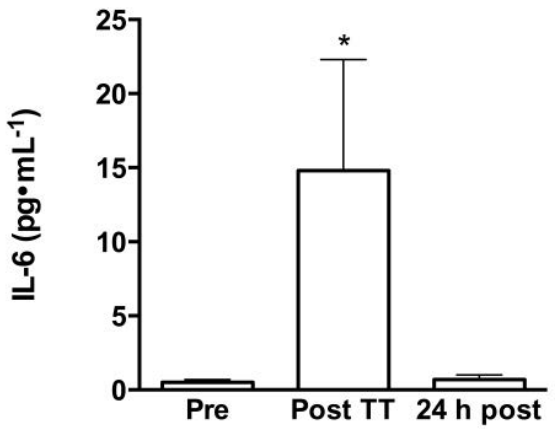

Fig. 1. *Changes in plasma IL-6 concentrations with exercise. Plasma IL-6 levels (pg•mL^{-1}) before (PRE), immediately following (Post TT) and 24 hours after (24 h post) a bout of prolonged exercise. Plasma IL-6 levels increased immediately following the bout of prolonged exercise and then returned to baseline 24 h post-exercise ($F=30.190$, $p\leq0.05$). *Significantly higher than Pre and 24 h post ($p<0.005$).*

In contrast, 114 CpG sites showed a correlation between IL-6 protein levels and methylation of CpG sites (unadjusted $p=0.001$). Eleven of these CpG sites and IL-6 protein concentrations (Figs. 2C, 3A, 3B and Table I) ($p\leq0.05$) were still significant after adjusting for multiple testing with a trend towards significance for a further seven CpG sites ($p=0.06$) after adjusting for multiple testing. Although the fold changes (Table I) were small, there is a clear relationship between IL-6 protein levels and individual CpG site methylation (Table I; Fig. 3, A and B). DAVID identified enriched KEGG pathways among the top 114 genes including the "T cell receptor signalling pathway" ($p=0.01$); "leukocyte transendothelial migration" ($p=0.02$); "natural killer cell mediated cytotoxicity" ($p=0.02$); "primary immunodeficiency" ($p=0.03$) and "systemic lupus erythematosus" ($p=0.05$).

We used IPA to investigate whether genes altered immediately after exercise, or when associated with circulating IL-6 (before adjusting the associations for multiple testing) shared any common biological pathways. Using IPA we identified 17 out of the top 104 genes associated with circulating IL-6 that were overrepresented in genes relating to the inflammatory response ($p=2.5\times10^{-9}$). Within these 17 genes, we also found a network of six genes (Fig. 4a); central to this network is a protein tyrosine phosphatase (PTPN6). In addition, among the top 50 genes whose methylation was altered immediately after exercise we generated a network of 19 interconnected proteins that play a role in infectious disease (Fig. 4b;

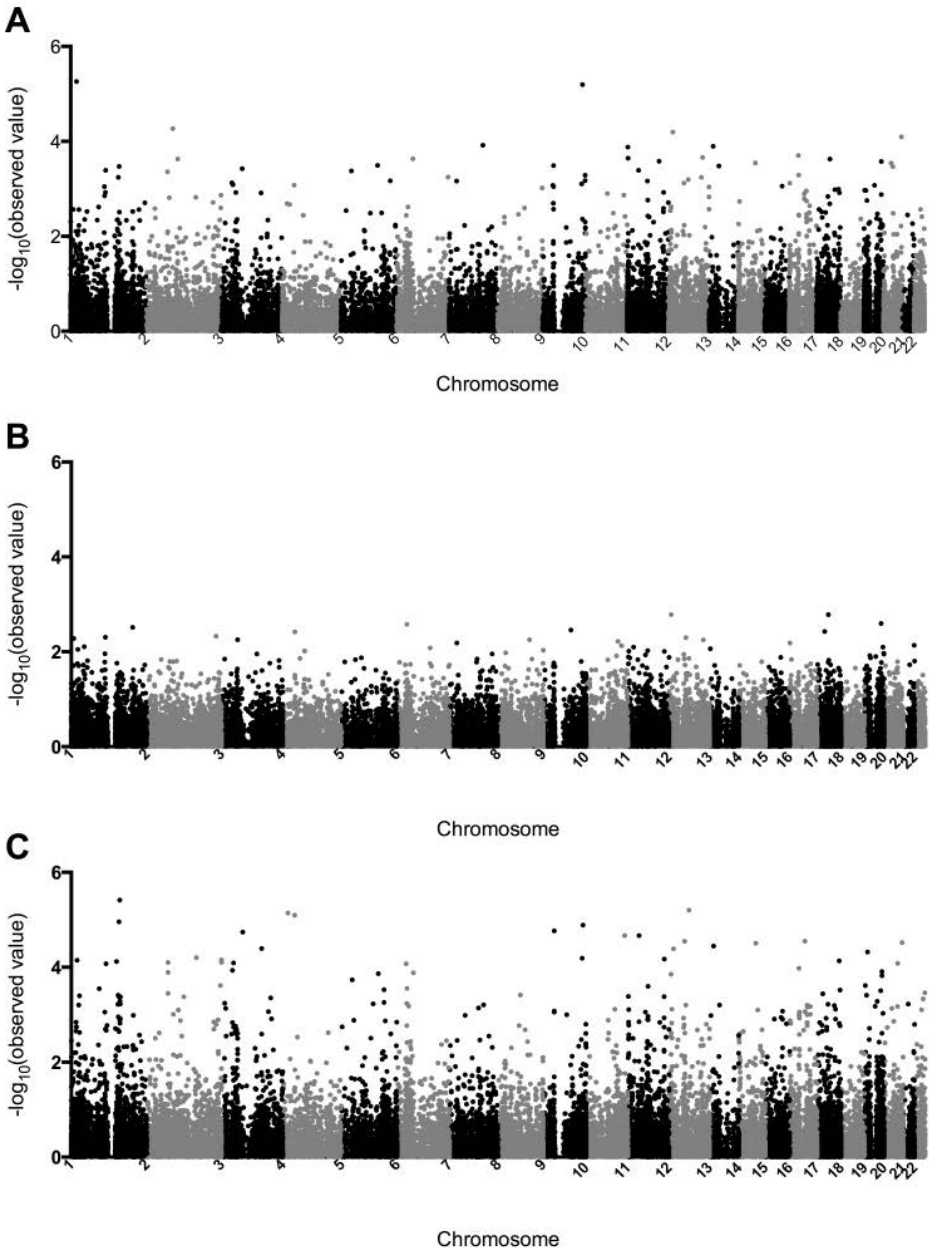

Fig. 2. *Associations between individual CpG site methylation. Comparison of DNA from PBMCs before and immediately following a bout of prolonged exercise (panel **A**); comparison of DNA from PBMCs before and 24 hours after a bout of prolonged exercise (panel **B**); levels of IL-6 proteins levels measured before, immediately after and 24 hours after a bout of prolonged exercise (panel **C**).*

Fisher's exact test p-value: $1x10^{-45}$), indicating that this network represents true relationships between these genes.

DISCUSSION

In the present study we investigated, for the first time, the effect of an acute bout of prolonged exercise on global and specific DNA methylation status in PBMCs and exercise-induced elevations in circulating IL-6 concentration. Whilst global DNA methylation was not altered by an acute bout of exercise *per se*, a relationship was determined between site-specific changes in DNA methylation

Table I. *CpG sites correlated IL-6 concentration.*

CpG site	Chromosome	Position	Gene	GENE_ID	Adjusted P-value	Fold Change	Correlation R^2
cg20535085	1	158883228	SLAMF1	6504	0.05	1.02	0.743
cg20395892	12	64869047	IRAK3	11213	0.05	0.99	-0.779
cg03368758	4	16509831	LDB2	9079	0.05	0.98	-0.732
cg02131853	4	38711032	TMEM156	80008	0.05	1.02	0.766
cg11921829	1	156013554	FCRL2	79368	0.05	0.98	-0.768
cg08999352	9	129587031	CDK9	1025	0.05	0.99	-0.743
cg15518883	9	35640561	SIT1	27240	0.05	1.02	0.759
cg14870461	3	69144793	AER61	285203	0.05	0.98	-0.704
cg23324787	11	36576270	RAG2	5897	0.05	1.02	0.726
cg09419900	10	124729456	C10orf89	118672	0.05	0.99	-0.729
cg02992767	X	135557639	CD40LG	959	0.05	1.01	0.717
cg23580000	16	48879657	ADCY7	113	0.06	0.98	-0.803
cg22566906	12	50685980	GRASP	160622	0.06	0.99	-0.685
cg09076077	20	58063710	C20orf197	284756	0.06	0.98	-0.647
cg22143352	14	74967594	JDP2	122953	0.06	0.99	-0.740
cg12836863	13	31787023	BRCA2	675	0.06	0.98	-0.707
cg18303397	3	130642825	MBD4	8930	0.06	1.02	0.721
cg00431549	12	14930292	MGP	4256	0.06	0.98	-0.713

Table II. *Functional properties of encoded proteins, whose gene methylation is associated with Il-6 protein levels.*

Gene	Encoded protein	Functional properties of encoded protein
SLAMF1	Signalling lymphocytic activation molecule	Induce proliferation and immunoglobulin synthesis by activated human B cells.Important for regulation of T-B cell interaction (22).
IRAK3	Interleukin-1 receptor-associated kinase	A key inhibitor of inflammation in association with obesity and metabolic syndrome [23].
LDB2	LIM domain binding 2	Capable of binding to a variety of transcription factors and are likely to function at enhancers to bring together diverse transcription factors. Plays a role in cell migration and normal neuronal development (23).
TMEM156		Unknown
FCRL2	FC receptor-like 2	Transmembrane protein expressed by memory B cells with a potentially negative immunomodulatory function (24).
CDK9	Cyclin-dependent kinase 9	CKD family members are important cell cycle regulators – CKD9 specifically involved in neutrophil lifespan and inhibiting apoptosis (25).
SIT1	Signalling threshold-regulating transmembrane adapter 1	Important modulator of TCR-mediated signalling that regulated T-cell activation, homeostasis and tolerance (26)
AER61		Unknown
RAG2	Recombinant activating gene 2	Involved in the initiation of V(D)J recombination during B and T cell development (27).
C10orf89		Unknown
CD40LG	CD40 ligand	Expressed on the surface of T cells. Involved in regulation of B cell function by engaging CD40 on to B cell surface (28).
ADCY7	Adenylate cyclase 7	Catalyses the formation of cyclic AMP from ATP and is inhibitable by calcium. Involved in modulation of mood and identified as a risk factor for depression (29).
GRASP/GRP1	General receptor for phosphoinositides 1-associated scaffold protein	A molecular scaffold protein linking receptors to neuronal proteins (30).
C20orf197		Unknown
JDP2	Jun dimerization protein 2	Involved in inducing cellular senescence and suppressing adipocyte differentiation by regulating histone modification (31).
BRCA2	Breast cancer 2	This gene is involved in maintenance of genome stability, specifically the homologous recombination pathway for double-strand DNA repair. BRCA2 is considered a tumour suppressor gene, gene mutations associated with risk of breast or ovarian cancer (32).
MBD4	Methyl-CpG binding domain 4	Mediates biological consequences of methylation signal and may have some function in DNA repair (33).
MGP	Matrix GLA protein	Matrix Gla protein (MGP), an inhibitor of calcification, limits calcium phosphate deposition in the vessel wall – play a role in prevention of coronary heart disease, hypertension (34).

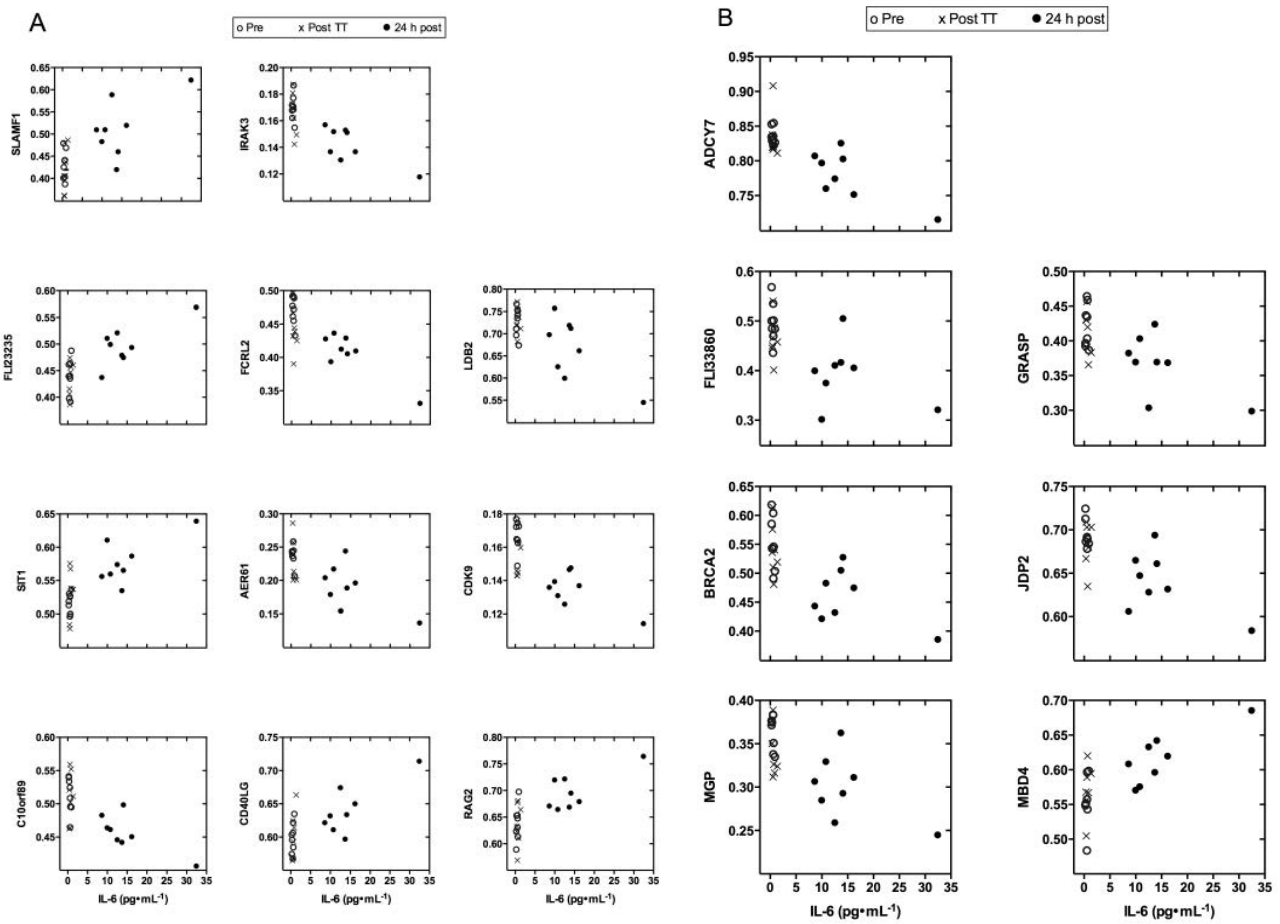

Fig. 3. *IL-6 protein levels and methylation of genes. Individual plots of IL-6 protein levels and methylation of genes that were significantly (panel **A**) and closely (panel **B**) associated with IL-6 proteins following a genome wide methylation scan (Table I). The x-axes represent methylation (beta values ~ intensity of the methylated bead type / combined locus intensity) of individual CpG sites for the corresponding genes (see Table I). The y-axis represents of IL-6 protein levels (pg□mL^{-1}): pre (open circles); post (crosses); and 24 h post (closed circles) a prolonged bout of exercise.*

of CpG sites in 11 individual genes (Table I) and exercise-induced IL-6 protein levels. These findings suggest that changes in the DNA methylation pattern may have some regulatory role on IL-6 levels following an acute bout of prolonged exercise.

Although the biological role of some of these CpG sites in relation to IL-6 activity has yet to be determined, some of the genes (descriptions of proposed functional properties of encoded proteins provided in Table II) are involved in inflammatory processes and are suggested to play a role in diseases associated with inflammation. For example, we observed that methylation of IRAK3, a key inhibitor of inflammation associated with obesity and metabolic syndrome (17), was inversely associated with plasma IL-6 concentrations. In our study, we showed that acute transient increases in IL-6 during exercise were associated with demethylation of IRAK3, potentially impacting upon transcriptional expression. The consequence of elevated IRAK3 being regulation of plasma IL-6.

A similar observation was evident between MGP methylation status and IL-6 concentration; MGP acts as an inhibitor of calcium deposition in vessel walls and plays a role in the prevention of coronary heart disease (18). Matrix Gla protein, synthesised by chondrocytes and vascular smooth muscle cells, has been shown to be a strong inhibitor of vascular

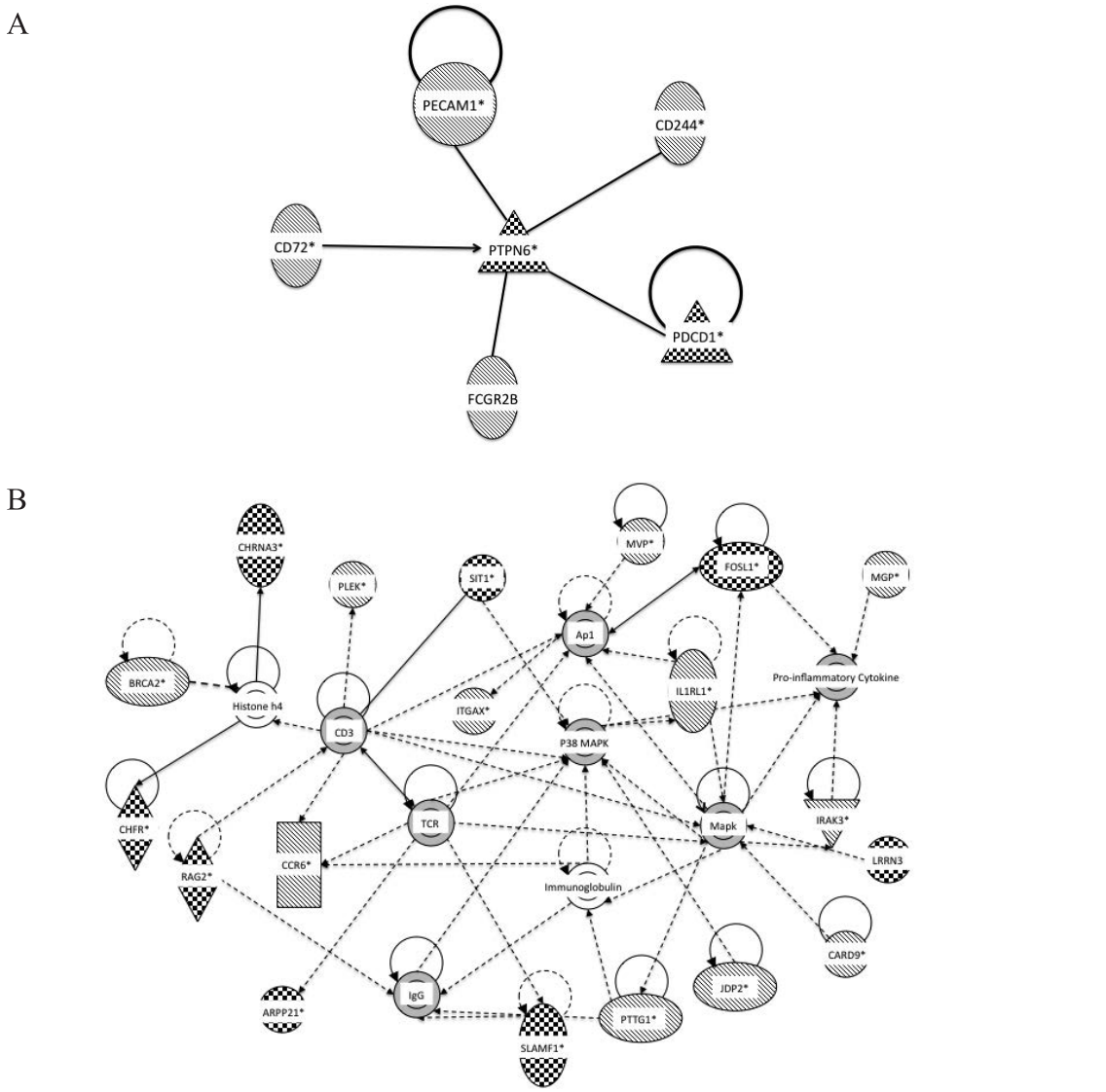

Fig. 4. *Pathway analysis of associated genes. We found a limited number of CpG sites were associated with circulating IL-6, and none were altered immediately after exercise after adjusting for multiple testing. We used IPA to assess if genes that were associated with our outcomes of interest (before adjusting for multiple testing) were enriched in biological pathways. Using IPA we identified that 17out of the top 104 genes associated (before adjusting for multiple testing) with circulating IL-6 that were overrepresented in genes relating to the inflammatory response. Within these 17 genes, we identified a network of 6 genes known to be related to the inflammatory response (panel **A**). We also found that nineteen out of the top fifty genes whose methylation status was altered immediately after exercise (before adjusting for multiple testing) were enriched in networks important in Infectious disease (panel **B**). The genes with diagonal stripes have increased methylation and those with checkered patterns have decreased methylation. The genes in grey are those whose methylation was not altered after exercise but are shown to complete pathway links. Proteins are depicted as nodes in various shapes representing the functional class of the protein. Lines depict the biological relationships between nodes. Circular lines or arrows represent self-regulation.*

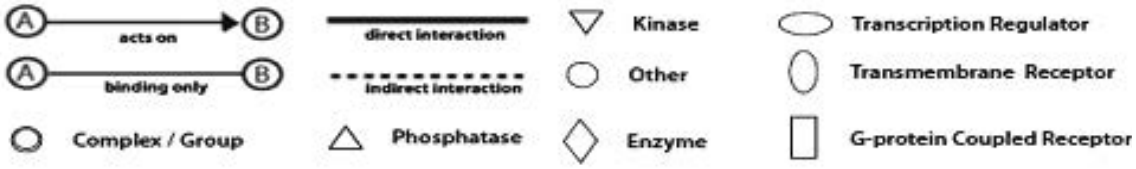

calcification (19). Inflammatory processes play an important role in the development of adverse vascular events and have been associated with cytokines, namely IL-6, tumour necrosis factor-α (TNF-α) as well as C-reactive protein (19). Our data suggest that elevations in IL-6 concentration are associated with demethylation (activation) of the MGP gene as a potential mechanism to protect the vasculature from elevated levels of IL-6. We propose that these 'dynamic' changes in the methylation status of genes such as IRAK3 and MGP are essential for appropriate regulation of IL-6 and physiological responses mediated by the cytokine following an acute bout of exercise. Whilst our findings indicate that overall an acute bout of exercise does not affect methylation globally, a novel finding itself, we were able to correlate the methylation status of individual genes to IL-6 concentrations and tentatively suggest that the acute effects of exercise on methylation may be site-specific.

These findings suggest that the epigenome is dynamic and can change due to environmental exposures/stressors such as exercise. The effects of short-term versus chronic alterations in the inflammatory environment on DNA methylation/ gene expression and physiological changes warrant further study and were not the scope of the present investigation.

Research demonstrates that epigenetic factors, including DNA methylation, are influenced by the environment (20); our data suggests that this can happen with relatively short exposure to environmental stimuli such as exercised-induced elevations in circulating IL-6 concentrations. Relationships were only found between IL-6 and 11 CpG sites despite evaluating 27,578 CpG dinucleotides spanning 14,000 genes, therefore caution should be exercised when interpreting the physiological relevance of these findings. In addition, DAVID pathway analysis demonstrated that the top 114 associated genes (before adjusting for multiple testing) are enriched for pathways important in the immune response such as the "T cell receptor-signalling pathway". In addition, Ingenuity pathway analysis demonstrated that genes associated with circulating IL-6 and altered immediately after exercise were enriched in genes important in the inflammatory response and infectious disease. Indeed, exercise does induce stress on the human body, resulting in an immune response (21) and IL-6 elevation (10). Therefore it would be expected that gene pathways associated with the immune response, including "leukocyte transendothelial migration", "natural killer cell mediated cytotoxicity" and "infectious disease", be enriched due to their functional interaction with cytokine processes.

In the present study, we found associations between elevated protein concentrations of IL-6 and altered methylation of genes that potentially regulate IL-6 and the inflammatory response, such as IRAK3or, potentially act downstream of increasing plasma IL-6, such as MGP, that protect the vasculature from adverse inflammatory processes. We suggest further studies to include mRNA expression analysis of IRAK3 and MGP genes associated with methylation and demethylation in response to exercise to confirm interaction with IL-6. These were not within the scope of the present study but warrant further exploration.

Presently, we cannot draw a conclusion as to whether differential IL-6 expression is a consequence rather than a cause of changes in methylation. It is not clear whether changes in DNA methylation subsequently regulate IL-6 production or altered IL-6 levels change the methylation of some gene promoters. It is plausible that there may be synergistic interaction between DNA methylation changes and IL-6 concentrations.

In summary, our study provides novel data suggesting that exercise-induced temporal increases in systemic IL-6 concentration are associated with dynamic alterations in DNA methylation status in certain genes, although the physiological relevance of these preliminary findings requires further study. Nonetheless, the data add support to the growing body of research indicating the potential impact of the external environment on DNA methylation in humans, which may provide an intermediate step between environment and chronic lifestyle-associated diseases.

ACKNOWLEDGEMENTS

The research was supported by the National Institute for Health Research (NIHR) Diet, Lifestyle & Physical Activity Biomedical Research Unit

based at University Hospitals of Leicester and Loughborough University.

The views expressed are those of the authors and not necessarily those of the NHS, the NIHR or the Department of Health. The authors were fully responsible for conducting the trial and analysing the data.

REFERENCES

1. Zhang FF, Cardarelli R, Carroll J, et al. Physical activity and global genomic DNA methylation in a cancer-free population. Epigenetics 2011; 6(3):293-9.
2. Berger SL, Kouzarides T, Shiekhattar R, Shilatifard A. An operational definition of epigenetics. Genes Dev 2009; 23(7):781-3.
3. Jaenisch R, Bird A. Epigenetic regulation of gene expression: How the genome integrates intrinsic and environmental signals. Nat Genet 2003; 33(S):245-54.
4. Yoder JA, Bestor TH. A candidate mammalian DNA methyltransferase related to pmt1p of fission yeast. Hum Mol Genet 1998; 7(2):279-84.
5. Anderson OS, Sant KE, Dolinoy DC. Nutrition and epigenetics: An interplay of dietary methyl donors, one-carbon metabolism and DNA methylation. J Nutr Biochem 2012; 23(8):853-9.
6. Barrès R, Yan J, Egan B, et al. Acute exercise remodels promoter methylation in human skeletal muscle. Cell Metab 2012; 15(3):405-11.
7. Robson-Ansley P, Walshe I, Ward D. The effect of carbohydrate ingestion on plasma interleukin-6, hepcidin and iron concentrations following prolonged exercise. Cytokine 2011; 53(2):196-200.
8. Hodge DR, Xiao W, Clausen PA, Heidecker G, Szyf M, Farrar WL. Interleukin-6 regulation of the human DNA methyltransferase (HDNMT) gene in human erythroleukemia cells. J Biol Chem 2001; 276(43):39508-11.
9. Robson-Ansley P, Barwood M, Canavan J, Hack S, Eglin C, Davey S, et al. The effect of repeated endurance exercise on IL-6 and sil-6r and their relationship with sensations of fatigue at rest. Cytokine 2009; 45(2):111-6.
10. Robson-Ansley P, Barwood M, Eglin C, Ansley L. The effect of carbohydrate ingestion on the interleukin-6 response to a 90-minute run time trial. Int J Sports Physiol Perform 2009; 4(2):186-94.
11. Kishimoto T. IL-6: From its discovery to clinical applications. Int Immunol 2010; 22(5):347-52.
12. Pedersen BK, Steensberg A, Fischer C, et al. The metabolic role of IL-6 produced during exercise: Is IL-6 an exercise factor? Proc Nutr Soc 2004; 63(2):263-7.
13. World Medical Association WMA. Declaration of helsinki. Ethical principles for medical research involving human subjects. 2008. Sixth Revision 2011.
14. Hull JH, Ansley P, Ansley L. Human tissue act: Implications for sports science. Br J Sports Med 2008; 42(4):236-7.
15. Walshe I, Robson-Ansley P, St Clair Gibson A, Lawrence C, Thompson KG, Ansley L. The reliability of the IL-6, sil-6r and sgp130 response to a preloaded time trial. Eur J Appl Physiol 2010; 110(3):619-25.
16. Huang DW, Sherman BT, Lempicki RA. Systematic and integrative analysis of large gene lists using DAVID bioinformatics resources. Nat Protoc 2009; 4(1):44-57.
17. Hulsmans M, Geeraert B, De Keyzer D, Mertens A, Lannoo M, Vanaudenaerde B, et al. Interleukin-1 receptor-associated kinase-3 is a key inhibitor of inflammation in obesity and metabolic syndrome. PLoS One 2012; 7(1):e30414.
18. Herrmann SM, Whatling C, Brand E, et al. Polymorphisms of the human matrix gla protein (MGP) gene, vascular calcification, and myocardial infarction. Arterioscler Thromb Vasc Biol 2000; 20(11):2386-93.
19. Wallis DE, Penckofer S, Sizemore GW. The "sunshine deficit" and cardiovascular disease. Circulation 2008; 118(14):1476-85.
20. Jirtle RL, Skinner MK. Environmental epigenomics and disease susceptibility. Nat Rev Genet 2007; 8(4):253-62.
21. Robson PJ, Blannin AK, Walsh NP, Castell LM, Gleeson M. Effects of exercise intensity, duration and recovery on *in vitro* neutrophil function in male athletes. Int J Sports Med 1999; 20(2):128-35.
22. Punnonen J, Cocks BG, Carballido JM, Bennett B, Peterson D, Aversa G, de Vries JE. Soluble and membrane-bound forms of signaling lymphocytic activation molecule (SLAM) induce proliferation and Ig synthesis by activated human B lymphocytes. J Exp Med 1997; 185(6):993-1004.

23. Storbeck CJ, Wagner S, O'Reilly P, McKay M, Parks RJ, Westphal H, Sabourin LA. The Ldb1 and Ldb2 transcriptional cofactors interact with the Ste20-like kinase SLK and regulate cell migration. Mol Biol Cell 2009; 20(19):4174-82.
24. Jackson TA, Haga CL, Ehrhardt GR, Davis RS, Cooper MD. FcR-like 2 inhibition of B cell receptor-mediated activation of B cells. J Immunol 2010; 185(12):7405-12.
25. Wang K, Hampson P, Hazeldine J, Krystof V, Strnad M, Pechan P, M J. Cyclin-dependent kinase 9 activity regulates neutrophil spontaneous apoptosis. PLoS One 2012; 7(1):e30128.
26. Arndt B, Krieger T, Kalinski T, et al. The transmembrane adaptor protein SIT inhibits tcr-mediated signaling. PLoS One 2011; 6(9):e23761.
27. Kassmeier MD, Mondal K, Palmer VL, et al. VprBP binds full-length RAG1 and is required for b-cell development and V(D)J recombination fidelity. EMBO J 2012; 31(4):945-58.
28. Liao J, Liang G, Xie S, et al. CD40L demethylation in CD4(+) T cells from women with rheumatoid arthritis. Clin Immunol 2012; 145(1):13-8.
29. Joeyen-Waldorf J, Nikolova YS, Edgar N, et al. Adenylate cyclase 7 is implicated in the biology of depression and modulation of affective neural circuitry. Biol Psychiatry 2012; 71(7):627-32.
30. Truschel ST, Zhang M, Bachert C, Macbeth MR, Linstedt AD. Allosteric regulation of GRASP protein-dependent golgi membrane tethering by mitotic phosphorylation. J Biol Chem 2012; 287(24):19870-5.
31. Huang YC, Hasegawa H, Wang SW, et al. Jun dimerization protein 2 controls senescence and differentiation via regulating histone modification. J Biomed Biotechnol 2011; 2011:569034.
32. Schlacher K, Wu H, Jasin M. A distinct replication fork protection pathway connects fanconi anemia tumor suppressors to RAD51-BRCA1/2. Cancer Cell 2012; 22(1):106-16.
33. Sjolund AB, Senejani AG, Sweasy JB. MBD4 and TDG: Multifaceted DNA glycosylases with ever expanding biological roles. Mutat Res 2012; 743-744:12-25.
34. Jia G, Stormont RM, Gangahar DM, Agrawal DK. Role of matrix gla protein in angiotensin ii-induced exacerbation of vascular calcification. Am J Physiol Heart Circ Physiol 2012; 303(5):H523-32.

ASSOCIATION BETWEEN THE EXPRESSION OF LHR, FSHR AND CYP19 GENES, CELLULAR DISTRIBUTION OF ENCODED PROTEINS AND PROLIFERATION OF PORCINE GRANULOSA CELLS IN REAL-TIME

B. KEMPISTY[1,2], A. ZIÓŁKOWSKA[1], S. CIESIÓŁKA[1], H. PIOTROWSKA[3], P. ANTOSIK[4], D. BUKOWSKA[4], M. NOWICKI[1], K.P. BRÜSSOW[5] and M. ZABEL[6]

[1]Department of Histology and Embryology, Poznań University of Medical Sciences, Poznań, Poland; [2]Department of Anatomy, Poznań University of Medical Sciences, Poznań, Poland; [3]Department of Toxicology, Poznań University of Medical Sciences, Poznań, Poland; [4]Department of Veterinary, Poznań University of Life Sciences, Poznań, Poland; [5]Institute of Reproductive Biology, Leibniz Institute for Farm Animal Biology, Dummerstorf, Germany; [6]Department of Histology and Embryology, Wroclaw Medical University, Poland

Received May 29, 2014 – Accepted July 15, 2014

The process of granulosa cell luteinization is part of the main process determining growth, differentiation and proliferation of these cells. Although the mechanisms underlying the regulation of luteinizing hormone receptor (LHR), follicle stimulating hormone receptor (FSHR) and cytochrome P450 aromatase expression in mammalian granulosa cells is well understood, still little is known about the expression of mRNA and encoded proteins in relation to cell proliferation and luteinization *in vitro*. Porcine granulosa cells were observed *in vitro* at a168-h period while undergoing real-time proliferation using an RTCA system. Furthermore, LHR, FSHR and CYP19 mRNA expression were detected using RQ-PCR after 168 h of *in vitro* culture (IVC) at 24-h intervals, and LHR, FSHR and P450arom were examined by confocal microscopic observation at 0 h, 24 h, 48 h, 96 h, and 168 h of IVC. We found increased expression of LHR and CYP19 mRNA at 24 h and 48 h of IVC compared to the other stages ($P<0.01$, $P<0.001$), whereas FSHR mRNA was higher only at 0 h ($P<0.001$). In contrast, LHR, FSHR and P450arom protein expression was significantly higher at the end of the168-h IVC period compared to 0 h, 24 h, 48 h and 96 h ($P<0.001$). LHR, FSHR and P450arom were distributed in the cytoplasm of porcine GCs at each time point of IVC. When analyzing cell proliferation, differences in cell index were observed (at least $P<0.05$) between the first (0-24 h) and the last period (144-168 h) of IVC; however, soon after 24 h of IVC a logarithmic increase in proliferation was also seen. We assume that the expression of LHR, FSHR and CYP19 mRNAs depends on the period of *in vitro* cultivation and may be linked with the luteinization process of porcine GCs. Furthermore, the patterns of mRNA and protein expression suggest a post-transcriptional regulation of LHR, FSHR and P450arom. In summary, it can be presumed that mRNA and protein expression and *in vitro* luteinization and proliferation of porcine GCs are regulated by different mechanisms, because not all of these processes are correlated.

Ovarian follicle maturation and ovulation is regulated by endocrine mechanisms that include

Key words: gene expression, granulosa cells, cell proliferation, pig

Mailing address: Bartosz Kempisty PhD,
Department of Histology and Embryology,
Department of Anatomy, Poznań University of Medical Sciences,
6 Święcickiego St.,
60-781 Poznań, Poland
Tel./Fax: +48 61 8546419 / +48 61 8546455
e-mail: etok@op.pl

0393-974X (2014)

several extracellular and intracellular interactions. Understanding these processes in more detail is a key to gaining insight into ovarian function and may be a target of pharmaceutical interventions that aim to provide new forms of fertility treatment in (domestic) animals. Since McFarland et al. and Sprengel et al. (1, 2) first cloned and sequenced the gonadotropin-related receptors, it has been recognized that gonadotropins form membrane associated receptors that are structurally related to G-protein receptors, such as TSHR and GHR (3). The first description regarding the existence of FSHR in granulosa cells (GCs) was given by Zeleznik et al. (4), who used autoradiographic analysis to examine the localization of ^{125}I-labelled FSH in rat ovarian sections. Camp et al. (5) found LHR mRNA present in the theca cells of immature follicles and in theca and granulosa cells of mature antral follicles.

Ovulation induced by pre-ovulatory estradiol and LH surge leads to activation of a gene transcription cascade in GCs. The induction of FSH and LH actions in GCs further leads to the activation of post-receptor mechanisms, which are related to a response of GC to gonadotropins. It has been shown that FSHR and LHR may be differentially expressed in GCs, which may be explained by the fact that LHR is more effectively coupled to cAMP (6). Furthermore, an LH surge during ovulation is responsible for the induction of the expression of "high-tone" cAMP-related genes that regulate GC differentiation and follicle rupture (6).

It was found that cytochrome P450 aromatase (CYP19), which is also called estrogen synthetase, catalyzes the conversion of androgens to estrogens and is involved in regulation of LHR and FSHR expression through ovulation (7-9). P450 aromatase is an enzyme that is highly expressed and its encoded protein is distributed in the ovary and placenta. Here, this enzyme participates in the regulation of reproductive functions, especially in stimulation of cell growth and differentiation (10-12). The function of P450 aromatase in the regulation of reproductive functions via activation of several growth factor-induced signaling pathways is well understood in mammals; however, the relation between GC proliferation and CYP19 expression or cellular distribution is not yet well known.

It is accepted that differentiation of GCs is regulated by endocrine and paracrine systems and related to follicle growth and development as well as to protein synthesis activity in oocytes (13). However, there is still a lack of data explaining GC ability to proliferate *in vivo* or *in vitro* that simply could be explained by a granulosa cell-cumulus cell differentiation enigma. Recently, we were able to demonstrate a link between cumulus cell proliferation and Cdk4 and Cx43 protein expression and subcellular distribution (14). We showed that oocyte-separated cumulus cells can proliferate *in vitro* using a cell proliferation index based on cell impedance measurement. However, to date there are only few published studies examining the expression of proteins that may be recognized as differentiation markers in cumulus cells, such as AMH, Slc38a3, Has2, Ptgs2, Ptx3 and Tnfaip6 (15).

The present study was aimed at finding a relationship between porcine GC proliferation and the expression of LHR, FSHR and CYP19, as well as to characterize the cellular distribution of these proteins during different periods of real-time *in vitro* cultivation.

MATERIALS AND METHODS

Animals

A total of 30 crossbred Landrace gilts with a median age of 120 days and a median weight of 98 kg were used in this study. All of the animals were kept under the same housing conditions. All of the experiments were approved by the local ethics committee.

Collection of porcine ovaries and in vitro cultivation of porcine granulosa cells (GCs)

The ovaries and reproductive tracts were recovered immediately after slaughter and transported within 10 min to the laboratory in a solution of 38°C, 0.9% NaCl. To provide optimum conditions for subsequent oocyte maturation *in vitro*, the ovaries of each animal were placed in 5% fetal bovine serum (FBS; Sigma-Aldrich Co., St. Louis, MO, USA) in PBS (15, 16). Thereafter, single follicles were opened by puncturing them using a 5-ml syringe and 20-G needle in a sterile Petri dish, and the cumulus-oocyte-complexes (COCs) and follicular fluid (FF) were recovered.

The *in vitro* cultivation medium consisted of Dulbecco's Modified Eagle's Medium (DMEM/F12, Sigma-Aldrich, USA), 2% fetal calf serum FCS (PAA, Austria), 10 mg/ml ascorbic acid (Sigma-Aldrich, USA),

0.05 µM dexamethasone (Sigma-Aldrich, USA), 200 mM L-glutamine (Invitrogen, USA), 10 mg/ml gentamicin (Invitrogen, USA), 10,000 units/ml penicillin and 10,000 µg/ml streptomycin (Invitrogen, USA). Cells were cultivated at 38.5°C under aerobic conditions (5% CO2). Once the adherent cells were more than 80% confluent, they were detached with 0.05% trypsin-EDTA (Invitrogen, USA) for 10 min and counted using a Z2 counter or cell viability analyzer (Vi-Cell XR 2.03; both Beckman Coulter, USA).

In vitro GC cultivation using a real-time cellular analyzer (RTCA)

The recovered GCs were transferred into an E-Plate 48 of a real-time cell analyzer (RTCA, Roche-Applied Science, GmbH, Penzberg, Germany), which consisted of an RTCA analyzer, an RTCA SP station and RTCA software. The GCs were then cultured in 200 µl of standard porcine IVM culture medium that consisted of Dulbecco's Modified Eagle's Medium (DMEM/F12, Sigma-Aldrich, USA), as mentioned above. The GCs were cultured for 0-168 h at 38.5°C under 5% CO_2 in air. The cultivation medium was replaced every 44 h. After each period of cultivation, the GCs were treated with trypsin (0.25% trypsin in a balanced salt solution, Sigma-Aldrich, St. Louis, MO, USA), and the collected pool of proliferating cells was used in further confocal microscopy analysis. After each cultivation period, the cell index (CI) was used to evaluate the relative and quantitative changes in electrical cell impedance. The cell status was determined using the RTCA software.

Confocal microscope analysis of protein levels and distribution in GCs

At period of proliferation (0 h, 24 h, 48 h, 96 h, 168 h), GCs were collected and fixed using acetone-methanol (1:1) for 10 min at -20ºC and washed three times in PBS/PVP (0.2%). To block non-specific binding, the samples were incubated in 3% BSA in PBS with 0.1% Tween-20 for 30 min at room temperature (RT). GCs were incubated for 1 h at RT with a goat polyclonal anti-LHR antibody (Ab) (K-15), goat polyclonal anti-FSHR Ab (N-20), and goat polyclonal anti-P450arom Ab from Santa Cruz Biotechnology (Santa Cruz, CA, USA). The antibodies were diluted 1:500 in PBS with 1.5% BSA and 0.1% Tween-20. After several washes with PBS containing 0.1% Tween-20, the samples incubated with anti-LHR, anti-FSHR and anti-P450arom primary antibodies were treated with a fluorescein isothiocyanate (FITC)-conjugated goat anti-rabbit IgG Ab diluted 1:500 in PBS with 0.1% Tween-20 for 1 hour at RT. After washing in PBS with 0.1% Tween-20, the GCs were stained with

Table I. *Oligonucleotide sequences used for RQ-PCR analysis.*

Gene	Gene accesion number	Primer sequence (5'-3')	Produkt size (bp)
CYP19	NM_214429.1	AAAGACGCAGGATTTTCACA TCTTTTGTCAGTTCACCACGT	97
FSHR	NM_214386.2	GAATTGAAAAGGCCAACAAC CTTTCAAAACTTAGTCCCACG	214
LHR	NM_214449.1	AAGCACAGCAAGGAGACCAA AAGAGGACAGTCACGTTTCC	231
ACTB	XM_003124280.3	CCCTTGCCGCTCCGCCTTC GCAGCAATATCGGTCATCCAT	69
PBGD	NM_001097412.1	GAGAGTGCCCCTATGATGCT ATGATGGCACTGAACTCCT	214
18S rRNA	AB117609	GTGAAACTGCGAATGGCTC CCGTCGGCATGTATTAGCT	105

0.1 µg/ml 4,6-diamino-2-phenylindole (DAPI, Santa Cruz Biotechnology, Santa Cruz, CA, USA) in mineral oil, mounted in an anti-fade medium on glass slides and examined by an LSN 510 confocal system with an Olympus Fluoview 10i microscope. Additionally, the GCs were stained with goat polyclonal anti-vimentin antibody (data not shown). The FITC was excited at 488 nm using an argon laser, and the emission was imaged through a 505-530 nm filter. All confocal microscopic images were analyzed using Imaris 7.2 software (BitPlane, Zurich, Switzerland).

Real-time quantitative polymerase chain reaction (RQ-PCR) analysis

Total RNA was isolated from GCs before (at 0 h) and after (24 h, 48 h, 72 h, 96 h, 120 h, 144 h, and 168 h) of IVC using an RNeasy mini column from Qiagen GmbH (Hilden, Germany). The RNA samples were re-suspended in 20 µl of RNase-free water and stored in liquid nitrogen. RNA samples were then treated with DNase I and reverse-transcribed (RT) into cDNA. RQ-PCR was conducted in a LightCycler real-time PCR detection system (Roche Diagnostics GmbH, Mannheim, Germany) using SYBR® Green I as a detection dye, and target cDNA was quantified using the relative quantification method. The relative abundance of LHR, FSHR and CYP19 transcripts in each sample was standardized to the internal standard glyceraldehyde-3-phosphate dehydrogenase (GAPDH). For amplification, 2 µl of cDNA solution was added to 18 µl of QuantiTect® SYBR® Green PCR (Master Mix Qiagen GmbH, Hilden, Germany) and primers (Table I). One RNA sample of each preparation was processed without the RT-reaction to provide a negative control for subsequent PCR.

To quantify the specific genes expressed in the GCs, the expression levels of specific oocyte mRNAs in each sample were calculated relative to PBGD and ACTB. To ensure the integrity of these results, the additional housekeeping gene 18S rRNA was used as an internal standard to demonstrate that PBGD and ACTB mRNAs were not differentially regulated in the groups of GCs. The gene for 18S rRNA expression has been identified as an appropriate housekeeping gene for use in quantitative PCR studies. Expression of PBGD, ACTB and 18S rRNA mRNA was measured in cDNA samples from isolated GCs.

Statistical analysis

A one-way ANOVA followed by Tukey's post-hoc test was used to compare the results of the real-time quantification of the proliferation index. The experiments were carried out in at least two replicates. The results quantifying the cell proliferation index were obtained using an RTCA system. The differences were considered to be significant at $*P<0.05$, $**P<0.01$ and $***P<0.001$ for the RQ-PCR and RTCA analyses and were evaluated by comparing the results obtained in five replicates of the same recovered granulosa cells. Statistical calculations were applied to the highest normalized proliferation index at each time point for each investigated group to compare the results. All statistical analyses were performed using the software program GraphPad Prism version 4.0 (GraphPad Software, San Diego, CA, USA).

RESULTS

After RQ-PCR analysis, we found an increased expression of CYP19 mRNA after 48 h of IVC compared to all other periods ($P<0.001$) and at 24 h compared to GCs before cultivation (at 0 h) ($P<0.01$) (Fig. 1A). The expression of FSHR was approximately 9-fold higher at 0 h of IVC compared to the other time points ($P<0.001$) (Fig. 1B). LHR mRNA was higher expressed at 24 h and 48 h of IVC compared to all other observed time points of IVC ($P<0.001$). Significant differences ($P<0.01$) in the LHR transcript level were also found at 48 h of IVC compared to 24 h (Fig. 1C).

We used a real-time cellular analyzer system to evaluate the proliferation index of porcine granulosa cells during 168 h of IVC (Fig. 2A). We found differences in the proliferation index at 0 h-24 h and 24 h-48 h of IVC in two of the twelve groups of replicates ($P<0.01$, $P<0.05$, respectively) (Fig. 2 B, C). When analyzing the proliferation index between 48 h-72 h of IVC we observed differences in three of the twelve groups of replicates ($P<0.05$) (Fig. 2D). Differences in two replication groups were analyzed at 72 h-96 h (Fig. 2E), 96 h-120 h (Fig. 2F) and at 144-168 h of IVC (Fig. 2H) and in three groups at 120-144 h (Fig. 2G), respectively ($P<0.05$ to $P<0.001$).

Imaris 7.2 software was used to analyze the expression and cellular distribution of LHR, FSHR and P450arom in porcine granulosa cells at 0 h 24 h, 48 h, 96 h and 168 h of real-time *in vitro* cultivation. Regarding LHR expression, we found an increased level of this protein at 168 h of IVC compared to all other time points ($P<0.001$, difference between 168 h and 0 h, 24 h, and 48 h), ($P<0.05$ between 168 h and 96 h), (Fig. 3 A-F). Similarly, FSHR expression revealed the same pattern of protein expression,

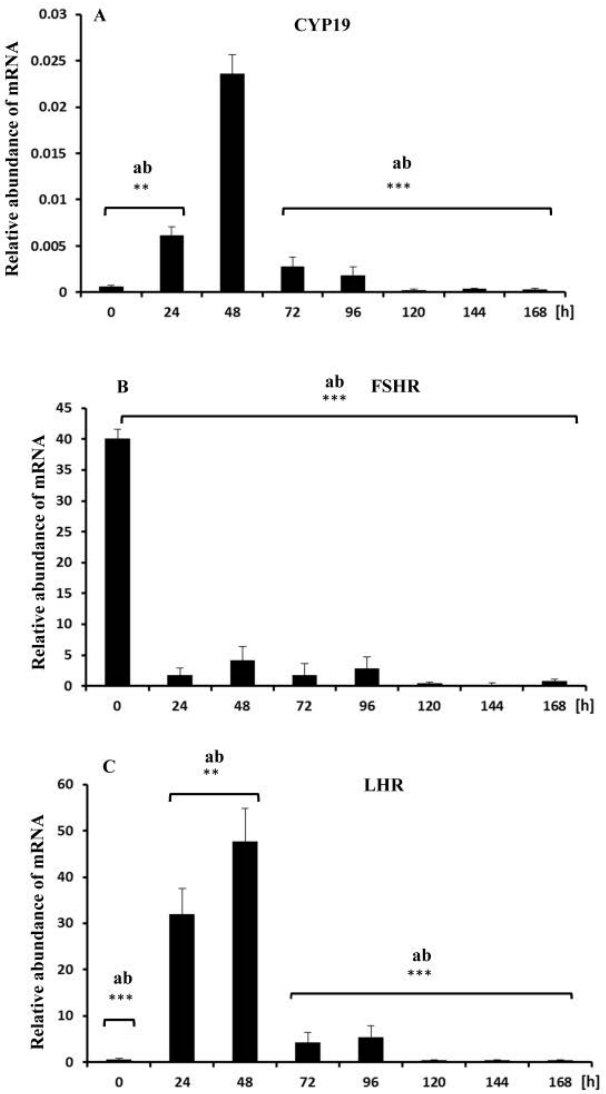

Fig. 1. *Relative abundance of CYP19, FSHR and LHR transcripts in porcine GCs analyzed before at 0 h, 24 h, 48 h, 72 h, 96 h, 120 h, 144 h and 168 h of IVC. Porcine GCs were isolated from follicles of pubertal gilts and immediately used to isolate RNA, which was reverse-transcribed into cDNA. The relative abundance of CYP19 (**A**), FSHR (**B**), and LHR (**C**) mRNAs was evaluated by RQ-PCR analysis before and after IVC. The results are presented as the mean ± SEM with the level of significance shown as * P<0.05, ** P<0.01, *** P<0.001.*

with the highest levels detected at 168 h (P<0.001, P<0.05) (Fig. 4 A-F). With regard to P450arom, we observed different expression levels between 0 h, 24 h, 48 h and after 96 h of IVC (P<0.01), between the 96 h and 168 h (P<0.05) and between the 0 h, 24 h, 48 h, 96 h levels and 168 h (P<0.001) (Fig. 5 A-F). Moreover, all of the investigated proteins were distributed in the cytoplasm rather than in the nucleus of the granulosa cells.

DISCUSSION

The granulosa cells belong to the population of ovarian cells that play a crucial role in oocyte maturation as well as having an important function during follicle growth and development. It was recently clearly demonstrated that follicular GCs and theca cells expressed LHR, FSHR and P450 aromatase on both the mRNA and protein level. However, there are conflicting results regarding how these proteins are expressed in GCs at different stages of the follicle development. There are only a few reports available that describe the expression profile and distribution of LHR, FSHR and P450 aromatase within the porcine ovary.

Mamluk et al. (18) characterized the cDNA sequence encoding bovine LHR and evaluated the effect of different luteinization protocols on the steroidogenic capacity and of LHR mRNA expression in granulosa-luteal cells. In this experiment, bovine granulosa cells were cultured with either forskolin or LH. They found that LHR mRNA was not present in luteal granulosa cells (LG), but in luteal theca cells (LT), where the expression of LHR was similar to that in forskolin- and LH-treated cells. Moreover, the expression of P450 aromatase was lower in luteal cells cultured with LH compared to those cultured with forskolin, and the differences were much more visible in LT- than in LG-cells. They concluded that LHR mRNA was primarily restricted to theca-dependent luteal cells rather than granulosa luteal cells. They also suggested that differences in LHR and P450 aromatase transcript contents indicate the existence of different mechanisms regulating the expression of mRNAs within the bovine ovary. In another study, Prochazka et al. (19) found that freshly isolated COCs displayed limited responses to LH and did not possess a sufficient number of functional LHR in porcine COCs. They also found that incubation of COCs with LH and FSH resulted in the completion of meiosis, activation of the PKA signaling pathway, expression of hyaluronan synthase 2, synthesis of hyaluronic acid and progesterone, and extensive

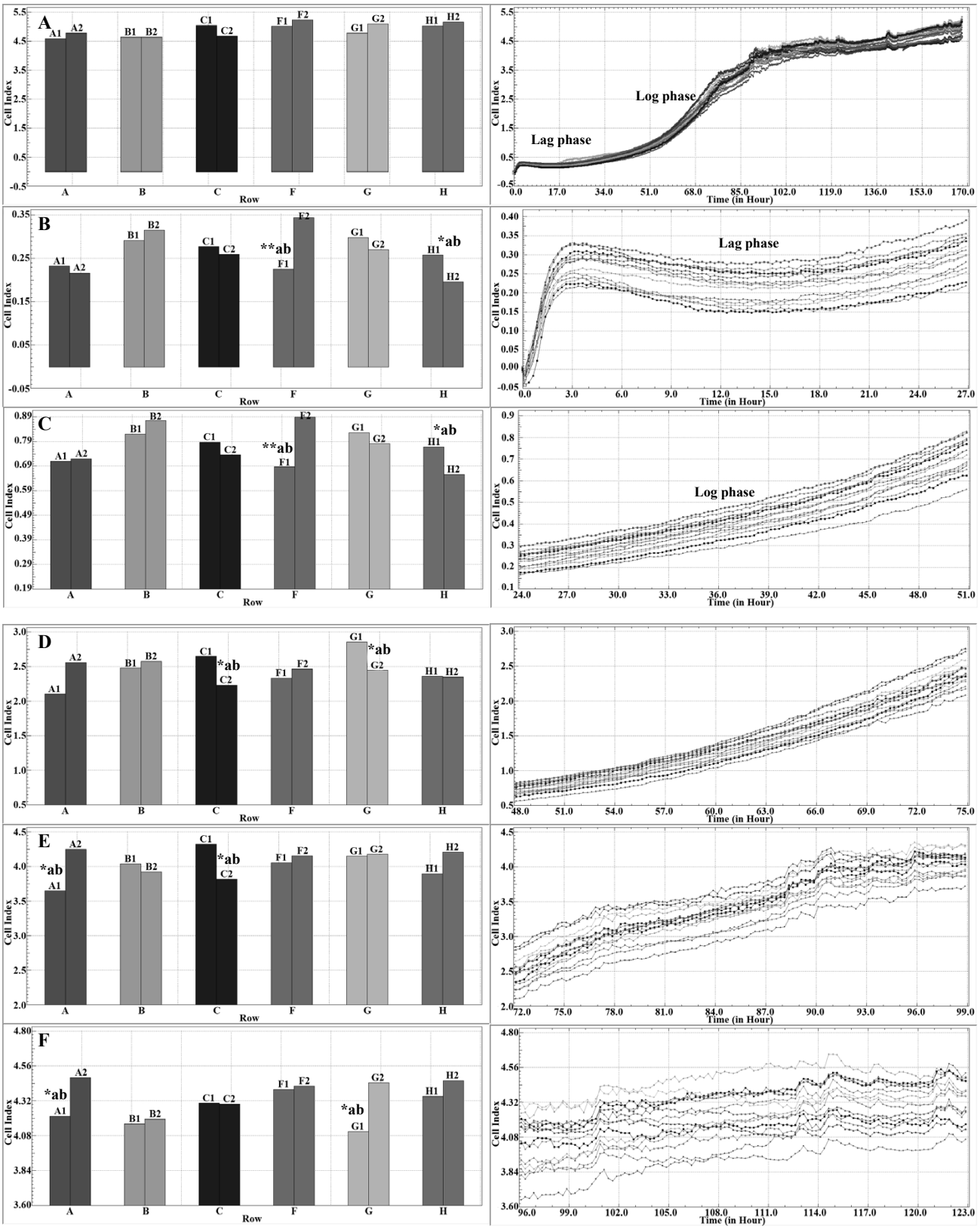
A
B
C
D
E
F
Cell Index
Row
Time (in Hour)
Lag phase
Log phase
*ab
**ab

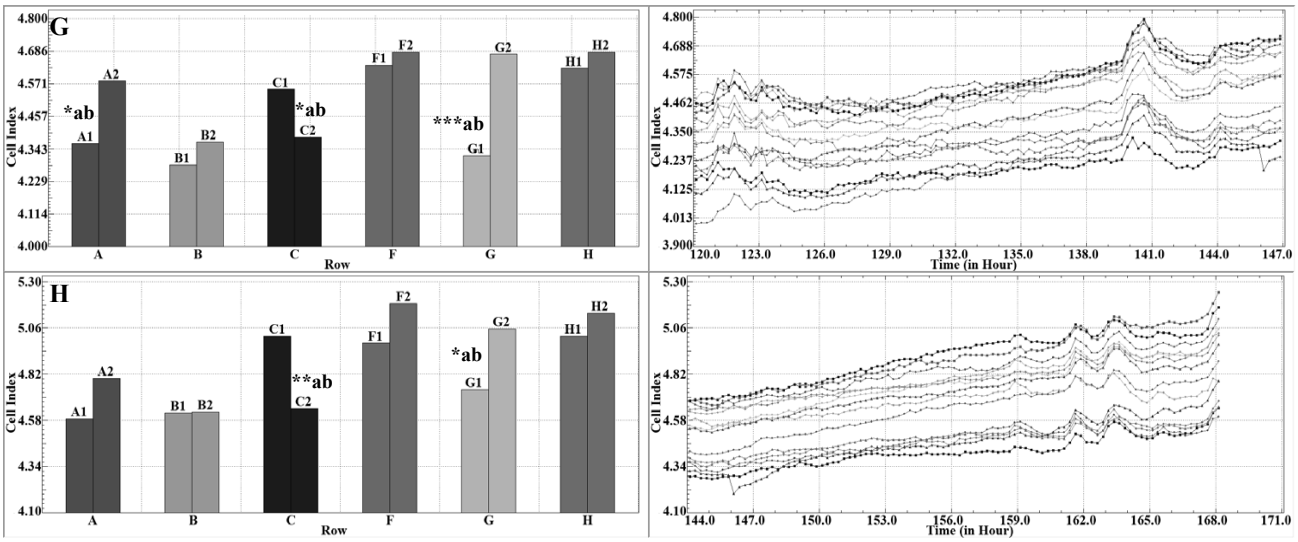

Fig. 2. *Normalized proliferation index of porcine GCs cultivated for 168 hours. Porcine granulosa cells were recovered from follicles of puberal gilts and treated with collagenase for 10 min at 38.5ºC. The cells were immediately transferred into an E-Plate 48 of a real-time cell analyzer (RTCA, Roche-Applied Science, GmbH, Penzberg, Germany). The experiment consisted of six replicates involving the cultivation of the same population of collected cells. At each step of the experiment, the normalized proliferation index was assessed for real-time in vitro cultivation for the time periods of 0-169 h (**A**), 0-24 h (**B**), 24-48 h (**C**), 48-72 h (**D**), 72-96 h (**E**), 96-120 h (**F**), 120-144 h (**G**), 144-168 h (**H**). The differences were considered to be significant at the level of $^{*}P<0.05$, $^{**}P<0.01$ and $^{***}P<0.001$. The different superscripts described significant differences (ab). At first 0-24 h (B) the cell are in lag phase. After 24-48 h the cells proliferation index is increased and the cells are in log phase (C).*

expansion of cumulus cells. It was concluded that the expression and presence of functional LHR in porcine COCs is related to the time of *in vitro* cultivation and dependent on the availability of hormones in the medium or follicular fluid. Moreover, the formation of functional LHR was dependent on cAMP pathway activation. Concordant with the results of these studies, an increased expression of LHR mRNA after 24 h and 48 h compared to the other time points of IVC was observed in our experiment. It may be assumed that a decreased expression of LHR before IVC (0 h) may be due to lack of necessary supplementation of hormones in medium during culture. The increased level of LHR expression after 24 h and 48 h of IVC, however, may be related to the process of luteinization and follicular-luteal transition of granulosa cells. At later stages of IVC, a decreased expression of LHR may reflect a lower sensitivity or susceptibility of granulosa cells in LH-dependent pathway activation.

Durlej et al. (20) looked for an association between FSHR mRNA and protein expression and antiandrogen flutamide treatment in the neonatal porcine ovary. They observed positive expression of FSHR in the oocytes, GCs of primary follicles and surface epithelium of the ovaries from both control and flutamide-treated groups. They concluded that FSHR is involved in the formation of early follicles and that androgens play a crucial role in the early stages of follicle growth and development. The role of FSHR expression in preovulatory follicle growth was recently investigated by Paradis et al. (21). They used proteomic analysis to investigate alterations in protein and gene expressions in oocytectomized cumulus cells (OOX) and found that oocyte co-culture inhibited FSHR mRNA expression in OOX and that the oocyte stimulated HSD3B transcript expression. This indicates a significant role of cumulus cells in progesterone synthesis. Cardenas and Pope (22) observed that FSHR mRNA

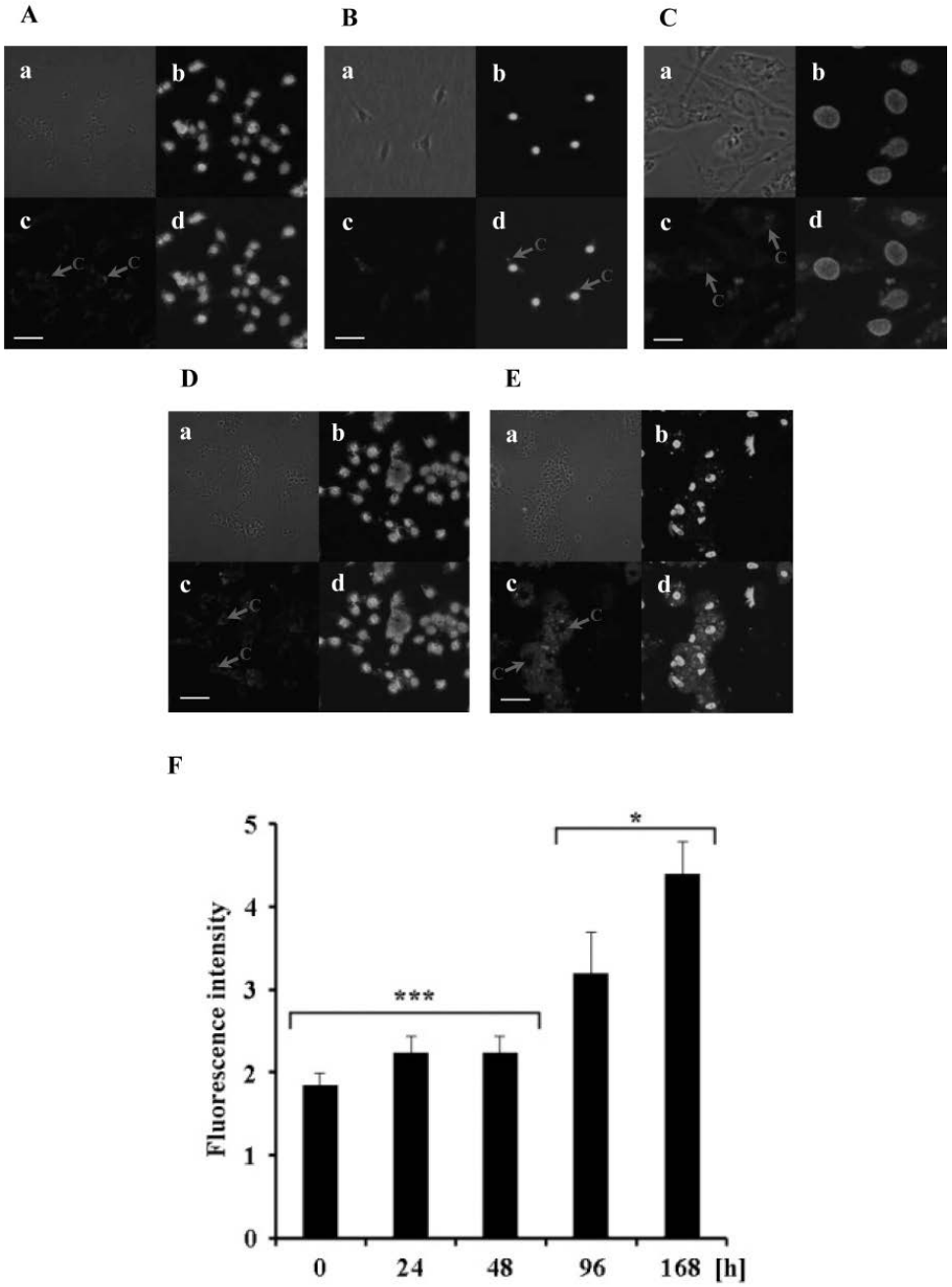

Fig. 3. *Confocal microscopic observation of LHR protein levels and cellular distribution in porcine GCs before at 0 h, 24 h, 48 h, 96 h and 168 h of IVC. The GCs that were collected before (**A**) and after 24 h (**B**), 48 h (**C**), 96 h (**D**) and 168 h (**E**) of IVC were stained with 0.1 µg/ml 4,6-diamino-2-phenylindole (DAPI; Santa Cruz Biotechnology, Santa Cruz, CA, USA) in mineral oil following staining for porcine LHR (goat polyclonal anti-LHR antibody (Ab) (K-15)). Secondary antibodies were labeled with FITC (fluorescence isothiocyanate), which emits a green fluorescent signal after excitation at 488 nm. The fluorescence intensity was measured using Imaris software. The differences were considered to be significant at P<0.05, P<0.01 and P<0.001 (**F**). GraphPad Prism version 4.0 (GraphPad Software, San Diego, CA, USA) was used for statistical calculations. All confocal microscopic images were analyzed using Imaris 7.2 (BitPlane, Zurich, Switzerland) software. The arrows indicate the cytoplasmic localization of investigated proteins in GCs in both before and after IVC. a-Nomarski, b-DAPI stained nucleus, c-antibody stained cells, d-merge. The scale bars represent 40 µm (A, B, D, E), and 20 µm (C).*

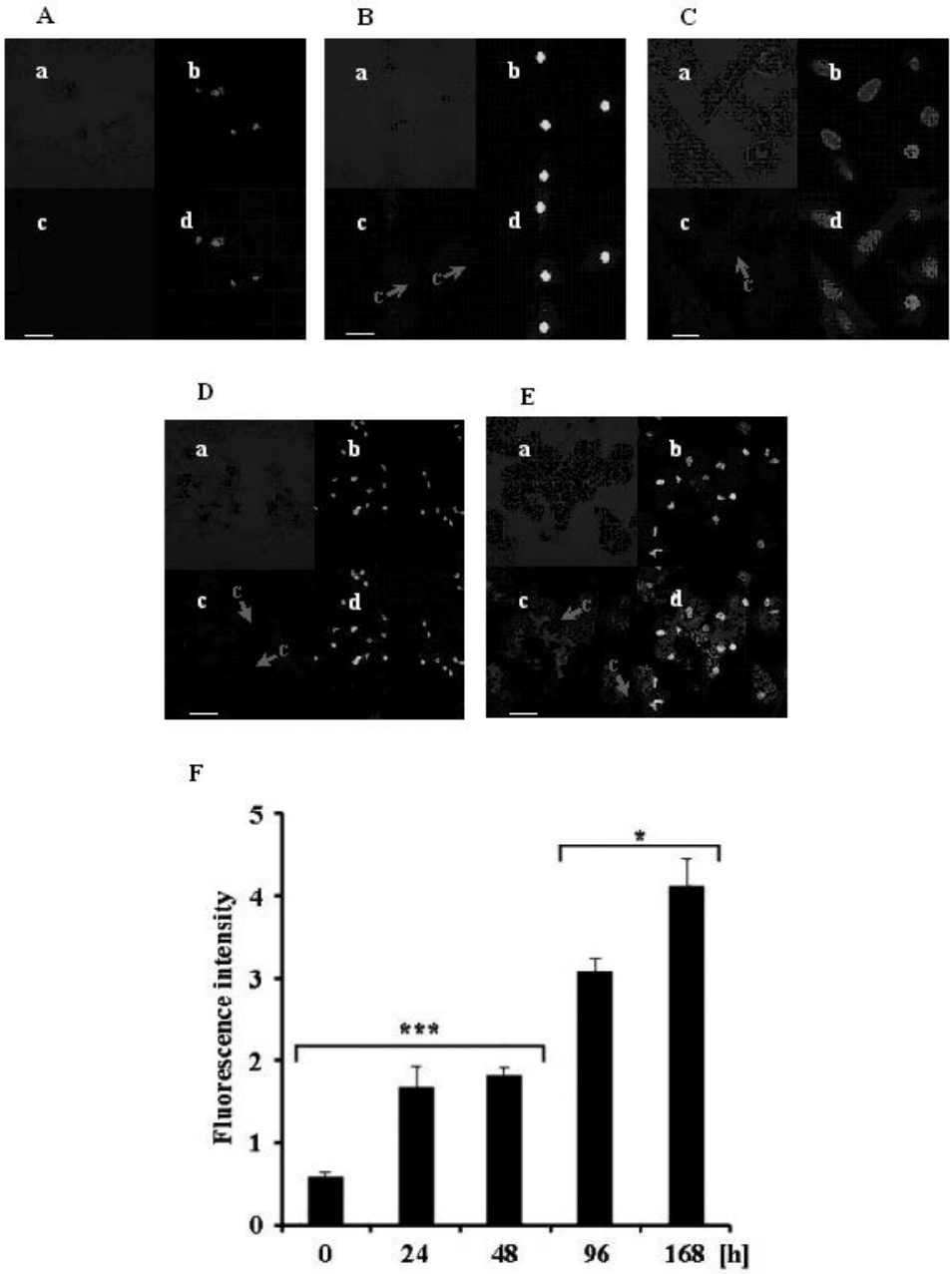

Fig. 4. *Confocal microscopic observation of FSHR protein levels and cellular distribution in porcine GCs before at 0 h, 24 h, 48 h, 96 h and 168 h of IVC. The GCs that were collected before (**A**) and after 24 h (**B**), 48 h (**C**), 96 h (**D**) and 168 h (**E**) of IVC were stained with 0.1 µg/ml 4,6-diamino-2-phenylindole (DAPI; Santa Cruz Biotechnology, Santa Cruz, CA, USA) in mineral oil following staining for porcine FSHR [goat polyclonal anti-FSHR Ab (N-20)]. Secondary antibodies were labeled with FITC (fluorescence isothiocyanate), which emits a green fluorescent signal after excitation at 488 nm. The fluorescence intensity was measured using Imaris software. The differences were considered to be significant at P<0.05, P<0.01 and P<0.001 (**F**). The arrows indicate the cytoplasmic localization of investigated proteins in GCs in both before and after IVC. a-Nomarski, b-DAPI stained nucleus, c-antibody stained cells, d-merge. The scale bars represent 40 µm (A, B, D, E), and 20 µm (C).*

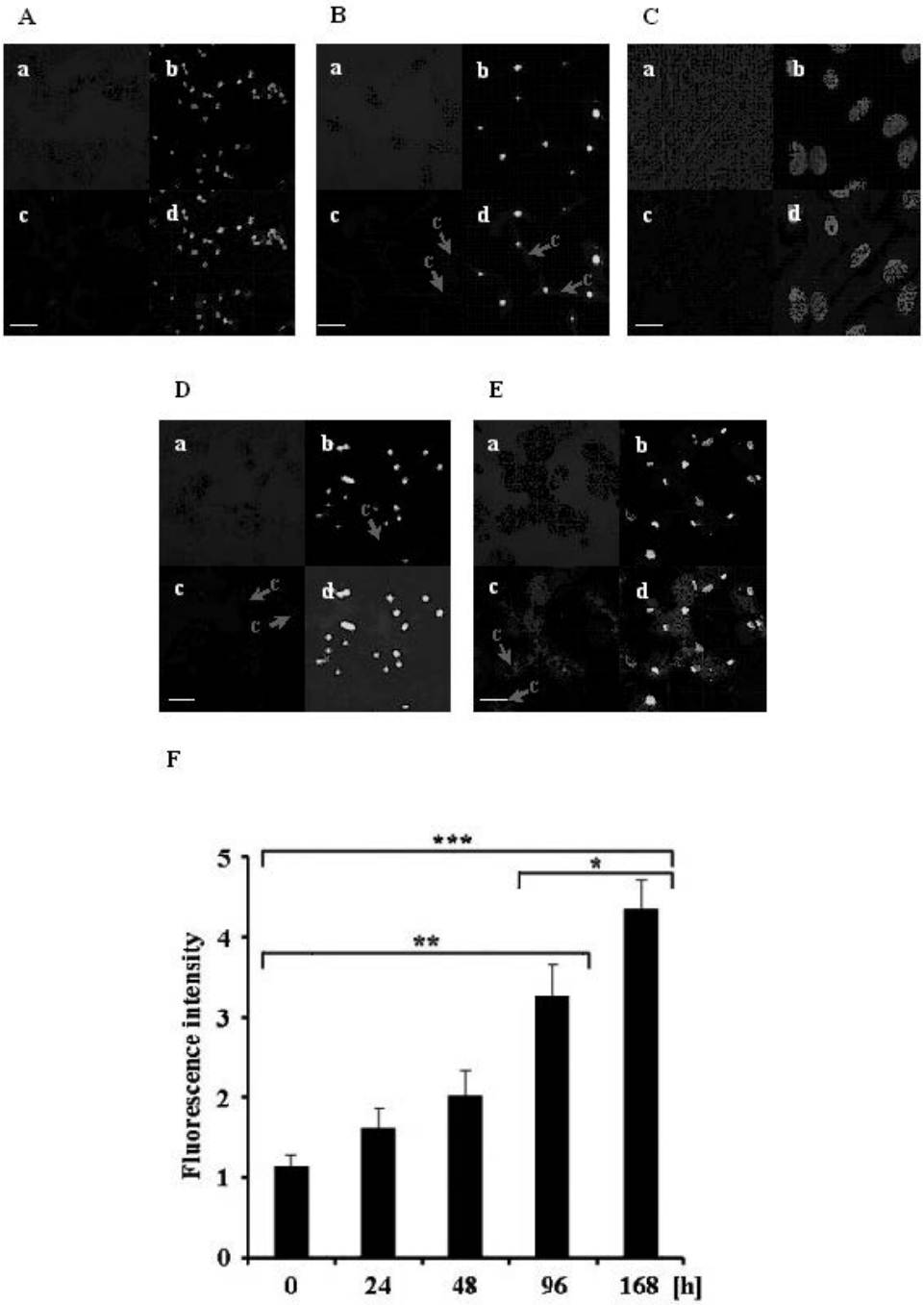

Fig. 5. *Confocal microscopic observation of P450arom protein levels and cellular distribution in porcine GCs before at 0 h, 24 h, 48 h, 96 h and 168 h of IVC. The GCs that were collected before (**A**) and after 24 h (**B**), 48 h (**C**), 96 h (**D**) and 168 h (**E**) of IVC were stained with 0.1 µg/ml 4,6-diamino-2-phenylindole (DAPI; Santa Cruz Biotechnology, Santa Cruz, CA, USA) in mineral oil following staining for porcine P450arom goat polyclonal anti-P450arom. Secondary antibodies were labeled with FITC (fluorescence isothiocyanate), which emits a green fluorescent signal after excitation at 488 nm. The fluorescence intensity was measured using Imaris software. The differences were considered to be significant at P<0.05, P<0.01 and P<0.001 (**F**). The arrows indicate the cytoplasmic localization of investigated proteins in GCs in both before and after IVC. a-Nomarski, b-DAPI stained nucleus, c-antibody stained cells, d-merge. The scale bars represent 40 µm (A, B, D, E), and 20 µm (C).*

decreased significantly in preovulatory follicles by day 19 of the estrous cycle. Our results, similar to those mentioned above, showed that the expression of FSHR mRNA was up-regulated at 0 h of IVC, when the GCs were not under the influence of external hormonal supplementation from cultivation medium. Moreover, we suppose that, contrary to the expression of LHR, the expression of FSHR mRNA in porcine GCs is decreased and unchanged during follicular growth and luteinization, respectively.

In the present study, we found a significant increase in the expression of CYP19 after 24 and 48 h of IVC. Likewise, Picton et al. (23) found that CYP19 mRNA decreased during cell luteinization after 144 h of IVC using a long-term culture of porcine granulosa cells. Moreover, using an *in vivo* and *in vitro* luteinization model, Pescador et al. (24) determined the expression of steroidogenic acute regulatory protein (StAR) and P450arom in the porcine ovary. Furthermore, they found that *in vitro* luteinization of porcine granulosa cells occurred after 96 h of IVC, during which time the P450arom transcript was present at 1 h after cell isolation but not detectable at 6 h. Furthermore, they observed that cytochrome P450 side-chain cleavage mRNA (P450scc) together with StAR expression was elevated throughout 96 h of IVC. Contrary to these observations, Garret et al. (25) found that P450arom mRNA in small non-atretic follicles decreased between days 3 and 7, which was independent of morphological and biochemical signs of atresia. Our results indicate that decreased expression of P450arom soon after 72 h of IVC may reflect the occurrence of luteinization of porcine GCs *in vitro*.

It was hypothesized that cumulus cells that surround oocytes and are responsible for oocyte-somatic cell "cross-talk", as well as granulosa and theca cells that form the follicle during development, may be connected by biochemical pathways. Moreover, it was shown by Knight and Glister (26) that cumulus cells, granulosa and theca cells are closely associated by transport of small proteins through these cells layers and by expression of specific marker genes. They found that TGFB superfamily proteins such as GDF9, BMP-2,-5,-6, BMP-4, BMP-6, BMP-7, BMP-15, AMH, inhibin and activin are commonly expressed in these three cells populations. Therefore, it may be suggested that these proteins are expressed through oocyte development and follicle growth during folliculogenesis and may also be served as markers of these three cell populations during antral follicle formation.

Our results, since conflicting with those of other studies, are the first to be performed using a quantitative real-time proliferation system. They demonstrated that the expression of LHR, FSHR and CYP19 mRNA was not correlated with GC proliferation in pigs. However, an increased expression of LHR, FSHR and P450arom proteins was detected after 168 h at the end of the IVC. These reversible mRNA and protein expression levels may be explained by alternative splicing occurring during the induction of the luteinization process of porcine GCs during IVC. It can be hypothesized further that the expression of LHR, FSHR and CYP19 mRNA depends on follicle growth (and possibly atresia) and is under hormonal control during the luteinization process of porcine GCs.

ACKNOWLEDGEMENTS

This study was made possible by grants number 2011/03/B/NZ4/02411 "OPUS" from the Polish National Centre of Science.

REFERENCES

1. McFarland KC, Sprengel R, Phillips HS, Köhler M, Rosemblit N, Nikolics K, Segaloff DL, Seeburg PH. Lutropin-choriogonadotropin receptor: an unusual member of the G protein-coupled receptor family. Science 1989; 245:494-9.
2. Sprengel R, Braun T, Nikolics K, Segaloff DL, Seeburg PH. The testicular receptor for follicle stimulating hormone: structure and functional expression of cloned cDNA. Mol Endocrinol 1990; 4:525-30.
3. Baumann G. Growth hormone-binding proteins: state of the art. J Endocrinol 1994; 141:1-6.
4. Zeleznik AJ, Midgley AR Jr, Reichert LE Jr. Granulosa cell maturation in the rat: increased binding of human chorionic gonadotropin following treatment with follicle-stimulating *hormone in vivo*. Endocrinology 1974; 95:818-25.
5. Camp TA, Rahal JO, Mayo KE. Cellular localization and hormonal regulation of follicle-stimulating

hormone and luteinizing hormone receptor messenger RNAs in the rat ovary. Mol Endocrinol 1991; 5:1405-17.
6. Richards JS, Russell DL, Robker RL, Dajee M, Alliston TN. Molecular mechanisms of ovulation and luteinization. Mol Cell Endocrinol 1998; 145:47-54.
7. Park SB, Han M. Inhibitory effects of androstenedione on endometrial cells: implications for poor reproductive outcome among women with androgen excess. Eur J Obstet Gynecol Reprod Biol 2013; 171:295-300.
8. Ptak A, Ludewig G, Robertson L, Lehmler HJ, Gregoraszczuk EL. *In vitro* exposure of porcine prepubertal follicles to 4-chlorobiphenyl (PCB3) and its hydroxylated metabolites: effects on sex hormone levels and aromatase activity. Toxicol Lett 2006; 164:113-22.
9. Karpeta A, Barc J, Ptak A, Gregoraszczuk EL. The 2,2',4,4'-tetrabromodiphenyl ether hydroxylated metabolites 5-OH-BDE-47 and 6-OH-BDE-47 stimulate estradiol secretion in the ovary by activating aromatase expression. Toxicology 2013; 305:65-70.
10. Nakamura E, Otsuka F, Inagaki K, et al. Mutual regulation of growth hormone and bone morphogenetic protein system in steroidogenesis by rat granulosa cells. Endocrinology 2012; 153:469-80.
11. Zhou P, Baumgarten SC, Wu Y, Bennett J, Winston N, Hirshfeld-Cytron J, Stocco C. IGF-I signaling is essential for FSH stimulation of AKT and steroidogenic genes in granulosa cells. Mol Endocrinol 2013; 27:511-23.
12. Hsieh M, Thao K, Conti M. Genetic dissection of epidermal growth factor receptor signaling during luteinizing hormone-induced oocyte maturation. PLoS One 2011; 6:e21574.
13. Hillier SG. Gonadotropic control of ovarian follicular growth and development. Mol Cell Endocrinol 2001; 179:39-46.
14. Kempisty B, Ziółkowska A, Piotrowska H, et al. Real-time proliferation of porcine cumulus cells is related to the protein levels and cellular distribution of Cdk4 and Cx43. Theriogenology 2013; 80:411-20.
15. Diaz FJ, Wigglesworth K, Eppig JJ. Oocytes determine cumulus cell lineage in mouse ovarian follicles. J Cell Sci 2007; 120:1330-40.
16. Al-aghbari AM, Menino AR. Survival of oocytes recovered from vitrified sheep ovarian tissues. Anim Reprod Sci 2002; 71:101-10.
17. Nascimento AB, Albornoz MS, Che L, Visintin JA, Bordignon V. Synergistic effect of porcine follicular fluid and dibutyryl cyclic adenosine monophosphate on development of parthenogenetically activated oocytes from pre-pubertal gilts. Reprod Domest Anim 2010; 45:851-9.
18. Mamluk R, Wolfenson D, Meidan R. LH receptor mRNA and cytochrome P450 side-chain cleavage expression in bovine theca and granulosa cells luteinized by LH or forskolin. Domest Anim Endocrinol 1998; 15:103-14.
19. Procházka R, Nemcová L, Nagyová E, Scsuková S, Mlynarcíková A. Development of functional LH Receptors on pig cumulus-oocyte complexes cultured *in vitro* by a novel two-step culture system. Mol Reprod Dev 2009; 76:751-61.
20. Durlej M, Knapczyk-Stwora K, Duda M, Galas J, Slomczynska M. The expression of FSH receptor (FSHR) in the neonatal porcine ovary and its regulation by flutamide. Reprod Domest Anim 2011; 46:377-84.
21. Paradis F, Moore HS, Pasternak JA, Novak S, Dyck MK, Dixon WT, Foxcroft GR. Pig preovulatory oocytes modulate cumulus cell protein and gene expression *in vitro*. Mol Cell Endocrinol 2010; 320:87-96.
22. Cárdenas H, Pope WF. Androgen receptor and follicle-stimulating hormone receptor in the pig ovary during the follicular phase of the estrous cycle. Mol Reprod Dev 2002; 62:92-8.
23. Picton HM, Campbell BK, Hunter MG. Maintenance of oestradiol production and expression of cytochrome P450 aromatase enzyme mRNA in long-term serum-free cultures of pig granulosa cells. J Reprod Fertil 1999; 115:67-77.
24. Pescador N, Stocco DM, Murphy BD. Growth factor modulation of steroidogenic acute regulatory protein and luteinization in the pig ovary. Biol Reprod 1999; 60:1453-61.
25. Garrett WM, Mack SO, Rohan RM, Guthrie HD. *In situ* analysis of the changes in expression of ovarian inhibin subunit mRNAs during follicle recruitment after ovulation in pigs. J Reprod Fertil 2000;

118:235-42.
26. Knight PG, Glister C. TGF-beta superfamily members and ovarian follicle development. Reproduction 2006; 132:191-206.

GASTROINTESTINAL SYMPTOMS IN IDIOPATHIC PULMONARY FIBROSIS PATIENTS TREATED WITH PIRFENIDONE AND HERBAL MEDICINE

Y. SHIMIZU[1,2], Y. SHIMOYAMA[3], A. KAWADA[3], M. KUSANO[4], Y. HOSOMI[5], M. SEKIGUCHI[5], T. KAWATA[1], T. HORIE[1], Y. ISHII[2], M. YAMADA[3], K. DOBASHI[6] and A. TAKISE[1]

[1]Department of Respiratory Medicine, Maebashi Red Cross Hospital, Maebashi, Gunma, Japan; [2]Department of Pulmonary Medicine and Clinical Immunology, Dokkyo Medical University School of Medicine, Mibu, Tochigi, Japan; [3]Department of Medicine and Molecular Science, Gunma University Graduate School of Medicine, Maebashi, Gunma, Japan; [4]Department of Endoscopy and Endoscopic Surgery, Gunma University Hospital Gastroenterology, Maebashi, Gunma, Japan; [5]Clinical laboratory Center, Maebashi Red Cross Hospital, Maebashi, Gunma, Japan; [6]Gunma University School of Health Sciences, Maebashi, Gunma, Japan

Received February 24, 2014 – Accepted July 25, 2014

Pirfenidone is an antifibrotic agent for patients with pulmonary fibrosis, but this drug has adverse gastrointestinal (GI) effects. The first aim of this study was to assess GI symptoms due to pirfenidone by using a new questionnaire for reflux symptoms and dismotility symptoms. Whether adding herbal medicine of rikkunshi-to improved GI symptoms due to pirfenidone therapy was also investigated. This was a randomized controlled trial performed on 17 IPF patients. The patients were assigned to two groups, and the study period was 8 weeks. The pirfenidone group received pirfenidone therapy for 8 weeks with add-on rikkunshi-to from 4 weeks, while the control group did not receive either of these agents. To assess the effects of RK, plasma levels of acyl-ghrelin and des-acyl-ghrelin, serum KL-6 and surfactant protein-D, and pulmonary function tests were monitored. GI symptoms were most severe during the initial 2 wks of pirfenidone therapy at a dose of 600 mg/day. Both reflux symptoms and dismotility symptoms deteriorated. Rikkunshi-to improved GI symptoms to the level prior to pirfenidone therapy. Plasma levels of des-acyl-ghrelin and acyl-/des-acyl-ghrelin ratio changed significantly at 8 weeks compared to 2 weeks. GI adverse events due to PFD were most severe in the first 2 weeks of treatment at a dose of 600 mg/day, and both reflux and dismotility symptoms deteriorated, but the drug was well tolerated at 1200 mg/day. Rikkunshi-to contributed to improvement of GI symptoms, but plasma ghrelin levels did not reflect the improvement of GI symptoms.

Idiopathic pulmonary fibrosis (IPF) is a specific form of chronic, progressive fibrosing interstitial pneumonia of unknown etiology that primarily occurs in older adults and has a poor prognosis (1). Until recently, there was no specific pharmacological therapy for IPF. However, 5-methyl-1-phenyl-2-[1H]-pyridone (pirfenidone: PFD; Shionogi and Co., Ltd., Osaka, Japan; Marnac Inc., Dallas,

Key words: idiopathic pulmonary fibrosis, pirfenidone, ghrelin, FSSG, rikkunshi-to

Mailing address: Yasuo Shimizu MD, PhD
Department of Pulmonary Medicine
and Clinical Immunology, Dokkyo Medical University
School of Medicine, 8 80 Kitakobayashi, Mibu,
Tochigi 321-0293, Japan
Tel.: +81 282 87 2151 Fax: +81 282 86 5080
e-mail: yasuo-s@dokkyomed.ac.jp

0393-974X (2014)

TX), a novel compound with anti-inflammatory, antioxidant, and antifibrotic effects in experimental models of pulmonary fibrosis (2, 3), has been proven to show efficacy in IPF patients (4-7). PFD has various adverse effects, including gastrointestinal (GI) symptoms, photosensitivity, rash, and dizziness, and a recent meta-analysis of randomized controlled trials showed a high rate of GI adverse events (nausea, dyspepsia, diarrhea, and anorexia) related to PFD therapy (8).

Different medications are required for two major classes of GI symptoms, i.e., reflux and dismotility symptoms. For reflux symptoms, such as heartburn and regurgitation, anti-acid therapy with proton pump inhibitors (PPIs) or H_2 receptor antagonists (H_2 blockers) is prescribed, while prokinetic agents are used for dismotility symptoms. Although various GI symptoms have been reported as adverse events due to PFD, effective drugs for these symptoms have not been identified.

Rikkunshi-to (RK) is a Chinese herbal medicine (Lin-Jun-Zi-Tang, TJ-43, Tsumura Pharmaceutical Co., Tokyo, Japan) that can be used to treat GI symptoms, including both reflux and dismotility symptoms (9, 10). One of the mechanisms by which RK improves GI symptoms is through an action on ghrelin (11).

Ghrelin is a motilin-related peptide that was discovered in the stomach where it acts as an endogenous ligand of growth hormone secretagogue receptor (GSH-R) (12). Acyl-ghrelin undergoes post-translational modification by O-n-octanoylation at serine 3, while des-acyl-ghrelin lacks O-n-octanoylation at serine 3. Acyl-ghrelin stimulates gastric antral motility and induces fasting motor activity in the duodenum, while des-acyl ghrelin decreases food intake and inhibits gastric emptying (13, 14).

As well as acting as a regulator of GI motility, ghrelin has anti-inflammatory effects, and it has been shown to attenuate sepsis-induced and bleomycin-induced lung injury in animals (15, 16).

In the present study, GI adverse events caused by pirfenidone were investigated with a new questionnaire for detection of reflux symptoms and dismotility symptoms (17). The GI medications employed by IPF patients on PFD therapy were also investigated using the questionnaire. Furthermore, the effect of RK on GI symptoms was examined along with measurement of the plasma acyl-ghrelin and des-acyl-ghrelin levels, while the anti-inflammatory effect of RK was assessed by measuring serum KL-6 and surfactant protein-D (SP-D), and by pulmonary function tests.

MATERIALS AND METHODS

Subjects

The diagnosis of IPF was determined according to the American Thoracic Society/European Respiratory Society (ATS/ERS) International Multidisciplinary Consensus Classification of the Idiopathic Interstitial Pneumonia (18). One patient had undergone video-assisted thoracoscopic surgery (VATS) for lung, but the other patients did not have surgery. Patients were excluded if they had a history of esophageal, gastric, or duodenal surgery, were currently using acid-suppressing drugs (PPIs, H2 blockers) or prokinetic agents such as selective serotonin (5HT4) agonists, or were mentally incompetent.

Study design and procedures

This study was performed as a randomized controlled trial. The IPF patients were randomly assigned to a group receiving PFD and RK therapy (PFD group) or a group that did not receive these agents (control group). Randomization was performed with the envelope method and the study period was 8 weeks (wks). In the PFD group, PFD was administered orally at 200 mg t.i.d (600 mg/day) for the initial 2 wks, and then at 400 mg t.i.d (1200 mg/day) for the remaining 6 wks. RK was also administered orally at 2.5 g t.i.d (7.5 g/day) from 4 to 8 wks after starting PFD treatment. The patients in the PFD group were reviewed every two wks and parameters were measured. In the control group, patients did not receive PFD or any immunosuppressive agents. The patients in the control group visited the hospital every 4 wks and parameters were measured (Table I). This study was conducted according to the guidelines of the Declaration of Helsinki, and all patients provided written informed consent before enrollment. This study was approved by the Human Research Committee of Maebashi Red Cross Hospital.

Assessment of gastrointestinal symptoms

The assessment of GI symptoms was performed with a new questionnaire, the modified frequency scale for the symptoms of gastroesophageal reflux disease (MFSSG), which can clearly distinguish symptoms of GERD (reflux symptoms) from symptoms of functional dyspepsia (FD) (dismotility symptoms). The MFSSG was modified

FSSG by adding two questions regarding interdigestive and postprandial epigastric pain (17, 19). The MFSSG questionnaire is composed of 14 questions, which are scored to indicate the frequency of symptoms as follows: never=0, occasionally=1, sometimes=2, often=3, and always=4. The unique feature of the MFSSG is that the questions cover both acid regurgitation-related symptoms (reflux symptoms, questions 1-6) and gastric dysmotility-related symptoms (dismotility symptoms, questions 7-12). To determine the dominant symptom in a patient, the total scores of acid regurgitation-related symptoms (reflux symptoms) or gastric dysmotility-related symptoms (dismotility symptoms) were compared.

Blood sampling and analysis

Measurement of the peripheral blood levels of KL-6 and SP-D was carried out by electrochemiluminescence immunoassay (ECLIA). Anti-*Helicobacter Pylori* IgG antibody (*H. Pylori* Ag) was determined by enzyme-linked immunoassay (EIA). Plasma acyl-ghrelin and des-acyl-ghrelin levels were also determined by EIA. For the measurment of plasma acyl-ghrelin and des-acyl-ghrelin, the patients were in a fasting state from 9pm the previous evening, and sampling was performed the following morning. Peripheral blood was drawn into tubes containing EDTA-2Na (1 mg) and aprotinin (500 U/ml). After centrifugation at 4°C, 1 N HCl was added at a 1/10 volume for plasma, and then stored at -20°C until assay. The levels were determined using Enzyme-Linked immunoassay (Mitsubishi Chemical Medience Inc, Tokyo, Japan). All samples were measured within one month from blood collection.

Pulmonary function tests

Pulmonary function tests were performed using a Chestac-55V (CHEST MI, Tokyo, Japan) on the first day of the study (week 0) and after 8 wks to evaluate the % vital capacity (%VC) and % forced vital capacity (%FVC).

Statistical analysis

Data are expressed as the mean (± SD). Comparison between the two groups was carried out with Student's *t*-test. Statistical significance was accepted at * $P<0.05$.

RESULTS

Profile of the patients

A total of 17 patients, who met the criteria for diagnosis of IPF, were enrolled in the present study. One patient had previously been diagnosed with IPF, while the others were referred to Maebashi Red Cross Hospital and IPF was newly diagnosed. All patients were Japanese, and they were randomly assigned to the PFD group or the control group. Two of the patients enrolled in the PFD group could not complete this study, one because of heart failure and the other due to diarrhea. Both these patients recovered after treatment. Thus, a total of 15 patients completed the study. The characteristics of the PFD group (n=8) and the control group (n=7) are shown in Table I. All the patients were men, and the median age was over 70 years in both groups. BMI showed no significant difference, but smoking was significantly more frequent in the control group than the PFD group ($p< 0.05$). The positive rate for of *H. pylori* Ag was 25.0% in the PFD group and 57.1% in the control group. Spirometric analysis of %VC and %FVC did not show statistical differences between the PFD and control groups. Mean KL-6 and SP-D levels were higher in the control group, but both levels were not statistically different between the PFD and control groups. The major comorbidities were diabetes mellitus and hypertension in both groups.

Changes of GI symptoms assessed by the MFSSG

When changes of the mean total MFSSG score were assessed in the PFD group, the score was highest 2 wks after starting PFD therapy at 600 mg/day, and it improved by 4 wks despite dose escalation to 1200 mg/day. Four weeks after starting treatment with PFD, RK was added. The total MFSSG score showed further improvement at 6 wks and at 8 wks, returning to the baseline value at 0 wks before starting PFD (Fig. 1A). The mean scores for reflux and dismotility showed a similar pattern of changes to the total score (Fig. 1 B, C). In the control group, the total score, as well as the reflux and dismotility scores, were stable during the study period (Fig. 1A-1C). There was statistically significant improvement of reflux score after commencement of RK therapy in the PFD group at 8 wks compared to 2 wks of before RK therapy. There was statistically significant improvement of motility score after commencement of RK therapy in the PFD group at 8 wks compared to 4 wks of before RK therapy. There were fewer *H. pylori* positive patients in the PFD group (n=2) than in the control group (n=4). Of the two patients with *H. pylori* infection in the PFD group, one patient showed the same score for reflux symtoms and

Table I. *Characteristics of the patients.*

Groups	Pirfenidone	Control
Number of subjects	8	7
M/F	8/0	7/0
Age	71.6(5.3)	70.3(9.4)
BMI	22.8(5.8)	25.4(2.8)
smoking status (pack-yrs)	16.0(16.1)	41.1(7.0)*
never,/ex/curr	2/6/0	0/6/1
H.Pyroi Ag(+/-)	2/6	4/3
DM	3	2
HL	1	1
HT	2	2
Arrythmia	0	3
HU	0	1
SAS	1	0
Acyl-ghrelin, fmol/ml	7.6(8.3)	5.5(1.4)
Des-acyl-ghrelin, fmol/ml	58.2(39.2)	49.1(15.0)
KL-6, U/ml	639.3(269.2)	1320(707.6)
SP-D, ng/ml	241.9(135.7)	326.7(119.3)
VC, % predicted	77.1(13.1)	85.0(15.3)
FVC, % predicted	78.1(11.8)	84.5(14.3)

*The number of males or females is indicated as M/F, and body mass index is indicated as BMI. Anti-Helicobacter pylori IgG antibody positive/negative (+/-). Comorbidities are diabetes mellitus (DM), hyperlipidemia (HL), hypertension (HT), arrhythmia, hyperuricemia (HU), and sleep apnea syndrome (SAS). Data are shown as the mean (±SD). *Statistically significant difference between groups.*

dismotility symptoms, with both scores worsening at 2 wks after starting PFD. The other patient with *H. pylori infection* had dominant dismotility symptoms at 0 wks, but reflux symptoms became worse than dismotility symptoms at 2 wks after starting PFD. The majority of patients in the PFD group without *H. pylori* infection showed deterioration of both reflux and dismotility symptoms.

Changes of plasma acyl-ghrelin and des-acyl-ghrelin

The plasma level of acyl-ghrelin decreased by 4 wks after starting PFD, and the acyl-ghrelin level did not increase after addition of RK, but the levels were not statistically different. In contrast, the acyl-ghrelin level showed a slight increase over 8 wks in the control group (Fig. 2A). In the PFD group, the plasma des-acyl-ghrelin level was decreased at 2 wks, but the level gradually increased to 8 wks after dose escalation of PFD at 2 wks, despite adding RK from 4 wks ($p<0.05$). In the control group, the des-acyl-ghrelin level was decreased at 4 wks, but returned to baseline at 8 wks (Fig. 2B). The acyl-ghrelin/des-acyl-ghrelin ratio decreased after the start of PFD treatment, and the decrease was not improved by adding RK in the PFD group. The ratio was statistically different between 2 wks and 8 wks in the PFD group ($p<0.05$). In the control group, the ratio did not show marked changes (Fig. 2C).

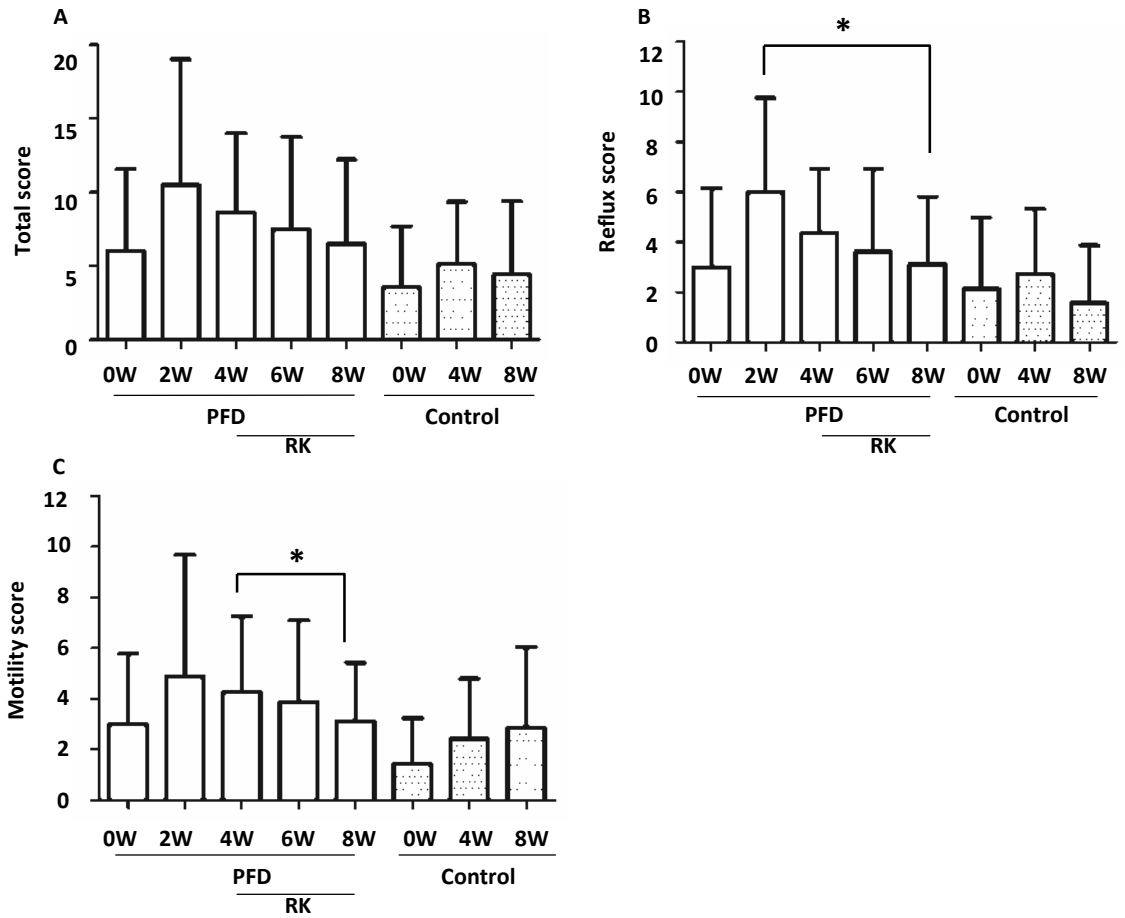

Fig. 1. *Changes of the mean scores for gastrointestinal symptoms. Total score for both reflux symptoms and dismotility symptoms (**A**), reflux symptoms score (**B**), and dismotility symptoms score (**C**). IPF patients receiving pirfenidone (PFD) with add-on rikkunshi-to (RK) from four weeks were monitored every two weeks (PFD group). Score for reflux symptoms at 2 weeks were statistically improved at 8 weeks (*p<0.05). Score for motility symptoms at 4 weeks were statistically improved at 8 weeks (*p<0.05). IPF patients without such therapy were monitored every four weeks (control group).*

Changes of IPF disease state parameters

The plasma KL-6 level was increased after 4 wks of PFD therapy, but decreased to the baseline level at 8 wks in the PFD group. In contrast, the KL-6 levels gradually decreased over 8 wks in the control group (Fig. 3A). The SP-D level was slightly decreased in both the PFD group and the control group after 8 wks (Fig. 3B). Neither KL-6 nor SP-D showed statistically significant changes during the study period. The pulmonary function parameters (% changes from base line of VC or FVC) did not show statistical changes between 0 wks and 8 wks in either group, but decline in FVC was within 5%, and this was better in the PFD group than the control group (Fig. 3 C, D).

DISCUSSION

This study investigated the changes of GI symptoms during 8 wks of PFD therapy, and demonstrated that reflux and dismotility symptoms were well tolerated in IPF patients receiving PFD at a daily dose of 1200 mg. In addition, the combined administration of PFD and RK improved GI symptoms to the level prior to starting PFD. The findings of this study are of importance for IPF therapy. To our knowledge, this is the first serial examination of the changes of GI symptoms, focusing on reflux symptoms and

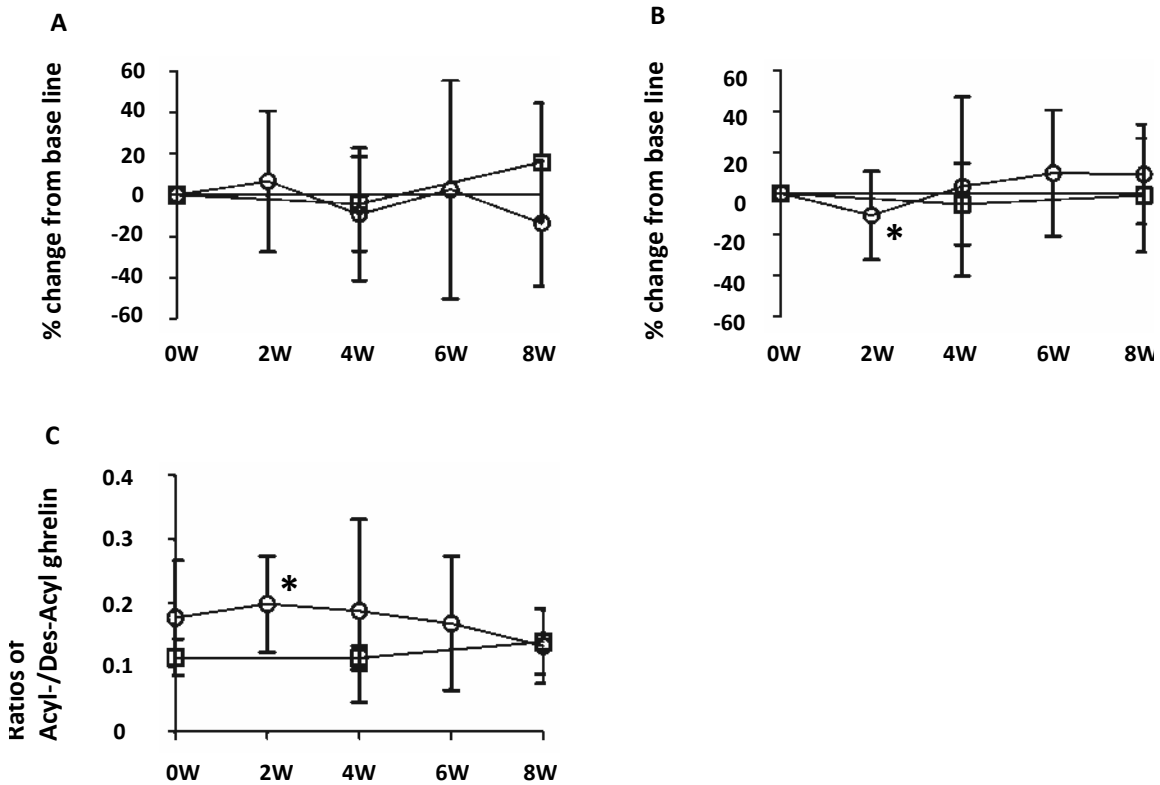

Fig. 2. *Changes of plasma acyl-ghrelin and des-acyl ghrelin. The percent (%) changes from baseline (week 0) of plasma acyl-ghrelin (**A**) and des-acyl-ghrelin (**B**) are shown. The acyl-ghrelin /des-acyl-ghrelin ratio was calculated from measured values, and is not the ratio of the % change of acyl-ghrelin relative to the % change of des-acyl-ghrelin (C). IPF patients receiving pirfenidone (PFD) with add-on rikkunshi-to (RK) were monitored every two weeks (PFD group, ○). IPF patients without such therapy were monitored every four weeks (control group, □). Changes of % changes of des-acyl-ghrelin or acyl-ghrelin/des-acyl-ghrelin ratio in PFD group were statistically different between 2 weeks and 8 weeks (*p<0.05).*

dismotility symptoms, along with investigation of the effects of RK on GI symptoms caused by PFD.

Both reflux and dismotility symptoms were exacerbated by PFD. GI symptoms (assessed from the total MFSSG score) were most severe at 2 wks with the initial dose of 600 mg. Unexpectedly, GI symptoms improved slightly without any treatment from 2 wks to 4 wks when the dose was escalated to 1200 mg. The mechanisms involved are unknown, but the number of GI adverse events did not differ significantly between doses of 1800 mg/day and 1200 mg/day in Japanese subjects receiving 52 wks of therapy (20). Although the severity of GI symptoms related to PFD therapy seems to not only depend on the dose, a recent study suggested that GI symptoms are improved by dose reduction, and continuation of PFD therapy with dose reduction rather than cessation of PFD was recommended (21). *H. pylori* infection has been reported to increase the occurrence of dismotility symptoms (22). Although only a small number of patients were investigated in the present study, *H. pylori* infection did not seem to affect the pattern of either reflux or dismotility symptoms.

RK reduced the GI symptoms. Previous clinical studies of PFD therapy for IPF patients showed that dismotility symptoms, such as anorexia, nausea, and dyspepsia, were more frequent than other GI symptoms (8). In the present study, reflux symptoms also deteriorated to a similar degree as dismotility symptoms after the start of PFD therapy. When RK was added to PFD, it contributed to improving both

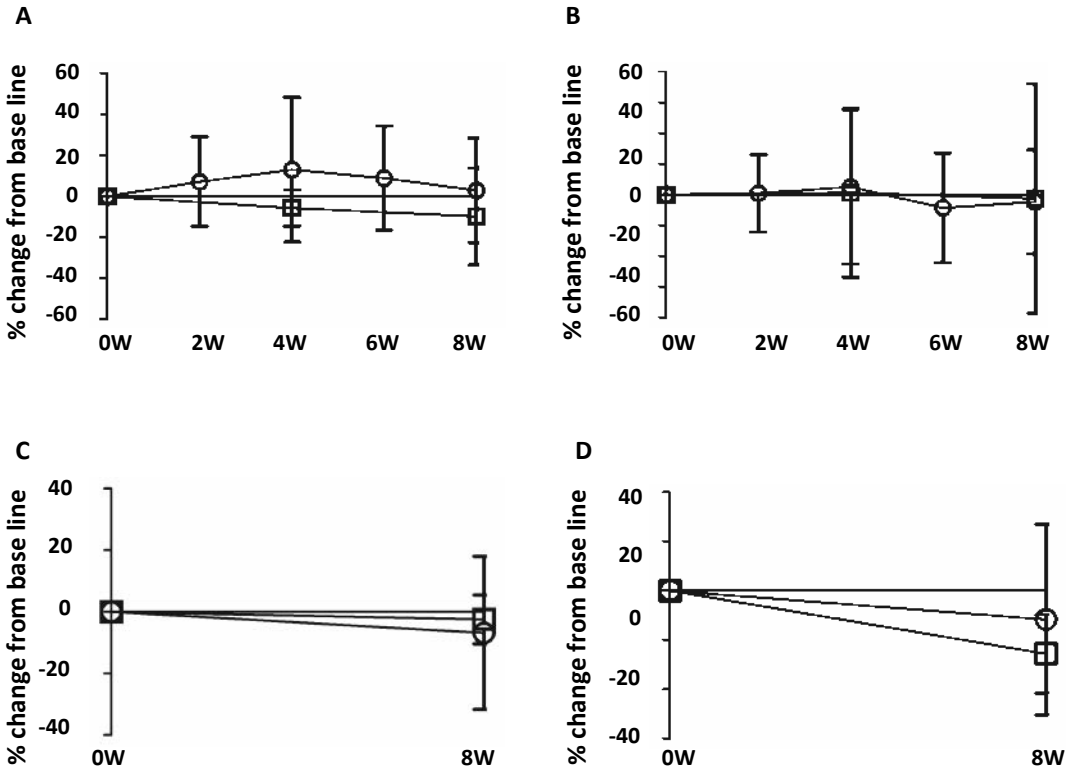

Fig. 3. *Changes of indicators of IPF disease status. Changes are indicated as the percent (%) change from baseline (week 0) for KL-6 (**A**), SP-D (**B**), % VC (**C**), and % FVC (**D**). IPF patients received pirfenidone (PFD) with add-on rikkunshi-to (RK) in the PFD group (○). IPF patients without such therapy formed the control group (□). Changes were not statistically significant.*

reflux and dismotility symptoms to the level before starting PFD, and RK seemed to be more effective for dismotility symptoms.

RK did not affect the plasma acyl-ghrelin level in IPF patients receiving PFD. RK has been reported to improve both reflux and dismotility symptoms (9), and RK also reduces adverse events due to chemotherapy such as cisplatin-induced anorexia (11). A role of ghrelin in these effects of RK has been reported. The acyl-ghrelin level was decreased by PFD therapy, and adding RK did not prevent a further decline in the present study. It has been reported that RK suppresses a decrease of the acyl-ghrelin level, so a change of acyl-ghrelin was expected to underlie the improvement of GI symptoms, but the acyl-ghrelin level was not influenced by RK in the present study.

In this study, RK was administered orally at a dose of 7.5 g/ day, which is the dose for adults according to previous reports (14, 23). However, a dose-response study into the effects of RK performed on dogs showed that intragastric administration of RK at 4.0 g (for a 10-12 kg dog) induced an increase in the plasma level of acyl-ghrelin, but 2.7 g or 1.3 g of RK did not increase plasma acyl-ghrelin (24). Thus, a low dose of RK may be one of the reasons for no increase of acyl-ghrelin in the present study, although GI symptoms were improved.

The acyl-ghrelin/des-acyl-ghrelin ratio declined during PFD therapy. Des-acyl-ghrelin was reported to be a strong inhibitor of acyl-ghrelin in animals (25). RK was expected to prevent a decrease of the acyl-ghrelin/des-acyl-ghrelin ratio, but this effect

could not be seen in the present study.

Several factors, such as body weight (BW), comorbidities, and cigarette smoking, have an influence on ghrelin levels (26-29). In the present study, the body mass index (BMI) of patients in the PFD and control groups did not change significantly during the study period, and disease status parameters were unchanged. Although the smoking history assessed by pack-years was significantly greater in the control group than the PFD group, acyl-ghrelin was lower in the control group compared with the PFD group at 0 wks. How smoking status affects the ghrelin level has not been determined (28, 29).

Ghrelin has other roles in addition to being a regulator of gut motility, including an anti-inflammatory effect on lung injury (15, 16). In the present study, biomarkers of IPF disease activity (KL-6 and SP-D) (7) and pulmonary function tests were not affected by RK. PFD treatment reduces the decline of % FVC from baseline (4-7). In this study, the decline was not statistically different, but the degree of dceline in % changes of FVC from base line was better in the PFD group compared to the control group.

There were several limitations to the present study. Since IPF is not a common disease, we found it difficult to enroll many patients, so the study was small in size. Also, we focused on evaluating the improvement of GI symptoms by RK rather than its anti-inflammatory effect. We predicted that GI symptoms would be most severe at 4 wks when the maximum dose of PFD was being administered. Therefore, we focused on the effect of RK by assessing the extent to which it improved GI symptoms after being added at 4 wks. Unexpectedly, we found that GI symptoms were most severe at 2 wks with the low dose of PFD. To determine the effect of RK more clearly, further studies may be needed.

In conclusion, GI adverse events due to PFD therapy were most severe after 2 wks of treatment at a dose of 600 mg/day, and both reflux and dismotility symptoms showed deterioration. Addition of RK seemed to contribute to improvement of GI symptoms, but further investigation is needed.

ACKNOWLEDGEMENTS

The authors thank the medical staff for assisting with blood sampling and pulmonary function tests.

Conflict of interests: K.D. was temporarily consultant for Shionogi. None of the other authors has a financial interest in the subject of this manuscript.

REFERENCES

1. Raghu G, Collard HR, Egan JJ, et al. ATS/ERS/JRS/ALAT Committee on Idiopathic Pulmonary Fibrosis. An official ATS/ERS/JRS/ALAT statement: idiopathic pulmonary fibrosis: evidence-based guidelines for diagnosis and management. Am J Respir Crit Care Med 2011; 183:788-824.
2. Oku H, Nakazato H, Horikawa T, Tsuruta Y, Suzuki R. Pirfenidone suppresses tumor necrosis factor-alpha, enhances interleukin-10 and protects mice from endotoxic shock. Eur J Pharmacol 2002; 446:167-76.
3. Oku H, Shimizu T, Kawabata T, et al. Antifibrotic action of pirfenidone and prednisolone: different effects on pulmonary cytokines and growth factors in bleomycin-induced murine pulmonary fibrosis. Eur J Pharmacol 2008; 590:400-408.
4. Azuma A, Nukiwa T, Tsuboi E, et al. Double-blind, placebo-controlled trial of pirfenidone in patients with idiopathic pulmonary fibrosis. Am J Respir Crit Care Med 2005; 17:1040-47.
5. Taniguchi H, Kondoh Y, Ebina M, et al. Pirfenidone Clinical Study Group in Japan The clinical significance of 5% change in vital capacity in patients with idiopathic pulmonary fibrosis: extended analysis of the pirfenidone trial. Respir Res 2011; 12:93.
6. Azuma A, Taguchi Y, Ogura T, et al. Pirfenidone Clinical Study Group in Japan Exploratory analysis of a phase III trial of pirfenidone identifies a subpopulation of patients with idiopathic pulmonary fibrosis as benefiting from treatment. Respir Res 2011; 12:143.
7. Noble PW, Albera C, Bradford WZ, et al. CAPACITY Study Group. Pirfenidone in patients with idiopathic pulmonary fibrosis (CAPACITY): two randomised trials. Lancet 2011; 377:1760-69.
8. Jiang C, Huang H, Liu J, Wang Y, Lu Z, Xu Z. Adverse events of pirfenidone for the treatment of

pulmonary fibrosis: a meta-analysis of randomized controlled trials. PloS One 2012; **7**:e47024.

9. Tatsuta M, Iishi H. Effect of treatment with liu-jun-zi-tang (TJ-43) on gastric emptying and gastrointestinal symptoms in dyspeptic patients. Aliment Pharmacol Ther 1993; **7**:459-62.
10. Tominaga K, Iwakiri R, Fujimoto K, et al. GERD 4 Study Group Rikkunshito improves symptoms in PPI-refractory GERD patients: a prospective, randomized, multicenter trial in Japan. J Gastroenterol 2012; 47:284-92.
11. Takeda H, Sadakane C, Hattori T, Katsurada T, Ohkawara T, Nagai K, Asaka M. Rikkunshito, an herbal medicine, suppresses cisplatin-induced anorexia in rats via 5-HT2 receptor antagonism. Gastroenterology 2008; 134:2004-13.
12. Kojima M, Hosoda H, Date Y, Nakazato M, Matsuo H, Kangawa K. Ghrelin is a growth-hormone-releasing acylated peptide from stomach. Nature 1999; 402:656-60.
13. Ogiso K, Asakawa A, Amitani H, Inui A. Ghrelin: a gut hormonal basis of motility regulation and functional dyspepsia. J Gastroenterol Hepatol 2011; 26(S)3:67-72.
14. Arai M, Matsumura T, Tsuchiya N, et al. Rikkunshito improves the symptoms in patients with functional dyspepsia, accompanied by an increase in the level of plasma ghrelin. Hepatogastroenterology 2012; 59:62-66.
15. Wu R, Dong W, Zhou M, Zhang F, Marini CP, Ravikumar TS, Wang P. Ghrelin attenuates sepsis-induced acute lung injury and mortality in rats. Am J Respir Crit Care Med 2007; 176:805-13.
16. Imazu Y, Yanagi S, Miyoshi K, et al. Ghrelin ameliorates bleomycin-induced acute lung injury by protecting alveolar epithelial cells and suppressing lung inflammation. Eur J Pharmacol 2011; 672:153-58.
17. Kusano M, Hosaka H, Kawada A, Kuribayashi S, Shimoyama Y, Kawamura O, Moki F. Development and evaluation of a modified Frequency Scale for the Symptoms of Gastroesophageal Reflux Disease to distinguish functional dyspepsia from non-erosive reflux disease. J Gastroenterol Hepatol 2012; 27:1187-91.
18. American Thoracic Society; European Respiratory Society/ American Thoracic Society/European Respiratory Society International Multidisciplinary Consensus Classification of the Idiopathic Interstitial Pneumonias. This joint statement of the American Thoracic Society (ATS), and the European Respiratory Society (ERS) was adopted by the ATS board of directors, June 2001 and by the ERS Executive Committee, June 2001. Am J Respir Crit Care Med 2002; 165:277-304.
19. Kusano M, Shimoyama Y, Sugimoto S, et al. Development and evaluation of FSSG: frequency scale for the symptoms of GERD. J Gastroenterol 2004; 39:888-91.
20. Taniguchi H, Ebina M, Kondoh Y, et al. Pirfenidone Clinical Study Group in JapanPirfenidone in idiopathic pulmonary fibrosis. Eur Respir J 2010; 35:821-29.
21. Okuda R, Hagiwara E, Baba T, Kitamura H, Kato T, Ogura T. Safety and efficacy of pirfenidone in idiopathic pulmonary fibrosis in clinical practice. Respir Med 2013; 107:1431-37.
22. Suzuki H, Moayyedi P. *Helicobacter pylori* infection in functional dyspepsia. Nat Rev Gastroenterol Hepatol 2013; 10:168-74.
23. Matsumura T, Arai M, Yonemitsu Y, et al. The traditional Japanese medicine Rikkunshito increases the plasma level of ghrelin in humans and mice. J Gastroenterol 2010; 45:300-307.
24. Yanai M, Mochiki E, Ogawa A, et al. Intragastric administration of rikkunshito stimulates upper gastrointestinal motility and gastric emptying in conscious dogs. J Gastroenterol 2013; 48:611-19.
25. Kumar R, Salehi A, Rehfeld JF, Höglund P, Lindström E, Håkanson R. Proghrelin peptides: Desacyl ghrelin is a powerful inhibitor of acylated ghrelin, likely to impair physiological effects of acyl ghrelin but not of obestatin A study of pancreatic polypeptide secretion from mouse islets. Regul Pept 2010; 164:65-70.
26. Delporte C. Recent advances in potential clinical application of ghrelin in obesity. J Obes 2012; 2012:535624.
27. Saad MF, Bernaba B, Hwu CM, Jinagouda S, Fahmi S, Kogosov E, Boyadjian R. Insulin regulates plasma ghrelin concentration. J Clin Endocrinol Metab 2002; 87:3997-4000.
28. Kokkinos A, Tentolouris N, Kyriakaki E, Argyrakopoulou G, Doupis J, Psallas M, Kyriaki

D, Katsilambros N. Differentiation in the short- and long-term effects of smoking on plasma total ghrelin concentrations between male nonsmokers and habitual smokers. Metabolism 2007; 56:523-27.

29. Tomoda K, Kubo K, Nishii Y, Yamamoto Y, Yoshikawa M, Kimura H. Changes of ghrelin and leptin levels in plasma by cigarette smoke in rats. J Toxicol Sci 2012; 37:131-38.

FREQUENCY OF BACTERIA CAUSING URINARY TRACT INFECTIONS AND THEIR ANTIMICROBIAL RESISTANCE PATTERNS AMONG PEDIATRIC PATIENTS IN WESTERN IRAN FROM 2007-2009

M. YASEMI[1], H. PEYMAN[1], K. ASADOLLAHI[2], A. FEIZI[1], S. SOROUSH[3,4], A. HEMATIAN[4], F.A. JALILIAN[3,4], M. EMANEINI[5], M.Y. ALIKHANI[6] and M. TAHERIKALANI[3,4]

[1]Student Research Committee, Ilam University of Medical Sciences Ilam, Iran; [2]Department of Clinical Epidemiology, School of Medicine, Ilam University of Medical Sciences, Ilam, Iran; [3]Clinical Microbiology Research Center, Ilam University of Medical Sciences, Ilam, Iran; [4]Department of Medical Microbiology, School of Medicine, Ilam University of Medical Sciences Ilam, Iran; [5]Department of Microbiology, School of Medicine, Tehran University of Medical Sciences, Tehran, Iran; [6]Department of Microbiology, School of Medicine, Hamadan University of Medical Sciences, Hamadan, Iran

Received January 9, 2013 – Accepted July 25, 2014

Urinary Tract infections (UTIs) are among the most common infections in infants and neonates. The aim of the current study was to evaluate the frequency of bacteria causing UTI and their relevant drug resistance patterns among infants and neonates hospitalized in Ilam province, Western Iran during 2007-2009. A total of 220 cases of UTI were enrolled in this cross-sectional retrospective study. A standard checklist was used for demographic and clinical data to be collected from their health records. Data was then analysed using SPSS version 16.0. More than two-thirds (64.8%) of the cases were female. *E. coli* (44.5%), *Klebsiella spp.,* (18.6%), *Enterobacter spp.,* (15%) and *Staphylococcus spp.* (12.7%) were the most common microorganisms isolated from UTIs, respectively. High rates of resistance to tetracycline, ampicillin, and nalidixic acid were observed among these isolates. Similar to other studies, *E. coli* was the most common bacteria causing UTI and showed a high rate of resistance against most of the antimicrobial agents. Determining the antimicrobial sensitivity can be helpful for physicians in choosing an appropriate treatment for patients suffering from UTI, and also to reduce the complications related to serious UTI.

Urinary tract infections (UTIs) are among the most common infections in infants and neonates (1, 2) which can cause permanent renal failure especially among children with vesicoureteral reflux. The diagnosis of UTI is difficult in the neonatal period because the signs and symptoms are non-specific in this age group. The incidence rate of UTI infection in neonates is 0.01-1% and increases to 10% in low birth weight and preterm babies. Early diagnosis, appropriate antimicrobial treatment and precise follow-up of patients could be the key solutions to reducing the occurrence of this condition (1-4). Approximately 3-5% of girls and 1% of boys acquire an UTI (5). It has been shown that 8.4% of girls and

Key words: urinary tract infection, drug resistance, infant, neonates, Iran

Mailing address:
Dr Morovat Taherikalani,
Clinical Microbiology Research Center, Department of Medical Microbiology, School of Medicine, Ilam University of Medical Sciences, Ilam, Iran
e-mail: taherikalani@gmail.com.

0393-974X (2014)

1.7% of boys will be, at least once, infected before the age of 7 and that the prevalence of UTI among neonates is reported as 5% and among children as 2% (6-8). However, the epidemiology and etiology of UTI, both in community and nosocomial infections, and the resistance pattern of the causative organisms has changed compared to previous years (9, 10). Antibiotic resistance, as an important issue affecting the treatment of infectious bacteria, has increased during recent years (11). Resistance rate varies among different countries (12).

The aim of the present study was to determine the antibiotic resistance pattern of the most common bacteria causing UTI among paediatric patients admitted to a hospital in Ilam.

MATERIALS AND METHODS

During the current cross-sectional retrospective study, children and neonates infected with urinary tract infection, admitted to Imam Khomeini Hospital in Ilam, were surveyed during 2007-2009. The Ilam province, with a population of 560,000, is located in Western Iran. All the children and neonates who need to be hospitalized are referred to the paediatrics unit and neonatal Intensive Care Unit at Imam Khomeini Hospital in Ilam. The current study can, therefore, be extrapolated to the total population of paediatrics in the Ilam province. A total of 220 patients, infected with UTI, were evaluated in this study among whom 7 patients were admitted as outpatients who had been referred to hospitals in other provinces in Iran to continue their treatments. These patients were excluded from the study and the data analysis was carried out based on the 213 remaining patients.

In the present study, the samples were confirmed as UTI by a pediatrician, according to the clinical and paraclinical indexes. Patients were children aged from 1 week to 16 years without history of genitourinary abnormalities, recent hospitalization, or antibiotic usage. Patients were hospitalized for evaluation and treatment with signs and symptoms of acute pyelonephritis, including temperature ≥ 38°C, chills, frequency, dysuria, urgency, suprapubic and/or flank tenderness, pyuria (defined as ≥5WBC/hpf), and fever of unknown source in children and in neonates (7–30 days of age) with clinical evidence of sepsis.

The demographic and clinical data associated with hospitalized children and neonates infected with urinary tract infections were extracted from the patients' documents using appropriate check lists. Other data such as year, season and the unit of admission were also recorded. The data were analyzed using the Statistical Package for the Social Sciences (SPSS) 16.0 for Windows. The normality of data and homogeneity of variance were checked before analysis. The nonparametric Kruskal-Wallis test or *chi*-squared test, were used for different variables accordingly.

RESULTS

A total of 220 infected patients were surveyed during 2007-2009, among whom 3.2% (n=7) were admitted as outpatients who had been referred to hospitals in other provinces in Iran to continue their treatments. These patients were, therefore, excluded from the study due to the lack of access to their information, and the assessment of data was carried out based on the 213 remaining patients.

Less than two-thirds of the samples (58.7%) were obtained from girls and more than one-third (41.3%) were from boys. The ratio of boys to girls was 0.7. The samples referred to the laboratory belonged to NICU (63.8%) and the paediatrics ward (36.2%). Among the 213 samples surveyed, the most common bacteria were as follows: *E.coli* (45.1%), *Klebsiella spp*. (17.8%), *Enterobacter spp*. (15.5%), *Staphylococcus spp*. (12.2%) and other bacteria (9.4%) (Table I).

The most effective antibiotics against *E. coli*, *Klebsiella spp*., *Enterobacter* and *Staphylococcus spp*. were nitrofurantoin (75.3%), SXT (58.8%), nitrofurantoin (62.5%) and cephalothin (50%), respectively. Other bacteria were also more sensitive to nitrofurantoin (43.7%) compared to other antibiotics (Table II and III).

DISCUSSION

Urinary tract infections (UTIs) are among the most common bacterial infections encountered by primary care physicians. Although UTIs do not occur with as great a frequency in children as in adults, they can be a source of significant morbidity in children. In this study, the prevalence of UTI was higher in females compared to males.

The most frequent bacteria identified were *E. coli*, *Klebsiella spp.*, *Enterobacter spp.,* and *Staphylococcus spp*., respectively. The most common bacteria identified were associated to the summer season whilst the least common were associated to spring. The highest prevalence of UTI

Table I. *The frequency of bacterial isolated from paediatric patients with UTI according to gender, seasonal pattern and hospital wards.*

			Bacterial isolates						
			E. coli	*Klebsiella Spp*	*Enterobacter spp*	*Staphylococcus spp*	Others	P value	**Total**
Gender	**Female**	**N**	**60**	**24**	**20**	**14**	**7**	**0.88**	**125**
		%	**48**	**19.2**	**16**	**11.2**	**5.6**		**58.7**
	Male	**N**	**36**	**14**	**13**	**12**	**13**		**88**
		%	**40.9**	**15.9**	**14.8**	**13.6**	**14.8**		**41.3**
Season	**Spring**	**N**	**25**	**9**	**5**	**4**	**-**	**0.006**	**43**
		%	**58.1**	**20.9**	**11.6**	**9.3**	**-**		**20.2**
	Summer	**N**	**27**	**17**	**11**	**7**	**3**		**65**
		%	**41.5**	**26.2**	**16.9**	**10.8**	**4.6**		**30.5**
	Autumn	**N**	**30**	**2**	**8**	**7**	**9**		**56**
		%	**53.6**	**3.6**	**14.3**	**12.5**	**16.1**		**26.3**
	Winter	**N**	**14**	**10**	**9**	**8**	**8**		**49**
		%	**28.6**	**20.4**	**18.4**	**16.3**	**16.3**		**23**
Ward	**NICU**	**N**	**56**	**31**	**23**	**15**	**11**	**0.09**	**136**
		%	**41.2**	**22.8**	**16.9**	**11**	**8.1**		**63.8**
	Pediatric	**N**	**40**	**7**	**10**	**11**	**9**		**77**
		%	**51.9**	**9.1**	**13**	**14.3**	**11.7**		**36.2**
	Total	**N**	**96**	**38**	**33**	**26**	**20**		**213**
		%	**45.1**	**17.8**	**15.5**	**12.2**	**9.4**		**100**

Table II. *The resistance pattern of the most common bacteria identified in paediatric patients with UTI.*

	Ampicillin			Gentamicin			Cephalotin			SXT			Nitrofurantion		
	S	I	R	S	I	R	S	I	R	S	I	R	S	I	R
E. coli	17.1	5.7	77.1	32.3	41.9	25.8	15.6	22.2	62.2	20	10	70	75.3	16.4	8.2
Klebsiella spp	-	7.1	92.9	50	17.9	32.1	22.2	22.2	55.6	58.8	11.8	29.4	40	23.3	36.7
Enterobacter spp	8.3	8.3	88.3	35	50	15	16.7	16.7	66.6	55.6	-	44.4	62.5	8.3	29.2
Staphylococcus spp	-	50	50	28.6	35.7	35.7	50	12.5	37.5	44.4	11.2	44.4	100	-	-
Others	33.3	-	66.7	20	50	30	9.1	9.1	81.8	37.5	12.5	50	43.7	12.5	43.8
P value		0.05			0.34			0.45			0.17			0.000	
Total	13.6	7.6	78.8	35.1	38.1	26.9	19.1	19.1	61.7	36.1	9.6	54.2	66.2	14.4	19.4

Table III. *The antibiotic resistance pattern of bacteria among paediatric patients with UTI during the years 2007-2009.*

	Ampicillin			Gentamicin			Cephalotin			SXT			Nitrofurantion		
	S	I	R	S	I	R	S	I	R	S	I	R	S	I	R
2007	9.4	-	90.6	56.1	29.3	14.6	12.9	35.5	51.6	43.5	4.3	52.2	54.8	21.4	23.8
2008	18.5	18.5	63	23	43.2	33.8	23.5	11.8	64.7	27.5	7.5	65	75	12.5	12.5
2009	14.3		85.7	36.8	36.8	26.3	16.7	8.3	75	45	20	35	50	9.1	40.9
P value		0.04			0.01			0.07			0.14			0.01	
Total	13.6	7.6	78.8	35.1	38.1	26.9	19.1	19.1	61.7	36.1	9.6	54.2	66.2	14.4	19.4

was associated to the years 2008 (53.5%), 2007 (30%) and 2009 (23.5%), respectively. The prevalence of UTI in males was less than that in females which was consistent with the results of the study carried out by Tseng et al. in Taiwan. The prevalence of UTI in the study of Tseng was 48.2% in males and 51.8% in females (1). In another study carried out by Ghedira et al. in Tunisia, a higher prevalence of UTI was reported in the male gender (13).

There was a significant correlation between the antibiotic resistance patterns of the identified bacteria and the antibiotics ampicillin and nitrofurantoin. An

increase in the rate of resistance to gentamicin and nitrofurantoin was seen during 2007-2009.

In the current study, *E. coli* was the most common bacteria (45.1%) causing urinary tract infection among the population under survey and this result was consistent with that reported by other studies (1, 3, 13-20). The other most frequent bacteria identified were *Klebsiella spp*., (17.8%), *Enterobacter spp*., (15.5%) and *Staphylococcus spp*., (12.2%), respectively. The frequencies of the bacteria *E. coli*, *Klebsiella spp*., and *Enterobacter spp*. were higher in the females compared to males whilst the frequency of *Staphylococcus spp*. was higher in the male gender. There was no significant correlation between gender and the prevalence of the identified bacteria (p=0.88).

E. coli is the most common member of the family Enterobacteriaceae which is responsible for 75-90% of UTI cases (21). The prevalence of infections caused by *E.coli* differs in different parts of the world and has been reported as a range of 56.2-87% (3, 13, 17-20). In a study carried out in Taiwan, the most common bacteria causing UTI were *E.coli* (81%), *Klebsiella spp*. (6.5%), *Enterococcus spp*. (6%) and *Proteus spp*. (3.5%). These results were similar to those reported by other studies (1, 14-16).

In the current study, the highest prevalence of bacteria causing UTI was associated to the spring season. The most common bacteria seen in the spring and summer were *E.coli* and *Klebsiella spp*. respectively, while *Enterobacter spp.,* and *Staphylococcus spp.,* were more frequent in winter. There was a significant correlation between the seasonal pattern and the prevalence of the identified bacteria (p=0.006).

The highest resistance of *E. coli* was against ampicillin, SXT and cephalothin, respectively. The results of the recent studies showed that ampicillin resistance has increased among *E. coli spp.* from 70.8% to 91.7% compared to 15 years ago (1). However, the interesting point in these studies was the consistency of gentamicin-resistance pattern (16.2%-19.8%) among all pathogens and the minor change in the nitrofurantoin-resistance pattern within the last 15 years (1). Other studies have reported an antibiotic resistance pattern of 44.1% to 74% for *E. coli* against ampicillin (18, 22, 23).

The antibiotic resistance of *E. coli* was reported as 96.6% against nitrofurantoin and 19.1% against ampicillin whilst the antibiotic resistance of *Klebsiella spp*., and *Proteus spp*. were 8.3% against ampicillin and 7.7% against furantoin, respectively. The highest antibiotic resistance, in the mentioned study, was against ampicillin (77.4%) whilst the lowest was against nitrofurantoin (8.4%).

The highest antibiotic resistance among *Klebsiella spp*., similar to that of *Enterobacter spp*., was against ampicillin and cephalothin, respectively. *Staphylococcus spp*., were more resistant against ampicillin whilst other bacteria were more resistant against ampicillin, cephalothin and SXT, respectively. There was a significant correlation between the frequency of antibiotic resistance of the identified bacteria and the year of study for the antibiotics nitrofurantoin (p=0.000) and ampicillin (p= 0.05) whilst there was no such a correlation for other antibiotics (p> 0.05). Resistance to gentamicin had increased from 14.6% in 2007 to 26.9% in 2009, while it had increased from 51.6% in 2007 to 75% in 2009 for cephalothin and from 23.8% in 2007 to 40.9% in 2009 for nitrofurantoin. This increase in resistance pattern was significant for gentamicin and nitrofurantoin (p=0.001) whilst it was not significant for cephalothin (p=0.07).

The maximum antibiotic sensitivity of *E. coli* to nitrofurantoin and ampicillin was 75.3% and 17.1%, respectively which were lower than those reported by Tseng (96.6% for nitrofurantoin and 19.1% for ampicillin) (1). The maximum sensitivity of *Klebsiella spp*., to SXT, gentamicin and nitrofurantoin was 58.8%, 50% and 40%, respectively, whilst the sensitivity rate against ampicillin was 0%. Similarly, in the study of Tseng sensitivity to ampicillin was very low (8.3%) (1).

In the current study, the rate of resistance to ampicillin was 78.8% which was higher than that reported by others (77.4%) (1). Different studies have shown that the rate of resistance to ampicillin is continuing to increase. Some instances of such studies have been carried out in different parts of Europe and Northern America. During a 22-year period in Britain, resistance to ampicillin had increased from 12% to 40% in hospitalized patients and from 33% to 46% in outpatients. In another study from Canada, the resistance rate of *E. coli* to ampicillin has been reported as 40% (24, 25). The resistance rate of *E. coli* to ampicillin has been reported as a range of

44.1% to 74% by other studies (1, 9, 11, 22, 26).

Finally, the results of this study show that antibiotic resistance among bacteria isolated from different infections in paediatrics in Iran is a big problem especially among hospitalized patients, as well as immuno-compromised patients. Therefore, the use of appropriate antibiotics against UTIs and establishment of annual surveillance programs on determining the antibiotic sensitivity of bacteria to routinely used antibiotics can be helpful for physicians in choosing an appropriate treatment for patients suffering from UTI and also to reduce the complications related to serious UTI.

ACKNOWLEDGEMENTS

This work was supported by Ilam University of Medical Sciences.

REFERENCES

1. Tseng MH, Lo WT, Lin WJ, Teng CS, Chu ML, Wang CC. Changing trend in antimicrobial resistance of pediatric uropathogens in Taiwan. Pediatr Int 2008; 50:797-800.
2. Gonzalez CM, Schaeffer AJ. Treatment of urinary tract infection: what's old, what's new, and what works. World J Urol 1999; 17:372-82.
3. Marcus N, Ashkenazi S, Yaari A, Samra Z, Livni G. Non-*Escherichia coli* versus *Escherichia coli* community-acquired urinary tract infections in children hospitalized in a tertiary center: relative frequency, risk factors, antimicrobial resistance and outcome. Pediatr Infect Dis J 2005; 24:581-85.
4. Gonzales ET, RDUTIIMJ, Feigin RD, DeAngelis CD. Urinary Tract Infection. In: McMillan JA, Feigin RD, DeAngelis CD, eds. In: 4 edn. Baltimore: Lippincott Williams & Willkins; 2006; 1836-40.
5. Elder J (ed.): Urologic disorders in infants and children. In: Behrman RE, Kliegman RM , Jenson HB, eds., 18 edn. Philadelphia: Saunders 2007.
6. Hoberman A, Chao HP, Keller DM, Hickey R, Davis HW, Ellis D. Prevalence of urinary tract infection in febrile infants. J Pediatr 1993; 123:17-23.
7. Hoberman A, Wald ER. Urinary tract infections in young febrile children. Pediatr Infect Dis J 1997; 16:11-17.
8. Shaw KN, Gorelick M, McGowan KL, Yakscoe NM, Schwartz JS. Prevalence of urinary tract infection in febrile young children in the emergency department. Pediatrics 1998; 102:e16.
9. Manges AR, Natarajan P, Solberg OD, Dietrich PS, Riley LW. The changing prevalence of drug-resistant Escherichia coli clonal groups in a community: evidence for community outbreaks of urinary tract infections. Epidemiol Infect 2006; 134:425-31.
10. Kahan NR, Chinitz DP, Waitman DA, Dushnitzky D, Kahan E, Shapiro M. Empiric treatment of uncomplicated urinary tract infection with fluoroquinolones in older women in Israel: another lost treatment option? Ann Pharmacother 2006; 40:2223-27.
11. Akram M, Shahid M, Khan AU. Etiology and antibiotic resistance patterns of community-acquired urinary tract infections in J N M C Hospital Aligarh, India. Ann Clin Microbiol Antimicrob 2007; 6:4.
12. Gales AC, Jones RN, Turnidge J, Rennie R, Ramphal R. Characterization of Pseudomonas aeruginosa isolates: occurrence rates, antimicrobial susceptibility patterns, and molecular typing in the global SENTRY Antimicrobial Surveillance Program, 1997-1999. Clin Infect Dis 2001; 32:S146-55.
13. Ghedira Besbes L, Messaoudi A, Ben Meriem C, Guediche MN. [Profile of antimicrobial resistance of agents causing urinary tract infections in children]. Tunis Med 2004; 82:299-305.
14. Yen CW, Chen DH. Urinary tract infection in children. J Microbiol Immunol Infect 1999; 32:199-205.
15. Wu CY, Chiu PC, Hsieh KS, Chiu CL, Shih CH, Chiou YH. Childhood urinary tract infection: a clinical analysis of 597 cases. Acta Paediatr Taiwan 2004; 45:328-33.
16. Wang SF, Huang FY, Chiu NC, Tsai TC, Ho UY, Kao HA, Hsu CH, Hung HY. Urinary tract infection in infants less than 2 months of age. Zhonghua Min Guo Xiao Er Ke Yi Xue Hui Za Zhi 1994; 35:294-300.
17. Lutter SA, Currie ML, Mitz LB, Greenbaum LA. Antibiotic resistance patterns in children hospitalized for urinary tract infections. Arch Pediatr Adolesc Med 2005; 159:924-28.

18. Fan SY, Zhang BL, Wang WH, Zhang X. [Bacterial pathogens and resistance patterns in community acquired pediatric urinary tract infection: experience of 152 cases]. Zhongguo Dang Dai Er Ke Za Zhi 2006; 8:115-17.
19. van Pinxteren B, van Vliet SM, Wiersma TJ, Goudswaard AN. [Summary of the practice guideline 'Urinary-tract infections' (second revision) from the Dutch College of General Practitioners]. Ned Tijdschr Geneeskd 2006; 150:718-22.
20. Hernandez-Porras M, Salmeron-Arteaga G, Medina-Santillan R. Microbial resistance to antibiotics used to treat urinary tract infections in Mexican children. Proc West Pharmacol Soc 2004; 47:120-21.
21. Dromigny JA, Nabeth P, Juergens-Behr A, Perrier-Gros-Claude JD. Risk factors for antibiotic-resistant *Escherichia coli* isolated from community-acquired urinary tract infections in Dakar, Senegal. J Antimicrob Chemother 2005; 56:236-39.
22. Prado V, Trucco O, Duran C, Mamani R, Royer M. [Profile of antimicrobial resistance of agents causing urinary tract infections in Chilean children. PRONARES surveillance program]. Rev Med Chil 2001; 129:877-85.
23. Katosova LK, Zorkin SN, Alekhina VM, Chashchina IL, Abramov KS. [Resistance of urinary tract infection pathogens and choice of antibacterial therapy in pediatric urologic practice]. Antibiot Khimioter 2004; 49:34-39.
24. Mazzulli T. Resistance trends in urinary tract pathogens and impact on management. J Urol 2002; 168:1720-22.
25. Sotto A, De Boever CM, Fabbro-Peray P, Gouby A, Sirot D, Jourdan J. Risk factors for antibiotic-resistant *Escherichia coli* isolated from hospitalized patients with urinary tract infections: a prospective study. J Clin Microbiol 2001; 39:438-44.
26. Soroush S, Haghi-Ashtiani MT, Taheri-Kalani M, et al. Antimicrobial resistance of nosocomial strain of *Acinetobacter baumannii* in children's medical center of Tehran: A 6-year prospective study. Acta Med Iran 2010; 48:178-84.

CHLAMYDOPHILA PNEUMONIA AND INCREASED *TLR4* GENE EXPRESSION IN LEUKOCYTES ARE ASSOCIATED WITH ACUTE MYOCARDIAL INFARCTION

L.G. LIMA-NETO[1,2], R.D.C. HIRATA[1], A.D. LUCHESSI[1], V.N. SILBIGER[1], D. CAVICHIOLI[1], E.S. DOS SANTOS[3], A.G.M. SOUSA[3], S.R.S. SPROVIERI[4], E.B. DE SOUSA-JUNIOR[4], F.C.P. DOS SANTOS[5], S. COLOMBO[5] and M.H. HIRATA[1]

[1]School of Pharmaceutical Sciences, University of Sao Paulo, Sao Paulo, Brazil; [2]Laboratory of Immunology, CEUMA University, Sao Luis, Brazil; [3]Institute Dante Pazzanese of Cardiology, Sao Paulo, Brazil; [4]School of Medical Sciences, Santa Casa of Sao Paulo, Sao Paulo, Brazil; [5]Institute Adolfo Lutz, Sao Paulo, Brazil

Received June 28, 2013 – Accepted May 26, 2014

We investigated the relationship of the positivity for *Chlamydophila pneumoniae* (*Cpn*) and *Mycoplasma pneumonia* (*Mpn*), inflammatory and metabolic markers, and mRNA expression and polymorphisms of the *TLR2, TLR4, IL-6* and *TNFA* genes with acute myocardial infarction (AMI). Two hundred and eighteen individuals (98 AMI and 120 non-AMI) were selected at two Clinical Centers. Blood samples were drawn to extract DNA and RNA and to measure laboratory variables including anti-*Cpn* IgM and IgG. *Cpn* and *Mpn* genomic DNA as well as *TLR2, TLR4, IL-6* and *TNFA* mRNA expression were evaluated by quantitative real-time PCR (qPCR). Gene polymorphisms were detected by PCR-HRM. AMI patients had higher positivity for *Cpn*-DNA (17.3%) than non-AMI group (6.7%, p=0.018). In addition, *Cpn*-DNA positivity was an independent predictor of risk for AMI (OR: 2.56, CI: 1.08 - 6.04, p=0.031). Positivity for anti-*Cpn* IgG and *Mpn*-DNA was similar between AMI and non-AMI (p>0.05). *TLR4* mRNA expression was higher in AMI than non-AMI individuals (p=0.005). *CD14* -260C>T, *TNFA* -308A>G, *TLR2 c.2258G>A*, *TLR4* c.896A>G and *TLR4* c.1196C>T variants were not associated with increased risk for AMI (p>0.05). In the AMI group, individuals carrying *CD14* -260CC genotype had higher hsCRP levels than CT/TT carriers (p=0.041). These results are suggestive that *Cpn*-DNA positivity and increased *TLR4* mRNA expression in blood leukocytes may be associated with AMI and could be useful markers to evaluate the severity and progression of the atherosclerotic disease in AMI patients.

Atherosclerosis is considered to be an inflammatory disease, secondary to endothelial injury, associated with various risk factors, such as cigarette smoking, hypercholesterolaemia, high arterial blood pressure and, more recently, with infectious agents (1-3).

Several infectious agents have been investigated for being part of the instability of the atheroma plaque. *Chlamydophila pneumoniae* (*Cpn*), an obligate intracellular bacterium, was detected in atheroma plaque and it has been suggested to participate in the atherosclerotic process leading to

Key words: Chlamydophila pneumonia, acute myocardial infarction, gene expression, polymorphisms

Mailing address: Dr Lidio G. Lima-Neto
Laboratory of Immunology,
CEUMA University
1, Josué Montello Street, Renascença II
65075120, São Luís, MA, Brazil
Tel.: +55 98 3214 4336 Fax: + 55 98 3214 4124
e-mail: lidio.neto@outlook.com

0393-974X (2014)

acute myocardial infarction (AMI) (4). Our group previously demonstrated that a co-infection with *Cpn* and *Mycoplasma pneumoniae* (*Mpn*) was linked to coronary plaque rupture, in association with vessel dilatation and adventicial inflammation (5) using an aortic atherosclerosis aneurysm study. A relationship between the positivity for anti-*Mpn* antibodies and coronary artery disease (CAD) was found only in patients with *Cpn* positivity (6), suggesting that coinfection may be an important risk factor for CAD, but the pathophysiological mechanisms remain to be elucidated.

Cpn and *Mpn* infect mucosal surfaces of the human respiratory tract causing pneumonia and bronchitis. *Cpn* can survive into immune cells by disarming mechanisms of innate immunity likely because *Cpn* infection blocks type I interferon (IFN) induction by preventing phosphorylation and nuclear translocation of the IFN regulatory factor 3 (IRF3), as demonstrated in infected epithelial cells (7). Thus, this respiratory bacterium may disseminate through peripheral blood leukocytes until reaching coronary arteries. Therefore, the detection of *Cpn* and *Mpn* in peripheral blood leukocytes of AMI patients may support the participation of these pathogens in the development of atherosclerosis. Although several studies have shown the presence of *Cpn* and *Mpn* within atheroma plaque (5, 8, 9), it is not clear whether *Cpn* and *Mpn* are passive inhabitants of the plaque or if these bacteria induce and/or intensify the inflammatory process in the arterial wall.

Toll-like receptors (TLR) and CD14 are receptors involved in microbial recognition by immune cells causing an inflammatory response. Increased expression of TLR encoding genes was found in coronary atherosclerotic lesion of patients with acute coronary syndrome (ACS) or stable angina pectoris suggesting that some types of bacteria could trigger the up-regulation of inflammatory-related genes in affected patients (10). Moreover, increased plasma inflammatory markers, such as interleukin (IL)-4 and IL-8, and intercellular adhesion molecule-1 (ICAM-1) have also been found in CAD patients after infection with *Cpn* IgA, and may make an important contribution to CAD progression (11).

Common variants in genes encoding CD14 (*CD14* -260C>T) and tumor necrosis factor alpha (*TNFA* -308G>A) have been reported to be associated with increased gene expression leading to an enhanced inflammatory process in elderly myocardial infarction patients (12). It is likely that *CD14* -260C>T and *TNFA* -308G>A polymorphisms contribute to inter-individual differences in susceptibility to *Cpn* and *Mpn* infections. It was also observed that individuals carrying *CD14* -260TT genotype are more susceptible to *Cpn* infection (13). In addition, variants in the *TLR4* (c.896A>G and c.1196C>T) and *TLR2* (c.2258G>A) have been shown to alter protein activity in leukocytes, which could reduce cytokine response and increase susceptibility to infection (12, 14). We investigated the association of the *Cpn* and *Mpn* positivity, metabolic and inflammatory markers, mRNA expression and polymorphisms of inflammatory-related genes with acute myocardial infarction (AMI).

MATERIALS AND METHODS

Subjects

Two hundred eighteen non-related individuals (<70 y) with AMI (n=98) and without AMI (non-AMI, n=120) were selected at two Clinical Centers (Institute Dante Pazzanese of Cardiology (IDPC) and Santa Casa of Sao Paulo (SCSP), Sao Paulo city, Brazil. AMI was diagnosed by clinical and laboratory evaluation according to the World Health Organization (WHO) criteria (15).

Biodemographic data and information on age, height and weight, cigarette smoking, alcohol consumption, hypertension and diabetes were evaluated. Each individual declared his ethnic group during the interview as required by Brazilian legislation. Those with increased systolic/diastolic blood pressure (≥140/90 mmHg) or under anti-hypertensive therapy were considered hypertensive (16). Diabetics were considered as those individuals with increased fasting glycemia (≥ 7.0 mmol/l, 126 mg/dl) or those receiving any hypoglycemic medication. Current cigarette smokers consumed three or more cigarettes/day. An alcohol consumer was considered one who takes a daily intake dose of 1 g or more of beer, wine, or 6 distilled spirits. Individuals practicing any physical activity or sport were considerate active.

Exclusion criteria were individuals with acute respiratory disease, renal or liver insufficiency, thyroid dysfunction, familial hypercholesterolemia, inflammatory disease, unstable angina, peripheral vascular disease, myocardiopathy, pericardiopathy and hematological disease.

The study protocol was approved by the Ethics Committee of the IDPC, SCSP and School of Pharmaceutical Sciences of the University of Sao Paulo (USP), Sao Paulo

city, Brazil, and each participant gave informed consent.

Blood sampling and laboratory analyses

Blood was drawn from an antecubital vein after at least 8 h of fasting. Trisodium citrate-anticoagulated blood was centrifuged for 25 min at 4°C and used for fibrinogen analysis. EDTA-anticoagulated blood was used for DNA and RNA analyses. Serum was used for biochemical measurements and kept at -80°C until used for detection of anti-*Cpn* IgG and IgM.

Serum glucose, total cholesterol, high-density lipoprotein (HDL) cholesterol and triglycerides were determined by routine laboratory procedures using a fully automated Hitachi mod. 912 system (Roche Diagnostic, São Paulo, Brazil). Low-density lipoprotein (LDL) cholesterol and very low-density lipoprotein (VLDL) cholesterol were calculated using Friedewald´s formula when the triglyceride concentration did not exceed 4.52mmol/l (17).

Serum apolipoprotein (apo) B and AI were determined by immunonephelometry (Dade Behring Marburg GmbH, Marburg, Germany). Serum ultrasensitive C-reactive protein (hsCPR) and IL-6 were measured by chemiluminescence immunoassay (Roche Diagnostic, Sao Paulo, Brazil). Plasma fibrinogen was determined by spectrophotometry using Electra mod. 1400C (Beckman coulter Inc, Palo Alto, CA, USA).

The detection of anti-*Cpn* IgG and IgM was performed using an indirect immunofluorescence assay as previously described (18). The titer >1/512 was considered a cut-off value for positive result, because it is representative for acute infection (19).

Genomic DNA and RNA extraction

The genomic DNA and the total RNA were extracted from EDTA-treated whole blood samples using QIAamp DNA Blood Mini Kit and QIAamp RNA Blood Mini Kit, respectively (QIAGEN, GmbH, Germany) following the manufacturer's protocols, immediately after the venipuncture blood collection.

Cpn-DNA and Mpn-DNA detection

Cpn-DNA and *Mpn*-DNA were detected in blood samples by quantitative real-time PCR (qPCR) using the TaqMan® system. Primers and probes used for the detection of *Cpn*-DNA and *Mpn*-DNA, shown in Table I, were selected using Primer Express software v.1.0 (Applied Biosystems, Foster City, CA, USA). The sequences were based on species-specific highly conservative regions from the 16S rRNA gene. The species-specific primers and probes were identified by multiple sequence alignment using the ClustalW software.

DNA samples were assayed in a 25 µl reaction mixture containing 50 ng template DNA, 200 nM primers and probe, and TaqMan Universal PCR Master Mix (Applied Biosystems, Foster City, CA, USA). PCR were carried out in a ABI Prism 7500 SDS (Applied Biosystems, Foster City, CA, USA) using the cycling conditions: 95°C for 10 min, 40 cycles at 95°C for 15 s and 60°C for 1 min. PCR product sequences were confirmed to be from the 16S rRNA gene by sequencing at the Human Genome Research Center of the USP, São Paulo city, Brazil.

In order to establish positive controls, we cloned plasmids containing the amplified region of each target bacteria. Reference strains were grown as recommended by the American Type Culture Collection (ATCC). The bacterial species used in this study were: *M. pneumonia* strain FH (ATCC 15531) and *C. pneumonia* strain AR39 (ATCC 53592). PCR was performed using 200 nM reverse and forward primers (Table I) (Invitrogen Corporation, CA, USA), 50 ng genomic DNA, 200 µM dNTPs (GE Healthcare, Buckinghamshire, England), 1.0 U termostable DNA polymerase and PCR buffer (50 mM KCl, 20 mmol/l $(NH_4)_2SO_4$, 2 mM $MgCl_2$, 75 mM Tris–HCl (pH 9.0)) (Biotools, Madrid, Spain) in 25 µl total volume. The PCR program consisted of one cycle at 95°C for 3 min; 29 cycles at 95°C for 1 min, 64°C for 1 min, 72°C for 1 min; and one cycle at 72°C for 10 min. Amplification was carried out in a PTC-200 Thermal Cycler (MJ Research Inc., MA, USA). *Cpn* and *Mpn* PCR products were purified using the *QIAquick* PCR purification kit (QIAGEN, GmbH, Germany) and inserted separately into the pGEM-T Easy vectors (Amersham Biosciences, Piscataway/NJ, USA). Clones were sequenced using M13 forward and reverse primers (Table I).

Chemically competent *Escherichia coli* strain DH5-α were transformed with recombinant plasmids (pGEM-*Cpn* and pGEM-*Mpn*) and inserted fragments were detected by restriction fragment analysis using agarose gel electrophoresis. Plasmids were purified with a MaxiPrep (Qiagen, GmbH, Germany) and concentrations were determined by spectrophotometry using ChemiImager 4400 v5.5 (Alpha Innotech Corporation, San Leandro, CA, USA). Plasmid DNA solutions were diluted in water as 10-fold dilutions containing 10^1 to 10^9 plasmid copies. These dilutions of positive plasmid controls for two target microorganisms were run in triplicate by quantitative real-time PCR (qPCR) and standard curves were obtained as previously described (20). pGEM-*Cpn* and pGEM-*Mpn* sequences were confirmed by DNA sequencing.

Gene expression analysis

Total RNA (1 µg) extracted from blood leukocytes was treated with DNAse (Qiagen, Valencia, CA, USA) and then reverse-transcribed with 200U of SuperScript II reverse transcriptase (Invitrogen, MD, USA). *TLR2, TLR4, IL-6* and *TNFA* mRNA levels were determined

by qPCR using TaqMan® system (Applied Biosystems, Foster City, CA, USA). qPCR were assayed in a 25 µl reaction mixture containing of 1 µL cDNA, 200 nM of primers and probe, and TaqMan Universal PCR Master Mix (Life Technologies, Foster City, CA, USA) diluted in nuclease-free water. The thermal cycling protocol consisted of one cycle at 95°C for 10 min, and 40 cycles at 95°C for 15 s and 60°C for 1 min. The amplification was carried out in a 7500 fast real-time system (Life Technologies).

The mRNA expression was calculated for each target gene using the comparative cycle threshold (Ct) method, as previously described (21). Genorm software [http://medgen.ugent.be/genorm] was used to select the most stable endogenous reference gene and the most stable in the experimental conditions was glyceraldehyde-3-phosphate dehydrogenase (*GAPD*) (21).

Gene polymorphism analysis

CD14 -260C>T (rs2569190), *TNFA* -308G>A (rs1800795), *TLR2 c.2258G>A* (rs5743708), *TLR4* c.896A>G (rs4986790) and *TLR4* c.1196C>T (rs4987233) variants were detected by PCR followed by high-resolution melting (HRM) analysis. PCR-HRM assays contained 25 ng genomic DNA, 200 nM of primers (Table I) (Applied Biosystems, Foster City, CA, USA) and 450 nM of SYTO® 9 green fluorescent nucleic acid stain (Invitrogen, Gathersburg, USA) in a 20 µl reaction mixture. PCR was performed on ABI Prism 7500 SDS (Applied Biosystems, Foster City, CA, USA) in conditions as follows: 1 cycle at 95°C for 15 min; 45 cycles at 95°C for 10 s and at 60°C for 30s. Melting curve data were generated by increasing the temperature from 50°C to 95°C at 0.1°C per second and recording fluorescence. HRM curve analysis was performed using HRM v.2.0.1 software (Applied Biosystems, Foster City, CA, USA). Genotyping assays were repeated for 25% of the DNA samples randomly selected. Different genotypes for *CD14, TNFA, TLR2* and *TLR4* polymorphisms were confirmed by DNA sequencing, and thereafter used as reference samples in the genotyping assays.

Statistical analysis

Statistical analyses were performed using Prism v.5.0 for Windows (Graph Pad Software Inc., CA, USA) and SPSS v. 17.0 for Windows (SPSS Inc., Madrid, Spain). Variables without normal distribution were log transformed for analysis. Continuous variables were presented as mean ± SD and compared by *t*-test. Analysis of mRNA expression data were performed using Mann-Whitney *U* test and presented as median. Categorical variables were compared by a *chi*-squared test. Multiple logistic regression analysis was carried out to search for an association between *Cpn*-DNA and *Mpn*-DNA positivity, polymorphisms and other variables with AMI using Wald Stepwise criteria to select variables. For this purpose, the independent variables were grouped into quartiles. High mRNA levels were considered to be values higher than the third quartile. The level of significance was considered 5%.

RESULTS

Characteristics of the study groups

Biodemographic, clinical and laboratory results of the AMI patients and non-AMI subjects are shown in Table II. The AMI group had increased frequency of hypertension, diabetes, cigarette smoking, and even higher age and BMI values, than non-AMI groups ($p<0.05$).

The AMI group also had higher concentrations of glucose, triglycerides, VLDL cholesterol, hsCRP, IL-6 and fibrinogen, and lower HDL cholesterol and Apo AI, when compared with the non-AMI group ($p<0.001$).

Bacterial DNA detection

Positive samples for *Cpn*-DNA were found more frequent in the AMI group (17.3%) than in the non-AMI group (6.7%, p=0.018) (Table II). On the other hand, positivity for anti-*Cpn* IgG (titer >1/512) was similar between AMI (7.1%) and non-AMI (3.8%, p=0.719), while all samples were negative for anti-*Cpn* IgM (titer < 1/16) (data not shown). *Mpn*-DNA positivity was similar between AMI (5.0%) and non-AMI (5.8%, p=1.000) groups (Table II).

According to the multiple logistic regression analysis, individuals positive for *Cpn*-DNA have two times more susceptibility for AMI (OR: 2.56, 95%CI: 1.08-6.04, p=0.031) than those with negative results for *Cpn*-DNA (Table III). However, *Cpn*-DNA positivity was not associated with increased levels of hsCRP, IL-6 and fibrinogen ($p>0.05$) (Data not shown).

Gene expression in blood leukocytes

Results from analysis of mRNA expression in blood leukocytes are shown in Fig. I. AMI individuals showed higher levels of *TLR4* mRNA expression when compared with non-AMI individuals (p=0.005). On the other hand, *TLR2*, *IL6* and *TNFA* mRNA expression was not associated

with AMI condition (Fig. 1). *TLR2* and *TNFA* mRNA leukocyte expression was higher than *TLR4* and *IL6* in both AMI and non-AMI groups ($p<0.05$, data not shown). Results from multiple logistic regression analysis showed that high levels of *TLR2, TLR4, IL-6* and *TNFA* mRNA were not related to AMI (Table III).

Positivity for *Cpn*-DNA was not associated with variability in *TLR4*, *TLR2*, *IL6* and *TNFA* mRNA expressions in AMI individuals ($p>0.05$, Fig. 2). Likewise, AMI subjects with positivity for *Mpn*-DNA had similar *TLR4*, *TLR2*, *IL6* and *TNFA* mRNA expression levels than those with negative results for *Mpn*-DNA (Data not shown). According to the multiple logistic regression analysis, positive individuals for *Cpn*-DNA were not associated with increased mRNA expression of *TLR2, TLR4, IL-6* and *TNFA* (data not shown).

Genetic polymorphisms

Genotype distributions of the *CD14, TNFA*, *TLR2* and *TLR4* polymorphisms were in Hard-Weinberg Equilibrium (HWE), indicating that the

Table I. *Primers and probes sequences used for real time PCR.*

Gene	Primers and Probes	Sequence 5' → 3'	Size (bp)
M13	Forward	GTAAAACGACGCCCAG	280
	Reverse	CAGGAAACAGCTATGAC	
Cpn-DNA	Forward	GGACCTTACCTGGACTTGACATG	70
	Reverse	TGTGTATCTGTCCTTGCGGAAA	
	Probe	FAM-TTGACAACTGTAGAAATAC-MGBNFQ	
Mpn-DNA	Forward	GACCTGCAAGGGTTCGTTATTT	68
	Reverse	GGCCGTTACCCCACCAA	
	Probe	FAM-TGAGGGTGCGCCATA-MGBNFQ	
TLR2	Forward	ATACAGACAAAGGCATACA'	103
	Reverse	ACCATAAACCCAACAACT	
	Probe	FAM-TTTATCGTCTTCCTGGTTCAAGCC-TAMRA	
TLR4	Forward	TGCGTGAGACCAGAAAGC	123
	Reverse	GTCCAGGTTCTTGGTTGA	
	Probe	FAM-ATGTCTGCCTCGCGCCTGGC-TAMRA	
IL6	Forward	GATTGTGCAATGTGACGTCCTT	125
	Reverse	GCTGCACTTTTCCCCCTAGTT	
	Probe	FAM-CGCCTCCAGGAGCCCAGCTATGA-TAMRA	
TNFA	Forward	GTAGGACCCTGGAGGCTGAAC	80
	Reverse	CCCAAAAGAAATGGAGGCAAT	
	Probe	FAM-CCCCCTCCTTCAGACACCCTCAACC-TAMRA	
GAPD	Forward	GGAAGGTGAAGGTCGGAGTCA	130
	Reverse	CTGGAAGATGGTGATGGGATTTC	
	Probe	FAM-CATGGCACCGTCAAGGCTGAGAACG-TAMRA	
CD14 -269C>T	Forward	AACCTAATTCTACCCCCCTTGG	78
(rs2569190)	Reverse	TCAGAGGCAGCCGAAGAGTT	
TNFA -308G>A	Forward	AGCCTCAATGACGACCTAAGCC	84
(rs1800795)	Reverse	AATGAGCCTCAGACATCTCCAGT	
TLR4 c.896A>G	Forward	GATTAGCATACTTAGACTACTACCTCGAAG	98
(rs4986790)	Reverse	CTTCTGAAAAAGCATTCCCACC	
TLR4 c.1196C>T	Forward	GGTTGCTGTTCTCAAAGTGATTTTGGGTCA	104
(rs4986791)	Reverse	AGGAAGTTTTCCTGGAAAGAATTGCCAGC	
TLR2 c2258G>A	Forward	CCATTCCCCAGCGCTTCT	58
(rs57437080)	Reverse	TGAACACCAAGACCTACCTGGA	

Cpn: Chlamydophila pneumoniae; Mpn: Mycoplasma pneumoniae; MGB: minor groove binding; NFQ: nonfluorescente quencher; TAMRA: Carboxytetramethylrhodamine; TLR: Toll-like receptor; IL6: interleukin-6; TNFA: Tumor necrosis factor alpha; GAPD: Glyceraldehyde 3-phosphate dehydrogenase.

Table II. *Biodemographic, clinical and laboratory data of AMI and non-AMI groups.*

Variables	AMI (98)	Non-AMI (120)	*p-value*
Age, years	61.4 ± 10.4	56.2 ± 9.1	<0.001
Men, %	65.0 (65)	75.0 (90)	0.137
Caucasian/African, %	65.0/35.0	65.9/34.1	1.00
BMI, Kg/m²	28.6 ± 3.5	24.0 ± 3.4	<0.001
Hypertension, %	62.0 (62)	20.0 (24)	<0.001
Diabetes, %	20.0 (20)	5.0 (6)	<0.001
Cigarette smoking, %	75.0 (75)	33.3 (40)	<0.001
Alcohol consumption, %	30.0 (30)	23.3 (28)	0.683
Physical activity, %	11.0 (11)	12.5 (15)	0.836
Glucose, mmol/l*	6.6 ± 3.2	5.1 ± 0.6	<0.001
Total cholesterol, mmol/l*	4.7 ± 1.4	4.5 ± 1.1	0.984
HDL cholesterol, mmol/l	1.1 ± 0.2	1.4 ± 0.4	<0.001
LDL cholesterol, mmol/l*	2.8 ± 1.1	2.8 ± 0.9	0.937
VLDL cholesterol, mmol/l*	0.8 ± 0.4	0.5 ± 0.3	<0.001
Triglycerides, mmol/l*	2.1 ± 2.0	1.1 ± 0.6	<0.001
Apolipoprotein AI, g/l	1.3 ± 0.3	1.4 ± 0.3	<0.001
Apolipoprotein B, g/l*	1.0 ± 0.3	0.9 ± 0.2	0.683
hsCRP, ng/ml	0.4 ± 0.9	0.1 ± 0.2	<0.001
IL-6, ρg/ml	11.4 ± 11.6	0.9 ± 1.2	<0.001
Fibrinogen, g/l	4.7 ± 1.9	2.7 ± 0.7	<0.001
Cpn-DNA	17.3 % (17)	6.7 % (8)	0.018
Mpn-DNA	5.0 % (5)	5.8 % (7)	1.000
Anti-*Cpn* IgG	7.1 % (7)	3.8 % (5)	0.719
Minor allele frequency			
TNFA -308G>A	11.0 %	8.3 %	0.364
CD14 -260C>T	36.7 %	32.9 %	0.364
TLR4 Asp299Gly, c.896A>G	4.6 %	3.3 %	0.620
TLR4 Thr399Ile, c.1196C>T	3.6 %	5.0 %	0.492
TLR2 Arg753Gln, c.2258G>A	0.5 %	0.8 %	1.000

Number of individuals in parenthesis. Continuous variables are presented as mean ± SD and compared by t-test. Categorical variables were compared by chi-square test. (*) Log transformed data. AMI: Acute Myocardial Infarction; BMI: Body mass index; HDL: High-density Lipoprotein; LDL: Low-density Lipoprotein; VLDL: Very Low-density Lipoprotein; Cpn: Chlamydophila pneumonia; Mpn: Mycoplasma pneumonia; Ig: Immunoglobulin; hsCRP: high sensitive C-reactive protein; IL-6: Interleukin-6; TNF: Tumor Necrosis Factor; CD14: Cluster of differentiation 14; TLR: Toll-Like receptor.

Table III. *Predictors of susceptibility to AMI. Multiple logistic regression model.*

Predictors	O.R	95%CI	p-value
Cpn-DNA	2.56	1.08 - 6.04	**0.031**
Mpn-DNA	0.86	0.26 - 2.80	0.803
High *TLR4* mRNA	1.74	0.94 - 3.25	0.078
High *IL6* mRNA	1.17	0.63 - 2.17	0.611
High *TLR2* mRNA	1.17	0.63 - 2.17	0.611
High *TNFA* mRNA	0.96	0.51 - 1.78	0.903
TNFA -308G>A	0.56	0.21 - 2.41	0.419
CD14 -260C>T	0.65	0.19 - 2.73	0.512
TLR4 Asp299Gly, c.896A>G	0.89	0.49 - 2.12	0.823
TLR4 Thr399Ile, c.1196C>T	0.76	0.42 - 1.91	0.720
TLR2 c.2258G>A	0.92	0.41-2.32	0.913

High mRNA levels were considered to be values higher than the third quartile. Non-AMI group was used as reference. All polymorphisms were introduced as dummy variables for the presence of less frequent allele. Models were adjusted for age, body mass index, hypertension, diabetes, cigarette smoking and alcohol consumption. OR: odds ratio; CI: confidence interval; Cpn: Chlamydophila pneumoniae; Mpn, Mycoplasma pneumoniae; IL6: Interleukin-6; TNFA: Tumor necrosis factor alpha; TLR: Toll-like receptor.

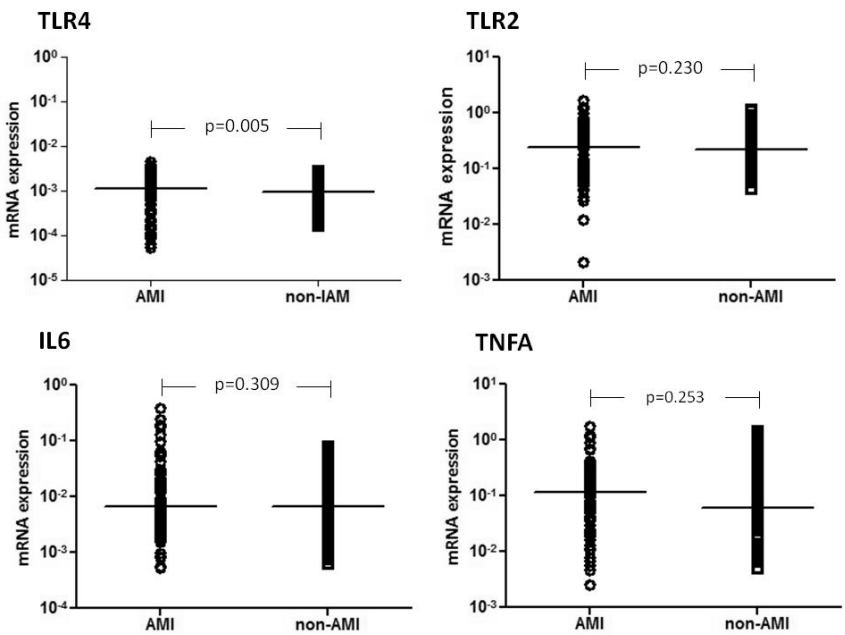

Fig. 1. *TLR4, TLR2, IL6 and TNFA mRNA expression in peripheral blood leukocytes. Values are presented as a dispersion plot with bars indicating median values and compared by Mann-Whitney U test and expressed as a relative value of mRNA quantification to the control ($2^{-\Delta CT}$).*

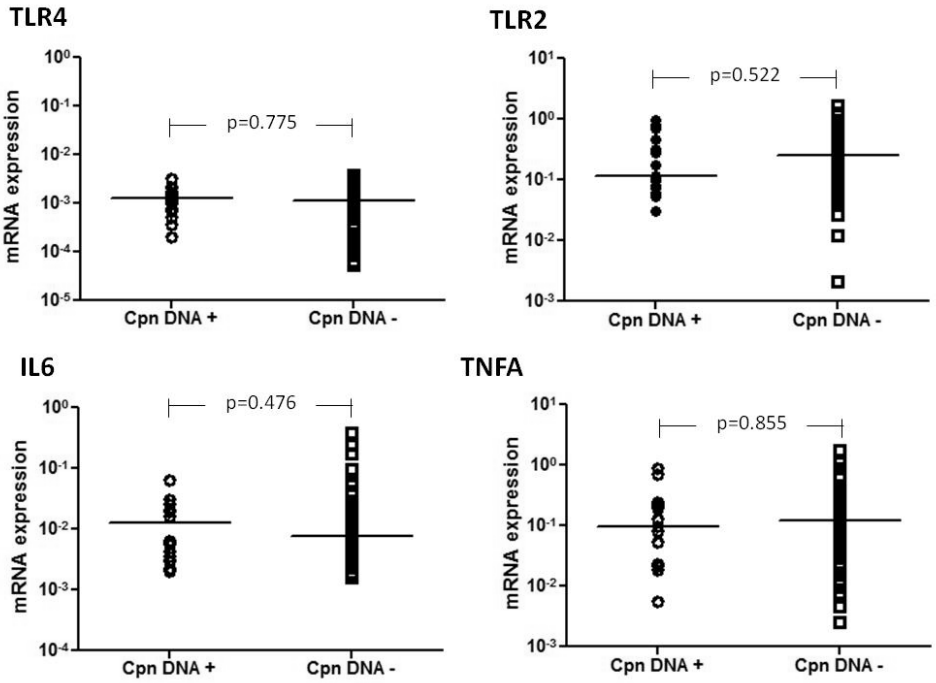

Fig. 2. *TLR4, TLR2, IL6 and TNFA mRNA expression in AMI patients according to Cpn-DNA positivity. Values are presented as a dispersion plot with bars indicating median values and compared by Mann-Whitney U test and expressed as a relative value of mRNA quantification to the control ($2^{-\Delta CT}$).*

sampling method was appropriate and the number of cases is representative (data not shown). Allelic frequencies of *TNFA* -308G>A, *CD14* -260C>T, *TLR2 c.2258G>A*, *TLR4* c.896A>G and *TLR4* c.1196C>T variants were similar between AMI and non-AMI individuals (p>0.05) as shown in Table II. Multiple logistic regression analysis confirmed that these polymorphisms were not associated with AMI (Table III).

CD14 -260T allele (CT/TT genotypes) tended to be associated with positivity for *Cpn*-DNA in AMI group (p=0.055). Lack of relationship was found between positivity for *Cpn*-DNA and *TNFA* -308A>G (Table IV), *TLR2 c.2258G>A*, *TLR4* c.896A>G or *TLR4* c.1196C>T variants (data not shown). Nor was positivity for *Mpn*-DNA related to the studied variants in AMI group (Data not shown).

The influence of *CD14* -260C>T and *TNFA* -308A>G polymorphisms on inflammatory and metabolic markers in AMI group was also investigated, as shown in Table IV. Individuals carrying *CD14* -260CC genotype had higher hsCRP levels than CT/TT carriers (p=0.041). No statistical significance was observed between *CD14* -260C>T genotypes for other inflammatory markers (IL-6 and fibrinogen) or metabolic variables (p>0.05). In the same way, *TNFA* -308A>G, *TLR2 c.2258G>A*, *TLR4* c.896A>G and *TLR4* c.1196C>T polymorphisms were not associated with variability in inflammatory and metabolic markers (p>0.05).

DISCUSSION

In this study, the presence of *Cpn*-DNA and *Mpn*-DNA was detected in peripheral blood leucocytes and positivity for *Cpn*-DNA associated with AMI. These results contribute with previous studies that have found an association between *Cpn*-DNA and atherosclerosis using peripheral blood leukocytes (22) and atheroma plaque as study models (21-23). Prager et al. detected *Cpn*-DNA in 86.9% of the peripheral blood leukocytes and in 82.6% of the

Table IV. *Relationship of the TNFA and CD14 polymorphisms with Cpn-DNA and Mpn-DNA positivity and inflammatory and metabolic markers in AMI group.*

Variable	*CD14* -260C>T genotypes			*TNFA* -308G>A genotype		
	-260CC (40)	-260CT/TT (58)	*p*	-308GG (76)	-308GA/AA (22)	*p*
Cpn-DNA +	7.5 % (3)	24.1 % (14)	0.055	15.8 % (12)	22.7 % (5)	0.543
Mpn-DNA +	5.0 % (2)	5.2 (3)	0.928	5.3 % (4)	4.5 % (1)	1.000
Anti-*Cp* IgG +	2.5 % (1)	10.3 % (6)	0.234	5.3 % (4)	13.6 % (3)	0.353
hsCRP, ng/mL	0.6 ± 0.8	0.3 ± 1.1	**0.041**	0.4 ± 1.0	0.3 ± 0.4	0.868
IL-6, pg/mL	13.5 ± 12.1	9.9 ± 11.1	0.064	10.8 ± 11.2	13.2 ± 12.8	0.551
Fibrinogen, g/l	4.8 ± 2.1	3.9 ± 1.7	0.107	4.2 ± 1.7	4.8 ± 2.0	0.866
Glucose, mmol/l	5.86±3.14	4.84±4.14	0.411	5.71±3.17	5.98±3.89	0.741
Total cholesterol, mmol/l	4.37±1.41	3.76±0.90	0.184	4.28±1.36	4.49±1.43	0.709
HDL cholesterol, mmol/l	0.99±0.29	0.94±0.41	0.554	1.23±0.33	1.09±0.29	0.079
LDL cholesterol, mmol/l	2.72±1.08	2.49±0.54	0.738	2.76±1.10	2.31±0.44	0.347
VLDL cholesterol, mmol/l	0.42±0.25	0.47±0.38	0.065	0.73±0.49	0.60±0.34	0.841
Triglycerides, mmol/l	1.87±1.1.45	1.23±0.87	0.072	1.83±2.00	1.25±0.92	0.241
Apolipoprotein A1, g/l	1.32±0.39	1.15±0.18	0.399	1.37±0.33	1.53±0.18	0.074
Apolipoprotein B, g/l	0.97±0.31	0.82±0.23	0.338	0.97±0.31	0.90±0.32	0.487

Number of individuals in parenthesis. Continuous variables are presented as mean ± SD and compared by t-test. Categorical variables were compared by chi-square test. AMI: acute myocardial infarction; Cpn: Chlamydophila pneumonia; Mpn: Mycoplasma pneumonia; IgG: immunoglobulin G; hsCRP: high sensitive C-reactive protein; IL-6: interleukin-6; HDL: high-density lipoprotein; LDL: low-density lipoprotein; VLDL: very low-density lipoprotein; TNFA: Tumor necrosis factor alpha; CD14: Cluster of differentiation 14.

atherosclerotic plaques from 46 patients undergoing carotid endarterectomy showing that *Cpn* may be associated with atherosclerosis (21). Sessa et al. reported a similar distribution pattern of the *Cpn*-DNA among carotid plaque and peripheral blood mononuclear cells (PBMC), but not in lymph nodes, in 30 patients with carotid atherosclerotic disease. The authors suggested PBMC model as a less invasive procedure to detect *Cpn* in patients with chlamydia-positive atherosclerotic plaques (23). Jha et al. showed high prevalence of *Cpn*-DNA in the aorta (64.7%) and in the coronary artery (58.3%) of CAD patients (24). The presence of circulating *Cpn*-DNA was also evaluated in a sample of CAD 296 patients and this interesting study showed an association between positivity for *Cpn*-DNA and advanced CAD, suggesting that *Cpn* infection may be a contributing factor to progression of coronary atherosclerosis (25). Although the *Cpn*-DNA positivity in our study was lower than that observed in other studies using CAD patients, we found association between *Cpn*-DNA and AMI, which is the main manifestation of atherosclerosis. Taken together, these results are suggestive that *Cpn*-infection is involved in the pathophysiology of atherosclerosis, and the exacerbation of the inflammatory response may result in the disruption of the atheroma plaque and AMI.

In a previous study, we found 100% positivity for *Mpn* antigens in 27 tissues from patients with aortic atherosclerosis aneurysm (AAA) using immunohistochemistry (IHC) assays (5). We concluded that infection by *Mpn* participates in the pathogenesis of AAA as well as the symbiotic co-infection by *Cpn* and *Mpn*. In this study, *Mpn*-DNA positivity in blood leukocytes was not associated with AMI, whereas we found a low frequency of *Mpn*-DNA (5%) in AMI patients. On the other hand, Weiss et al. detected the presence of *Mpn*-DNA in 13 (36.1%) atherosclerotic plaques and 27 (25%) blood leukocytes of 36 samples from patients undergoing carotid endarterectomy (26), but no association was

observed between the presence of *Mpn*-DNA in leucocytes and atherosclerotic plaques. Therefore, the authors concluded that the random distribution of *Mpn* in tissue samples does not support a role for *Mpn* in the development of atherosclerosis. These contradictory results are suggestive that the relationship between positivity for *Mpn* and atherosclerosis or CAD depends on the study model, size sample, severity of the atherosclerotic disease and other factors. Therefore, more studies are necessary to elucidate the mechanisms by which *Mpn* infection contributes to the development and progression of the coronary atherosclerotic process.

In our study, increased *TLR4* mRNA expression in blood leukocytes was associated with AMI, which is suggestive of the TLR4 involvement in the inflammatory response related to AMI. Increased *TLR4* mRNA levels in circulating monocytes were also reported in CAD patients (27). In addition, Fukushima et al. showed that *TLR4* mRNA expression levels in coronary plaques was higher in ACS patients than in those with stable angina pectoris using coronary plaques (10). The TLR2 and TLR4 are transmembrane receptors involved in the innate immune system response to the presence of foreign microorganisms in the host organism. Associated with theirs ligand, TLR2 and TLR4 induce the production of inflammatory markers (28). Therefore, leukocyte *TLR4* mRNA expression may be a potential marker to evaluate the progress of the atherosclerotic disease in AMI patients, as well as to monitor the pharmacological therapy.

We evaluated whether positivity for *Cpn*-DNA was associated with altered *TLR4* mRNA expression in blood leukocytes and no relationship was found. Indeed, chlamydial components such as lipopolysaccharide (LPS) and chlamydial heat shock protein 60 (cHSP60) are recognized by TLR4 and the intact organisms stimulate the innate immune cells through TLR2 (29). Nevertheless, *Cpn* is a highly adapted pathogen that can productively infect macrophages and disarm essential aspects of innate immunity, whereas *Cpn* infection targets TRAF3 for degradation as demonstrated in infected epithelial cells (7). This degradation may explain why *Cpn*-DNA positivity was not associated either with increased mRNA expression of *TLR4* nor with *TLR2, IL6* and *TNFA* gene expression.

Our previous study demonstrated that *CD14* -260C>T, *IL6* -174G>C and *TLR4* c.896A>G and *TLR4* c.1196C>T variants were not associated with AMI in young patients (30). Likewise, in this study, these variants and *TNFA* -308A>G polymorphism were not associated with AMI in older patients. A meta-analysis covering a total of 8,299 AMI cases and 6,849 controls indicated that the *TLR4* c.896A>G polymorphism was not associated with AMI risk (31) corroborating our findings. On the other hand, Pu et al. performed a meta-analysis of 28 studies involving 13,335 coronary heart disease (CHD) cases and 7,979 controls and found that *CD14* -260C>T polymorphism was a risk factor for CHD (32). The relationship between *TNFA* -308A>G polymorphism and AMI was investigated by Ghaderian et al. in a case-control study with AMI patients (33). The authors found that *TNFA* -308A>G polymorphism might be helpful for determining susceptibility to AMI in Iranian patients.

An interesting tendency of association was observed between *Cpn*-DNA positivity and *CD14* -260C>T polymorphism, and it is likely that the *CD14* variant alters the expression of CD14 protein, which may increase the susceptibility to chlamydial infection in macrophages. Poikonen et al. evaluated the effects of the *CD14* -260C>T, *TLR2* Arg753Gln and *TLR4* Asp299Gly polymorphisms on *Cpn* growth in human macrophages *in vitro*. They found that the *Cpn* growth was high in *CD14* -260TT genotype carrying cells and the other polymorphisms had no effect on chlamydial growth (34).

We found an association between *CD14* -260CC genotype and higher levels of hsCRP in AMI patients. Conversely, *CD14* -260TT genotype was independently associated with increased hsCRP levels in one study with a sample of CAD patients (35). These contradictory results are suggestive that the relationship between *CD14* -260C>T polymorphisms and hsCRP levels may depend on genetic, epigenetic and environmental factors as well as the study model, size sample, and severity of the CHD.

In conclusion, the results from this study are suggestive that positivity for *Cpn*-DNA and increased mRNA expression of *TLR4* in blood leukocytes may be associated with AMI and could be useful markers to evaluate the severity and progression of the

atherosclerotic disease in AMI patients.

ACKNOWLEDGEMENTS

This study was supported by grants from FAPESP (# 2006/04163-8), Brazil. The authors thank Elvira Maria Guerra-Shinohara and Alvaro Cerda for support in statistical analysis and Cristina Fajardo for technical support. Andre D. Luchessi, Mario H. Hirata and Rosario D.C. Hirata are recipients of fellowships from CNPq, Brazil. Lidio G Lima Neto and Vivian N. Silbiger were recipients of fellowships from FAPESP, Brazil.

REFERENCES

1. Ross R. Atherosclerosis--an inflammatory disease. N Engl J Med 1999; 340(2):115-26.
2. Campbell LA, Kuo CC. Chlamydia pneumoniae--an infectious risk factor for atherosclerosis? Nat Rev Microbiol 2004; 2(1):23-32.
3. Schiavoni G, Di Pietro M, Ronco C, et al. Chlamydia pneumoniae infection as a risk factor for accelerated atherosclerosis in hemodialysis patients. J Biol Regul Homeost Agents 2010; 24(3):367-75.
4. Sessa R, Di Pietro M, Schiavoni G, et al. Detection of Chlamydia pneumoniae in atherosclerotic coronary arteries. Int J Immunopathol Pharmacol 2004; 17(3):301-6.
5. De Assis, RM, Higuchi ML, Reis MM, Palomino SAP, Hirata RDC, Hirata MH. Involviment of TLR2 and TLR4, *Chlamydophila pneumoniae* and *Mycoplasma pneumoniae* in adventitial inflammation of aortic atherosclerotic aneurysm. World J Cardiovasc Dis 2014; (4):14-22.
6. Momiyama Y, Ohmori R, Taniguchi H, Nakamura H, Ohsuzu F. Association of Mycoplasma pneumoniae infection with coronary artery disease and its interaction with chlamydial infection. Atherosclerosis 2004; 176(1):139-44.
7. Wolf K, Fields KA. Chlamydia pneumoniae impairs the innate immune response in infected epithelial cells by targeting TRAF3. J Immunol 2013; 190(4):1695-701.
8. Di Pietro M, Filardo S, De Santis F, Sessa R. Chlamydia pneumoniae infection in atherosclerotic lesion development through oxidative stress: a brief overview. Int J Mol Sci 2013; 14(7):15105-20.
9. Liuzzo G, Ciervo A, Niccoli G, Mancini F, Fusco B, Montone RA, et al. Chlamydia pneumoniae in coronary atherosclerotic plaques and coronary instability. Int J Cardiol 2011; 147(1):176-8.
10. Fukushima R, Soejima H, Fukunaga T, Nakayama M, Oe Y, Oshima S, Sugiyama S, Ogawa H. Expression levels of Toll-like receptor genes in coronary atherosclerotic lesions of patients with acute coronary syndrome or stable angina pectoris. Circ J 2009; 73(8):1479-84.
11. Jha HC, Srivastava P, Sarkar R, Prasad J, Mittal AS. Association of plasma circulatory markers, Chlamydia pneumoniae, and high sensitive C-reactive protein in coronary artery disease patients of India. Mediators Inflamm 2009; 2009:561532.
12. Olivieri F, Antonicelli R, Cardelli M, Marchegiani F, Cavallone L, Mocchegiani E, Franceschi C. Genetic polymorphisms of inflammatory cytokines and myocardial infarction in the elderly. Mech Ageing Dev 2006; 127(6):552-9.
13. Eng HL, Chen CH, Kuo CC, Wu JS, Wang CH, Lin TM. Association of CD14 promoter gene polymorphism and Chlamydia pneumoniae infection. J Infect Dis 2003; 188(1):90-7.
14. Ferwerda B, McCall MB, Verheijen K, Kullberg BJ, van der Ven AJ, Van der Meer JW, Netea MG. Functional consequences of toll-like receptor 4 polymorphisms. Mol Med 2008; 14(5-6):346-52.
15. Mendis S, Thygesen K, Kuulasmaa K, Giampaoli S, Mahonen M, Ngu Blackett K, Lisheng L. World Health Organization definition of myocardial infarction: 2008-09 revision. Int J Epidemiol 2011; 40(1):139-46.
16. Hanon O, Anagnostopoulos K, Franconi G, Amah G, Safar M, Girerd X. Are the 1999 World Health Organization-International Society of Hypertension recommendations applicable to clinical practice? Arch Mal Coeur Vaiss 2000; 93(8):953-7.
17. Friedewald WT, Levy RI, Fredrickson DS. Estimation of the concentration of low-density lipoprotein cholesterol in plasma, without use of the preparative ultracentrifuge. Clin Chem 1972; 18(6):499-502.
18. Melles HH, Colombo S, Linhares IM, Siqueira LF. Evaluation of parameters for laboratory diagnosis of genital female infection by Chlamydia trachomatis.

Rev Soc Bras Med Trop 2000; 33(4):355-61.

19. Wang S. The microimmunofluorescence test for Chlamydia pneumoniae infection: technique and interpretation. J Infect Dis 2000; 181(S):S421-5.
20. Rodrigues AS, Louren OD, Lima Neto LG, et al. Clinical and microbiological evaluation, by real-time PCR, of non-surgical treatment of aggressive periodontitis associated with amoxicillin and metronidazole. J Periodontol 2011; 83(6):744-52.
21. Silbiger VN, Luchessi AD, Hirata RD, et al. Novel genes detected by transcriptional profiling from whole-blood cells in patients with early onset of acute coronary syndrome. Clin Chim Acta 2013; 5(421):184-90.
22. Prager M, Turel Z, Speidl WS, et al. Chlamydia pneumoniae in carotid artery atherosclerosis: a comparison of its presence in atherosclerotic plaque, healthy vessels, and circulating leukocytes from the same individuals. Stroke 2002; 33(12):2756-61.
23. Sessa R, Di Pietro M, Schiavoni G, et al. Measurement of Chlamydia pneumoniae bacterial load in peripheral blood mononuclear cells may be helpful to assess the state of chlamydial infection in patients with carotid atherosclerotic disease. Atherosclerosis 2007; 195(1):e224-30.
24. Jha HC, Srivastava P, Divya A, Prasad J, Mittal A. Prevalence of Chlamydophila pneumoniae is higher in aorta and coronary artery than in carotid artery of coronary artery disease patients. APMIS 2009; 117(12):905-11.
25. Wang SS, Tondella ML, Bajpai A et al. Circulating Chlamydia pneumoniae DNA and advanced coronary artery disease. Int J Cardiol 2007; 118(2):215-9.
26. Weiss TW, Kvakan H, Kaun C, et al. No evidence for a direct role of Helicobacter pylori and Mycoplasma pneumoniae in carotid artery atherosclerosis. J Clin Pathol 2006; 59(11):1186-90.
27. Ashida K, Miyazaki K, Takayama E, et al. Characterization of the expression of TLR2 (toll-like receptor 2) and TLR4 on circulating monocytes in coronary artery disease. J Atheroscler Thromb 2005; 12(1):53-60.
28. Van der Pouw Kraan TC, Bernink FJ, Yildirim C, et al. Systemic toll-like receptor and interleukin-18 pathway activation in patients with acute ST elevation myocardial infarction. J Mol Cell Cardiol 2014; 67:94-102.
29. Joyee AG, Yang X. Role of toll-like receptors in immune responses to chlamydial infections. Curr Pharm Des 2008; 14(6):593-600.
30. Lima-Neto LG, Hirata RD, Luchessi AD, Silbiger VN, Stephano MA, Sampaio MF, Armaganijan D, Hirata MH. CD14 and IL6 polymorphisms are associated with a pro-atherogenic profile in young adults with acute myocardial infarction. J Thromb Thrombolysis 2012; 36(3): 332-40.
31. Yin YW, Sun QQ, Hu AM, Liu HL, Wang Q, Zhang BB. Toll-like receptor 4 gene Asp299Gly polymorphism in myocardial infarction: a meta-analysis of 15,148 subjects. Hum Immunol 2014; 75(2):163-9.
32. Pu H, Yin J, Wu Y, Zhang D, Wang Y, Zhou R, Jiang P, Liu Y. The association between CD14 gene C-260T polymorphism and coronary heart disease risk: a meta-analysis. Mol Biol Rep 2013; 40(6):4001-8.
33. Ghaderian SM, Akbarzadeh Najar R, Tabatabaei Panah AS. Tumor necrosis factor-alpha: investigation of gene polymorphism and regulation of TACE-TNF-alpha system in patients with acute myocardial infarction. Mol Biol Rep 2011; 38(8):4971-7.
34. Poikonen K, Lajunen T, Silvennoinen-Kassinen S, Leinonen M, Saikku P. Effects of CD14, TLR2, TLR4, LPB, and IL-6 gene polymorphisms on Chlamydia pneumoniae growth in human macrophages in vitro. Scand J Immunol 2009; 70(1):34-9.
35. Bernardo E, Angiolillo DJ, Ramirez C et al. Influence of the CD14 C260T promoter polymorphism on C-reactive protein levels in patients with coronary artery disease. Am J Cardiol 2006; 98(9):1182-4.

ALLERGY-RELATED CHANGES IN LEVELS OF $CD8^+CD25^+FOXP3^{bright}$ TREG CELLS AND FOXP3 mRNA EXPRESSION IN PERIPHERAL BLOOD: THE ROLE OF IL-10 OR TGF-β

M. EUSEBIO[1], P. KUNA[2], L. KRASZULA[1], M. KUPCZYK[2] and M. PIETRUCZUK[1]

[1]*Department of Laboratory Diagnostics, Medical University of Lodz, Poland;* [2]*Department of Internal Medicine, Medical University of Lodz, Poland*

Received October 7, 2013 – Accepted June 27, 2014

There is an increasing body of evidence that alterations of regulatory T (T_{reg}) cell numbers and functions lead to immune disorders. Accordingly, understanding the regulatory mechanisms that maintain peripheral regulatory T (T_{reg}) cell homeostasis is key to the development of effective targeted biologic therapies. We previously demonstrated the effects of IL-10 or TGF-β on distinct $CD8^+CD28^-$ T cell subsets *in vitro*. Allergy-related changes of $CD8^+CD25^+FoxP3^{bright}$ T_{reg} cells and FoxP3 mRNA expression in peripheral blood were assessed by means of multicolor flow cytometry and real-time polymerase chain reaction (RT-PCR). Co-stimulation of $CD8^+CD25^+$ T cells with anti-CD3/CD28 in the presence of either IL-10 or TGF-β increased the frequency of $CD8^+CD25^+FoxP3^{bright}$ T_{reg} cells in patients with asthma and controls. Likewise, $CD8^+CD25^+$ T cell activation with anti-CD3/CD28 and TGF-β increased FoxP3mRNA expression in all groups. Anti-CD3/CD28 and IL-10 appeared to regulate FoxP3 mRNA expression in a phenotype-dependent manner. Specifically, co-stimulation by anti-CD3/CD28 and IL-10 markedly increased FoxP3 mRNA expression in the severe asthma group whereas it had opposite effects on this value in other groups. Taken altogether, these data suggest that IL-10 and TGF-β may modulate FoxP3 expressions at the protein and mRNA levels in respect to their need for peripheral tolerance.

Allergic asthma is a Th_2 cell-mediated chronic inflammatory syndrome characterized by bronchial hyperresponsiveness to a variety of allergic stimuli (1). It has been previously demonstrated that a subpopulation of T cells known as regulatory T (T_{reg}) cell, plays a role in various physiological and pathological immune responses. Although much attention and funding have been devoted to the role of $CD4^+$ T_{reg} cell in allergy and other immune-mediated diseases, the role of $CD8^+$ T_{reg} cell in immunity, tolerance, and disease remains unclear. A limited number of reports have suggested that T_{reg} cells number and function may be altered in patients with allergic mediated airway inflammation (2). $CD8^+$ T_{reg} cells were shown to regulate Th_2-type cytokine signaling *in vitro* (3). Cytokines are important mediators that regulate leukocyte recruitment during allergic inflammation (4). Specifically, Th_2 cell-related cytokines promote the recruitment of T cells into the inflamed airways. Allergen specific immunotherapy can hinder or limit allergic response by increasing the patterns of cytokines produced by Th_2 and T_{reg} cells (5). Over the past few decades there have been a plethora of attempts to decipher the

Key words: IL-10, TGF-β, allergy, asthma, $CD8^+$ Treg cells

Mailing address: Makandjou-Ola Eusebio, MD, PhD
Department of Laboratory Diagnostics,
II Chair of Internal Medicine,
Medical University of Lodz,
Kopcinski 22 str., 90-153 Lodz, Poland
Tel.: +48 42 677 69 83 Fax: +48 42 678 28 33
e-mail: eusemak@yahoo.com

0393-974X (2014)

implication of $CD8^+$ T_{reg} cell and relevant cytokines including IL-10 and TGF-β in immune tolerance (6). These cytokines are emerging as major regulators of airway immune responses in healthy (7) and allergic (8) subjects. Accordingly, IL-10 and TGF-β appear to mediate immunity and chronic inflammation (9). Anti-IgE antibody has been demonstrated to exert its clinical effects by increasing the levels of IL-10 and TGF-β in patients with allergic asthma (10). TGF-β and IL-10 polymorphisms have been associated with allergy and asthma (11). Although the effects of these cytokines on the differentiation of lymphocytes have been somehow previously investigated (12), their direct role on $CD8^+CD25^+FoxP3^{bright}$ T_{reg} cells and FoxP3 mRNA expression remains unclear. The present study was designed to investigate the changes of $CD8^+CD25^+FoxP3^{bright}$ T_{reg} cells and FoxP3 gene expression in the peripheral blood of allergic asthma subjects (AA) and healthy controls (NC) after short-term culture. Co-stimulation of $CD8^+CD25^+$ cells with anti-CD3/CD28 in the presence of either IL-10 or TGF-β increased the frequency of $CD8^+CD25^+FoxP3^{brigh}$ T_{reg} cells in patients with asthma and controls. Similarly, co stimulation of $CD8^+CD25^+$ T cells by anti-CD3/CD28 and TGF-β increased FoxP3 mRNA expression in all groups. Activation of $CD8^+CD25^+$ T cells by anti-CD3/CD28 and IL-10 appeared to regulate Foxp3 mRNA expression in a phenotype-dependent manner. Specifically, co-stimulation by anti-CD3/CD28 and IL-10 markedly increased Foxp3 mRNA expression in severe asthma (SA) group whereas it had opposite effects on this value in other groups. Taken together, these data suggest that IL-10 and TGF-β may modulate Foxp3 expressions at the protein and mRNA levels in respect to their need for peripheral tolerance.

MATERIALS AND METHODS

Patients and controls

The study protocol was approved by the Local Ethics Committee of the Medical University of Lodz. Each subject provided written informed consent before screening and blood sample collection. Skin-prick tests, total serum immunoglobulin E and forced expiratory volume in 1 second (FEV_1) were measured as previously described (13). Asthma diagnosis was based on several factors, including lung function tests and a detailed medical history of wheezing, breathlessness, and chest tightness as indicated in the GINA (The Global Initiative for Asthma) guidelines. Patients with asthma (AA) (n=50) were stratified into severe (SA) (n=25) or mild to moderate (MA) (n=25) categories according to ENFUMOSA (European Network For Understanding Mechanisms Of Severe Asthma) criteria. Subjects without history of allergy or lung disease and who had negative skin prick test reaction served as controls. All participants were non-smokers and had not had a respiratory tract infection in the preceding month.

Blood samples and cell separation

PBMC were isolated using Ficoll-HyPaque 1077 density gradient centrifugation (Sigma-Aldrich, St Louis, Missouri). PBMCs (1 x 10^6 cells/100 µl) were incubated for 15 min with 5 µl of Human $CD8^+$ T Cell Enrichment Cocktail. Cells were washed with buffer and centrifuged at 1500 r/min for 10 min. The pellet was resuspended in buffer and incubated for 30 min with streptavidin beads. Cells were filtered using magnetic-activated cell sorting protocol. The resulting $CD8^+$ T cell fraction was subsequently incubated for 15 min with CD25-coated magnetic beads conjugated to anti-CD25 mAb (Miltenyi Biotec, mouse IgG1), followed by incubation with anti-human $CD25^{PE}$ mAb (Miltenyi Biotec, clone 4E3, Mouse IgG2b, k). The $CD8^+CD25^+$ fraction was enriched by passing the suspension through LD-columns set on the MACS device (Miltenyi Biotec, USA). The entire procedure was carried out at 4°C. The purity of $CD8^+CD25^+$ T cell was > 97% as assessed by flow cytometry.

In vitro cell activation

For quantitative analysis, freshly isolated $CD8^+CD25^+$ T cells (1x10^6 cells/100µl) were cultured with purified NA/ LE anti-human CD3 mAb (BD Pharmingen, clone UCHT1, Mouse IgG1, k) (10 ug/ ml), in combination with purified NA/LE anti-human $CD28^{PE}$ mAb (BD Pharmingen, clone CD28.2, Mouse IgG1, k) (1ug/ ml) in complete RPMI medium containing 10% fetal bovine serum, 20 mM Hepes buffer, non-essential amino acids, sodium pyruvate, 2 mM L-glutamine, 100 µg/ ml streptomycin and 100 units/ ml penicillin (Sigma-Aldrich). $CD8^+CD25^+$ T cell cultures were stimulated with 10ng/ ml of recombinant anti-human $IL\text{-}10^{PE}$ mAb (BD Pharmingen, clone JES3-19F1, Rat IgG2a, k) or anti-human $TGF\text{-}\beta^{PE}$ mAb (Abcam, clone 2AR2, Rat IgG1, k). The cells were incubated for 72 h in 24-well flat bottom sterile plates (Thermo Fisher Scientific Inc.) at 37°C in a 5% CO_2-humidified atmosphere.

Immune staining and flow cytometry analysis

After isolation, the single-cell suspension (1x10^6/100µl)

of activated or non-activated $CD8^+CD25^+$ T cells were incubated for 30 min at 4°C with anti-human $CD8^{AmCyan}$ mAb (BD Biosciences, clone SK1, Mouse IgG1, k), and anti- human $CD25^{FITC}$ mAb (BD Biosciences, clone M-A251, Mouse IgG1, k). Surfaced labeled cells were washed with Foxp3 permeabilization buffer for 30 min at 4°C. For intracellular Foxp3 staining, cells were incubated with anti- human $FoxP3^{APC}$ mAb (eBioscience, clone 236A/E7, Mouse IgG1, k) for 45 min at 4°C. The frequency of $CD8^+CD25^+$ T cell subsets was measured using a FACS Canto II cytometer equipped with FACS Diva software (Becton Dickinson, San Jose, CA, USA) as previously described (14). The acquisition and analysis were restricted to the lymphocyte gate as determined by their forward (FSC) and side-scatter (SSC) characteristics. Lymphocytes were gated based on their CD8 expression and each subpopulation was gated on CD25, and FoxP3 expression (Fig. 1). All experiments were carried out in triplicate. The same gate specifications were used for each sample.

Real-time reverse transcription–PCR of FoxP3 mRNA

Total RNA was extracted from sorted $CD8^+CD25^+$ T cells using NucliSens Minimag Extraction Reagents kit in accordance with the manufacturer's instructions (BioMérieux Industry, Durham, NC, USA). Taqman reaction was achieved with template cDNA (corresponding to 1 µg total RNA). FoxP3 mRNA was quantified by real-time polymerase using the Brilliant II FAST SYBR QPCR Master kit (Stratagene, USA) in a Light Cycler instrument (Roche Molecular Biochemicals) as described elsewhere (15). Results are presented as folds relative to the expression of GAPDH and are expressed in pmol/µl. The sequences of the primers are as follows: Human FoxP3: Forward primer (FP) 5-CAGCACATTCCCAGAGTTCCT-3 and reverse primer (RP) 5-GCGTGTGAACCAGTGGTAGAT-3. GAPDH: Forward primer (FP) 5-GGCTGCTTTTAACTCTGG-3 and reverse primer (RP) 5-GGAGGGATCTCGCTCC.

Statistical analysis

All statistical analyses were performed using Statistica Polska software (Stat Soft, Poland). The results were compared between groups by Mann-Whitney test. P value less than 0.05 was considered significant.

RESULTS

Patients' characteristics

The characteristics of the AA patients did not differ from those of their healthy gender and age-matched peers. The mean age of the study population was: SA (48±14), MA (42±13), and NC (48.5±14.5).

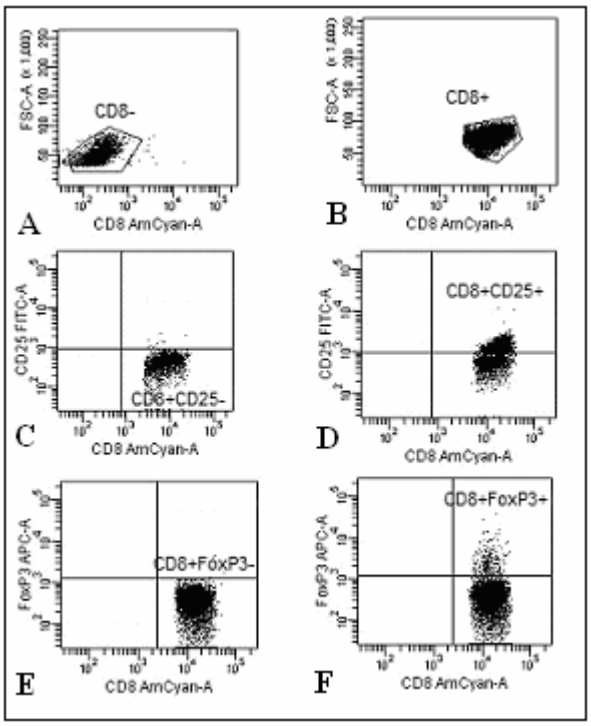

Fig. 1. *Flow cytometric analysis of the expression of CD25 and FoxP3 in $CD8^+$ T cells. Cells were stained for CD8, CD25 and FoxP3 co-expression as described in Materials and Methods. The gates in panel defining $CD8^+$, $CD8^+CD25^+$, $CD8^+FoxP3^+$ T cells events of fully stained cells (***B***, ***D***, ***F***) and their controls (***A***,***C***,***E***), respectively, were created based on FMOs (fluorescence minus one-CD8, CD25 and FoxP3). The FMO gate line is applied to a specific channel to differentiate cells. Dot plots represent the standard data for three independent measurements. Data are representative of allergic asthma subjects and controls groups.*

The AA group included 25 (50%) males and 25 (50%) females. The SA group comprised 12 (48%) men and 13 (52%) women whereas the MA and NC groups included 13 (52%) men and 12 (48%) women. SA patients were taking high doses of inhaled steroids (800-1600 µg/day) of budesonide. MA patients were taking inhaled steroids (200-800 µg/day) of budesonide *pro re nata*.

Severe asthma group had the lowest percentage of $CD8^+CD25^+FoxP3^{bright}$ T_{reg} cells parallel with the highest percentage of $CD8^+CD25^+FoxP3^-$ T cells after enrichment (baseline)

Patients with allergic asthma had lower

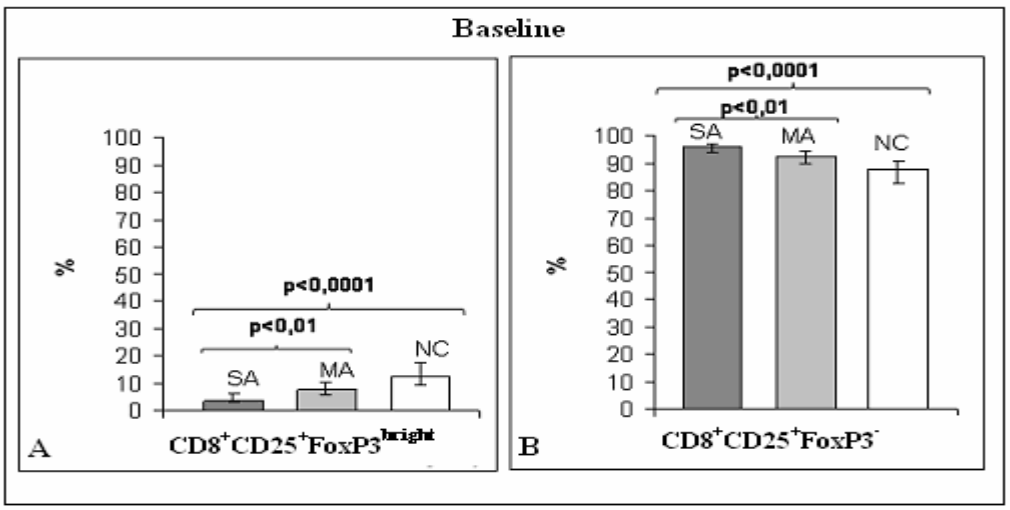

Fig. 2. *Increase of the frequency of CD8⁺CD25⁺FoxP3^{bright} T_{reg} cells and decrease of the frequency of CD8⁺CD25⁺FoxP3⁻ T cells in severe asthma. Purified CD8⁺CD25⁺ T cells from allergic asthma subjects and healthy controls were co-stained for CD8, CD25 and FoxP3 co-expression. The proportions of CD8⁺CD25⁺FoxP3^{bright} Treg cells and CD8⁺CD25⁺FoxP3⁻ T cells subsets were quantified. Bar diagrams indicate the frequency of CD8⁺CD25⁺FoxP3^{bright} T_{reg} cells and CD8⁺CD25⁺FoxP3⁻ T cells subsets. Data are expressed as median percentages ± interquartiles and are representative of three independent experiments. P <0.05 was considered significant.*

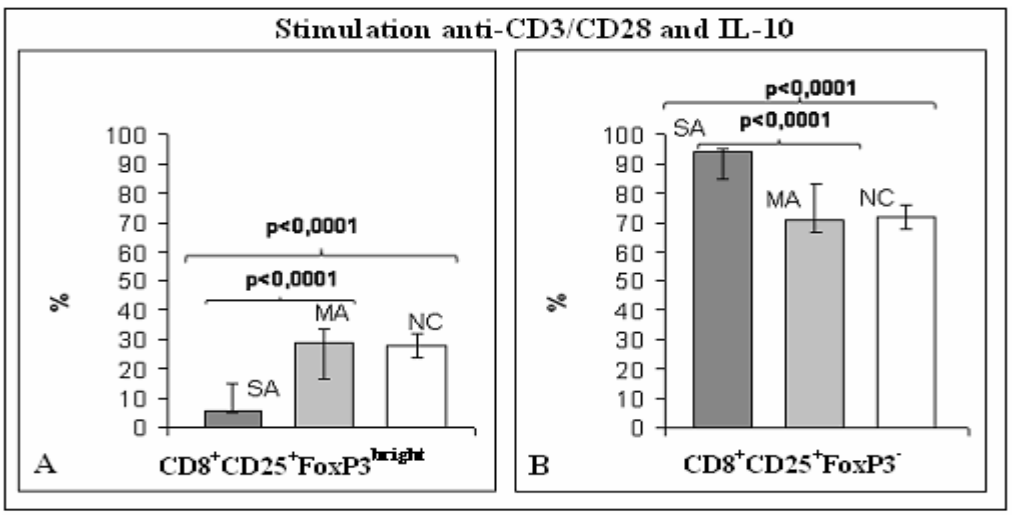

Fig. 3. *Comparison of the effects of anti-CD3/CD28 and IL-10 on the proportion of CD8⁺CD25⁺FoxP3^{bright} Treg cells and CD8⁺CD25⁺FoxP3⁻ T cells in vitro. Freshly isolated CD8⁺CD25⁺ T cells were co stimulated with anti-CD3/CD28 and IL-10. The proportions of CD8⁺CD25⁺FoxP3^{bright} Treg cells and CD8⁺CD25⁺FoxP3⁻ T cells subsets were quantified. Bars represent the median percentages ± interquartiles of three independent experiments. Statistical analysis was performed using Mann-Whitney test. P< 0.05 was considered significant.*

percentages of CD8⁺CD25⁺FoxP3^{bright} T_{reg} cells [(SA (3.4±4.55) *vs* MA (7.5±8.15)] than controls NC (12.1 ±13.2). Moreover, patients with severe asthma had a significantly lower percentage of CD8⁺CD25⁺FoxP3^{bright} Treg cells (3.4±4.55) than those with mild to moderate asthma (7.5±8.15), p<0.01, and age-matched controls (12.1±13.2), p<0.0001 (Fig. 2A). In contrast, subjects with allergic

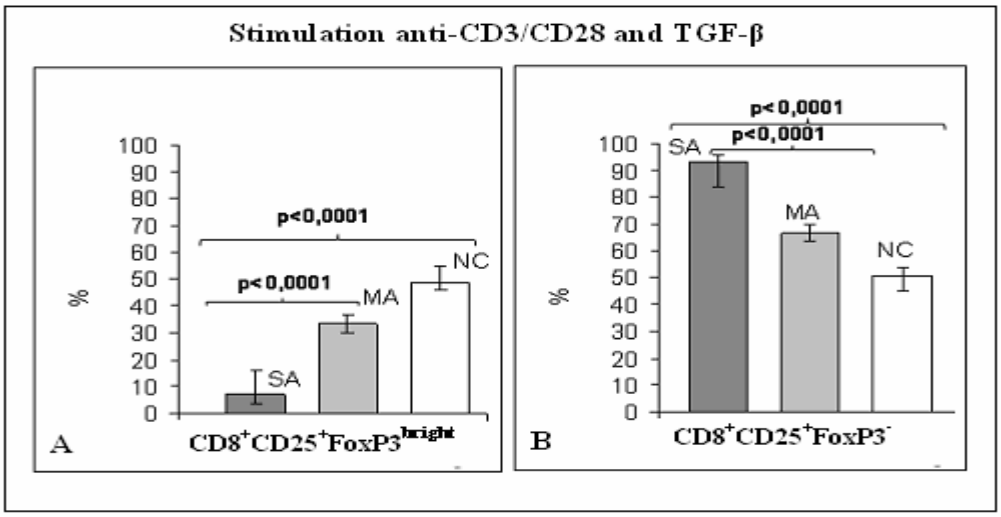

Fig. 4. *Comparison of the effects of anti-CD3/CD28 and TGF-β on the proportion of $CD8^+CD25^+FoxP3^{bright}$ T_{reg} cells and $CD8^+CD25^+FoxP3^-$ T cells in vitro. Freshly isolated $CD8^+CD25^+$ T cells were co stimulated with anti-CD3/CD28 and TGF-β. The proportions of $CD8^+CD25^+FoxP3^{bright}$ Treg cells and $CD8^+CD25^+FoxP3^-$ T cells subsets were quantified. Bars represent the median percentages ± interquartiles of three independent experiments. Statistical analysis was performed using Mann-Whitney test. P< 0.05 was considered significant.*

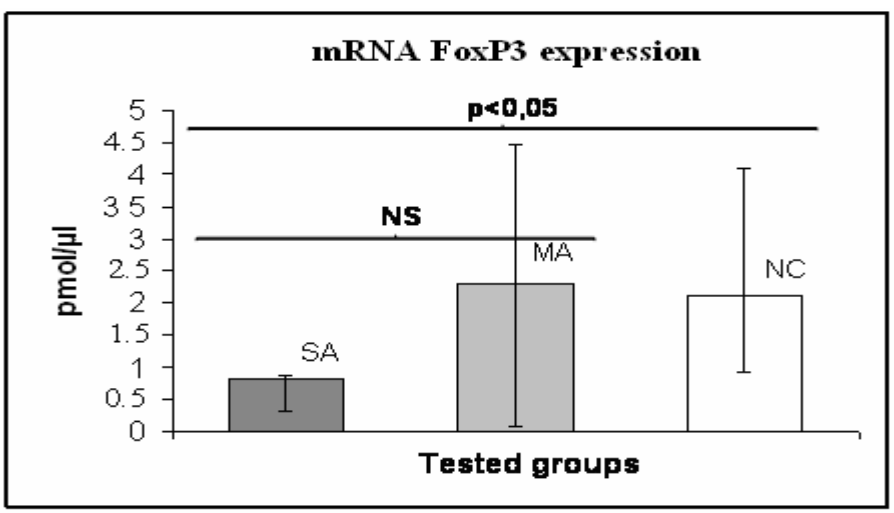

Fig. 5. *Decrease in the Foxp3 mRNA expression in purified $CD8^+CD25^+$ T cells of severe asthma patients compared with controls. The levels of FOXP3 mRNA expression in non stimulated $CD8^+CD25^+$ T cells were assessed by RT-PCR. Bars represent the median percentages ± interquartiles of three independent experiments. There was a significant difference between the Foxp3 mRNA expressions in severe asthma (SA) patients and healthy subjects (NC) (Mann-Whitney test. P< 0.05 was considered significant).*

asthma had higher percentages of $CD8^+CD25^+FoxP3^-$ T cells than controls. Subjects with severe asthma had a significantly higher percentage of these cells (96±95.5) than their mild to moderate asthma counterparts (92.5±91.85), p<0.01 and controls (87.9±86.9) p<0.0001 (Fig. 2B).

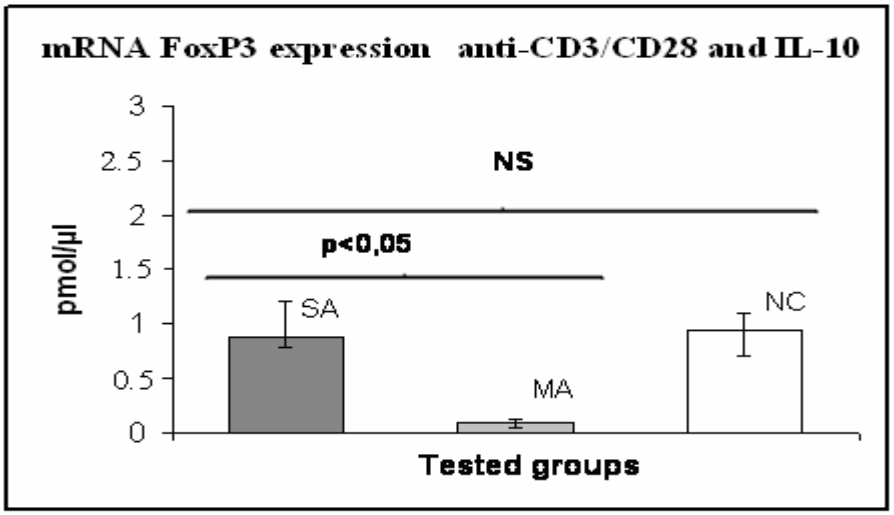

Fig. 6. *Decrease in the Foxp3 mRNA expression in stimulated $CD8^+CD25^+$ T cells of severe asthma patients compared with controls. The levels of FoxP3 mRNA expression in anti-CD3/CD28 and IL-10 stimulated $CD8^+CD25^+$ T cells were assessed by RT-PCR. There were no significant differences between the severe asthma and controls groups with respect to the level of FoxP3 mRNA expression (Mann-Whitney test. P< 0.05 was considered significant).*

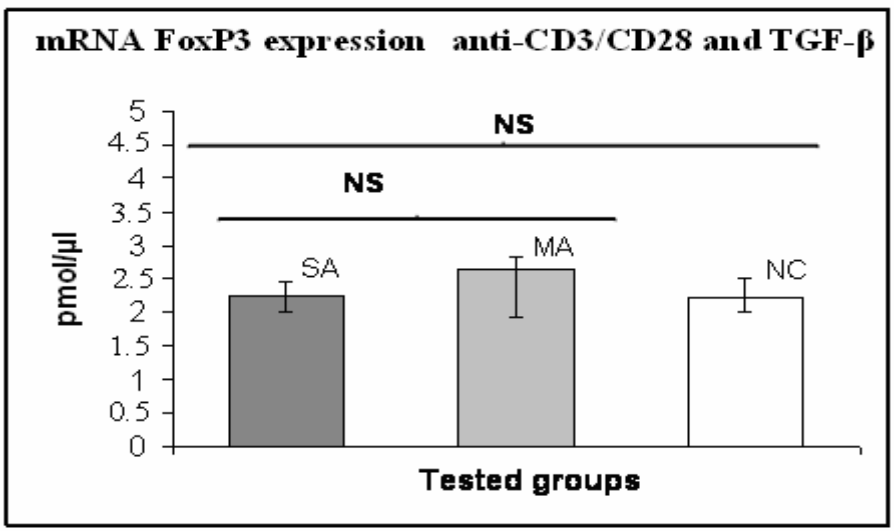

Fig. 7. *Decrease in the Foxp3 mRNA expression in stimulated $CD8^+CD25^+$ T cells of severe asthma patients compared with controls. FoxP3 mRNA expression in anti-CD3/CD28 and TGF-β stimulated $CD8^+CD25^+$ T cells were assessed by RT-PCR. There were no significant differences between the severe asthma and controls groups with respect to the level of FoxP3 mRNA expression (Mann-Whitney test). P< 0.05 was considered significant.*

Co-stimulation of anti-CD3/CD28 activated $CD8^+CD25^+$ T cells in the presence of either IL-10 or TGF-β increased the frequencies of $CD8^+CD25^+FoxP3^{bright}$ T_{reg} cells

Co-stimulation of $CD8^+CD25^+$ T cells with anti-CD3/CD28 in the presence of IL-10 resulted in a 1.57-fold increase in the percentage of $CD8^+CD25^+FoxP3^{brigh}$ T_{reg} cells in patients with severe asthma (3.4±4.55 to 5.5±10) compared with a 3.86-fold increase in this parameter in patients with

mild to moderate asthma (7.5±8.15 to 29.0±25.1) and a 2.31-fold increase in this parameter in controls (12.1±13.2 to 28.0±27.85) (Fig. 3A). Similarly, co-stimulation with anti-CD3/CD28 in the presence of TGF-β induced a 2.14-fold increase in the percentage of this subset in severe asthma subjects (3.4±4.55 to 7.3±10) compared with a 4.49-fold increase in this value in subjects with mild to moderate asthma (7.5±8.15 to 33.7±33.2) and a 4.03-fold increase in this parameter in controls (12.1±13.2 to 48.8±50.5) (Fig.4A).

TGF-β exerted more potent effect on FoxP3 expression in anti-CD3/CD28 activated $CD8^+CD25^+$ T cells than IL-10

Although both cytokines increased the level of FoxP3 expression in anti-CD3/CD28 activated $CD8^+CD25^+$ T cells from severe asthma subjects, the effect of TGF-β was 1.36-fold higher than that induced by IL-10 [(TGF-β=2.14) *vs* (IL-10=1.57)]. Likewise, the effect of TGF-β on the frequency of $CD8^+CD25^+FoxP3^{bright}$ T_{reg} cells from patients with mild to moderate asthma was 1.6-fold higher than that induced by IL-10 [(IL-10=3.86) *vs* TGF-β=4.49)]. The effect of TGF-β on the frequency of $CD8^+CD25^+FoxP3^{bright}$ T_{reg} cells from controls was 4.03-fold higher than that induced by IL-10 [(IL-10=2.31) *vs* (TGF-β= 4.03)].

Severe allergic asthma subjects had the lowest FoxP3 mRNA expression in peripheral blood enriched $CD8^+CD25^+$ T cells at baseline

At early time points (before culture), circulating $CD8^+CD25^+$ T cells from patients with severe asthma (0.82±0.58) expressed a significantly lower level of FoxP3 mRNA than similar cells from healthy donors (2.11±2.5) $p<0.05$. Moreover, patients with severe asthma (0.82±0.58) had a non-significantly lower level of FoxP3 mRNA expression than those with mild to moderate asthma (2.29±2.29), $p>0.05$ (Fig. 5).

Stimulation of $CD8^+CD25^+$ T cells from patients with severe allergic asthma with anti-CD3/CD28 in the presence of either IL-10 or TGF-β increased the level of FoxP3 mRNA expression

Co-stimulation of $CD8^+CD25^+$ T cells from severe asthma subjects with anti-CD3/CD28 and TGF-β induced a 2.71 (0.82±0.58 to 2.23±2.23)-fold increase in the expression of FoxP3 mRNA (Fig. 7). Co-stimulation of these cells with anti-CD3/CD28 and IL-10 induced a 1.07 (0.82±0.58 to 0.88±0.99)-fold increase in the level of FoxP3 mRNA expression (Fig. 6).

TGF-β increased the level of FoxP3 mRNA expression in anti-CD3/CD28 treated $CD8^+CD25^+$ T cells from patients with mild to moderate asthma and controls whereas IL-10 had opposite effects on this parameter

Compared with baseline, co-stimulation of $CD8^+CD25^+$ T cells with anti-CD3/CD28 and TGF-β induced a 1.15 (2.29±2.29 to 2.64±2.38)-fold and a 1.05 (2.11±2.5 to 2.22±2.25)-fold increase in the levels of FoxP3 mRNA expression in patients with mild to moderate asthma and healthy subjects, respectively (Fig. 7). In contrast, co-stimulation of $CD8^+CD25^+$ T cells from healthy subjects with anti-CD3/CD28 and IL-10 induced a 2.27 (2.11±2.5 to 0.93±0.9)-fold decrease in the level of FoxP3 mRNA expression (Fig. 6).

DISCUSSION

IL-10 and TGF-β are key factors in maintaining T-cell tolerance (16). Previous studies have characterized $CD8^+$ T_{reg} cells expressing IL-10 and TGF-β in aberrant immune response in the lung (17). However, the regulatory mechanisms ascribed to this subset in the contest of asthma are not well understood. Environmental factors including T-cell receptor (TCR) stimulation (18) and TGF-β (19) have been shown to regulate the expressions of CD25 and Foxp3. Our previous studies have described the influence of IL-10 and TGF-β on the relative percentages of $CD8^+CD28^-$ T cell subsets from AA subjects and controls (20).

The present study demonstrates the role of activation signals delivered by IL-10 and TGF-β in allergy-related changes in the percentages of circulatory $CD8^+CD25^+FoxP3^{bright}$ T_{reg} cells. The second main observation is that co stimulation of $CD8^+CD25^+$ T cells through anti-CD3/CD28 and TGF-β increased FoxP3 mRNA expression in all groups. Interestingly, anti-CD3/CD28 and IL-10 regulated FoxP3 mRNA expression in a phenotype-

dependent manner. Specifically, anti-CD3/CD28 and IL-10 greatly increased the FoxP3 mRNA expression in the severe asthma group whereas it markedly decreased this parameter in the other groups. The significance of these differential effects of IL-10 on FoxP3 mRNA expression levels is not clear. It is known, however, that weak TCR stimulation enhances Foxp3 induction *in vivo* (21) whereas enhanced TCR stimulation in the presence of anti-CD28, induces NF-κB signaling, which down-regulates Foxp3 induction (22). These preliminary findings may provide explanations for those observations. It has been shown that higher concentration of TGF-β has stimulatory effects on Foxp3 expression (23). Our study demonstrates differences between $CD8^+CD25^+$ T cells from patients with severe and mild to moderate asthma in respect to their response to anti-CD3/CD28 stimulation in the presence of TGF-β. Severe asthma patients showed a remarkable increase in the level of FoxP3 mRNA expression following co-stimulation of $CD8^+CD25^+$ T cells with TGF-β when compared with subjects from the mild to moderate asthma and controls groups. These findings suggest an increased response of $CD8^+CD25^+$ T cells from severe asthma subjects to TGF-β stimulation. Although the present study has demonstrated differences between Foxp3 expressions at the protein and mRNA levels under basal conditions and after short-term culture in a group of allergy asthma patients compared with healthy subjects, it has certain limitations. Co-stimulation with IL-10 resulted in a tremendous decrease in FoxP3 mRNA levels in patients with mild to moderate asthma. It has been previously demonstrated that different drugs influence the level of Foxp3 mRNA and the number of T_{reg} cell. Therefore, although this finding is difficult to explain, it may be related to different treatment protocols in allergy asthma groups. Epigenetic modulation of Foxp3 mRNA expression and T_{reg} cells may provide another plausible explanation to our unexpected finding. It has been hypothesized that epigenetic changes contribute, to some extent, to the differentiation of T-cell (24**),** FoxP3 expression (25), and chronic inflammatory diseases (26). Genetic variants of IL-10 and changes in the pattern of IL-10 methylation appear to play a role in the development of asthma and allergy (27). The role of other genetic/epigenetic factors including the ADAM33 DNA methylation (28) in the pathogenesis of asthma has also been described. TGF-β isoforms namely TGF-β_1 and TGF-β_2 are thought to be involved in the regulation of inflammation, cell growth, and differentiation (29). Specifically, it has also been demonstrated that TGF-β2 inhibits ADAM33 mRNA expression by chromatin modification through DNA methylation (30). Further studies are needed to investigate whether the tremendously decreased levels of FoxP3 mRNA that we observed after co-stimulation with IL-10 were effectively caused by decreased gene expression, or were strongly influenced by the treatment protocol or epigenetic modulation of T_{reg} cell.

In conclusion, we suggest that IL-10 and TGF-β may modulate Foxp3 expressions at the protein and mRNA levels in respect to their need for peripheral tolerance. A better understanding of the values of T_{reg} cells and their markers in asthma may provide clues for prospective therapy and non-invasive diagnosis of allergy. Ongoing trials of target therapies that modulate T_{reg} cells to restore tolerance deserve better attention. Moreover, our preliminary findings, together with additional evidence depicting the role of IL-10 and TGF- β in chronic inflammation, may open new avenues for the selective modulation of cytokine signaling to

ACKNOWLEDGEMENTS

This work was supported by the Polish Academy of Sciences grant KBN nr N N402 517339.

REFERENCES

1. Ciprandi G, De Amici M, Tosca MA, Pistorio A, Marseglia GL. Sublingual immunotherapy affects specific antibody and TGF-beta serum levels in patients with allergic rhinitis. Int J Immunopathol Pharmacol 2009; 22(4):1089-96.
2. Fu R, Li J, Zhong H, Yu D, Zeng X, Deng M, Sun Y, Wen W, Li H. Broncho-Vaxom attenuates allergic airway inflammation by restoring GSK3β-related T regulatory cell insufficiency. Plos One 2014; 9(3):e92912.
3. Adams B, Dubois A, Delbauve S, Debock I, Lhommé F, Glodman M, Flamand V. Expansion of regulatory

CD8+CD25+ T cells after neonatal alloimmunization. Clin Exp Immunol 2011; 163(3):354-61.
4. Di Sciascio MB, Vianale G, Verna N, et al. Eosinophil recruiting chemokines are down-regulated in peripheral blood mononuclear cells of allergic patients treated with deflazacort or desloratadine. Int J Immunopathol Pharmacol 2007; 20(4):745-51.
5. Ahmadiafshar A, Taymourzadeh B, Shaikhi A, Mazloomzadeh S, Torabi Z. Evaluation of IL10, TGF-B and specific IgE and IgG levels during sublingual rye grass immunotherapy. J Aller Ther 2013; 4:132.
6. Elrefaei M, Burke CM, Baker CA, Jones NG, Bousheri S, Bangsberg DR, Cao H. TGF-beta and IL-10 production by HIV-specific CD8+ T cells is regulated by CTLA-4 signaling on CD4+ T cells. PLoS One 2009; 4(12):e8194.
7. Hobbs K, Negri J, Klinnert M, Rosenwasser LJ, Borish L. Interleukin-10 and transforming growth factor-beta promoter polymorphisms in allergies and asthma. Am J respir Crit Care Med 1998; 158(6):1958-62.
8. Jarry A, Bossard C, Bou-Hanna C, Masson D, Espaze E, Denis MG, Laboisse CL. Mucosal IL-10 and TGF-beta play crucial roles in preventing LPS-driven, IFN-gamma-mediated epithelial damage in human colon explants. J Clin Invest 2008; 118(3):1132-42.
9. Herbert DR, Orekov T, Perkins C, Finkelman FD. IL-10 and TGF-beta redundantly protect against severe liver injury and mortality during acute schistosomiasis. J Immunol 2008; 181(10):7214-20.
10. Yalcin AD, Bisgin A, Gorczynski RM. IL-8, IL-10, TGF-β, and GCSF levels were increased in severe persistent allergic asthma patients with the anti-IgE treatment. Mediators Inflamm 2012; 2012:720976.
11. Kim SH, Yang EM, Lee HN, Cho BY, Ye YM, Park HS. Combined effect of IL-10 and TGF-beta1 promoter polymorphisms as a risk factor for aspirin-intolerant asthma and rhinosinusitis. Allergy 2009; 64(8):1221-5.
12. Sanjabi S, Zenewicz LA, Kamanaka M, Flavell RA. Anti-inflammatory and pro-inflammatory roles of TGF-beta, IL-10, and IL-22 in immunity and autoimmunity. Curr Opin Pharmacol 2009; 9(4):447-53.
13. Pietruczuk M, Eusebio M, Kraszula L, Kupczyk M, Kuna P. Phenotypic characterization of *ex vivo* CD4+CD25highCD127low immune regulatory T cells in allergic asthma: pathogenesis relevance of their FoxP3, GITR, CTLA-4 and FAS expressions. J Biol Regul Homeost Agents 2012; 26(4):627-39.
14. Eusebio M, Kraszula L, Kupczyk M, Kuna P, Pietruczuk M. Low frequency of CD8+CD25+FOXP3(BRIGHT) T cells and FOXP3 mRNA expression in the peripheral blood of allergic asthma patients. J Biol Regul Homeost Agents 2012; 26(2):211-20.
15. Hardick J, Yang S, Lin S, Duncan D, Gaydos C. Use of the Roche Light Cycler instrument in a real-time PCR for *Trichomonas vaginalis* in urine samples from females and males. J Clin Microbiol 2003; 41(12):5619-22.
16. Lavasani S, Dzhambazov B, Nouri M, et al. A novel probiotic mixture exerts a therapeutic effect on experimental autoimmune encephalomyelitis mediated by IL-10 producing regulatory T cells. PLoS One 2010; 5(2):e9009.
17. Jarnicki AG, Lysaght J, Todryk S, Mills KH. Suppression of antitumor immunity by IL-10 and TGF-beta-producing T cells infiltrating the growing tumor: influence of tumor environment on the induction of CD4+ and CD8+ regulatory T cells. J Immunol 2006; 177(2):896-904.
18. Kalia V, Sarkar S, Subramaniam S, Haining WN, Smith KA, Ahmed R. Prolonged interleukin-2Ralpha expression on virus-specific CD8+ T cells favors terminal-effector differentiation in vivo. Immunity 2010; 32(1):91-103.
19. Adalid-Peralta L, Fragoso G, Fleury A, Sciutto E. Mechanisms underlying the induction of regulatory T cells and its relevance in the adaptive immune response in parasitic infections. Int J Biol Sci 2011; 7(9):1412-26.
20. Eusebio M, Kraszula L, Kupczyk M, Kuna P, Pietruczuk M. The effects of Interleukin (IL-10) or transforming growth factor (TGF-β) on the anti-CD3/CD28 induced activation of CD8+CD28- and CD8+CD28+ T cells in allergic asthma. J Biol Regul Homeost Agents 2013; 27(3):00-00.
21. Gottschalk RA, Corse E, Allison JP. Expression of Helios in peripherally induced Foxp3+ regulatory T cells. J Immunol 2012; 188(3)976-80.

22. Thomas RM, Chen C, Chunder N, Ma L, Taylor J, Pearce EJ, Wells AD. Ikaros silences T-bet expression and interferon-gamma production during T helper 2 differentiation. J Biol Chem 2010; 285(4):2545-53.
23. Josefowicz SZ, Rudensky A. Control of regulatory T cell lineage commitment and maintenance. Immunity 2009; 30(5):616-25.
24. Larché M. Regulatory T cells in allergy and asthma. Chest 2007; 132(3):1007-14.
25. Lal G, Bromberg JS. Epigenetic mechanisms of regulation of Foxp3 expression. Blood 2009; 114(18):3727-35.
26. Zaina S, Lindholm MW, Lund G. Nutrition and aberrant DNA methylation patterns in atherosclerosis: more than just hyperhomocysteinemia? J Nutr 2005; 135(1):5-8.
27. Tobi EW, Lumey LH, Talens RP, Kremer D, Putter H, Stein AD, Slagboom PE, Heijmans BT. DNA methylation differences after exposure to prenatal famine are common and timing- and sex-specific. Hum Mol Genet 2009; 18(21):4046-53.
28. Tripathi P, Awasthi S, Gao P. ADAM metallopeptidase domain 33 (ADAM33): a promising target for asthma. Mediators Inflamm 2014; 2014:572025.
29. Howell JE, McAnulty RJ. TGF-beta: its role in asthma and therapeutic potential. Curr Drug Targets 2006; 7(5):547-65.
30. Yang Y, Wicks J, Haitchi HM, Powell RM, Manuyakorn W, Howarth P, Holgate ST, Davies DE. Regulation of a disintegrin and metalloprotease-33 expression by transforming growth factor-β. Am J Respir Cell Mol Biol 2012; 46(5):633-40.

ASSESSMENT OF BIOPHYSICAL THERAPY IN THE MANAGEMENT OF PAIN IN CURRENT MEDICAL PRACTICE COMPARED WITH IBUPROFEN AND PLACEBO: A PILOT STUDY

A. FOLETTI[1,2], P. BARON[2,3], E. SCLAUZERO[2,3], G. BUCCI[2,3], A. RINAUDO[2,3] and R. ROCCO[2,3]

[1]Institute of Translational Pharmacology, CNR, Rome, Italy; [2]Clinical Biophysics International Research Group, Lugano, Switzerland; [3]General Practictioner, Regione Friuli Venezia Giulia, Italy

Received July 9, 2013 – Accepted June 25, 2014

Pain management is a daily part of current medical practice. The aim of this pilot study was to assess the efficacy of a biophysical procedure (Med Select 729) compared to a usual pain killer drug (Ibuprofen), and to placebo in order to disclose some effective procedures to be employed especially in elderly people with multiple comorbidities, in patients with allergy to chemical drugs or previous side effects, in non-responders to usual medications, and in chronic diseases to reduce overload. A total of 66 patients were divided in 3 groups. After one week of biophysical therapy they showed similar effect to ibuprofen and after one month the statistical significance was achieved with $p<0.02$ in comparison to placebo. We conclude that biophysical therapy was shown to be an effective and safe procedure for the management of pain in current medical practice.

Pain management represents an important part of current daily medical practice since many pain-related diseases require medical treatment. Pain can be a maladaptive response to stress, a condition/state in which differences between afferent stimuli and the dynamic process responsible for maintaining stability in an organism (allostasis) activate adaptive responses to reduce these differences. Since allostasis aims to maintain stability while coping with both internal and external changes, it is a process that varies intrinsically with time. Allostatic load is the sum of the allostatic response to physiological status at a specific time, which occurs when activation of allostatic response is continuously restored (1-3). As part of an adaptive response, pain induces a faster recovery of allostasis in acute diseases, while it worsens allostatic load and slows recovery in chronic diseases (4-6). Thus, pain has to be considered not only from a symptomatic viewpoint but also from a systemic perspective (7-10). Several factors contribute to the current complexity in pain management: age increase in the general population with a corresponding increase of chronic disease comorbidities; increased number of drug allergies and/or side effects; increased number of multi-pharmacological treatment of patients for whom the choice of pain killer medication is difficult due to possible cross drug reactions. In addition, usual pharmacological treatments with painkillers or non-steroidal anti-inflammatory drugs can often result in increased stress in patients and thus, increase their allostatic load while significantly reducing

Key words: pain, allostasis, allostatic load, biophysical therapy, system information therapy, biolectromagnetic therapy, system medicine, personalized medicine

Mailing address: Alberto Foletti, MD PhD
Deptartment of Innovative Technologies,
University of Applied Sciences
of Southern Switzerland-SUPSI,
Galleria, 2, Manno 69, Switzerland
Tel.: +41 78 75 78 783 Fax: +41 91 972 40 42
e-mail: contact@albertofoletti.ch

0393-974X (2014)

DISCLOSURE: ALL AUTHORS REPORT NO CONFLICTS OF INTEREST RELEVANT TO THIS ARTICLE.

healing resources. For these reasons, an effective non-pharmacological strategy to cope with pain in an effective and safe way would benefit patients. Biophysical therapies using electro-medical devices (such as Med Select 729 in this trial) allow to perform very personalized treatment using endogenous electromagnetic signals of the patient, and is therefore consistent with the developing concept of personalized medicine without the need for pharmacological treatment (11, 12).

Following the understanding that the characteristics and behavior of a system are not the sum of its single parts, but a result of its complex interactions – a concept defined as Systems Medicine (7-10) – a new clinical approach has been developed (13). The System Information Therapy is an integrative clinical tool based on biophysical methods operating by endogenous and external electromagnetic signals simultaneously. Living organisms produce electromagnetic signals endogenously and use them in the coordination of their internal processes and cell-to-cell interaction (14-16). The anti-inflammatory effects of electronic signals derived from electromagnetic therapies have also been demonstrated (17). The System Information Therapy approach using biophysical procedures simultaneously produces a systemic and a local effect (18) and leads to a reduction of allostatic load as detected by evaluation of fluctuating asymmetry, a clinical marker of stress (19, 20). Here, we present a pilot study aimed at assessing the efficacy of biophysical therapy in treating pain. We utilised the transfer of electromagnetic signals to an aqueous system, in agreement with previous studies (21-26), to implement a cost reduced, easy-to-apply non-pharmacological treatment for pain.

MATERIALS AND METHODS

This pilot clinical trial was designed to assess the efficacy of a biophysical treatment recorded on an aqueous system compared to a common anti-inflammatory drug (ibuprofen) and compared to placebo. The purpose of the experimental design was to: i. Test the effectiveness of a biophysical therapy by the daily sublingual administration of drops of the recorded aqueous solution (Nomabit base) to patients with acute or chronic pain in a general practitioner's surgery; ii. Test the effectiveness of the administration of ipobrufen 600 mg twice a day, in patients with acute or chronic pain in a general practitioner's surgery; iii. Test the effectiveness of a generic liquid (Nomabit base), employed as placebo, in patients with pain in a general practitioner's surgery; iv. Compare the effectiveness between the three procedures. All patients signed an informed consent form and this study was performed in accordance with the declaration of Helsinki.

All patients were informed that they were part of a study in which they received treatment for pain without being aware of the treatment group they were part of (biophysics, pharmacologic or placebo group). This was a single-blind study since only the physician knew which drug was being given to the patient. Patients receiving biophysics therapy or placebo were therefore unaware of which therapy they were taking. To increase the reliability of the results obtained with biophysical therapy recorded on aqueous solution of trace elements in comparison with placebo, patients belonging to the placebo group were given the same aqueous solution used in the biophysical therapy, with the same weekly schedule but without recorded biophysical signals. Our aim was to avoid any psychological effects on the outcome of the study.

Inclusion criteria were the presence of pain (acute or chronic) and aged between 18 and 90 years. Exclusion criteria included: patients with allergy to the drugs used, patients who do not give their informed consent, patients with psychic diseases or severe illnesses.

Patients in the biophysical therapy group (Group 1) were treated following a 2-step protocol using a commercially available electro-medical device, Med Select 729 (Wega, Germany). This medical device operates in the low frequency range (between 0 and 20 KHz) using a magnetic field with an intensity similar to the Earth's magnetic field with a maximum of 50 μT (MicroTesla). It allows to record input signals using two electrodes and to send output signals to the patient through two magnetic electrodes for local use, for example, on the pain site, or through a magnetic carpet where the patient can lie down (in this way the entire body of the patient can be treated). Therefore, the device can offer a local and systemic treatment simultaneously, as previously described (18). The same device used for signal recording (Med Select 729) was always used. The experimental design was extremely easy to reproduce since the programs used for the 2-step treatment are already preset in the apparatus: anyone with access to a similar device can employ these settings and programs. The 1st step consisted of selecting the program 'regulation therapy' on the touch screen of the Med Select 729 device to record the endogenous input signals at the painful region of each patient and of delivering the therapeutic electromagnetic output signals to an electromagnetic, full body-sized carpet on which the patient lay for 10 minutes. Then, the program 'pain

therapy' was selected from the touch screen of the Med Select 729 to record the endogenous input signals at the painful region and deliver the therapeutic output signals at the pain site for 10 minutes.

These output therapeutic signals were recorded on a commercially available aqueous system (Nomabit Base) by placing the solution into a special output coil built-in for this purpose in the Med Select 729 device. The aqueous solution in which signals were recorded was inserted into a coil present in the device. The recording circuit and procedures are described in detail (26).

The Nomabit Base aqueous solution was subsequently self-administered by the patient in order to allow the therapeutic information recorded to be delivered according to a weekly plan starting on Monday with a single drop and increasing by one drop/day up to 6 drops on Saturday; no therapy was administered on Sunday (Table I). The Nomabit Base aqueous solution is composed of oligominerals currently marketed in Italy and used as a food supplement: it presents the advantage of already being provided with a dropper and stored in a cardboard coated aluminum container, which ensures that the signal is preserved on the aqueous solution and is protected from thermal shock and environmental interferences with electromagnetic signals. This is an "off label" use of a common dietary supplement, which is already suitable to be stored for a long period of time (up to three months after opening, as indicated on the label by the manufacturer without risk of bacterial or fungal contamination that may alter its characteristics).

Patients in the pharmacological treatment group (group 2) were treated with ibuprofen 600 mg twice a day, on a full stomach, for 10 days. Patients included in the placebo group (group 3) received Nomabit Base solution as placebo (Nomabit Base solution was therefore not placed into the Med Select and did not receive output signals), and followed the same protocol as patients from the biophysical group (Table I).

The evaluation of the pain was performed at 3 different time points: beginning of the study, after one week and after one month, using a visual analogue scale (VAS), a self-rating method currently in use in clinical management of pain. Criteria of evaluation of VAS self-rating modification in the follow up was the following: Reduction $\geq$ 2 points in VAS score was considered as improved; Reduction = 1 points in VAS score was considered as unchanged; Reduction $\leq$ 0 points in VAS score was considered as a worsening of the condition.

Statistical analysis

Comparisons between improvement in VAS score for the 3 treatment groups were carried out using the *Chi*-square test. All statistical tests were performed with a significance level of α=0.05 (two-sided). Statistical analysis was carried out using SAS software (version 9.2, Cary, NC, USA). Sequential analysis was used to assess the efficacy of treatment (Fig. 1). The validity limits of a triangular and sequential mirroring test were with a probability of error of $p<0.05$, an event probability of 80% and a relative risk of 0.75. The V axis corresponds to approximately one-quarter of the observed events. The Z axis is the number of observed events in the control group minus the number of expected events given by an equivalent treatment. A statistically positive and valid significance was obtained if the data sequence crossed over the line above, whereas it was considered negative if it crossed over the line below; if it stays within the two continuous lines (between the line above and line below) differences in the therapeutic response among the various groups cannot be considered statistically significant.

RESULTS

Baseline clinical characteristics

A total of 66 patients (40 females and 26 males) were enrolled in the present study. The number of patients was similar for 3 treatment groups: 26 in the Biophysical therapy group (17 females, 9 males), 23 in the pharmacological group (11 females, 9 males); 17 in the placebo group (12 females, 5 males). The age distribution of patients in the 3 groups is shown in Fig. 2. The mean age of patients in the Biophysical group was an average of 56.1 years; in the pharmacological group, 59.4 years and 55.3 years in the placebo group. The study included patients with both acute and chronic pain.

Table I. *Weekly protocol of therapy administration in the biophysical group*

Day	Treatment (drops)
Monday	1
Tuesday	2
Wednesday	3
Thursday	4
Friday	5
Saturday	6
Sunday	none

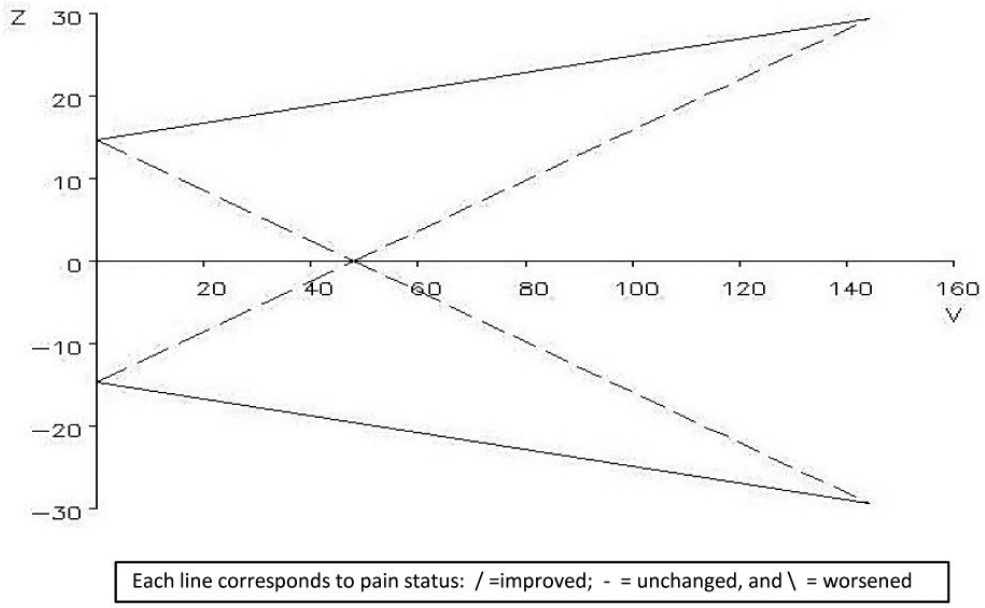

Fig. 1. *Sequential analysis was used to assess the efficacy of treatment. The V axis corresponds to approximately one quarter of the observed events. The Z axis is the number of observed events in the control group minus the number of expected events given by an equivalent treatment. A statistically positive and valid significance was obtained if the data sequence crosses over the above line, whereas it was considered negative if it crosses over the line below; if it stays within the two continuous lines differences in the therapeutic response among the various groups cannot be considered statistically significant. See Methods for further information (Statistical analysis).*

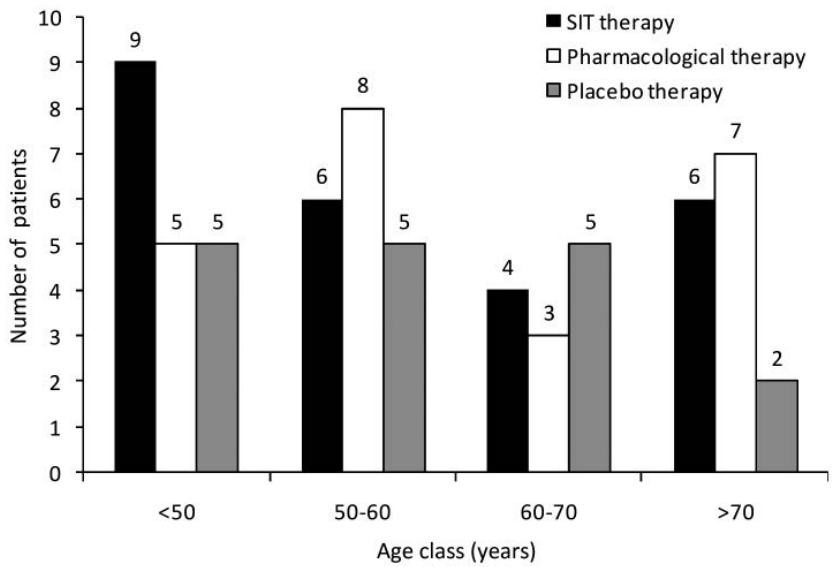

Fig. 2. *Age distribution among patients in the 3 groups.*

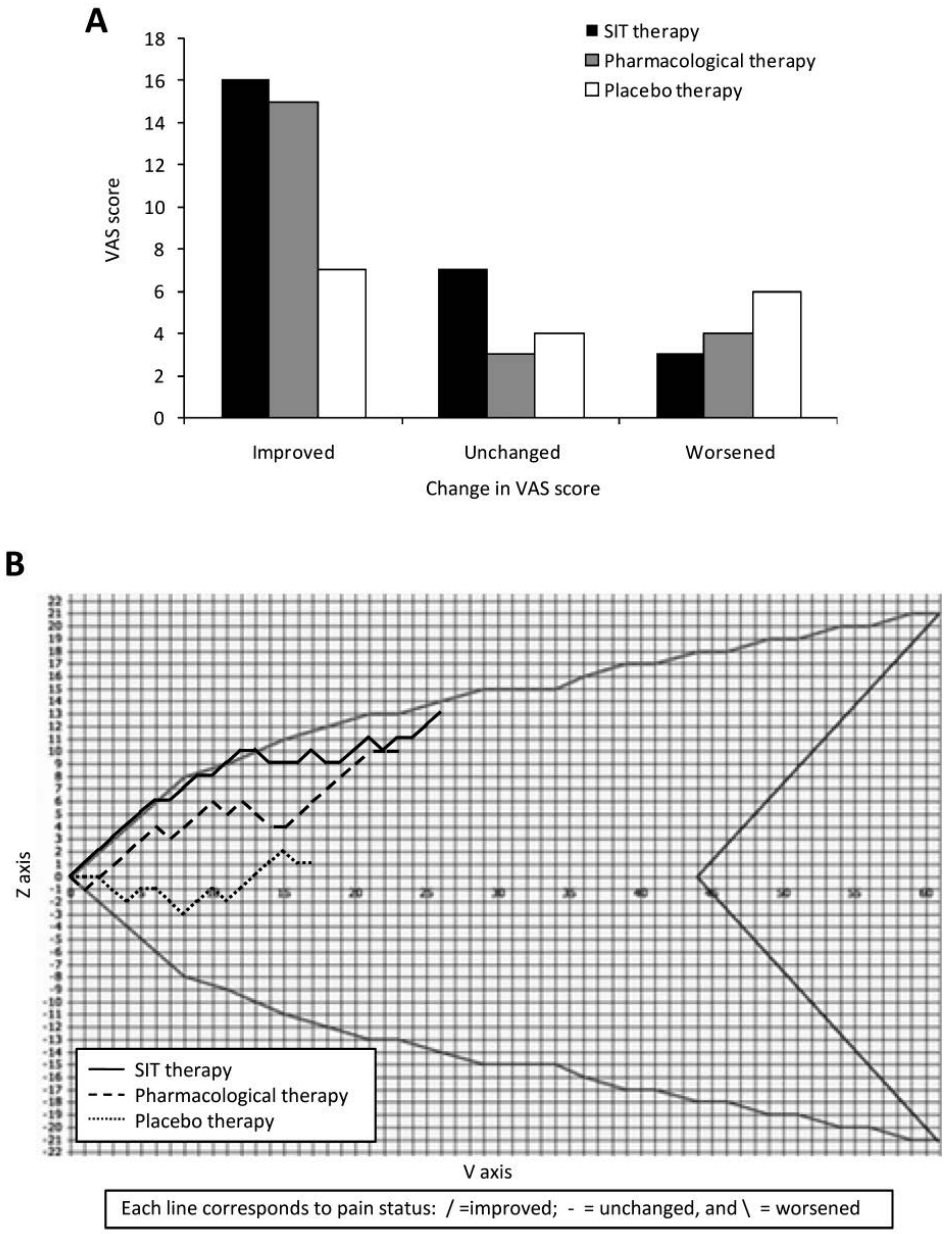

Fig. 3. *Change in pain intensity after 1 week of treatment. **A**) Change in pain intensity as self-rated by VAS after 1 week of treatment. **B**) Sequential analysis of data from each patient after 1 week of treatment.*

Effect of biophysical and pharmacological therapies on pain relief after 1 week of treatment

After one week of treatment, both biophysical and pharmacological therapies were effective in inducing pain relief as reported by a reduction of >2 points in VAS at the first follow-up assessment: improvement was reported by 61.5% of patients in the biophysical group (16/26) and 65.2% in the pharmacological group (15/23). At the same time point, only 41.2% of patients treated with placebo showed a reduction in pain perception (7/17). Of note, only 26.9% of patients (7/26) in the Biophysical group, 13% in the pharmacological group (3/23) and 23.5% of the placebo group (4/17) showed reported no change

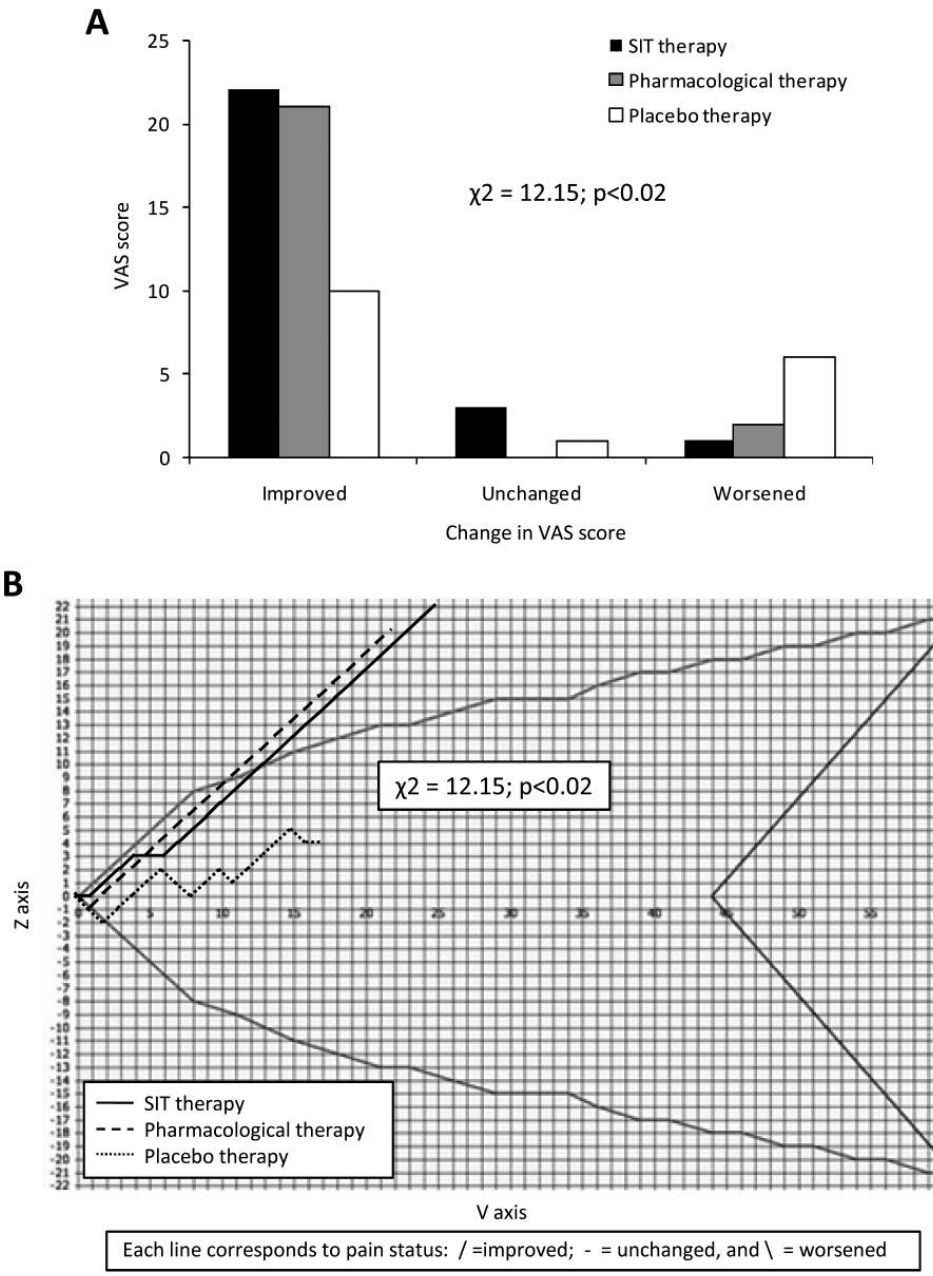

Fig. 4. *Change in pain intensity after 1 month of treatment. **A)** Change in pain intensity as self-rated by VAS after 1 week of treatment. **B)** Sequential analysis of data from each patient after 1 month of treatment.*

in VAS scores. Worsening of pain was reported in 11.5% of the Biophysical group (3/26), in 17.4% of the pharmacological group (4/23) and in 35.3% of the placebo group (6/17; Fig. 3A). A sequential analysis is also presented in Fig. 3B.

Effect of biophysical and pharmacological therapies on pain relief after 1 month of treatment

After 1 month of treatment, both biophysical therapy and ibuprofen (600 mg) were found to be effective in reducing pain compared to the placebo

group. A significant improvement, corresponding to 2 or more points in VAS score, was reported in 84.6% of biophysical-treated patients (22/26), in 91.3% of ibuprofen-treated patients (21/23) and in only 58.8% of placebo-treated patients (10/17). Only 11.5% of cases (3/26), in the biophysical group, no patients in the pharmacological group (0/23) and 5.9% cases of the placebo group (1/17) demonstrated unchanged pain perception (decrease of one point of VAS). Pain worsening, defined as an increase of VAS score between 0 and 1, was reported in 7.7% of cases in the Biophysical group (1/26), in 8.7% of cases in the pharmacological group (2/23) and in 35.3% of patients in the placebo group (6/17; Fig. 4A). Sequential analysis of the data demonstrated a similar trend in responsiveness to treatment between the Biophysical and Pharmacological groups compared to placebo at the end of the first month ($\chi^2 = 12.15$, $p<0.02$; Fig. 4B).

DISCUSSION

The main findings from the present study demonstrate that biophysical therapy is an effective method to relieve pain. Patients receiving biophysical treatment showed a similar reduction in pain perception (assessed by changes in VAS score) as those patients treated with the non-steroidal anti-inflammatory drug Ibubrofen (600 mg), administered twice a day. In contrast, patients treated with placebo did not present with any significant pain relief. In addition, biophysical and pharmacological therapies also demonstrated long-term efficacy: at the second follow-up assessment carried out after one month of treatment, a significant reduction in pain was observed in biophysical and pharmacological-treated patients, but not in placebo-treated patients.

These data suggest that biophysical therapy mimics the dynamics of the pharmacological treatment and produces long lasting effects. Interestingly, only a few patients showed a worsening of pain in the biophysical group and no reported side effects were derived from this treatment. Moreover, many patients in the Biophysical group reported a general relaxation following treatment, which was presumably due to a systemic effect of the biophysical therapy.

Importantly, the use of a single recording procedure during the entire biophysical therapy allowed to perform only one treatment, lasting only 20 minutes, in the presence of the physician. The rest of the treatment was self-administered, saving time and cost to the patient. Biophysical therapy can be therefore considered a time and cost-effective approach for pain treatment. In addition, the biophysical approach is a personalized therapy, since the pattern of signals recorded are endogenous electromagnetic signals, unique to each patient.

The recording of output signals on an aqueous system, a commercially available solution of micro elements Nomabit Base (by Named, Italy), has already been previously demonstrated (21-26). Here, we demonstrate that this procedure is clinically feasible and applicable as an integrative tool in general practice, in agreement with previous hypotheses that an aqueous system is capable of recording, storing, and transferring biophysical active information to biological targets (27-30). Further clinical trials are indeed required to confirm the data presented in this preliminary pilot study and to understand whether this system can be applied to other clinical areas besides pain management. Biophysical therapy may also be considered as a second line intervention in cases where pharmacological treatment is ineffective or leads to serious side effects or allergies. The progressive aging of the population raises a number of challenges in the management of pain and many other symptoms due to the increase of incidence of chronic diseases. We envisage that this biophysical approach can help to manage symptoms derived from these diseases by reducing the global allostatic load. We believe that biophysical treatments can help to reduce total morbidity and mortality, as previously documented from successful studies on aging (31, 32).

In summary, we present important findings from this pilot study in which biophysical therapy demonstrated the same efficacy thanthe usual pharmacological therapy with ibuprofen in pain management. Since the effectiveness of this procedure of recording electromagnetic signals in aqueous solutions has not previously been proven, it is important that the results of this pilot study are interpreted with caution. Regardless, the improvement in pain perception could be seen as early as one week of treatment with the effects of both therapeutic approaches still observed after

one month. The majority of biophysical treatment was self-administered (only the first treatment was performed in the presence of a physician) saving time and cost to the patient. The biophysical method presented here can therefore be considered as an effective, safe, and long lasting therapy for pain management in current medical practice.

REFERENCES

1. McEwen BS, Stellar E. Stress and the individual mechanisms leading to disease. Arch Intern Med 1993; 153:2093-101.
2. Seeman TE, Singer BH, Rowe JW, Horwitz RI, McEwen BS. Price of adaptation - allostatic load and its health consequences. MacAthur studies of successful aging. Arch Intern Med 1997; 157:2259-68.
3. McEwen BS. Stress, adaptation and disease. Allostasis and allostatic load. Ann NY Acad Sci 1998; 840:33-44.
4. McEwen BS, Seeman T. Protective and damaging effects of mediators of stress. Elaborating and testing the concepts of allostasis and allostatic load. Ann NY Acad Sci 1999; 896:30-47.
5. McEwen BS, Wingfield JC. The concept of allostasis in biology and biomedicine. Horm Behav 2003; 43:2-15.
6. Glein DA, Goldman N, Chuang Y-L, Weinstein M. Do chronic stressors lead to physiological dysregulation? Testing the theory of allostatic load. Psychosomatic Med 2007; 69:769-76.
7. Ahn AC, Tewari M, Poon C-S, Phillips RS**.** The clinical applications of a systems approach. PLoS Medicine 2006; 3:e209.
8. Ahn AC, Tewari M, Poon C-S, Phillips RS. The limits of reductionism in medicine: could systems biology offer an alternative? PLoS Medicine 2006; 3:e208.
9. Carlson RJ. Holism and reductionism as perspectives in medicine and patient care. West J Med 1979; 131:466-70.
10. Federoff HG, Gostin LO. Evolving from reductionism to holism: is there a future for System Medicine? JAMA 2009; 302:994-6.
11. Henney AM. The promise and challenge of personalized medicine: aging populations, complex diseases, and unmet medical need. Croat Med J 2012; 53:207-10.
12. Louca S. Personalized medicine – a tailored health care system: challenges and opportunities. Croat Med J 2012; 53: 211-3.
13. Foletti A. Managing biological complexity in the framework of Systems Medicine: the possible key role of Systems Information Therapy by biophysical methods in integrating medical practice., In Proceedings of the 1rst International Symposium "Biophysical Aspects of Complexity in Health and Disease. Milan, Italy, 2010; p. 20-1.
14. Liboff AR. Toward an electromagnetic paradigm for biology and medicine. J Altern Complement Med 2004; 10:41-7.
15. Cifra M, Fields JZ, Farhadi A. Electromagnetic cellular interaction. Prog Biophys Mol Biol 2010; 105:223-46.
16. Rossi C, Foletti A, Magnani A, Lamponi S. New perspectives in cell communication: bioelectromagnetics interactions. Seminar Cancer Biol 2011; 21:207-14.
17. Odell RHJr, Sorgnard RE. Anti-inflammatory effects of electronic signals treatment. Pain Physician 2008; 11:891-907.
18. Liboff AR. Local and holistic electromagnetic therapies. Electromagn Biol Med 2007; 26:315-25.
19. Parson PA. Fluctuating asymmetry: an epigenetic measurement of stress. Biol Rev Camb Philos Soc 1990; 65:131-45.
20. Foletti A, Grimaldi S. Systems Information Therapy and the central role of the brain in allostasis. J Phys Conf Ser 2011; 329:012027.
21. Jerman I, Berden M, Ružic R. Biological influence of ultraweak supposedly EM radiation from organisms mediated through water. Electro Magnetobiol 1996; 15:229-44.
22. Kreisl P. Test on the transduction of acetic acid information via an electronic amplifier. Acta Medica Empirica 1998; 47:17-24.
23. Jerman I, Ružic R, Krašovec R, Škarja M, Mogilnicki L. Electrical transfer of molecule information into water, its storage, and bioeffects on plants and bacteria. Electromagn Biol Med 2005; 24:341-53.
24. Heredia-Rojas JA, Torres-Flores AC, Rodriguez-De la Fuente AO, Mata-Cardenas BD, Rodriguez-

Flores LE, Barron-Gonzales MP, Torres-Pantoja AC, Alcocer-Gonzales GM. Entamoeba histolytica and Trichomonas vaginalis: Trophozoite growth inhibition by metronidazole electro-transferred water. Exp Parasitol 2011; 127:80-3.

25. Heredia-Rojas JA, Gomez-Flores AC, Rodriguez-De la Fuente AO, Monreal-Cuevas E, Torres-Flores AC, Rodriguez-Flores LE, Beltcheva M, Torres-Pantoja AC. Antibicrobial effect of amphotericin B electronically-activated water against Candida Albicans. African J Microbiology Res 2012; 6:3684-9.
26. Foletti A, Ledda M, D'Emilia E, Grimaldi S, Lisi A. experimental finding on the electromagnetic information transfer of specific molecular signals mediated through aqueous system on two human cellular models. J Altern Complement Med 2012; 18:258-61.
27. Thomas Y, Schiff M, Belkadi L, Jurgens P, Kahhak L, Benveniste J. Activation of human neutrophils by electronically transmitted phorbol-myristate acetate. Medical Hypotheses 2000; 54:33-9.
28. Smith CW. Quanta and coherence effects in water and living systems. J Altern Complement Med 2004; 10:69-78.
29. Widom A, Srivastava Y, Valenzi V. The biophysical basis of Benveniste experiments: Entropy, structure, and information in water. Int J Quantum Chem 2010; 110:252-6.
30. Foletti A, Grimaldi S, Lisi A, Ledda M, Liboff AR. Bioelectromagnetic medicine: The role of resonance signaling. Electromagn Biol Med 2013; 32:484-99.
31. Seeman TE, McEwen BS, Rowe JW, Singer BH. Allostatic load as a marker of cumulative biological risk: MacArthur studies of successful aging. Proc Natl Acad Sci USA 2001; 98:4770-5.
32. Karlamangla AS, Singer BH, McEwen BS, Rowe JW, Seeman TE. Allostatic load as a predictor of functional decline. MacArthur studies of successful aging. J Clin Epidemiol 2002; 55:696-710.

LUNG INVOLVEMENT IN SYSTEMIC SCLEROSIS: ROLE OF HIGH RESOLUTION COMPUTED TOMOGRAPHY AND ITS RELATIONSHIP WITH OTHER PULMONARY AND CLINICO-SEROLOGICAL FEATURES

M. COLACI[1], M. SEBASTIANI[1], A. MANFREDI[1], D. GIUGGIOLI[1], G. CASSONE[1], C.U. MANZINI[1], C. GHIZZONI[1], S. CERRI[2] and C. FERRI[1]

[1]Rheumatology Unit, Department of Medical and Surgical Science for Adults and Children, University of Modena and Reggio Emilia, Modena; [2]Center for Rare Lung Diseases, University of Modena and Reggio Emilia, Modena, Italy

Received November 22, 2013 – Accepted June 17, 2014

The first two authors contributed equally to the manuscript

The study investigated the characteristic of interstitial lung disease in a large series of systemic sclerosis (SSc) patients by means of HRCT and the correlations between functional lung parameters, serological features and the extent of lung involvement evaluated by high-resolution computed tomography (HRCT). One hundred and seven SSc patients, consecutively investigated by means of HRCT, standard chest X-ray, and pulmonary function tests, were retrospectively evaluated. Chest radiogram and HRCT scores were strongly associated (Pearson's r=0.82, p<.0001); moreover, the first significantly correlated with spirometric parameters, even if weakly. Anti-Scl70 and anti-centromere antibodies were associated with higher (p=0.01) and lower HRCT score (p=0.0002), respectively. The extension of interstitial lung involvement in SSc evaluated with HRCT is directly proportional to functional lung parameters. HRCT, spirometry and DLco should be considered essential in the core-set of non-invasive diagnostic tools for the first-line assessment of scleroderma lung involvement.

Systemic sclerosis (SSc) is a connective tissue disease clinically characterized by different degrees of skin and visceral organ involvement. The etiology of SSc still remains obscure; the disease appears to be the result of multistep and multifactorial processes, including immune-system alterations, altered fibroblasts activation and diffuse microvascular abnormalities. Both fibrotic and vascular alterations are responsible for SSc organ damage, mainly lung, heart, gastrointestinal tract, and/or kidney (1, 2).

Interstitial lung disease (ILD) is one of the most frequent clinical manifestations of SSc. The presence of bibasilar fibrosis at radiological investigation is one of the diagnostic hallmarks of SSc; however, clinical manifestations of ILD are extremely variable, from asymptomatic interstitial involvement to progressive fibrosis leading to respiratory failure (3). In addition, pulmonary arterial hypertension, alone or more often associated to lung fibrosis, represents one of the most harmful complications of ILD. On the whole, ILD may affect the overall prognosis of the disease; however, the natural history and outcome

Key words: systemic sclerosis, scleroderma, lung fibrosis, high resolution computed tomography, pulmonary arterial hypertension

Mailing address: Dr Marco Sebastiani,
Rheumatology Unit,
University of Modena and Reggio Emilia,
Via del Pozzo n° 71,
41121, Modena, Italy
Tel.: +39 059 4222279 Fax: +39 059 4224178
e-mail: marco.sebastiani@unimo.it

0393-974X (2014)

DISCLOSURE: ALL AUTHORS REPORT NO CONFLICTS OF INTEREST RELEVANT TO THIS ARTICLE.

of ILD may be unpredictable in a relevant number of patients. A correct evaluation of the activity and severity of ILD may be decisive for an adequate therapeutic approach. High resolution computed tomography (HRCT) has been included among non-invasive diagnostic procedures routinely employed in clinical practice for the study of SSc patients (4). The aim of the present study was to investigate the characteristic of ILD in a large series of SSc patients by means of HRCT; in addition, radiological findings were correlated with other non-invasive pulmonary investigations, and various SSc symptoms.

MATERIALS AND METHODS

One hundred and seven consecutive SSc patients followed-up in our Rheumatology Centre from the 1st January 2000 to 31st December 2010 were evaluated for ILD; all patients gave informed consent for the use of the data from their clinical records. Disease duration was calculated from the onset of the first non-Raynaud's phenomenon disease feature. In all subjects, SSc was classified at baseline according to the American College of Rheumatology preliminary criteria; patients were also classified on the basis of the extent of skin sclerosis according to LeRoy's cutaneous subset model (5), and standardized criteria were followed for the evaluation of clinical and serological parameters (6). For all patients, the follow-up was 10 years.

Lung radiological evaluation

Patients underwent both standard chest radiogram and HRCT scan. All scans were performed with a 3000 Sytec (GE, Milwaukee, Wisconsin, USA) with a scanning time of 1/sec. 1-mm sections were acquired at 10-mm intervals from apex to base, by using a 24-36 cm field of view, a 512 x 512-reconstruction matrix, 120 kV, and 160 mA. Images were reconstructed with a high-spatial-frequency algorithm for lung analysis, and reviewed at lung window (window width 1600 HU; window level –500 HU).

Lung evaluation was performed at the suspended end-inspiratory volume. Most patients underwent scanning in the prone position; in cases showing increased opacification in the postero-basal segments, a limited number of sections were also acquired through the lower zones of the lung, with the patient in the prone position, to ensure that opacification was not due to gravity-dependent perfusion.

Without knowledge of the patients' clinical conditions, two trained radiologists independently evaluated, in random order, both chest radiograms and HRCT scans modified from Schurawitzki et al. (7). The final conclusions were reached as the average interpretation; therefore, all discordant interpretations were resolved by consensus. For HRCT, the presence and the distribution of the following signs were detected: ground-glass opacities, septal and non-septal lines, subpleural curvilinear shadows, parenchymal bands, honeycombing areas, subpleural cysts, and bronchiectasis. Each lung was subdivided into three zones, upper, middle and lower, as follows: the upper zones were defined as the areas above the level of carina; the middle zones, between the level of carina and the level of the inferior pulmonary veins; and the lower zones, under the level of the inferior pulmonary veins. A score between 0 and 3, on the basis of the presence/absence and the kind of radiological signs was given as follows:

0: no signs of interstitial lung impairment;

1: ground-glass and/or septal lines;

2: non-septal lines and/or subpleural curvilinear shadows and/or parenchymal bands;

3: honeycombing areas and/or subpleural cysts.

The scores of the six lung areas were then summarized to obtain an overall score that was a value between 0 and 18 (minimum 0 and maximum 18).

The standard chest radiogram was evaluated as follows: score 0, in the absence of signs of interstitial lung involvement; 1 or 2, presence of mild or marked reticulo-nodular interstitial lung involvement, respectively; and 3, presence of severe reticulo-nodular interstitial lung involvement mimicking the HRCT honeycombing pattern.

Lung function tests

Forced vital capacity (FVC), forced expiratory volume in the first second (FEV1) were determined in all patients using a 9L water seal spirometer Baires (Biomedin, Padova, Italy); determination of the residual volume (RV) was obtained with the helium dilution method. Total lung capacity (TLC) was calculated by adding RV to inspiratory vital capacity (VC). The diffusing capacity for carbon monoxide (DLco) with the single breath method was also performed and corrected for alveolar volume and hemoglobin level. Values for FVC, FEV1, TLC, RV, and DLco were expressed as percentage of the normal predicted values for age, height, and sex (8-10). Results below 80% of the respective normal value were considered pathological; FEV1/VC was considered abnormal for values < 88% and < 89% in males and in females, respectively.

The FVC < 80% was assumed as criterion of restrictive lung defect. In this sample, the FVC was better distributed and more sensitive than TLC in describing a restrictive syndrome.

Apart from instrumental lung evaluations, all patients

underwent echocardiography. Left and right ventricular measures were obtained; moreover, pulmonary arterial systolic pressure (PAPs) was estimated using Doppler recordings of tricuspid regurgitation, measuring the peak velocity of the tricuspid regurgitation jet. If indicated, right heart catheterization was performed to make the diagnosis of pulmonary hypertension.

Statistical analysis and survival

Continuous variables were expressed as mean ± standard deviation. Group differences were tested for significance by *chi*-squared test, with Yates' correction, unpaired two-tailed Student's *t*-test, and ANOVA test where appropriate. Comparisons between continuous variables were performed by means of the Pearson's product-moment correlation coefficient. Simple and multiple regression analyses were also performed by means of SPSS version 17.0. A p value <0.05 was considered significant.

RESULTS

Main demographic and clinico-serological features of the 107 SSc patients (87 females, 20 males; mean age 52.1±12.3 years; mean disease duration 7±6 years) at baseline are summarized in Table I. The patient population consisted of limited cutaneous SSc (lcSSc) in 72% of cases, and diffuse cutaneous SSc (dcSSc) in 28%.

Table II shows the prevalence of the main symptoms of ILD along with the results of radiological and other non-invasive pulmonary investigations at baseline. Over two-thirds of patients referred dyspnea on exertion (72%), dyspnea at rest was present in 9% of individuals, and non-productive cough in 39%. 39% of SSc patients had a history of smoking (ongoing and/or former, ≥ 10 pack-years); the presence of smoking habit did not correlate with respiratory symptoms, HRCT score or other lung parameter alterations, and disease outcome. Standard chest X-ray and HRCT showed one or more alterations in the majority of cases, showing comparable mean total scores, namely 5.9±5.2 and 6.2±5.1, respectively (Table II). The most frequent findings at HRCT examination were ground-glass, septal, and non-septal lines, while honeycombing was detected in 21% of cases (Table II). Lung function tests revealed the presence of restrictive syndrome, generally mild or moderate, in almost half of the patients (47%). On

Table I. *Demographic and clinico-serological features of SSc patients.*

No. of patients		107
Female/male ratio		1/6
Mean age (years)		52.1±12.3
Mean dis dur (years)		7±6
SSc skin subsets		
	limited	72%
	diffuse	28%
Hypermelanosis		48%
Calcinosis		21%
Teleangectasias		72%
Skin ulcers		38%
Raynaud's phenomenon		95%
Sicca syndrome		50%
Arthralgias/arthritis		64%/5%
Esophageal involvement		59%
Lung involvement		58%
Autoantibodies		
	anti-centromere	44%
	anti-Scl70	36%

Table II. *Scleroderma lung involvement in 107 patients.*

	%	mean±SD
Chest X-ray alterations (total)	85	
mean total score (range 0-18)		5.9±5.2
HRCT alterations (total)	84	
ground-glass	58	
septal lines	66	
nonseptal lines	56	
subpleural curvilinear shadows	16	
parenchymal bands	24	
honeycombing	21	
subpleural cysts	21	
bronchiectases	23	
mean total score (0-18)		6.2±5.1
Pulmonary function tests		
TLC (<80%)	12	96±16
VC (<80%)	47	79±18
FVC (<80%)	42	80±18
FEV1 (<80%)	38	84±19
FEV1/VC (F <89%; M <88%)	9	106±14
DLco (<80%)	81	59±18
Restrictive syndrome (VC)	47	
Ostructive syndrome (FEV1/VC)	9	
Dyspnea on exertion/at rest	72/9	
Cough/Phlegm	39/4	
Smoking habit	39	

the contrary, obstructive syndrome evaluated on the basis of FEV1/VC reduction was found in only 9% of cases. DLco was abnormally reduced in a high percentage of patients (81%), comparable to that observed for radiological alterations. Clinically overt interstitial lung involvement evaluated on the basis of symptoms (dyspnea and/or cough), radiological, and spirometric alterations was observed in 58% of cases. The possible relationships between HRCT abnormalities and other lung parameter alterations were also investigated; in particular, HRCT score strongly correlated with chest X-ray score ($r=0.825$; $p<0.0001$), while the correlation with the main spirometric parameters, namely TLC ($p<0.033$), VC ($p<0.001$), FVC ($p<0.001$), FEV1 ($p=0.004$), and DLco (p=ns), was weaker (Fig. 1). Moreover, significantly higher HRCT scores were found in patients with dyspnea on exertion ($p=0.05$) or cough ($p=0.04$). Consistently, dyspnea on exertion was significantly associated with higher HRCT score ($p=0.01$), or pulmonary hypertension diagnosed by right heart catheterization ($p=0.032$).

A significantly higher HRCT score was found in patients with serum anti-Scl70 antibodies compared

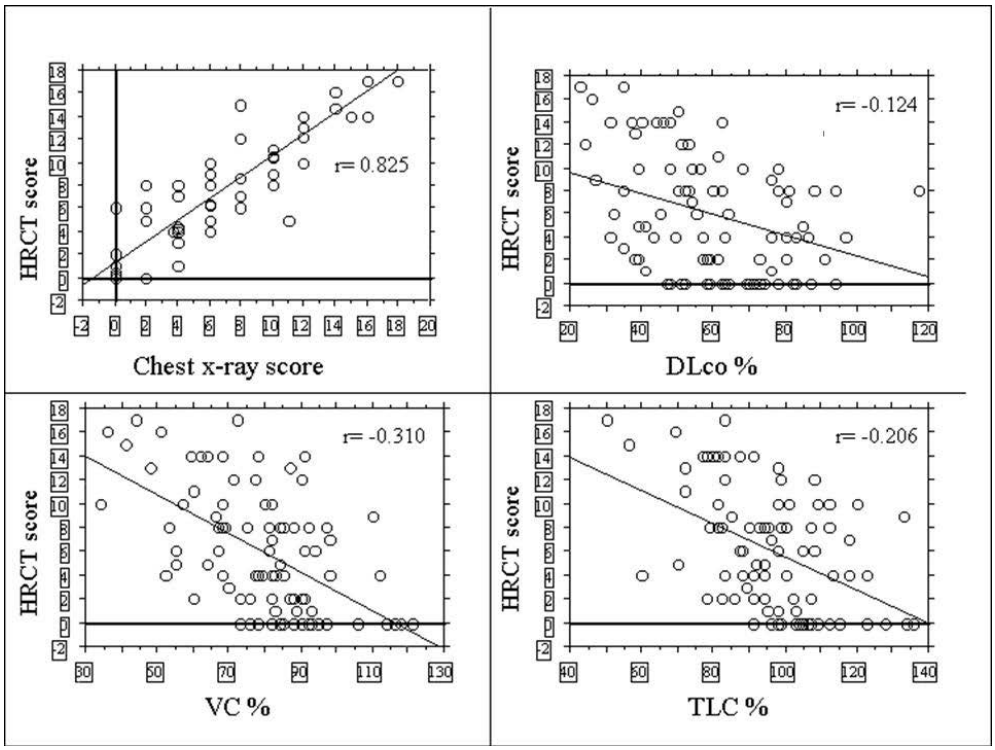

Fig. 1. *Correlation between HRCT score and standard chest X-ray score, DLCO, VC, and TLC values.*

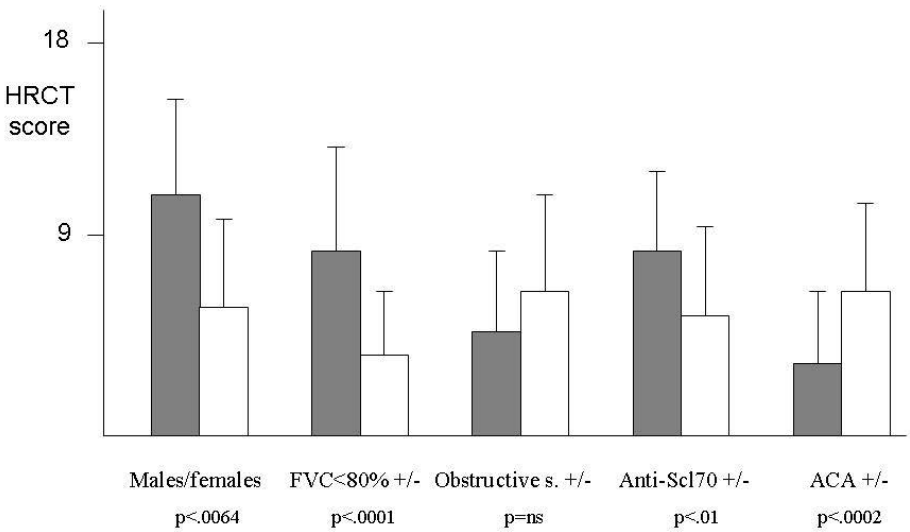

Fig. 2. *Mean total HRCT score in SSc patients divided according to gender, lung function parameters, and serology (ACA=anticentromere and anti-Scl70 autoantibodies). Statistical evaluations were performed by means of unpaired two-tailed Student's t-test.*

to anti-Scl70-negatives (p=0.01); conversely, ACA-positive individuals showed a significantly milder lung involvement as revealed by HRCT (p=0.0002) (Fig. 2). During the follow-up of study, 14 SSc patients died, 10 due to severe lung involvement (complicated by lung carcinoma in 3 cases), 1 due to cardiac involvement, and 1 due to sepsis; in 2 patients the cause of death remained unknown. The deceased patients had shown a significantly higher HRCT score (9.5±4.5 *vs* 5.7±5; p=0.01), with restrictive syndrome in 12/14 cases, a significantly lower DLco (41±10 *vs* 61±20; p=0.002), FVC (67±15 *vs* 82±18; p=0.02), and VC (66±18 *vs* 80±17; p=0.02); other adverse prognostic parameters were the patient age (58±12 *vs* 51±12; p=0.043), pulmonary hypertension (3/14 *vs* 0/97; p=0.001) and abnormally high erythrocyte sedimentation rate (35±30 *vs* 22±17; p=0.02) at the time of the first visit. On the contrary, patient age and sex, disease duration, and cutaneous subsets did not affect the SSc outcome.

DISCUSSION

The results of the present study on a large series of 107 unselected SSc patients demonstrated the presence of various lung alterations by means of HRCT in the majority of individuals. There was a good correlation between HRCT and standard chest X-ray scores, demonstrating a discrete capacity of the latter as digital imaging to evidence lung fibrosis, if evaluated by trained radiologists. These findings are in keeping with the study by Steele et al. (11), who demonstrated that physical examination and standard chest X-ray are good predictors of ILD in SSc patients, as a starting point for defining SSc-ILD in observational research; HRCT is then necessary in order to more deeply investigate lung interstitium, i.e. ILD pattern or its distribution and the severity. In half of the cases the presence of restrictive syndrome was suggested by spirometric parameter alterations (TLC and FVC), which were significantly correlated with HRCT score. The DLco was the functional index that better reflected the severity of ILD (12): the prevalence of impaired DLco was comparable to the whole HRCT alterations (81% *vs* 84%); moreover, DLco significantly correlated with radiological lung alterations quantified by HRCT score. However, in individual cases there was a discrepancy between HRCT score and DLco impairment, the latter being the result of interstitial lung fibrosis and/or lung vascular abnormalities. Mild or absent alterations on HRCT were observed in some patients with marked DLco reduction, often due to pulmonary hypertension. Dyspnea on exertion was the most common symptom of ILD; nonetheless, its origin is multifactorial, as suggested by the statistically significant association between dyspnea and pulmonary hypertension. On the whole, symptomatic lung involvement, evaluated on the basis of clinical manifestations, fibrotic and/or vascular alterations, was observed in almost two-thirds of SSc patients. Interestingly, no significant correlations were noticed between the prevalence of ILD and the extent of cutaneous involvement or other visceral organ involvement. On the contrary, the presence of scleroderma serological markers may have some important clinical implications: anti-Scl70 autoantibodies were significantly associated with more severe interstitial lung fibrosis, while anti-centromere (ACA)-positive individuals showed a milder lung involvement, as evidenced by HRCT score. These observations are in keeping with previous studies suggesting a worse prognostic value of anti-Scl70 and a possible "protective" role of ACA in the SSc outcome (13).

The detection of lung involvement is crucial in the clinical assessment and management of SSc patients. Bibasilar lung fibrosis is included among the SSc classification criteria, and its presence is particularly useful to diagnose patients with mild sclerodactyly or sine scleroderma SSc (14, 15). Moreover, the progression of ILD to respiratory failure and/or pulmonary heart disease may affect the overall prognosis of SSc (16, 17). Follow-up studies on large SSc series suggested that ILD, alone or in combination with other organ involvement, is one of the most frequent cause of death (13, 18). The outcome of ILD is often unpredictable - in a significant number of patients it may evolve insidiously since pulmonary symptoms may be very mild or absent, especially in the early SSc. Thus, diagnosis of fibrosing alveolitis and/or pulmonary hypertension may be delayed with negative consequences for the therapeutic decisions and prognosis.

An early evaluation of alveolitis is decisive to predict the progression of ILD to severe lung fibrosis;

ground glass alterations at HRCT could be indirect signs of active lung involvement (19). Since impaired DLco can be the consequence of interstitial fibrosis and/or pulmonary vascular disease (20), a screening evaluation of pulmonary arterial pressure by color-Doppler echocardiography, eventually confirmed by right heart catheterization, is mandatory.

The findings observed in our unselected SSc patients confirm in part the results of previous studies (21). Differences in the prevalence of lung involvement, in general, and of single pulmonary alterations among SSc series may be due to some important bias, firstly the large variability in the patient selection and/or in the employed study methodologies.

The quantification of both activity and severity of SSc manifestations is crucial in the disease management (13). For SSc patient assessment, the core set of non-invasive diagnostic procedures should include a clinical history and careful physical examination, standard chest X-ray, HRCT, spirometry with DLco, ECG, and color-Doppler echocardiography (6). These investigations are often sufficient to detect early both interstitial and/or vascular lung involvements. HRCT score and pulmonary function tests with DLco permit to quantify the severity of ILD and to monitor its variations during the follow-up.

Evaluation of ILD may be particularly difficult in the presence of discrepant clinical findings due to the different sensibility and specificity of diagnostic procedures and not secondarily to the single patient compliance. In this respect, a team of referral specialists, i.e. pneumologist, cardiologist, and radiologist, familiar with the most common SSc cardiopulmonary features is needed to correctly evaluate the results of diagnostic investigations and to diminish inter-observer variability.

REFERENCES

1. Ferri C, Valentini G, Cozzi F, et al. Systemic Sclerosis Study Group of the Italian Society of Rheumatology (SIR-GSSSc). Systemic sclerosis: demographic, clinical, and serologic features and survival in 1,012 Italian patients. Medicine 2002; 81:139-53.
2. LeRoy EC, Medsger TA. Criteria for the classification of early systemic sclerosis. J Rheumatol 2001; 28:1573-6.
3. Steen VD. The lung in systemic sclerosis. J Clin Rheumatol 2005; 11:40-6.
4. Wells AU. High-resolution computed tomography and scleroderma lung disease. Rheumatology 2008; 47:59-61.
5. LeRoy EC, Black C, Fleischmajer R, Jablonska S, Krieg T, Medsger TA Jr, Rowell N, Wollheim F. Scleroderma (systemic sclerosis): classification, subsets and pathogenesis. J Rheumatol 1988; 15:202-5.
6. Walker KM, Pope J; Scleroderma Clinical Trials Consortium; Canadian Scleroderma Research Group. Expert agreement on EULAR/EUSTAR_recommendations for the management of systemic sclerosis. J Rheumatol 2011; 38:1326-8.
7. Schurawitzki H, Stiglbauer R, Graninger W, Herold C, Pölzleitner D, Burghuber OC, Tscholakoff D. Interstitial lung disease in progressive systemic sclerosis: high-resolution CT versus radiography. Radiology 1990; 176:755-9.
8. Stocks J, Quanjer PH. Reference values for residual volume, functional residual capacity and total lung capacity. ATS Workshop on Lung Volume Measurements. Official Statement of The European Respiratory Society. Eur Resp J 1995; 8:492-506.
9. Cotes JE, Chinn DJ, Quanjer PH, Roca J, Yernault JC. Standardization of the measurement of transfer factor (diffusing capacity). Report Working Party Standardization of Lung Function Tests, European Community for Steel and Coal. Official Statement of the European Respiratory Society. Eur Resp J 1993; 16:41-52.
10. Liang B-M, Lam DCL, Feng Y-L. Clinical applications of lung function tests: a revisit. Respirology 2012; 17:611-9.
11. Steele R, Hudson M, Lo E, Baron M. Clinical decision rule to predict the presence of interstitial lung disease in systemic sclerosis. Arthritis Care Res 2012; 64:519-24.
12. Gatta G, Di Grezia G, Iacomino A, Russo A, Petrillo M, Feragalli B, Cappabianca S, Grassi R. HRCT in systemic sclerosis: correlation between respiratory functional indexes and extension of lung failure. J Biol Regul Homeost Agents 2013; 27:579-87.
13. Vettori S, Cuomo G, Abignano G, Iudici M, Valentini

G. Survival and death causes in 251 systemic sclerosis patients from a single Italian center. Reumatismo 2010; 62:202-9.
14. Walker JG, Pope J, Baron M, et al. The development of systemic sclerosis classification criteria. Clin Rheumatol 2007; 26:1401-9.
15. Toya SP, Tzelepis GE. The many faces of scleroderma sine scleroderma: a literature review focusing on cardiopulmonary complications. Rheumatol Int 2009; 29:861-8.
16. Launay D, Humbert M, Berezne A, et al. Clinical characteristics and survival in systemic sclerosis-related pulmonary hypertension associated with interstitial lung disease. Chest 2011; 140:1016-24.
17. Khanna D, Tseng C-H, Farmani N, et al. Clinical course of lung physiology in patients with scleroderma and interstitial lung disease: analysis of the Scleroderma Lung Study Placebo Group. Arthritis Rheum 2011; 63:3078-85.
18. Tyndall AJ, Bannert B, Vonk M, et al. Causes and risk factors for death in systemic sclerosis: a study from the EULAR Scleroderma Trials and Research (EUSTAR) database. Ann Rheum Dis 2010; 69:1809-15.
19. Shah RM, Jimenez S, Wechsler R. Significance of ground-glass opacity on HRCT in long-term follow-up of patients with systemic sclerosis. J Thor Imaging 2007; 22:120-4.
20. Mukerjee D, St George D, Knight C, Davar J, Wells AU, Du Bois RM, Black CM, Coghlan JG. Echocardiography and pulmonary function as screening tests for pulmonary arterial hypertension in systemic sclerosis. Rheumatology 2004; 43:461-6.
21. Bussone G, Mouthon L. Interstitial lung disease in systemic sclerosis. Autoimm Rev 2011; 10:248-55.

PHARMACOLOGICAL GSK-3β INHIBITION IMPROVES OSTEOBLAST DIFFERENTIATION ON TITANIUM SURFACES

S. LUMETTI[1], S. FERRILLO[2], S. MAZZOTTA[2], G.M. MACALUSO[1], M. BONANINI[1], G. PASSERI[2] and C. GALLI[1]

[1]Department of Biomedical, Biotechnological, and Translational Sciences, University of Parma, Italy; [2]Department of Clinical and Experimental Medicine, University of Parma, Italy

Received January 27, 2014 – Accepted June 5, 2014

Rough titanium surfaces enhance the activation of Wnt canonical signaling, a pathway required for osteoblast differentiation. The present study investigated the effects of GSK3b-inhibitor (2'Z,3'E)-6-Bromoindirubin-3′-oxime (BIO) on osteoblastic differentiation on titanium surfaces with different topography and wettability. C2C12 cells were plated on pickled, acid-etched/sand-blasted (SLA), modified hydrophilic SLA titanium discs (modSLA) and stimulated with increasing doses of BIO. Activation of Wnt canonical signaling was measured with a reporter system. Gene expression was measured in the same cell system by Real Time PCR. Osteoblastic MC3T3 cells were then plated on discs with or without BIO and the expression of osteoblast specific genes was assessed by Real Time PCR. One mM BIO activated Wnt canonical signaling in C2C12 cells on all surfaces, and the highest effect was on rough surfaces. BIO markedly increased the expression of Osteoprotegerin and Osteocalcin in MC3T3 cells on rough surfaces at the concentration of 100 nM, and on all surfaces at the concentration of 1 mM. BIO enhances Wnt signaling activation and the expression of osteoblastic genes on rough surfaces and could be a viable approach to improve cell response to implant surfaces.

Osseointegrated implants require close contact between the biomaterial and surrounding tissues. This process can be dramatically improved by surfaces that promote cell adhesion and the activation of signaling pathways that direct the commitment of undifferentiated cells from the marrow compartment toward the osteoblastic lineage (1, 2). The canonical Wnt signaling plays a fundamental role for the commitment of osteochondral progenitors (3), as disruption of this cascade severely impairs bone formation (4), and deletion of Wnt surface receptor Lrp5 leads to severe osteopenia (5). Moreover, this pathway contributes to maintain existing bone through modulating osteoclastogenesis and thus bone turnover (6, 7). The main regulator of the canonical Wnt signaling is b-catenin, a multi-role protein that can function both as a structural protein and as co-transcription factor (8). The fate of b-catenin is controlled by a multi-protein complex that includes the GSK3b kinase (9-11). This complex targets b-catenin for proteosomal degradation, thus controlling its activity. Inhibitors of GSK3b have been previously shown to stimulate cell proliferation and osteoblast differentiation *in vitro* and in rodent models *in vivo* (12, 13), and our group has recently demonstrated that GSK3b inhibition by Lithium Chloride is a viable strategy to improve osteoblast differentiation on hyperhydrophilic titanium

Key words: titanium, Wnt, BIO, osteoblast, implant

Mailing address: Dr Guido Macaluso,
Dep. Biomedical,
Biotechnological, and Translational Sciences,
Università di Parma,
Via Gramsci 14, 43100 Parma, Italy
Tel.: +39 0521 986722
e-mail: guidomaria.macaluso@unipr.it

0393-974X (2014)

DISCLOSURE: ALL AUTHORS REPORT NO CONFLICTS OF INTEREST RELEVANT TO THIS ARTICLE.

surfaces (14). Alternative inhibitors with broader spectrum may represent an important tool to improve osteoblast differentiation and bone formation around titanium implants with different surface treatment.

The present study investigated the effects of (2'Z,3'E)-6-Bromoindirubin-3′-oxime (BIO), a well known inhibitor of GSK3b, on the activation of Wnt canonical signaling and osteoblast differentiation in cells growing on titanium surfaces with different topography.

MATERIALS AND METHODS

Pickled, acid-etched, sand-blasted (SLA) and hydrophilic SLA (modSLA) commercially pure titanium samples were kindly provided by Straumann Institut AG (Basel, Switzerland). These surfaces have been extensively characterized and are an established model of commercially available implant surface (15-18). Pickled discs are a smooth surface with mean peak to valley roughness (R_a) of 0.2 µm. SLA and modSLA surfaces have an R_a of 3.2 µm. The samples were provided as sterile discs of 1 mm thickness, 16 mm diameter, and were used in 24 well plates (Corning, Amsterdam, The Netherlands) for biological assays.

Reagent (2'Z,3'E)-6-Bromoindirubin-3′-oxime (BIO) was purchased from Sigma-Aldrich (Sigma-Aldrich Italy, Milan, Italy). The C2C12 cell line was purchased from the European Catalog of Cell Cultures (Health Protection Agency Culture Collections, Salisbury, UK) and MC3T3 cells were obtained from the American Type Culture Collection (LGC Standards S.R.L., Sesto S.Giovanni, MI, Italy). C2C12 cells were chosen because they are a common model to study the Wnt canonical pathway, due to the abundance of the molecular machinery necessary for this pathway, whilst MC3T3 cells are an established model of osteoblastic cell. They were grown in Dulbecco's modified Eagle Medium (DMEM, Sigma-Aldrich Italy, Milan, Italy), 10% Fetal Bovine Serum (Euroclone, Pero, Italy), 1% Penicillin and Streptomycin (Penstrep, Sigma-Aldrich Italy, Milan, Italy) and 1% Glutamine (Sigma-Aldrich Italy, Milan, Italy). For viability and gene expression assays, 100000 C2C12 cells were plated on Pickled, SLA or modSLA discs in 1 ml of complete medium in 24 well plates (Euroclone, Pero, Italy), in triplicate and assayed 24 h after plating. For reporter assays, C2C12 cells were plated on titanium surfaces in 1ml/well OptiMEM (Life Technologies, Carlsbad, CA, USA), 5% FBS, 1% Penstrep at the density of 80000 cells/well and transfected. Attractene (Qiagen, Venlo, The Netherlands) was used to forward-transfect cells with reporter plasmids according to the manufacturer's instructions. Cells were then treated with 1.5 mM recombinant Wnt3a protein, similarly to what was previously published (19), to provide background stimulation for the canonical Wnt pathway, and with either vehicle or increasing doses of BIO. Cells were then assayed after 24 h. MC3T3 cells were plated on Pickled, SLA or modSLA discs in 1 ml of complete medium in 24 well plates at the density of 50000 cells/well, in triplicate. On the following day, complete medium enriched with 250 mM ascorbic acid (Sigma-Aldrich Italy, Milan, Italy) was added to the cells to promote differentiation. Cells were assayed 96 h after plating.

Reporter assays

The TCF-Luc assay kit was obtained from SABioscience (Frederick, MD, USA). The kit contains a vector carrying the Firefly Luciferase gene under the control of TCF-binding elements, and a control plasmid constitutively expressing Renilla Luciferase under the control of the CMV promoter. Luciferase activity was calculated as the ratio between Firefly and Renilla Luciferase. The reporter assays were performed with Dual-Luciferase Reporter assay system (Promega, Milan, Italy) according to the manufacturer's recommendations. The samples were read with a Glomax 20/20 Luminometer (Promega, Milan, Italy) with double injectors.

Cell viability assay

To evaluate cell viability on titanium surfaces, the MTT assay for cell viability was used (Roche Applied Science, Monza, Italy), according to the manufacturer's indications. Briefly, 50 µl MTT labeling reagent (final concentration 0.5 mg/ml) were added, and then incubated for 4 hours, then 500 µl of solubilization solution were added. After overnight incubation, absorbance was read at 570 nm using a Multiscan Ascent spectrophotometer (Titertek Instruments Inc., Huntsville, AL, USA).

Real Time PCR

Total RNA was extracted from cell cultures using TRizol (Life Technologies, Carlsbad, CA, USA), according to the manufacturer's indications. TaqMan quantitative RT-PCR was performed as previously described using the following primer probe sets from Life Technologies (Carlsbad, CA, USA): Alkaline Phosphatase (Mm00475834_m1); Osteoprotegerin (Mm00435451_m1); Cyclooxygenase-2 (Mm01307329_m1); Runx2 (Mm00501584_m1); Osteocalcin (for 5'-GCTGCGCTCTGTCTCTCTGA-3'; rev 5'-TGCTTGGACATGAAGGCTTTG-3'; probe 5'-FAM-AAGCCCAGCGGCC-NFQ-3'); the housekeeping gene used in the study was mouse ribosomal protein S2, ChoB (for 5'-CCCAGGATGGCGACGAT-3'; rev 5'-CCGAATGCTGTAATGGCGTAT-3'; probe,

5'-FAM-TCCAGAGCAGGATCC-NFQ-3'). qPCR was performed with a Real Time PCR machine (StepOne, Life Technologies, Foster City, CA, USA).

Statistical analysis

Data were analyzed using Prism 4 (Prism 4, GraphPad, La Jolla, CA, USA). All values are reported as the mean ± Standard Deviation of three repeated experiments performed in triplicate. Differences between group means were evaluated with ANOVA statistical test and Bonferroni post-test and differences were considered significant when $p<0.05$.

RESULTS

To investigate the effects of (2'Z,3'E)-6-Bromoindirubin-3'-oxime (BIO) on canonical Wnt signaling in cells of the mesenchymal lineage on different titanium surfaces, we cultured premyoblast C2C12 cells on Pickled (smooth), sand-blasted/acid-etched (SLA) and hyperhydrophilic SLA (modSLA). BIO significantly increased Wnt activation, with a peak at 1 mM, and Wnt stimulation was higher on modSLA surfaces than smooth and SLA surfaces at both 1 and 10 mM. The peak concentration of 1 mM induced also a higher Wnt activation on SLA than smooth surfaces, although this effect was not observed at the higher concentration (Fig. 1).

The mRNA levels were then measured for Wnt target genes at Real Time PCR in C2C12 cells cultured on titanium discs with different surface treatments in the absence or in the presence of 1 mM BIO, the concentration that exerted the highest effects based on the previous experiment. Addition of BIO significantly increased the expression of Wnt target Alkaline Phosphatase (ALP) and Osteoprotegerin (OPG) in cells on SLA and modSLA surfaces (Fig. 2). Noticeably, it elevated the expression of transcript for another known Wnt target, Cyclooxygenase-2 (Cox-2), a protein required for the synthesis of Prostaglandin, in cells on smooth and SLA surfaces, although no changes were observed on modSLA (Fig. 2).

To measure cell growth on pickled, SLA and modSLA surfaces, we performed MTT assay at 24, 48 and 72 h of culture in C2C12 cells (Fig. 3). Cells on pickled surfaces displayed a tendency to proliferate faster than cells on rough SLA and modSLA titanium, as previously reported, and addition of 1 mM BIO did not affect their behavior.

To investigate whether BIO could promote the

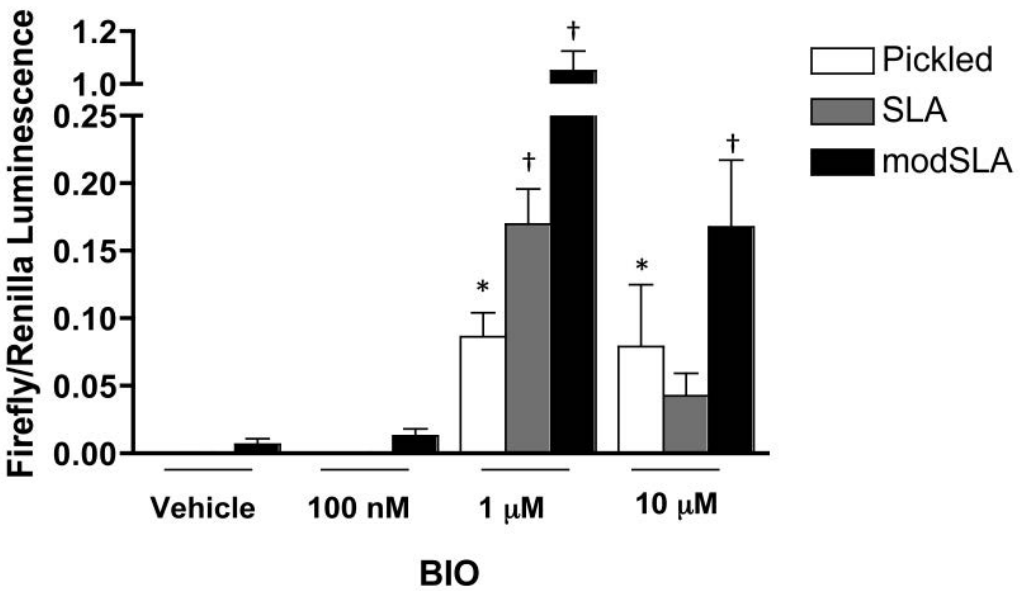

Fig. 1. *Luciferase activity of C2C12 cells cultured on pickled, sand-blasted/acid-etched (SLA) or hydrophilic SLA (modSLA) and transfected with both a reporter construct expressing firefly luciferase under the control of multiple β-catenin/TCF binding sites and a control plasmid constitutively expressing Renilla luciferase. Cells were treated with 1.5 mM Wnt3a and with either vehicle or increasing concentrations of BIO. * $p<0.05$, † $p<0.001$ vs vehicle group.*

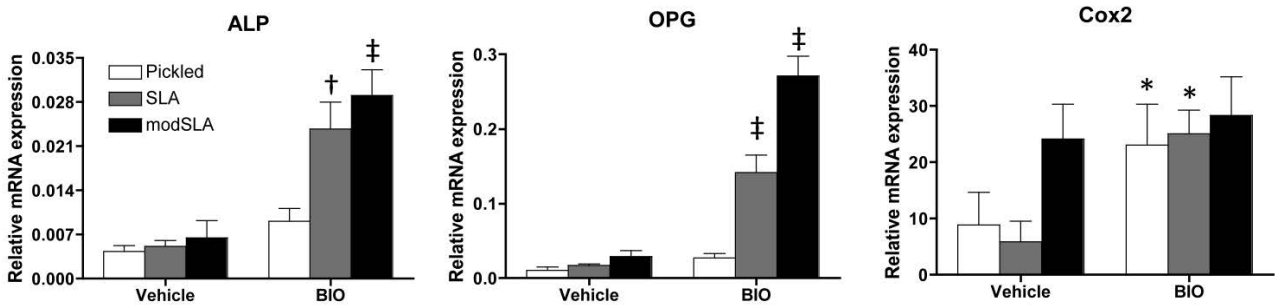

Fig. 2. *Quantitative RT-PCR of (**A**) Alkaline Phosphatase (ALP), (**B**) Osteoprotegerin (OPG) or (**C**) Cyclooxygenase-2 (Cox-2) mRNA from C2C12 cells cultured on pickled, SLA or modSLA titanium after addition of Wnt3a and treated with either vehicle or 1 mM BIO. All values were normalized to ribosomal protein S2 mRNA levels. All treatments were performed in triplicate. * p <0.05, † p <0.01 and ‡ p <0.001 vs vehicle group.*

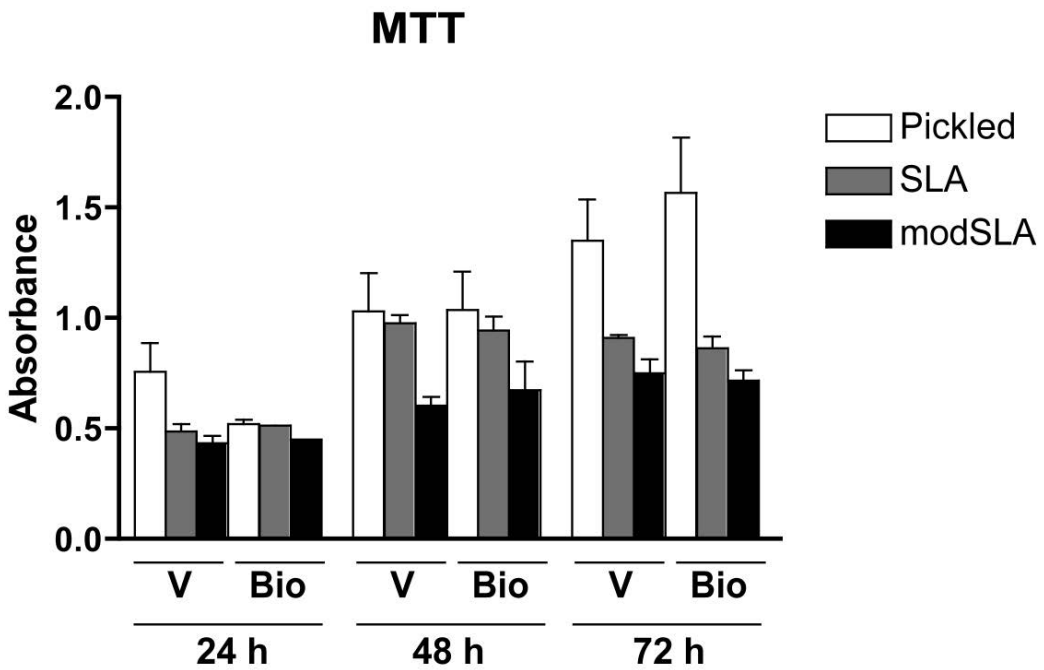

Fig. 3. *MTT viability assay of C2C12 cells on pickled, SLA or modSLA titanium surfaces in the presence of either vehicle or 1 mM BIO.*

expression of osteogenic genes on titanium surfaces, the murine calvaria cell line MC3T3 was stimulated with vehicle, 100 nM or 1 mM BIO (Fig. 4). One hundred nM BIO increased the expression of Wnt target genes and osteoblastic markers ALP and OPG in cells on SLA and modSLA surfaces, while 1 mM BIO significantly increased the mRNA levels of ALP on SLA and modSLA discs and of OPG on all three surfaces. Interestingly, BIO did not appear to affect the expression of Runx2, a gene required for osteoblast differentiation, but nevertheless increased the transcript levels for Osteocalcin (OCN), a marker with a pattern similar to that observed with OPG. One hundred nM BIO increased OCN expression on SLA and modSLA titanium and 1 mM BIO increased the mRNA levels for OCN on all surfaces (Fig. 4).

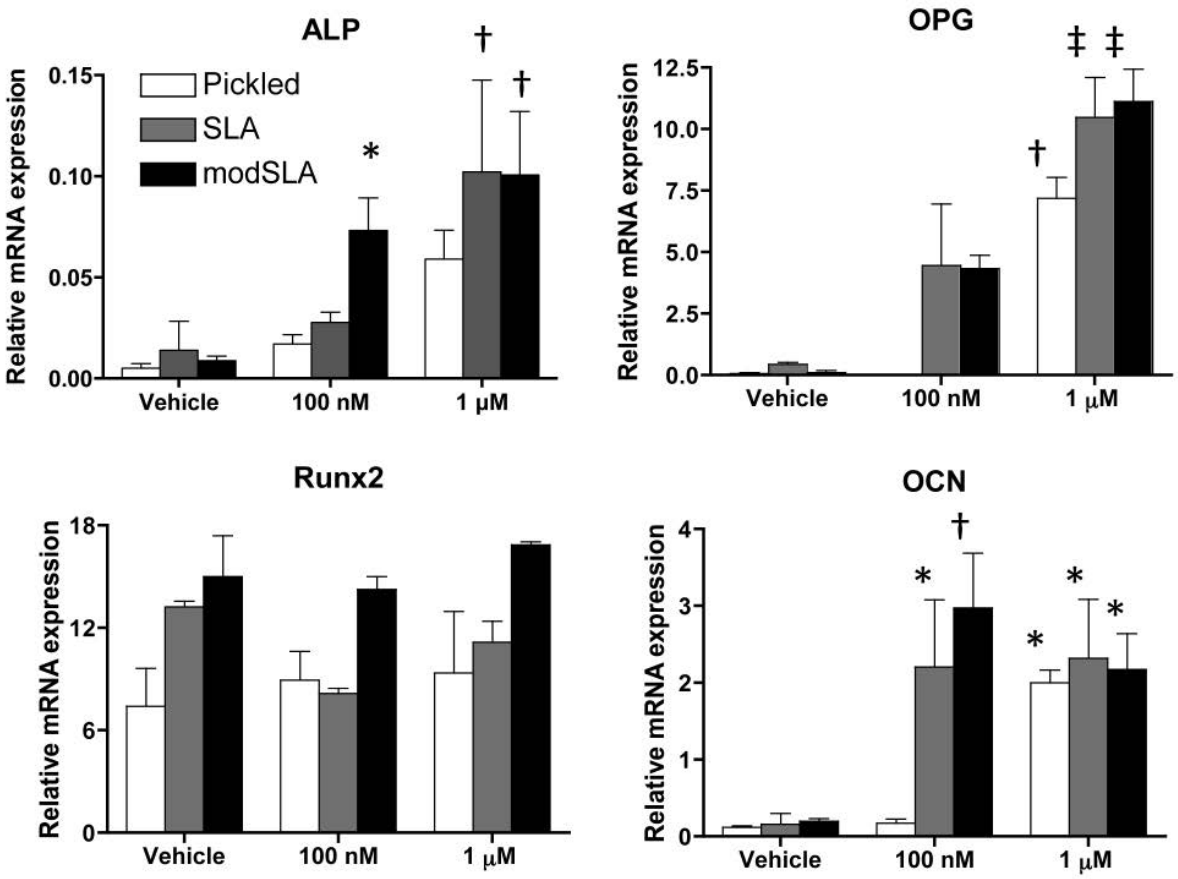

Fig. 4. *Quantitative Real Time-PCR of (**A**) ALP, (**B**) OPG, (**C**) Runx-2 or (**D**) Osteocalcin mRNA from MC3T3 cells cultured on pickled, SLA or modSLA titanium treated with either vehicle, 100 nM or 1 μM BIO. All values were normalized to ribosomal protein S2 mRNA levels. * p <0.05, † p <0.01 and ‡ p <0.001 vs vehicle group.*

DISCUSSION

The canonical Wnt signaling pathway is initiated upon binding of secreted glycoproteins of the Wnt family to membrane receptors, which then transduce the signal and activate alternative signaling cascades. It has been shown that rough implant topography can enhance the activation of the canonical Wnt pathway *in vitro* and *in vivo* (2, 20, 21), and we have reported that cytoskeletal organization affects canonical Wnt signaling, suggesting that surface topography can promote osteoblastic differentiation at least in part by directly regulating cell shape (22, 23). Therefore, this signaling pathway appears as an interesting candidate target to improve bone formation around endosseous implants. A pivotal role for the regulation of this pathway is played by b-catenin (24), a protein whose activity is regulated by a destruction complex that includes the GSK3b kinase (25). We have previously shown that Lithium Chloride (LiCl), a GSK3b inhibitor, could enhance activation of Wnt signaling and improve osteoblastic differentiation in murine cells on titanium surfaces. LiCl however presents with important drawbacks, which limit its potential use in a clinical perspective. Most significantly, LiCl has been reported to inhibit mineralization *in vivo* (26), which is obviously an undesirable phenomenon for implant integration. Moreover, LiCl is known to nonspecifically act on multiple signaling pathways (27). We therefore investigated an alternative, more specific GSK3b inhibitor, (2'Z,3'E)-6-Bromoindirubin-3′-oxime (BIO), which has been shown to maintain pluripotency of human and murine embryonic stem

cells (28). The present study showed that BIO, though not significantly affecting cell viability, enhances Wnt canonical signaling in murine cells growing on titanium surfaces by both reporter assay and gene expression. We decided to normalize our Real Time PCR data using the ribosomal S2 subunit, as this has shown good consistency as a housekeeping gene in bone cells (29-33). Although a stimulation is visible in all groups as compared to control, cells on rough or hyperhydrophilic surfaces appear to be more responsive to BIO. BIO thus appears to magnify the effects of surface topography on Wnt signaling activation. When we cultured osteoblastic MC3T3 cells on titanium surfaces and stimulated them with increasing concentrations of BIO we observed an increase in the expression levels of osteogenic genes, limited to rough surfaces at the lower dose and on every surface at the higher dosem, although no change in Runx2 expression was observed in the absence or in the presence of BIO, suggesting that the effect of BIO on osteoblastic differentiation is not mediated by an increase of activity of this transcription factor.

Based on the present data, BIO appears as a candidate molecule to improve cell differentiation on implant surfaces with different cell topography, in particular on hyperhydrophilic surfaces. Future studies will have to address the issue of how to deliver such a stimulus and how to properly release these molecules in the surrounding environment, thus controlling their concentrations in the peri-implant tissues.

ACKNOWLEDGEMENTS

The authors would like to thank Straumann Institut AG (and in particular Dr. Appert and Dr. Molenberg), Basel, Switzerland, for kindly providing the titanium surfaces used in the present study. The study was funded by grant 093_2010 from ITI Foundation (Basel, Switzerland) research grant from Fondazione Cariparma.

REFERENCES

1. Schwartz Z, Lohmann CH, Oefinger J, Bonewald LF, Dean DD, Boyan BD. Implant surface characteristics modulate differentiation behavior of cells in the osteoblastic lineage. Adv Dent Res 1999; 13:38-48.
2. Wall I, Donos N, Carlqvist K, Jones F, Brett P. Modified titanium surfaces promote accelerated osteogenic differentiation of mesenchymal stromal cells *in vitro*. Bone 2009; 45:17-26.
3. Krishnan V, Bryant HU, Macdougald OA. Regulation of bone mass by Wnt signaling. J Clin Invest 2006; 116:1202-9.
4. Rodda SJ, McMahon AP. Distinct roles for Hedgehog and canonical Wnt signaling in specification, differentiation and maintenance of osteoblast progenitors. Development 2006; 133:3231-44.
5. Cui Y, Niziolek PJ, MacDonald BT, et al. Lrp5 functions in bone to regulate bone mass. Nat Med 2011; 17:684-91.
6. Kramer I, Halleux C, Keller H, et al. Osteocyte Wnt/beta-catenin signaling is required for normal bone homeostasis. Mol Cell Biol 2010; 30:3071-85.
7. Glass DA, 2nd, Bialek P, Ahn JD, et al. Canonical Wnt signaling in differentiated osteoblasts controls osteoclast differentiation. Dev Cell 2005; 8:751-64.
8. Verheyen EM, Gottardi CJ. Regulation of Wnt/beta-catenin signaling by protein kinases. Dev Dyn 2010; 239(1):34-44.
9. Cselenyi CS, Jernigan KK, Tahinci E, Thorne CA, Lee LA, Lee E. LRP6 transduces a canonical Wnt signal independently of Axin degradation by inhibiting GSK3's phosphorylation of beta-catenin. Proc Natl Acad Sci U S A 2008; 105:8032-37.
10. Bonewald LF, Johnson ML. Osteocytes, mechanosensing and Wnt signaling. Bone 2008; 42:606-15.
11. Rokutanda S, Fujita T, Kanatani N, et al. Akt regulates skeletal development through GSK3, mTOR, and FoxOs. Dev Biol 2009; 328:78-93.
12. Clement-Lacroix P, Ai M, Morvan F, et al. Lrp5-independent activation of Wnt signaling by lithium chloride increases bone formation and bone mass in mice. Proc Natl Acad Sci U S A 2005; 102:17406-11.
13. Kulkarni NH, Onyia JE, Zeng Q, et al. Orally bioavailable GSK-3alpha/beta dual inhibitor increases markers of cellular differentiation in vitro and bone mass in vivo. J Bone Miner Res 2006; 21:910-20.
14. Galli C, Piemontese M, Lumetti S, Manfredi E, Macaluso GM, Passeri G. GSK3b-inhibitor lithium chloride enhances activation of Wnt canonical

signaling and osteoblast differentiation on hydrophilic titanium surfaces. Clin Oral Implants Res 2013; 24:921-27.

15. Zhao G, Raines AL, Wieland M, Schwartz Z, Boyan BD. Requirement for both micron- and submicron scale structure for synergistic responses of osteoblasts to substrate surface energy and topography. Biomaterials 2007; 28(18):2821-29.
16. Khandelwal N, Oates TW, Vargas A, Alexander PP, Schoolfield JD, Alex McMahan C. Conventional SLA and chemically modified SLA implants in patients with poorly controlled type 2 diabetes mellitus--a randomized controlled trial. Clin Oral Implants Res 2013; 24:13-19.
17. Hyzy SL, Olivares-Navarrete R, Hutton DL, Tan C, Boyan BD, Schwartz Z. Microstructured titanium regulates interleukin production by osteoblasts, an effect modulated by exogenous BMP-2. Acta Biomater 2013; 9:5821-29.
18. Klein MO, Bijelic A, Ziebart T, et al. Submicron scale-structured hydrophilic titanium surfaces promote early osteogenic gene response for cell adhesion and cell differentiation. Clin Implant Dent Relat Res 2013; 15:166-75.
19. Galli C, Piemontese M, Meikle ST, Santin M, Macaluso GM, Passeri G. Biomimetic coating with phosphoserine-tethered poly(epsilon-lysine) dendrons on titanium surfaces enhances Wnt and osteoblastic differentiation. Clin Oral Implants Res 2014; 25(2):e133-9
20. Galli C, Passeri G, Ravanetti F, Elezi E, Pedrazzoni M, Macaluso GM. Rough surface topography enhances the activation of Wnt/beta-catenin signaling in mesenchymal cells. J Biomed Mater Res A 2010; 95:682-90.
21. Ivanovski S, Hamlet S, Salvi GE, et al. Transcriptional profiling of osseointegration in humans. Clin Oral Implants Res 2011; 22:373-81.
22. Galli C, Piemontese M, Lumetti S, Ravanetti F, Macaluso GM, Passeri G. Actin cytoskeleton controls activation of Wnt/beta catenin signaling in mesenchymal cells on implant surfaces with different topographies. Acta Biomater 2012; 8:2963-68.
23. Lumetti S, Mazzotta S, Ferrillo S, Piergianni M, Piemontese M, Passeri G, Macaluso GM, Galli C. "RhoA Controls Wnt Upregulation on Microstructured Titanium Surfaces," BioMed Research International, vol. 2014, Article ID 401859.
24. Xu W, Kimelman D. Mechanistic insights from structural studies of beta-catenin and its binding partners. J Cell Sci 2007; 120:3337-44.
25. Angers S, Moon RT. Proximal events in Wnt signal transduction. Nat Rev Mol Cell Biol 2009; 10(7):468-77.
26. Baran DT, Schwartz MP, Bergfeld MA, Teitelbaum SL, Slatopolsky E, Avioli LV. Lithium inhibition of bone mineralization and osteoid formation. J Clin Invest 1978; 61:1691-96.
27. Li J, Khavandgar Z, Lin SH, Murshed M. Lithium chloride attenuates BMP-2 signaling and inhibits osteogenic differentiation through a novel WNT/GSK3- independent mechanism. Bone 2011; 48(2):321-31.
28. Sato N, Meijer L, Skaltsounis L, Greengard P, Brivanlou AH. Maintenance of pluripotency in human and mouse embryonic stem cells through activation of Wnt signaling by a pharmacological GSK-3-specific inhibitor. Nat Med 2004; 10: 55-63.
29. Onal M, Galli C, Fu Q, Xiong J, Weinstein RS, Manolagas SC, O'Brien CA. The RANKL distal control region is required for the increase in RANKL expression, but not the bone loss, associated with hyperparathyroidism or lactation in adult mice. Mol Endocrinol 2012; 26(2):341-48
30. Rhee Y, Allen MR, Condon K, et al. PTH receptor signaling in osteocytes governs periosteal bone formation and intracortical remodeling. J Bone Miner Res; 26(5):1035-46.
31. Galli C, Fu Q, Wang W, Olsen BR, Manolagas SC, Jilka RL, O'Brien CA. Commitment to the osteoblast lineage is not required for RANKL gene expression. J Biol Chem 2009; 284(19):12654-62.
32. O'Brien CA, Plotkin LI, Galli C, et al. Control of bone mass and remodeling by PTH receptor signaling in osteocytes. PLoS One 2008;3(8):e2942.
33. Galli C, Zella LA, Fretz JA, Fu Q, Pike JW, Weinstein RS, Manolagas SC, O'Brien CA. Targeted deletion of a distant transcriptional enhancer of the receptor activator of nuclear factor-kappaB ligand gene reduces bone remodeling and increases bone mass. Endocrinology 2008; 149(1):146-53.

CO(2) PNEUMOPERITONEUM INDUCES *IN VITRO* HYPOXIC RESPONSE CULMINATING IN APOPTOSIS OF HUMAN NEUROBLASTOMA CELLS

M. CURRÒ[1], A.S. MONTALTO[2], P. IMPELLIZZERI[2], E. MONTALTO[2], R. RISITANO[1], T. RUSSO[2], P. PERRONE[2], V. CHIRICO[2], T. ARRIGO[2], C. SALPIETRO[2], C. ROMEO[2] and R. IENTILE[1]

[1]Department of Biomedical Sciences and Morphological and Functional Imaging, University of Messina, Italy; [2]Department of Pediatric, Gynecological, Microbiological and Biomedical Sciences, University of Messina, Italy

Received February 5, 2014 – Accepted July 18, 2014

The first two authors contributed equally to this study

The ablative role of minimally invasive surgery (MIS) in neuroblastoma (NB) is still controversial due to the possible CO_2 pneumoperitoneum side-effects on tumor aggressiveness. It is known that CO_2 produces hypoxic condition with changes in tumor microenvironment influencing cell functions. Here we investigated whether CO_2 exposure affects the transcription factor HIF-1α and the apoptotic signalling pathway in SH-SY5Y NB cells. SH-SY5Y cells were exposed to a pressure of 15 mmHg CO_2 (100%) for 4 h (T_0) and then moved to normal condition for 24 h (T_{24}). In control and CO_2-exposed cells, we analyzed the mRNA levels and DNA binding activity of HIF-1α. We also evaluated the proliferative activity and cell viability as well as caspase-9/3 cleavage and nuclear fragmentation. A significant increase in HIF-1α activation was observed in SH-SY5Y cells exposed to CO_2 compared to control cells. CO_2 treatment also decreased the proliferation rate and the percentage of viable cells. In addition, the expression and cleavage of caspase-9 and -3 were significantly increased in NB cells exposed to CO_2. These data correlated with apoptotic feature observed in CO_2-treated NB cells. Our findings show that CO_2-induced hypoxic condition exerts cytotoxic effects on NB cells by eliciting mitochondrial apoptotic pathway and thereby improving the understanding of the possible clinical impact of CO_2 pneumoperitoneum on NB behavior.

The role of minimally invasive surgery (MIS) in neuroblastoma (NB) treatment is unclear. The clinical advantages of MIS regarding surgical morbidity and antitumor efficacy after NB resection are not conclusive (1). In parallel, molecular implications of CO_2 impact on tumor behaviour are an open issue. The few experimental studies predominantly report a negative CO_2 influence on liver metastasis, NB cell apoptosis, c-myc and HMGB-1 expressions as well as NB cell migration (2–4). However, in a recent work, we showed *in vitro* that simulated CO_2 pneumoperitoneum environment induced oxidative stress and cell DNA damage followed by a significant attenuation of cell proliferation mediated by p53

Key words: CO_2 pneumoperitoneum, neuroblastoma cells, HIF-1α, caspase-9, apoptosis

Mailing address: Dr. Angela Simona Montalto,
Unit of Pediatric Surgery, Department of Pediatric, Gynecological, Microbiological and Biomedical Sciences University of Messina, Italy
Policlinico G. Martino, Viale Gazzi, 98124 Messina, Italy
Tel.: +39 0902213025 Fax: +39 0902213025
e-mail: amontalto@unime.it

0393-974X (2014)

DISCLOSURE: ALL AUTHORS REPORT NO CONFLICTS OF INTEREST RELEVANT TO THIS ARTICLE.

activation (5).

It is known that CO_2 produces a hypoxic condition on cells and tissues (6). Hypoxic control of cell growth and death may be of general pathophysiological importance. The primary transcriptional responses to hypoxic stress are mediated by the Hypoxia Inducible transcription factors (HIFs) of which HIF-1α was shown to play a central role in the growth and survival of cancer cells. It has been reported that increased expression of HIF-1α and its regulated genes can be also associated with apoptotic pathway via activation of p53 protein (7). The balance between hypoxia-induced apoptosis and the increased resistance to cell death mediated by various hypoxia-induced pathways determines whether a tumor can survive and even grow under hypoxic conditions.

Several studies have shown that hypoxic NB cells adopt an immature, neural crest-like phenotype, which results in more aggressive tumor cells with increased potential to metastasize (8–10). In one clinical study, an up-regulation was demonstrated of HIF-1α associated with adverse clinic-pathological and biological factors in neuroblastomas (11).

On the other hand, it has been shown that hypoxia affect NB cell behavior in a time-relative manner, indeed apoptotic features were observed at an early period of exposure time, but these effects were reversed with the extension of hypoxic treatment (12). Therefore, the aim of this study was to investigate molecular mechanisms underlying hypoxic response associated with CO_2 insufflation in NB cells to evaluate the controversial effects associated with changes of HIF-1α pathway. Moreover, we evaluated the cell proliferation rate and characterized the apoptotic signalling pathway following CO_2 exposure of NB cells.

MATERIALS AND METHODS

Materials

The human SH-SY5Y NB cells (CRL-2266) were purchased from American Type Culture Collections (ATCC) (Rockville, MD, USA) and maintained in culture for no more than 20 passages. RPMI, penicillin/streptomycin mixture, glutamine, phosphate buffered saline solution (PBS), (3-(4,5-dimethylthiazol-2-yl)-2,5-diphenyl*tetrazolium* bromide (MTT), Hoechst 33258 and other chemicals of analytical grade, as well as mouse monoclonal antibody against α-tubulin were from Sigma (Milan, Italy). Rabbit antibody against caspase-3 was from Millipore (Milan, Italy); antibodies against procaspase-9 and active caspase-9 were from Abcam (DBA, Milan, Italy). Horseradish peroxidase-conjugated anti-mouse and -rabbit secondary antibodies, ECL Chemiluminescence detection kit and X-ray film were purchased from GE Healthcare (Milan, Italy). Developer, fixer, and Kodak X-ray film were from Kodak (Milan, Italy).

Fetal bovine serum (FBS), TRIzol reagent, High-capacity cDNA archive kit, TaqMan PCR master mix and TaqMan assay for human HIF-1α (Hs00936366_m1) and β-actin (Hs99999903_m1) were from Life Technologies (Milan, Italy).

Cell culture and treatment

SH-SY5Y NB cells were cultured in RPMI-1640 medium containing 10% (v/v) heat-inactivated FBS, L-glutamine (2 mM), 100 units/mL penicillin, and 100 mg/mL streptomycin, and maintained at 37°C in a humidified incubator with 5% CO_2 and 95% air. Sub-confluent SH-SY5Y cells were exposed to a pressure of 15 mmHg (100%) of CO_2 for 4 h into a pneumoperitoneum chamber located in an incubator set at 37°C, as previously reported (5). After gas treatment, cells were either immediately harvested (T_0) or incubated again in 5% CO_2 and 95% air for 24 h (T_{24}). Control cultures were maintained in a standard cell incubator (95% air/5% CO_2) at 37°C and either harvested after 4 h or further incubated for 24 h.

Analysis of gene expression by Real-Time PCR

Total RNA was isolated using TRIzol reagent, then two micrograms of RNA were reverse transcribed with High-Capacity cDNA Archive kit according to the manufacturer's instructions.

HIF-1α mRNA levels were analyzed by Real-Time PCR using a TaqMan gene expression assay (Life Technologies, Milan, Italy). β-actin was used as endogenous control. Quantitative PCR reactions were set up in duplicate in a 96-well plate and were carried out in 10 µl reactions containing 1x Gene Expression Mastermix, 1x TaqMan-specific assay, and 25 ng RNA converted into cDNA. RT-PCR was performed in a 7900HT Fast Real-Time PCR System with the following profile: one cycle at 50°C for 2 min, then 95°C for 10 min, followed by 40 cycles at 95°C for 15 s and 60°C for 1 min. Data were collected with SDS 2.3 software (Applied Biosystems, Foster City, CA, USA) and analyzed using the 2^{-DDCT} relative quantification method. Values are presented as fold change relative to unexposed T_0 cells.

Nuclear extracts and gel mobility shift assay

Nuclear extracts of CO_2-exposed and control cells were prepared as previously described (13). The presence

of HIF-1 DNA binding activity in cell nuclear extracts was evaluated by electrophoretic mobility shift assay (EMSA), using the EMSA HIF1 detection kit (Panomics, Redwood City, CA, USA) according to the manufacturer's instructions.

Proliferation assay and cytotoxicity study

To assess the effects of CO_2 exposure on cell proliferation, an MTT (3-(4,5-methylthiazol-2-yl)-2,5-diphenyl-tetrazolium bromide) reduction assay was performed.

At the end of the incubation periods (T_0 and T_{24}), control and CO_2 exposed cells, seeded at a density of $2.5 \cdot 10^4$ cell/well in 96-well culture plates, were incubated with fresh medium containing MTT (0.5 mg/mL) at 37°C for 4 h. Then, insoluble formazan crystals were dissolved in 100 µL of acidic isopropanol (0.04 M HCl in absolute isopropanol) at 37°C for 1 h. The optical density in each well was determined at 570 nm using a microplate reader (Tecan Italia, Cologno Monzese, Italy). Results were expressed as percentage of control T_0 cells. All experiments were performed in triplicate. Cytotoxic effects of CO_2 exposure were assessed by the trypan blue dye exclusion test, according to manufactured instructions.

Western blotting

After incubation, cells plated in 25 cm^2 flasks at a density of $2.5 \cdot 10^5$ cell/ml were scraped off and lysed using ice-cold RIPA buffer supplemented with Protease Inhibitor Cocktail (SIGMA Aldrich, Milan, Italy), followed by centrifugation at 8,000 x g at 4°C for 10 min to remove cell debris. Protein concentration was evaluated by the Bradford method and 30 µg proteins were loaded on a 10% denaturing SDS-polyacrylamide gel. After protein transfer, the nitrocellulose membranes were blocked with 5% non-fat dry milk at room temperature for an hour. Then membranes were incubated with mouse monoclonal antibody against α-tubulin (diluted 1:50000 in TBS-T), rabbit antibodies against caspase-3 (diluted 1:200), procaspase-9 or active caspase-9 (diluted 1:100) overnight at 4°C, followed by incubation with horseradish peroxidase-conjugated anti-mouse or anti-rabbit secondary antibodies (respectively diluted 1:50000 and 1:1000 in TBS-T) for 2 h at room temperature. Immunoblots were developed with ECL Plus chemiluminescent detection system kit using Kodak film. The band intensity was quantified by densitometric analysis with an AlphaImager 1200 System (Alpha Innotech, San Leandro, CA, USA).

Hoechst 33258 fluorescent microscopy

Hoechst microscopy analyses were performed to examine the apoptotic cell death as a result of morphological change in the nucleus.

Following treatment, the cells plated at a density of $2.5 \cdot 10^5$ cells/ml in 4-well chamber slides were washed with PBS and fixed with 4% paraformaldehyde for 15 min at room temperature. After three rinses with PBS, the cells were incubated for 15 min with Hoechst 33258 (20 µg/ml in PBS), and then the morphology of the nucleus was analyzed under a DM IRB fluorescence microscope (Leica Microsystem, Heidelberg, Mannheim, Germany), equipped with a digital camera (Canon Power Shot S50, Milan, Italy). Viable cells were identified by their intact nuclei with diffuse fluorescence, whereas apoptotic cells by their chromosome condensation and fragmentation of nuclei exhibiting highlight staining.

At random, 200 cells were observed in the fluorescent microscope at ×400 magnification and the percentage of cells reflecting pathological changes was calculated. Data were collected for three replicates and used to calculate the respective means and standard error of the mean (SEM).

Statistical analysis

All experiments were repeated at least three times and each experiment was performed in triplicate. All values are expressed as mean ± SEM. Statistical analysis was carried out using Student's *t*-test, with p-values less than 0.05 considered significant.

RESULTS

Given the well-known property of CO_2 to create a hypoxic environment, we firstly examined the effects of CO_2 exposure on HIF-1α expression/activation in SH-SY5Y NB cells.

HIF-1α mRNA levels were only weakly increased in NB cells exposed to 15 mmHg CO_2 for 4 h (T_0) with respect to control cells, and returned to basal levels in cells maintained up to 24 h of incubation in standard condition after removal of CO_2 (T_{24}) (Fig. 1A). Nevertheless, as highlighted by EMSA analysis, immediately after 4 h CO_2 exposure (T_0) we observed a significant increase in HIF-1 DNA binding activity in nuclear extracts of treated cells in comparison to control ones. No differences were found in HIF-1 activation between CO_2-exposed and unexposed cells 24 h after gas removal (T_{24}) (Fig. 1B).

We then evaluated the effect of CO_2-induced hypoxic stress on cell proliferation. As shown in Fig. 2A, CO_2 exposure exhibited anti-proliferative effects on NB cells. Although there was no significant difference in the cellular MTT reduction

between CO_2-exposed and unexposed T_0 cells, after 24 h of incubation in standard condition (T_{24}) the proliferative activity was slower in CO_2-treated cells (50%) than in control cells (80%). The MTT data was confirmed by counting the cells in a Neubauer hemocytometer chamber (data not shown).

The inhibitory effect of CO_2 treatment on cell proliferation was accompanied by the induction of cell death, evaluated by trypan blue dye exclusion test. The percentage of dead cells was similar in T_0-exposed and unexposed cells (9% *vs* 5%, $p>0.05$), but in the following 24 h we observed a significant increase in cell death of CO_2–exposed cells in comparison to control ones (27% *vs* 9%, $p< 0.01$) (Fig. 2B).

Considering that hypoxia may be associated with apoptosis in experimental models, we evaluated the activation of caspase pathway in CO_2-exposed SH-SY5Y. A significant up-regulation of procaspase-9 ($p<0.05$) was observed in NB cells treated with CO_2 for 4 h (T_0) compared to control cells, although in the following 24 h (T_{24}) protein amounts were similar to control ones (Fig. 3). The exposure of NB cells to CO_2 was also accompanied by a significant increase in caspase-9 cleavage both in T_0 and T_{24} cells compared with control cells ($p<0.05$) (Fig. 3).

Similarly, procaspase-3 expression levels were increased in CO_2-exposed T_0 cells (1.7-fold, $p<0.05$), increasing up to 2-fold ($p<0.05$) in CO_2-exposed T_{24} cells when compared to controls. In addition, fragments of activated caspase-3 (17 kDa subunit) appeared immediately after CO_2 exposure, and were more evident in CO_2-exposed T_{24} cells with 5.3-fold ($p<0.01$) increases in comparison to control cells (Fig. 4).

CO_2-induced apoptosis in SH-SY5Y cells was

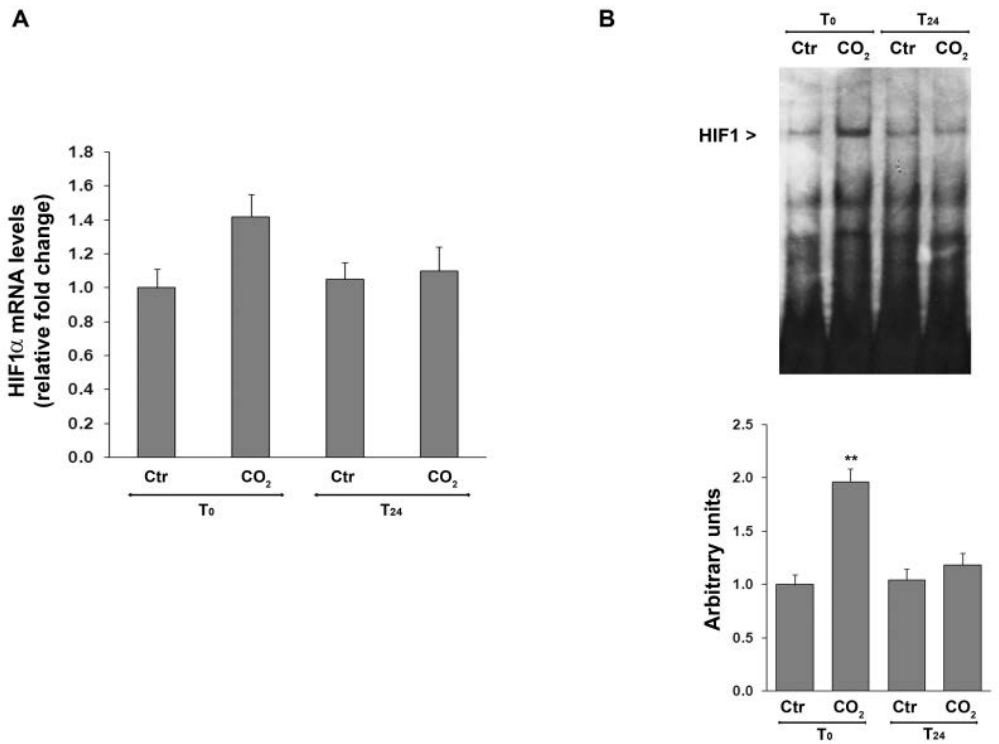

Fig. 1. *Effects of CO_2 exposure on HIF-1α transcription and activation in SH-SY5Y cells. After 4 h CO_2 insufflation, cells were either immediately harvested (T_0) or incubated again in 5% CO_2 and 95% air for 24 h (T_{24}). **A)** Total RNA was purified from cell cultures and the mRNA levels of HIF-1α was evaluated by Real-Time PCR. **B)** Nuclear extracts were incubated with an oligonucleotide probe containing the HIF-1α consensus motif and subjected to EMSA analysis. The densitometric analysis of HIF-1α bands is shown at the bottom. Values represent the mean ± SEM of three separate experiments. **$p<0.01$ significant differences in comparison to control.*

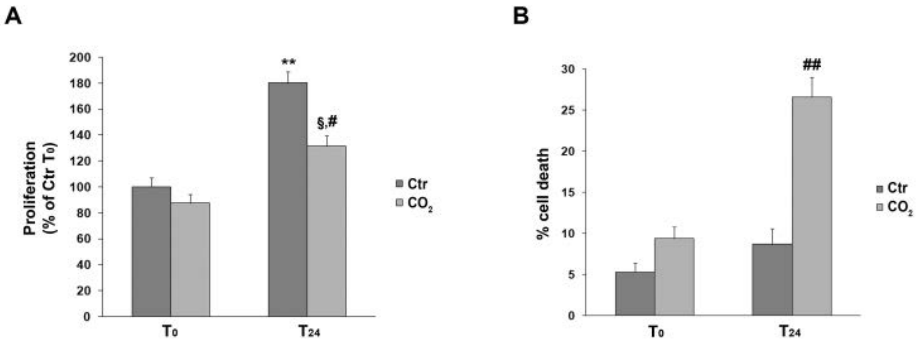

Fig. 2. *CO_2 exposure decreases NB cell growth and increases the percentage of dead cells.* ***A)*** *Proliferation rate was assessed by MTT assay. Results of MTT test are expressed as percentages of the values detected in untreated T_0 cells. Each value is the mean ± S.E.M. of at least three experiments.* ***B)*** *Cell death was evaluated using the trypan blue dye exclusion test. Data represent the mean ± S.E.M. of three different experiments. **$p<0.01$ significant differences in comparison to control T_0 cells; $^{§}p<0.05$ significant differences in comparison to CO_2 T_0 cells; $^{\#}p<0.05$ and $^{\#\#}p<0.01$ significant differences in comparison to control T_{24} cells.*

evaluated by fluorescence microscopy after Hoechst 33258 staining of CO_2-exposed and unexposed cells. As shown in Fig. 5, homogeneously stained nuclei were observed in control cells both at T_0 and T_{24}, as well as in CO_2-exposed T_0 cells, while CO_2-exposed T_{24} cells presented apoptotic features with fragmented nuclei.

Direct counting of apoptotic cells was carried out to quantify microscopic observations and the number of apoptotic cells was expressed as percent of the total number of cells. In control and CO_2-treated T_0 cultures we detected less than 1% apoptotic cells, whereas 12% of CO_2-exposed T_{24} cells showed apoptotic features ($p<0.01$).

DISCUSSION

In pediatric surgical oncology, the use of MIS can offer several advantages in comparison to open surgery, such as less pain, faster recovery time and improved cosmesis. In addition, this technique is mostly aimed to minimize the physiologic consequences of an operation which include scarring, stress response and disability (14, 15). To date, the applications of MIS in the management of NB are limited to selected conditions (diagnostic purpose, treatment of well encapsulated tumors with favorable prognostic factors or metastasis) (1). The relationship between laparoscopic tumor surgery and overall survival, event-free survival as well as surgical morbidity, is unclear in the pediatric population (1). A critical issue for the complete acceptance of MIS in NB resection is to elucidate the potential adverse effects of CO_2, a gas molecule used for pneumoperitoneum, on tumor cell behavior. NB is the most common heterogeneous solid tumor in children and it has been postulated that the exposure to CO_2 increases malignancy of tumor cells (2, 16). Conversely, in a recent study we highlighted cytotoxic effects induced by CO_2 insufflation on human NB cells via oxidative stress (5). In particular, we showed significantly increased ROS production in SH-SY5Y NB cells after CO_2 insufflation with marked DNA damage, p53 up-regulation and cell cycle arrest. These data suggested that CO_2 can interfere with the malignant potential of the NB cells and led us to investigate molecular mechanisms contributing to these effects.

CO_2 alters the chemical environment of cells through hypoxia influencing different cell functions (6). In a previous study, the hypoxic CO_2 effects on markers of malignancy as c-myc and HMGB-1 in SH-SY5Y NB cells were evaluated. The authors found strong molecular signs of malignant transformation

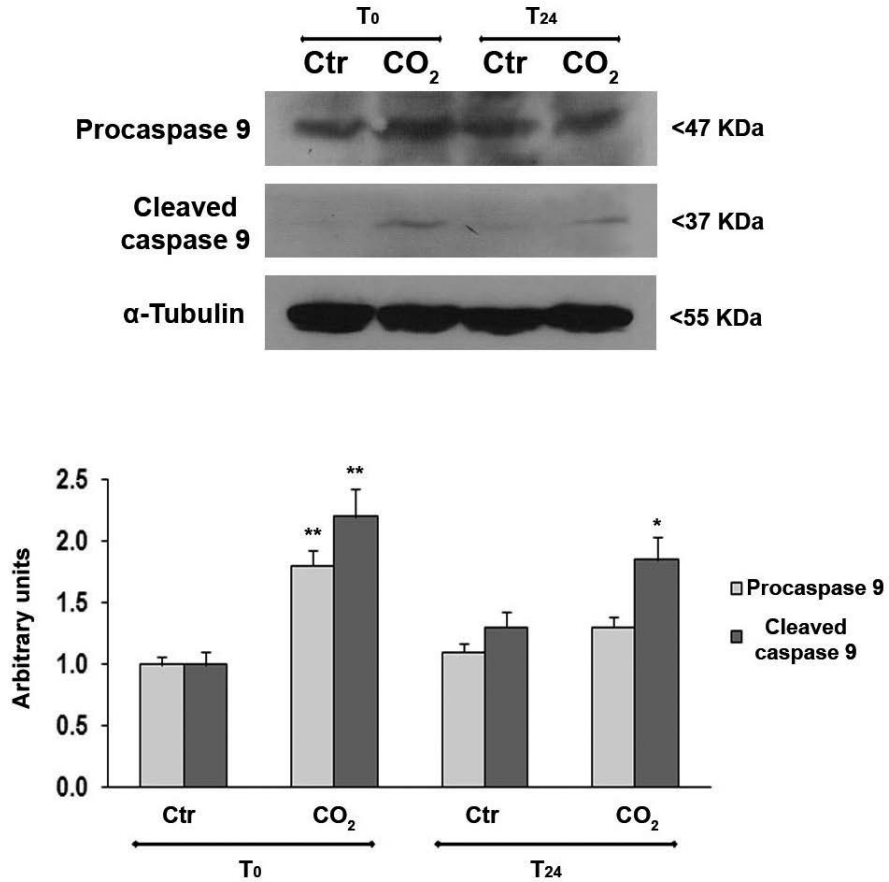

Fig. 3. *CO_2 treatment induces caspase-9 cleavage in SH-SY5Y NB cells. Cell lysates from CO_2 exposed and unexposed cell cultures were analyzed by Western blotting using specific antibodies against procaspase-9 and cleaved caspase-9. Densitometric analysis of immunoblots (bottom) was carried out after normalization against α-tubulin. The immunoblots are representative of three separate experiments. *p<0.05, and **p<0.01 significant differences in comparison to relative controls.*

in tumor cells subjected to CO_2 exposure (3).

The primary factor mediating the response to hypoxic stress is HIF-1, which consists of a constitutively expressed subunit, HIF-1β, and an oxygen-regulated subunit, HIF-1α. It is well known that HIF-1α plays a pivotal role in adaptive responses of cancer cells to hypoxic condition, inducing the expression of numerous genes involved in a broad range of cellular processes such as angiogenesis, proliferation, migration and invasion, but paradoxically it also mediates hypoxic cell death (17, 18). On the other hand, previous experiments on NIH3T3 normal fibroblasts demonstrated that hypoxic stress influenced Forkhead Box O3a transcription factor inhibiting HIF1-induced apoptosis and promoting cell survival (19).

In the present report, we evaluated HIF-1α involvement in NB cell response to CO_2. We highlighted an increase in HIF-1α activation after 4 h CO_2 exposure of SH-SY5Y NB cells, and no differences were observed between CO_2-exposed and unexposed cells 24 h after gas removal. Although several *in vitro* and *in vivo* studies showed a transcriptional regulation of HIF-1α (20, 21), in our experimental condition HIF-1α activation was associated only to a weak induction of its transcription. Thus, we can affirm that, based on the severity and duration of hypoxic exposure,

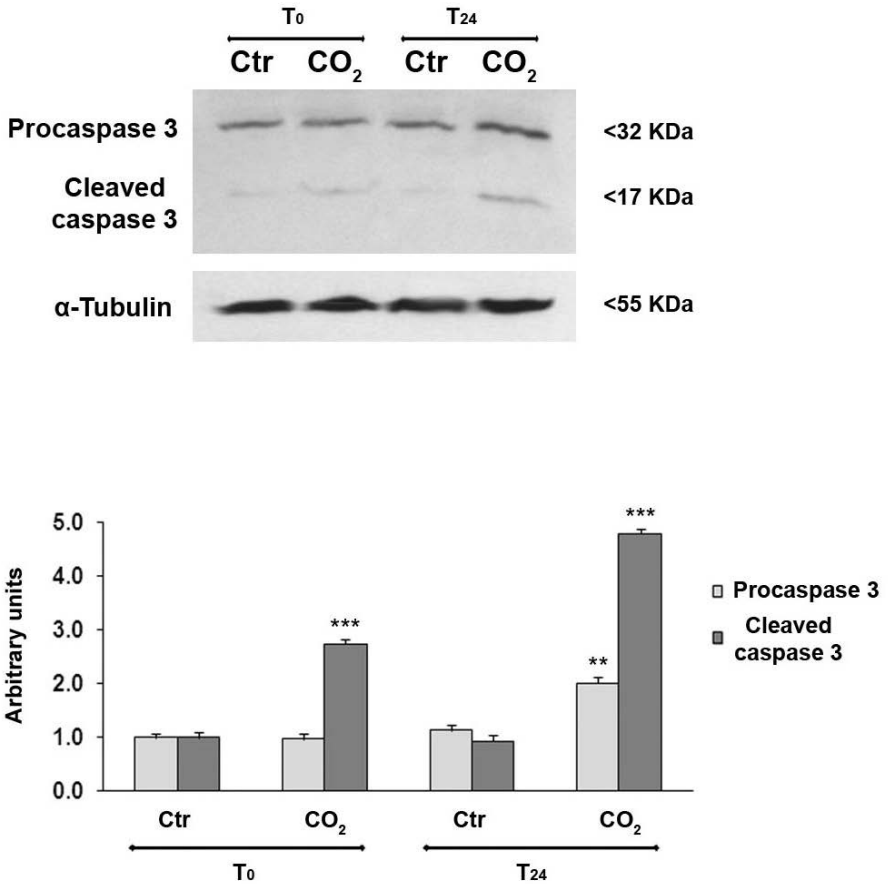

Fig. 4. *Caspase-3 expression and cleavage in SH-SY5Y NB cells treated with CO_2. After exposure to 15 mmHg CO_2, cellular proteins were extracted for the determination of the expression of procaspase-3 by Western blotting. The activation of caspase-3 was assessed by the presence of a 17 kDa fragment derived from the cleavage of proenzyme caspase-3 (32 kDa). Densitometric analysis of immunoblots (bottom) was carried out after normalization against α-tubulin. The immunoblots are representative of three separate experiments. **p<0.01, and ***p<0.005 significant differences in comparison to relative controls.*

HIF-1α was primarily regulated by posttranslational modifications at the level of its protein stability, as frequently is the case for transcription factors.

To further study the underlying mechanisms of the CO_2 effects on NB cells, we determined the proliferative activity and cell viability by MTT assay and trypan blue staining, respectively. CO_2 exposure showed growth inhibitory effects leading also to NB cell death. Our results are in line with previous data reporting a persistent decrease in NB cell proliferation after CO_2 incubation (22).

Cell response to hypoxic conditions is at least partly mediated by mitochondria attempting to reduce oxygen utilization. Mitochondrial dysfunction leads to increased ROS production which in turn triggers a cascade of events involving the activation of p53 and transcription factors, such as HIF-1 (23–25).

On the basis of this evidence, the present and previous results (5) suggest that the increase in ROS production caused by CO_2-induced hypoxic microenvironment is associated with HIF-1α activation and p53 up-regulation.

Because p53 engages the cell death pathway and HIF-1α contributes to programmed cell death during hypoxia, we explored the potential capacity of CO_2 to induce apoptosis on NB cells. Our results show that the early HIF-1α activation was accompanied by a significant increase in caspase-9

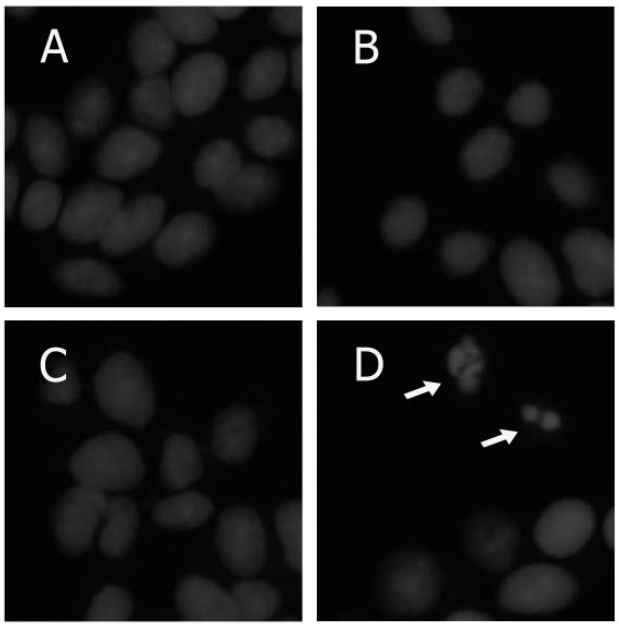

Fig. 5. *Apoptotic morphological changes in SH-SY5Y NB cells induced by CO_2 exposure, evaluated by Hoechst staining. Following treatment, the cells plated in 4-well chamber slides were stained with Hoechst 33258 and examined by fluorescence microscopy at ×400.* ***A)*** *Control cultures at T_0;* ***(B)*** *cells treated with CO_2 for 4 h (T_0);* ***(C)*** *control cells at T_{24};* ***(D)*** *cells exposed to CO_2 for 4 h and then incubated in standard condition for 24 h (T_{24}). The arrows designate the presence of apoptotic nuclear profiles.*

cleavage that persisted until 24 h after CO_2 removal. Once activated, caspase-9, the initiator caspase in mitochondrial apoptosis pathway, can process a group of downstream effector caspases, including caspase-3, which are responsible for the proteolytic cleavage of many intracellular proteins, resulting in the biochemical and morphological changes associated with apoptosis. In line with this evidence, our data demonstrated a marked increase of caspase-3 cleavage and apoptotic rate in CO_2-exposed NB cells following caspase-9 activation. Thus, in our experimental condition, HIF-1α appears to be a key candidate in the regulation of apoptotic cell death triggering the intrinsic mitochondrial/caspase-9 pathway. Our data are consistent with a previous study clearly showing that hypoxia-induced apoptosis relies on the intrinsic mitochondrial apoptotic pathway, while it is independent from the extrinsic pathway (death receptor-mediated) (26). A recent work also showed that $CoCl_2$, a well-characterized hypoxia-mimetic agent, induced canonical p53 mitochondrial apoptosis in the p53 wild-type NB cell lines, and caspase-independent cell death in both p53 mutated and knockout cells (27).

In contrast with our results, Reisman and coworkers (3) reported a reduction of caspase 3/7 activity in SH-SY5Y cells after CO_2 treatment when compared to unexposed cells. However, in this work the authors performed the CO_2-exposure of NB cells for 2 h and did not evaluate the effects at prolonged times after gas removal. Another study assessed the effects of CO_2 pneumoperitoneum on MKN-45 gastric cancer cells investigating the role of HIF-1α in CO_2-induced apoptosis. Data suggested that CO_2 insufflation increased the expression of HIF-1α which promoted apoptosis by activating Bax protein, a major core of the intrinsic apoptosis pathway at the mitochondria (28).

A mechanism by which HIF-1α can induce apoptosis is the stabilization of the tumor suppressor p53 (29). Several studies reported a cross-talk between the HIF-1α and p53 transcription factors, and both direct and indirect interactions have been proposed to explain this interplay (30). Chen et al. (31) described the formation of a trimeric complex containing p53, MDM2 and HIF-1α. In this ternary complex, the direct binding of HIF-1α to MDM2, the best-known physiological inhibitor of p53, suppresses the MDM2-dependent ubiquitination and nuclear export of p53 favoring its transcriptional activity (31).

However, the relationship between HIF-1α and p53 provides a potential negative feedback loop for the HIF-1α stabilization by promoting its MDM2-mediated ubiquitination and proteasomal degradation (32). Thus, once p53 becomes activated under hypoxic conditions, it contributes to terminating HIF-1 adaptive responses and exerts its anti-proliferative and pro-apoptotic activity.

In light of these observations and considering our previous data showing the CO_2-induced activation of the tumor suppressor p53 (5), we can hypothesize that following CO_2 exposure the HIF-1α activation increases the p53 protein stability, leading to apoptotic cell death.

Our results indicate that mimicking conditions of CO_2 pneumoperitoneum affect HIF-1α activity promoting apoptosis rather than cell proliferation in p53 wild-type SH-SY5Y NB cell line. These data corroborate our previous findings on CO_2-induced cell cycle arrest (5).

In conclusion, we emphasize that laparoscopic approach could have no side negative effects on NB cell behavior. However, the better characterization of the molecular mechanisms underlying the tumor cell response to CO_2, both in *in vitro* and *in vivo* experimental studies, should become a focus of research activities in pediatric surgical oncology. The demonstration that MIS is a safe and effective technique in NB treatment might extend its applicability to this heterogeneous tumor, and allow to benefit from its clinical and immunological qualities.

REFERENCES

1. Heloury Y, Muthucumaru M, Panabokke G, Cheng W, Kimber C, Leclair MD. Minimally invasive adrenalectomy in children. J Pediatr Surg 2012; 47:415-21.
2. Metzelder M, Kuebler J, Shimotakahara A, Vieten G, von Wasielewski R, Ure BM. CO(2) pneumoperitoneum increases systemic but not local tumor spread after intraperitoneal murine neuroblastoma spillage in mice. Surg Endosc 2008; 22:2648-53.
3. Reismann M, Wehrmann F, Schukfeh N, Kuebler JF, Ure B, Glüer S. Carbon dioxide, hypoxia and low pH lead to overexpression of c-myc and HMGB-1 oncogenes in neuroblastoma cells. Eur J Pediatr Surg Off J Austrian Assoc Pediatr Surg Al Z Für Kinderchir 2009; 19:224-27.
4. Yu Y, Kuebler J, Groos S, Metzelder M, Kurpanik S, Ure BM, Vieten G. Carbon dioxide modifies the morphology and function of mesothelial cells and facilitates transepithelial neuroblastoma cell migration. Pediatr Surg Int 2010; 26:29-36.
5. Montalto AS, Currò M, Russo T, et al. In vitro CO(2)-induced ROS production impairs cell cycle in SH-SY5Y neuroblastoma cells. Pediatr Surg Int 2013; 29:51-59.
6. Wildbrett P, Oh A, Naundorf D, Volk T, Jacobi CA. Impact of laparoscopic gases on peritoneal microenvironment and essential parameters of cell function. Surg Endosc 2003; 17:78-82.
7. Carmeliet P, Dor Y, Herbert JM, et al. Role of HIF-1alpha in hypoxia-mediated apoptosis, cell proliferation and tumour angiogenesis. Nature 1998; 394:485-90.
8. Jögi A, Øra I, Nilsson H, Lindeheim A, Makino Y, Poellinger L, Axelson H, Påhlman S. Hypoxia alters gene expression in human neuroblastoma cells toward an immature and neural crest-like phenotype. Proc Natl Acad Sci U S A 2002; 99:7021-26.
9. Jögi A, Vallon-Christersson J, Holmquist L, Axelson H, Borg A, Påhlman S. Human neuroblastoma cells exposed to hypoxia: induction of genes associated with growth, survival, and aggressive behavior. Exp Cell Res 2004; 295:469-87.
10. Löfstedt T, Jögi A, Sigvardsson M, Gradin K, Poellinger L, Påhlman S, Axelson H. Induction of ID2 expression by hypoxia-inducible factor-1: a role in dedifferentiation of hypoxic neuroblastoma cells. J Biol Chem 2004; 279:39223-31.
11. Dungwa JV, Hunt LP, Ramani P. HIF-1α up-regulation is associated with adverse clinicopathological and biological factors in neuroblastomas. Histopathology 2012; 61:417-27.
12. Wang D, Weng Q, Zhang L, He Q, Yang B. VEGF and Bcl-2 interact via MAPKs signaling pathway in the response to hypoxia in neuroblastoma. Cell Mol Neurobiol 2009; 29:391-401.
13. Caccamo D, Campisi A, Currò M, Aguennouz M, Li Volti G, Avola R, Ientile R. Nuclear factor-kappab activation is associated with glutamate-evoked tissue transglutaminase up-regulation in primary astrocyte cultures. J Neurosci Res 2005; 82:858-65.
14. Carter JJ, Whelan RL. The immunologic consequences of laparoscopy in oncology. Surg Oncol Clin N Am 2001; 10:655-77.
15. Novitsky YW, Litwin DEM, Callery MP. The net immunologic advantage of laparoscopic surgery. Surg Endosc 2004; 18:1411-19.
16. Hiyama E, Iehara T, Sugimoto T, et al. Effectiveness of screening for neuroblastoma at 6 months of age: a retrospective population-based cohort study. Lancet 2008; 371:1173-80.

17. Bruick RK. Expression of the gene encoding the proapoptotic Nip3 protein is induced by hypoxia. Proc Natl Acad Sci U S A 2000; 97:9082-87.
18. Kim J-Y, Ahn H-J, Ryu J-H, Suk K, Park J-H. BH3-only protein Noxa is a mediator of hypoxic cell death induced by hypoxia-inducible factor 1alpha. J Exp Med 2004; 199:113-24.
19. Bakker WJ, Harris IS, Mak TW. FOXO3a is activated in response to hypoxic stress and inhibits HIF1-induced apoptosis via regulation of CITED2. Mol Cell 2007; 28:941-53.
20. Chen Y-R, Dai A-G, Hu R-C, Jiang Y-L. Differential and reciprocal regulation between hypoxia-inducible factor-alpha subunits and their prolyl hydroxylases in pulmonary arteries of rat with hypoxia-induced hypertension. Acta Biochim Biophys Sin 2006; 38:423-34.
21. Görlach A. Regulation of HIF-1alpha at the transcriptional level. Curr Pharm Des 2009; 15:3844-52.
22. Schmidt AI, Reismann M, Kübler JF, et al. Exposure to carbon dioxide and helium reduces in vitro proliferation of pediatric tumor cells. Pediatr Surg Int 2006; 22:72-77.
23. Chandel NS, McClintock DS, Feliciano CE, Wood TM, Melendez JA, Rodriguez AM, Schumacker PT. Reactive oxygen species generated at mitochondrial complex III stabilize hypoxia-inducible factor-1α during hypoxia: a mechanism of O2 sensing. J Biol Chem 2000; 275:25130-38.
24. Chandel NS, Vander Heiden MG, Thompson CB, Schumacker PT. Redox regulation of p53 during hypoxia. Oncogene 2000;19:3840-48.
25. Hamanaka RB, Chandel NS. Mitochondrial reactive oxygen species regulate hypoxic signaling. Curr Opin Cell Biol 2009; 21:894–9.
26. Weinmann M, Jendrossek V, Handrick R, Güner D, Goecke B, Belka C. Molecular ordering of hypoxia-induced apoptosis: critical involvement of the mitochondrial death pathway in a FADD/caspase-8 independent manner. Oncogene 2004; 23:3757-69.
27. Stenger C, Naves T, Verdier M, Ratinaud M-H. The cell death response to the ROS inducer, cobalt chloride, in neuroblastoma cell lines according to p53 status. Int J Oncol 2011; 39:601-9.
28. Hao Y-X, Zhong H, Yu P-W, Zhang C, Zeng D-Z, Shi Y, Tang B. Effects of HIF-1alpha on human gastric cancer cell apoptosis at different CO(2) pressures. Clin Exp Med 2009; 9:139-47.
29. Greijer AE, van der Wall E. The role of hypoxia inducible factor 1 (HIF-1) in hypoxia induced apoptosis. J Clin Pathol 2004; 57:1009-14.
30. Sermeus A, Michiels C. Reciprocal influence of the p53 and the hypoxic pathways. Cell Death Dis 2011; 2:e164.
31. Chen D, Li M, Luo J, Gu W. Direct interactions between HIF-1 alpha and Mdm2 modulate p53 function. J Biol Chem 2003; 278:13595-98.
32. Ravi R, Mookerjee B, Bhujwalla ZM, et al. Regulation of tumor angiogenesis by p53-induced degradation of hypoxia-inducible factor 1? Genes Dev 2000; 14:34–44.

SYSTEMIC SCLEROSIS INTERSTITIAL LUNG DISEASE EVALUATION: COMPARISON BETWEEN SEMIQUANTITATIVE AND QUANTITATIVE COMPUTED TOMOGRAPHY ASSESSMENTS

A. ARIANI[1], F. LUMETTI[1], M. SILVA[2], D. SANTILLI[1], F. MOZZANI[1], G. LUCCHINI[1], G. DELSANTE[1] and N. SVERZELLATI[2]

[1]Department of Medicine, Internal Medicine and Rheumatology Unit, Azienda Ospedaliero-Universitaria di Parma, Parma, Italy; [2]Department of Clinical Sciences, Section of Radiology, University of Parma, Parma, Italy

Received March 18, 2014 – Accepted June 20, 2014

The pulmonary fibrosis extent in systemic sclerosis (SSc) has a prognostic value. Chest Computed Tomography (CT) is the gold standard to detect an interstitial lung disease (ILD). Semi-quantitative scores and quantitative methods can estimate the ILD. The first ones have a considerable inter-intra-observer variability, while quantitative scores, based on distribution of lung attenuation parameters (also called CT indexes), can be obtained through expensive and not so user-friendly software. The aim of this work is to investigate whether a DICOM-viewer open-source software (OsiriX) can obtain CT indexes correlating with semi-quantitative scores. Sixty-three chest CTs of ILD-SSc patients were assessed with two semi-quantitative methods (visual extent and limited/extensive ILD grading) and then blindly processed with OsiriX to obtain the distribution parameters of lung attenuation (kurtosis, skewness and mean). Semiquantitative assessment and CT indexes were compared through the Spearman rank test and Mann-Whitney test. All CT indexes showed a statistically significant correlation of moderate degree with the visual extent semi-quantitative assessment (p-value < 0.05). Skewness was the lung attenuation distribution parameter with the strongest correlation (r =-0.378, p-value = 0.0023). Moreover, CT indexes of patients with an extensive and limited disease were statistically different (p < 0.01). CT indexes correlating with a radiological semi-quantitative ILD assessment can be obtained through OsiriX. CT indexes can be considered very helpful to discriminate patients with extensive and limited ILD.

Systemic sclerosis (SSc) is a connective tissue disease secondary to both autoimmune and vascular etiology (1). SSc can affect any organ including the lung. In particular, interstitial fibrosis is the most frequent and prognostically relevant pulmonary alteration (2). Currently, the most suitable non-invasive instrumental examination to detect interstitial lung disease (ILD) is chest Computed Tomography (CT). During the last two decades, radiologists have developed semi-quantitative scores to describe the presence, extent and severity of pulmonary fibrosis (3, 4). Some of these scores have a prognostic value (5), but they are not suitable for clinical practice. Their usefulness is

Key words: interstitial lung disease, pulmonary fibrosis, systemic sclerosis, OsiriX, CT quantitative indexes, skewness, kurtosis, mean lung attenuation

Mailing address: Dott. Alarico Ariani,
Azienda Ospedaliero Universitaria di Parma,
Ospedale Maggiore di Parma,
Day Hospital del Dipartimento Medico Polispecialistico 2,
Reumatologia, Via Gramsci 14, 43100 Parma, Italy
Tel.: +39 0521 702776/702786 Fax: +39 0521 704793
e-mail: dott.alaricoariani@libero.it

0393-974X (2014)

due to the capability to distinguish whether the lung damage is mainly related to ground glass opacities or honeycombing lesions. However, even among experienced radiologists, the inter-observer agreements of semi-quantitative assessments range from weak to moderate (6).

In order to overcome this operator-dependent limit, special software was developed. This software can semi-automatically differentiate normal lung parenchyma from the ILD-affected part within chest CT images. The analysis of the histograms of lung attenuation (i.e. radiation absorption) distribution allows to obtain some parameters (such as kurtosis, skewness, mean lung attenuation - definitions in Table I) which permit a quantitative evaluation of pulmonary fibrosis (7, 8).

However, the software employed by the majority of authors (9, 10) to perform this kind of analysis (post-processing) is not very common due to both its cost and the challenging training required to achieve a proper use of such.

Over the last few years software capable of viewing radiological images (in Digital Imaging Communications in Medicine - DICOM, format), available online and free of charge, has opened a new approach to medical imaging (11). Recently, one paper demonstrated that one of these DICOM-viewers, OsiriX, can be a useful tool to achieve a post-processing analysis finalized to quantify the ILD extent through the kurtosis, skewness and mean lung attenuation calculation (12).

The main aim of this work is to verify the existence of a correspondence between two ILD semi-quantitative assessments and lung attenuation distribution parameters (kurtosis, skewness, mean lung attenuation - MLA), also called ILD quantitative CT indexes, obtained through OsiriX. In particular, we focused our research on: a) the correlations between OsiriX calculated CT indexes (i.e. quantitative assessment) and a visual extent assessment (i.e. one of the two semi-quantitative assessments); b) the differences among the distinct CT indexes of patients with an extensive *vs* limited disease according to Goh et al. ILD scoring - one of the most important radiological semi-quantitative assessments strongly related to severe pulmonary involvement.

MATERIALS AND METHODS

The study was conducted according to the Declaration of Helsinki and approved by the local Ethics Committee.

Table I. *Glossary.*

Attenuation	X-rays absorption (in HU) of a single spatial unit (voxel) in which chest CT subdivides the lung examined
Distribution hystogram	absolute frequency graphical representation of lung attenuation values
Mean Lung Attenuation (MLA)	arithmetic mean of all attenuation values
Kurtosis	dimensionless quantity related to the peakedness of the distribution histogram. Along with MLA and skewness, it is a lung attenuation distribution parameter
Skewness	dimensionless quantitiy related to the simmetry of the distribution histogram. Along with MLA and kurtosis, it is a lung attenuation distribution parameter

Patients

We included 63 consecutive patients admitted to our clinic between September and December 2013, with diagnosis of diffuse or limited SSc established according to the ACR/EULAR classification criteria (13). The descriptive statistics of these patients are summarized in Table II. All patients gave their informed consent.

Computed tomography

CT was always performed using 128- slice MDCT (Somatom FLASH, Siemens, Forcheim, Germany). CT images were reconstructed at section width slice thickness of 1 mm using a high spatial frequency algorithm. All patients were examined in the supine position from lung apices to lung bases at full-suspended inspiration using standard acquisition parameters: 100 effective mAs, 120kVp. All images were viewed at window settings optimized for assessment of lung parenchyma (window width, 1600–1600 HU; window level, -500 to -600 HU).

Semiquantitative assessments

Five levels in each CT were preselected by an observer who was not involved in subsequent scoring of the cases: i) the aortic arch; ii) 1cm below the level of the carina; iii) the right pulmonary venous confluence; iv) the midpoint between 3 and 5; and v) 1 cm above the dome of the right hemi-diaphragm.

The CT sections of each patient were assessed for the ILD extent to the nearest 5%. The mean value constituted the visual extent assessment.

All images were reviewed, according to the Goh et al. method, (4) at the preselected levels by one thoracic radiologist (9 years experience in scoring chest CT for ILD extent) using DICOM viewing software (DicomWorks, version 1.3; http://dicom.online.fr) at standard window settings for visualization of the lung parenchyma (centre -500 HU, window width 1600 HU). When ILD was indeterminate, Forced Vital Capacity was taken into account as described by Goh et al.

While scoring the study cases, the observer had no knowledge of other lung function data or other indicators of disease severity.

Table II. *Descriptive statistics of SSc patients.*

CHARACTERISTIC	RESULTS
Age, mean ± SD years	59.6±13.2
Gender, % female	92.1%
Race/ethnicity	
Caucasian	96.8 %
African	1.6 %
Other	1.6 %
SSc duration, mean ± SD years	8.6±6.3
Diffuse cutaneous SSc, %	39.7%
Current smoker, %	4.8%
Scl70 positive patients, %	47.6%
Forced Vital Capacity, mean ± SD %	83.6±13.2
Diffusion Lung capacity of CO, mean ± SD %	67.0±19.7

Quantitative assessment

OsiriX is a user-friendly DICOM-viewer, free of charge and available on the developer's website (www.osirix-viewer.com) (14). It allows even to an unskilled user to perform post-processing on CT and MR. The lung segmentation algorithm is the same presented by Ariani et al. (12). Voxels between -950 HU and -400 HU were selected using 3D Growing Region Upper/Lower Threshold algorithm with the seed inside pulmonary parenchyma. After the application of the brush ROI tool (closing with a "Structuring Element Radius" equal to 20) the whole lung was segmented. Finally, after applying Compute Volume command, CT indexes were displayed. Fig. 1 shows the CT indexes as the final result of the above-mentioned method.

Statistical analysis

Statistical analysis was performed using R software (www.r-project.org, version 3.0.1 with psy and ca package). Non-parametric tests were used for all parameters (even those that follow a Gaussian distribution according to the Functional test of D'Agostino-Pearson).

The Spearman rank order test was used to verify the correlation between lung attenuation distribution parameters and the visual extent semi-quantitative score. A Spearman rho value of 0-0.30 was considered fair, 0.31-0.50 moderate, 0.51-0.70 good, 0.71-1.00 excellent.

The difference between CT indexes of patients with an extensive and limited disease was carried out by the Mann-Withney test. A p-value <0.05 was considered statistically significant.

RESULTS

The CT index with the stronger degree of correlation with the visual extent assessment is the skewness ($r = -0.378$, p-value = 0.0023); kurtosis and MLA had a moderate correlation with the visual extent assessment (respectively $r = -0.332$, p-value = 0.0079 and $r = 0.366$, p-value = 0.0031).

Patients with extensive and limited disease had dissimilar CT index values; these differences were statistically significant (p-value < 0.01). Median, spread and shape of kurtosis, skewness and MLA in

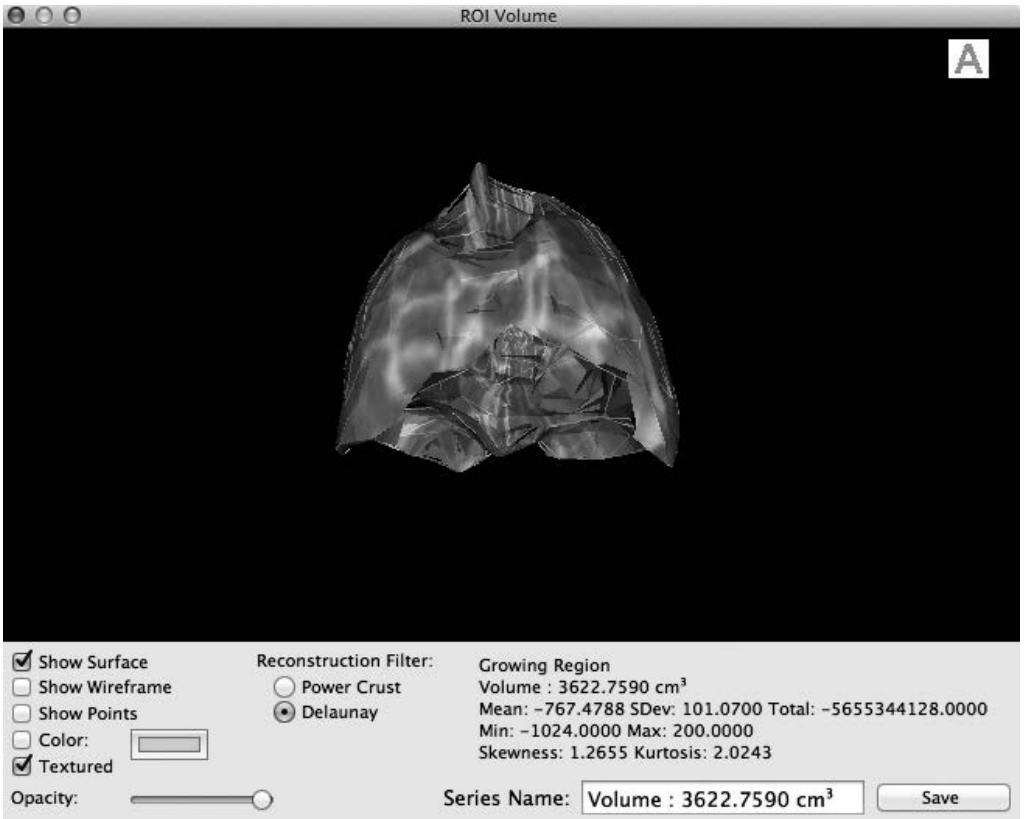

Fig. 1. *Example of OsiriX 3D ROI (Region Of Interest) lung CT indexes window. The final output of the segmentation process and CT indexes computation consists of a tridimensional lung recostruction (above) with a list of the related attenuation parameters (third column below, under "Growing Region").*

the above groups are reported in the box-plot graphs (Fig. 2).

DISCUSSION

CT chest is the best non-invasive exam to detect pulmonary fibrosis. The radiological score more widely used to assess ILD presence, severity and extent shows a moderate inter-observer agreement only if made by experienced radiologists. Otherwise the concordance can only be low (4). To overcome this problem, DICOM-viewer software capable of identifying (segment) the whole lung and the areas affected by fibrosis has been developed. From these segmentations it is possible to obtain histograms of lung attenuation and of their distribution parameters whose usefulness in quantifying pulmonary fibrosis has been demonstrated by several authors (15-17). The CT index inter- and intra-observer variability is lower than the one of the semi-quantitative score (18).

Although the determination of these parameters is really promising, the introduction into clinical practice of these types of DICOM-viewers is improbable due to the relatively high cost of licenses and to the difficulty in training new users. The software needed to perform a pulmonary fibrosis quantification is very sophisticated, proprietary (7, 9, 19) and, therefore, not so easily applicable in multi-center studies. Moreover, until now no study has been able to propose satisfactory CT index cut-offs to discern the patients with the worse prognosis (20).

A recent study described a positive experience with a free DICOM-viewer software, OsiriX, that achieves the same results as the proprietary programs (12). This very user-friendly and easy-to-learn DICOM viewer was able to calculate distribution parameters of the attenuation histograms referred both to the entire lung and to the non-fibrotic component.

Taking into account these results, the following

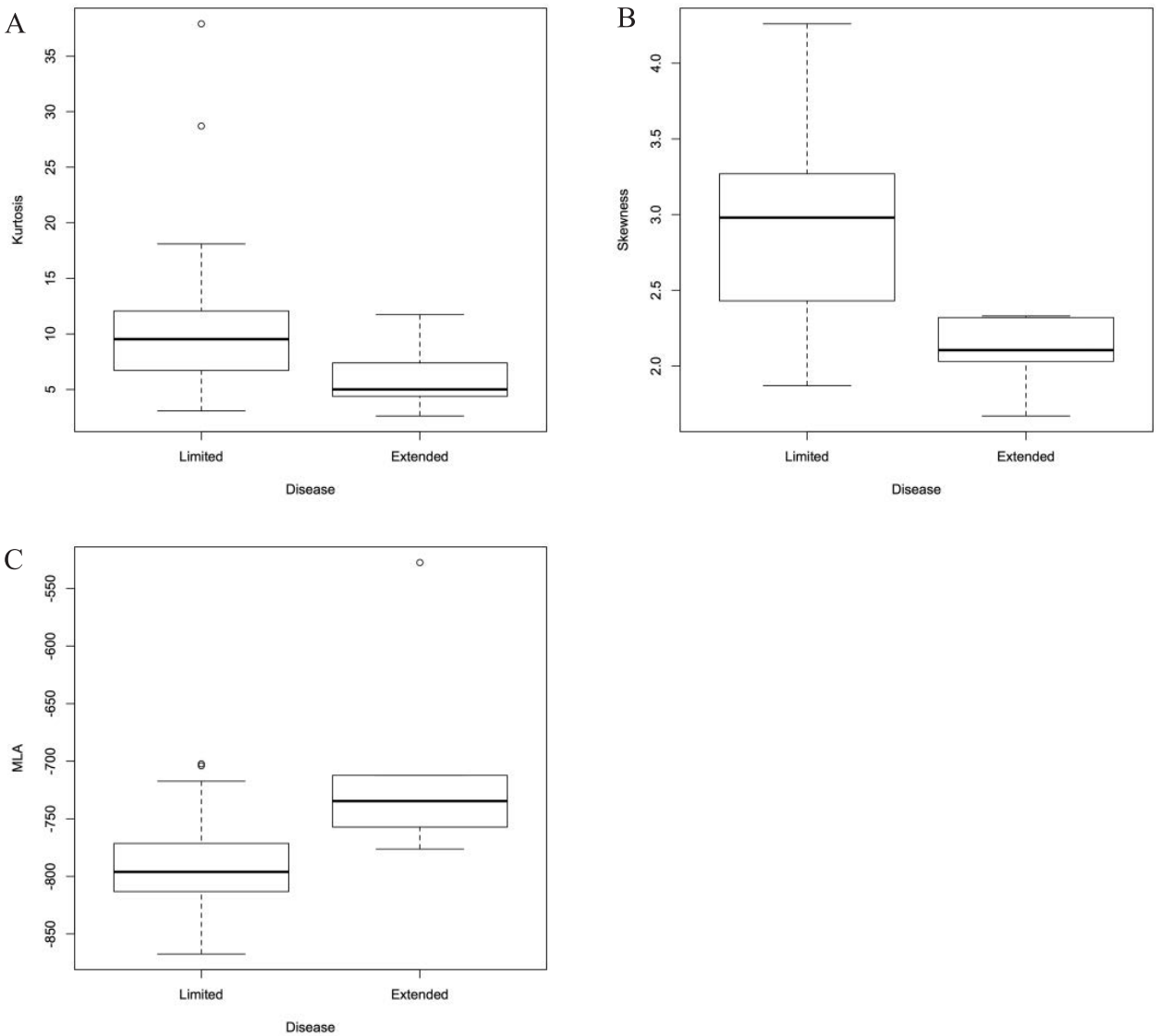

Fig. 2. *Box-plots showing the difference of kurtosis (**A**), skewness (**B**) and MLA (**C**) distribution between limited and extensive disease patient groups.*

considerations can be drawn: 1) all the distribution parameters had a moderate degree correlation with ILD visual extent semi-quantitative score performed by an experienced radiologist. 2) CT index distributions in limited and extensive disease groups are considerably different. 3) Skewness is the CT index that better correlates with the ILD visual extent assessment; it also showed the most remarkable difference in distribution values among the limited *vs* extensive disease groups.

The main limitations of this study are: i) the reduced sample size, ii) the selection of patients with not very aggressive SSc; iii) the absence of Osirix algorithm exploration in carrying out the fibrosis unaffected lung; iv) the lack of negative controls; v) having arbitrarily (although in line with the most recent papers) established to start the lung segmentation from a given interval (-950, -400 HU); vi) the need to use a computer running MacOsX, a not so widespread operative system.

Forthcoming research perspectives are the comparison of lung attenuation distribution parameters with spirometric values, the study of inter- and intra-observer variability of CT indexes

obtained through OsiriX, the investigation of CT index changes in follow-up chest CTs and a greater sample size.

In summary, our data suggest that lung attenuation distribution parameters have a good correspondence to an expert radiologist's ILD evaluation. These CT indexes (in particular skewness and kurtosis) could be easily introduced in clinical practice. OsiriX is a free DICOM viewer, easy to learn even by a non-radiologist user, and it can become a tool allowing the identification of patients with an extensive ILD resulting in poor prognosis. This work could be the starting point of the first stage of a change in the clinical approach to the assessment of pulmonary fibrosis because wider use of CT indexes may provide useful elements for evaluating the efficacy of anti-fibrotic therapy.

REFERENCES

1. Matucci-Cerinic M, Kahaleh B, Wigley FM. Review: evidence that systemic sclerosis is a vascular disease. Arthritis Rheum 2013; 65:1953-62.
2. Karassa FB, Ioannidis JPA. Mortality in systemic sclerosis. Clin Exp Rheumatol 2008; 26:S85-93.
3. Warrick JH, Bhalla M, Schabel SI, Silver RM. High resolution computed tomography in early scleroderma lung disease. J Rheumatol 1991; 18:1520-8.
4. Goh NSL, Desai SR, Veeraraghavan S, et al. Interstitial lung disease in systemic sclerosis: a simple staging system. Am J Respir Crit Care Med 2008; 177(11):1248-54.
5. Moore OA, Goh N, Corte T, et al. Extent of disease on high-resolution computed tomography lung is a predictor of decline and mortality in systemic sclerosis-related interstitial lung disease. Rheumatology 2013; 52:155-60.
6. Wells AU. High-resolution computed tomography and scleroderma lung disease. Rheumatology (Oxford) 2008; 47:v59-61.
7. Sumikawa H1, Johkoh T, Yamamoto S, et al. Computed tomography values calculation and volume histogram analysis for various computed tomographic patterns of diffuse lung diseases. J Comput Assist Tomogr 2009; 33:731-8.
8. Orlandi I, Camiciottoli G, Diciotti S, et al. Thin-section and low-dose volumetric computed tomographic densitometry of the lung in systemic sclerosis. J Comput Assist Tomogr 2006; 30:823-7.
9. Kim HG, Tashkin DP, Clements PJ, et al. A computer-aided diagnosis system for quantitative scoring of extent of lung fibrosis in scleroderma patients. Clin Exp Rheumatol 2010; 28:S26-35.
10. Sumikawa H1, Johkoh T, Colby TV, et al. Computed tomography findings in pathological usual interstitial pneumonia: relationship to survival. Am J Respir Crit Care Med 2008; 177:433-9.
11. Ratib O, Rosset A, Heuberger J. Open Source software and social networks: disruptive alternatives for medical imaging. Eur J Radio 2011; 78:259-65.
12. Ariani A, Carotti M, Gutierrez M, Bichisecchi E, Grassi W, Giuseppetti GM, Salaffi F. Utility of an open-source DICOM viewer software (OsiriX) to assess pulmonary fibrosis in systemic sclerosis: preliminary results. Rheumatol Int 2014; 34(4):511-6.
13. van den Hoogen F, Khanna D, Fransen J, et al. 2013 classification criteria for systemic sclerosis: an American college of rheumatology/European league against rheumatism collaborative initiative. Ann Rheum Dis 2013; 72:1747-55.
14. Rosset A, Spadola L, Pysher L, Ratib O. Informatics in radiology (infoRAD): navigating the fifth dimension: innovative interface for multidimensional multimodality image navigation. Radiographics 2006; 26:299-308.
15. Sverzellati N, Calabrò E, Chetta A, et al. Visual score and quantitative CT indices in pulmonary fibrosis: Relationship with physiologic impairment. Radiol med 2007; 112:1160-72.
16. Lynch DA. Quantitative CT of fibrotic interstitial lung disease. Chest 2007; 131:643-4.
17. Best AC, Meng J, Lynch AM, Bozic CM, Miller D, Grunwald GK, Lynch DA. Idiopathic pulmonary fibrosis: physiologic tests, quantitative CT indexes, and CT visual scores as predictors of mortality. Radiology 2008; 246:935-40.
18. Camiciottoli G, Orlandi I, Bartolucci M, et al. Lung CT densitometry in systemic sclerosis: correlation with lung function, exercise testing, and quality of life. Chest 2007; 131:672-81.
19. Zavaletta VA, Bartholmai BJ, Robb RA. High resolution multidetector CT-aided tissue analysis and quantification of lung fibrosis. Acad Radiol 2007;

14:772-87.

20. Shin KE, Chung MJ, Jung MP, Choe BK, Lee KS. Quantitative computed tomographic indexes in diffuse interstitial lung disease: correlation with physiologic tests and computed tomography visual scores. J Comput Assist Tomogr 2011; 35:266-71.

EXPRESSION OF TIR8 RECEPTOR IN CHICKEN TISSUES

L. TURIN, G. MANAROLLA and F. RIVA

Department of Veterinary Science and Public Health (DIVET), University of Milan, Italy

Received May 15, 2014 – Accepted July 24, 2014

The orphan receptor TIR8, also known as SIGIRR, belongs to the TLR/IL-1R (TIR) superfamily and plays an important role in the immune response. The signalling pathways of the receptors belonging to the TIR family are tightly regulated at multiple levels and through different mechanisms. TIR8 negatively modulates innate immunity and inflammatory responses in the areas where it is primarily expressed (gastrointestinal tract, kidney and lung). TIR8 has been well characterized in mouse, humans and in other Mammalian species, but it is still poorly known in chicken. Given the importance of gastrointestinal diseases in chicken, the aim of our study was to investigate the distribution of TIR8 in a wide panel of non-pathologic tissues and organs. TIR8 expression was analyzed in chicken samples at both levels of transcript mRNA and translated protein. The pattern of expression of TIR8 (ubiquitous) was similar to Mammals for some tissues (high levels in kidney and gastrointestinal tract), but it resulted unique for other tissues. High expression was detected in liver, pancreas and female reproductive tract. Interestingly, the receptor was highly expressed also in heterophils, the most common granulocytes of birds. Few isoforms of chicken TIR8 were detected by Western blot, suggesting the occurrence of different post-translational processing in different organs. Immunohistochemistry revealed TIR8 immunolabelling in chicken intestine and thymus. These results demonstrate that the receptor, although evolutionarily conserved, show species-specific peculiarities.

The orphan receptor TIR8 (Toll-like/interleukin-1 receptor-8), also known as SIGIRR (Single Immunoglobulin IL-1R-Related molecule), belongs to the IL-1R (Interleukin-1 receptor) family of the TIR (Toll-like/interleukin-1 receptors) super-family. Innate mechanisms of defense against pathogens involve different members of the TIR superfamily, which includes pro-inflammatory receptors TLRs (Toll-like receptors) and IL-1Rs, decoy receptors, negative regulator receptors, accessory and adapter molecules, all sharing the conserved intracellular TIR domain (1-4).

Upon stimulation by their ligands, TLRs and IL-1Rs interact with specific adaptor proteins and initiate a signalling pathway, which leads to the activation of transcription factors and to the synthesis of proinflammatory cytokines and chemokines (5).

Signalling pathways of TLR/IL-1Rs are very complex and tightly regulated to ensure the appropriate modulation of the innate and inflammatory responses and to limit deregulated activations that could cause uncontrolled inflammation or autoimmune responses (6, 7). TIR8 is a negative regulator of the inflammatory pathways in the epithelial tissues at mucosal sites, where it is highly expressed (8-11). The negative regulation of TLR and IL-1R signalling influences the communication among intestinal epithelial cells, immune system and commensal microorganisms (12).

Key words: chicken, gene expression, IL-1 receptors, TIR8/SIGIRR, Toll-like receptors, inflammation

Mailing address: Dr Lauretta Turin,
Department of Veterinary Science
and Public Health (DIVET),
University of Milan,
via Celoria 10, 20133 Milan, Italy
Tel.: +39 02 50318090 Fax: +39 02 50318089
e-mail: lauretta.turin@unimi.it

0393-974X (2014)

TIR8 inhibits NF-kB (nuclear factor kappa-light-chain-enhancer of activated B cells), JNKs (c-Jun N-terminal kinases) and AKT/PKB (AKT/protein kinase B) activation following the stimulation of IL-1R or TLR family members (13). It regulates potentially detrimental inflammatory responses associated to infections, autoimmune diseases or cancer (14-19).

Birds' immune systems are quite similar to the mammalian ones in terms of overall organization and mechanisms of immunity. The avian TIR family includes some orthologue members of the mammalian molecules and some unique to birds (20-22). TIR8, mainly studied in mouse and human models (2, 3, 9, 11-14, 17, 18), has been studied, more recently, also in other species (23, 24), but it is still poorly known in chickens.

The chicken has a long and distinguished history as a major model system for studies in different fields, including genetic and immunology. It was the first economically important species for which a genetic linkage map was constructed, the first non-mammalian amniote genome to be fully sequenced and the first species where the T- (thymus) and B- (Bursa of Fabricius) lymphocytes were discovered.

Considering the importance of TIR8 in innate immunity and inflammation, its evolutionary conservation and the lack of data on it in chicken, we focused our study on this receptor in such species. The detailed map of TIR8 expression, preliminary knowledge to any investigation on its role in the pathogenesis, was the major aim of this study. We examined the distribution of *Tir8* in a wide panel of chicken organs both at the transcriptional level (mRNA) by means of quantitative RT-Real-Time PCR and at the protein level by Western blot and immunohistochemistry. The presence of isoforms was evaluated by Western blot analysis, after the validation of a polyclonal antibody to human TIR8, which was cross-reactive with the chicken receptor.

MATERIALS AND METHODS

Samples

Samples (0.5 cm^3) of brain, cerebellum, Harderian gland, skin, trachea, thymus, air sac, heart, lung, liver, gizzard, proventriculus, small intestine, pancreas, caecum, large intestine, cloaca, bursa of Fabricius, spleen, kidney, adrenal gland, testicle, ovary, oviduct, skeletal muscle and bone marrow from a 56-day-old commercial broiler chicken were collected at a slaughterhouse, and immediately placed in sterile tubes containing 3 ml of RNA Later (Qiagen, Hilden, Germany) and stored at 4°C for 24 h. Duplicate samples were immediately frozen and stored at -80°C until Western blot analysis; other samples were fixed in 10% buffered formalin for immunohistochemistry.

Blood from 5 commercial broilers of the same age and breed was collected and pooled in tubes containing ethylenediamine-tetraacetic acid (EDTA) to isolate chicken heterophils, as reported (25). The blood diluted 1:2 with RPMI-1640 media (Invitrogen, Carlsbard, CA, USA) containing 1% methylcellulose was centrifuged at 35 g for 15 min at 4°C. The supernatant was transferred to a new tube and diluted 1:2 with Ca^{2+} and Mg^{2+}-free Hank's balanced salt solution, layered onto discontinuous Histopaque-1077 (Sigma Chemical Company, St. Louis, MO, USA) gradient and centrifuged at 190 g for 1 h at 4°C. The heterophil layer was collected, washed with Hank's solution and resuspended in Phosphate Buffered Saline (PBS).

The experimental protocol was approved by the Ethics Committee of the University of Milan (Protocol Number 121521500524).

RNA extraction

Total RNA was isolated from the samples by the guanidine isothiocyanate (4M) method with minor modifications. Briefly, the samples were homogenized in 3 ml of guanidine isothiocyanate using a rotor-stator system (Ultra Turrax T25 Ika-Werke, Staufen, Germany). The lysate (1.3 ml) was centrifuged overnight at 42,000 rpm at 18°C on a 5.7M cesium chloride layer (Optima TL ultracentrifuge, Beckman Instruments, Inc. Palo Alto, CA, USA). The pellet was dissolved in sterile water and the RNA was precipitated with absolute ethanol and sodium acetate 3M pH 5.4 in dry ice for 2 hours. After centrifugation in a microcentrifuge (Eppendorf, Hamburg, Germany) at maximum speed for 30 min at 4°C, the RNA pellet was dissolved in sterile water and stored at -20°C.

RNA determination and Reverse Transcription

The concentration of total RNA was determined using a spectrophotometer (BioPhotometer, Eppendorf, Hamburg, Germany) at 260 nm wavelength. About 1 µg of total RNA from each sample was reverse transcribed to cDNA using the High Capacity cDNA Archive kit with random hexamers (Applied Biosystem, Foster City, CA, USA) and the resulting cDNA was stored at -20°C before Real-Time PCR assays.

Real-Time PCR

The cDNA obtained from each sample was used as a

template for Real-Time PCR in optimized 25 µl reaction volume in MicroAmp optical 96-well plates. Each plate contained duplicates of each sample cDNA diluted 1:100 (9 µl), 2X Power Syber Green PCR Master Mix (12.5 µl) (Applied Biosystem, Foster City, CA, USA) and primers 300 nM each (0.3 µl of 10 µM solution). The species-specific primer pairs were designed using as target the most complete chicken sequence homologous to human and mouse *tir8* available in the NCBI nucleotide sequences database (gi:118091084); primers were also designed for the chicken housekeeping beta-actin gene (access number gi:45382926, NCBI) (26). Primers were custom synthesized by Invitrogen (Carlsbad, CA, USA).

In addition to the cDNA samples, duplicates of 10-fold serial dilutions of chicken kidney cDNA were used as templates to generate standard curves for estimation of the expression in relationship to the calibrator (kidney 1:100) (relative quantification). A duplicate no-template control (NTC) was also included in each plate.

Real-Time quantitative PCR was carried out in the 7000 Sequence Detection System (Applied Biosystem, Foster City, CA, USA) at the following thermal cycle conditions, 10 min at 95°C followed by 40 cycles of 15 s at 95°C and 1 min at 60°C. Quantification was determined after application of an algorithm to the data analyzed by the software of the 7000 Detection System (Applied Biosystem, Foster City, CA, USA).

For each sample tested the expression level was calculated following the results of the calibrator of the same run. The chicken *Tir8* expression was normalized using the calculated beta-actin cDNA expression (mean) of the same sample and run. We used the free software BLAST available on the PubMed web site for gene sequence search and alignment. Primer Express software (Applied Biosystem, Foster City, CA, USA) was used for the specific primer design.

Western blot

Chicken tissues stored at -80°C were processed for the extraction of proteins. Each sample was mechanically homogenized using a rotor-stator system in 1 ml of cold lysis buffer (50 mM Tris-HCl pH 7.6, 150 mM NaCl, 1% (v/v) NP40, 2% (v/v) TritonX100, 1% (w/v) Zwitterion, 1 mM EDTA) added with protease inhibitors cocktail and PMSF (Sigma-Aldrich, St. Louis, MO, USA) and incubated for 30 min on ice. After centrifugation for 10 min at 15,000 x g in minifuge at 4°C, the supernatant was collected and protein concentration was determined spectrophotometrically using the Bradford micromethod (BioRad Protein Assay, BioRad Laboratories, GmbH, Munich, Germany).

Aliquots of lysed organs, corresponding to 60 µg of total protein content were loaded on 10% SDS-PAGE and Western blotted on nitrocellulose membrane. Immunodetection was carried out overnight at 4°C using a polyclonal goat anti-hSIGIRR Antibody (R&D Systems, Minneapolis, MN, USA) as the primary antibody at a concentration of 0.1 mg/ml (1:500 dilution from stock solution). An HRP-conjugated anti-goat secondary antibody (Sigma-Aldrich, St. Louis, MO, USA) was used (1:2000 dilution, 1 hour at room temperature). Positive bands were detected using chemiluminescent HRP substrate (Millipore, Molsheim, France).

Immunohistochemistry

Formalin-fixed tissue samples sciatic nerve, bursa of Fabricius, thymus, spleen, lung, liver, proventriculus, gizzard, duodenum, jejunum, cecum, Harderian gland, kidney were routinely processed for histology. Four-µm thick paraffin-wax sections were stained for demonstration of TIR8 receptor using Avidin-Biotin-peroxidase Complex (ABC) immunohistochemistry (27). Additional sections were included as negative control. Briefly, after the quenching of endogenous peroxidase activity with 0.3% hydrogen peroxide in Phosphate Buffered Saline (PBS) pH 7.4 for 30 min, antigen retrieval was performed using microwave treatment at 750 W for 15 min (three cycles, 5 minutes each) in 10 mM citrate buffer (pH 6.0). After rinsing with PBS, 10% normal horse serum was applied for 30 min to block non-specific antibody binding. Subsequently, sections were incubated overnight at 4°C with the same primary antibody used for Western blot (polyclonal goat anti-hSIGIRR Antibody, R&D Systems, Minneapolis, MN, USA) diluted 1:100. Biotinylated horse anti-goat antibody (Vector Laboratories Inc., Burlingame, CA, USA) was used as secondary antibody, followed by ABC Vectastain Elite kit (Vector Laboratories Inc., Burlingame, CA, USA). Peroxidase activity was revealed with 3-amino-9-ethylcarbazole (Vector Laboratories Inc., Burlingame, CA, USA).

RESULTS

Tir8 mRNA expression analysis by Real-Time PCR

The expression pattern of *Tir8* was analyzed by mean of quantitative Real-Time PCR assays in a panel of 27 chicken organs and tissues. The complete mRNA sequence of chicken *Tir8* (gi:118091084) was selected to design specific primers spanning two adjacent exons. The primer pair with the best score localized in the middle of the sequence was used in Real-Time PCR assays to amplify the cDNA from each sample (26).

All the sampled organs resulted positive to the

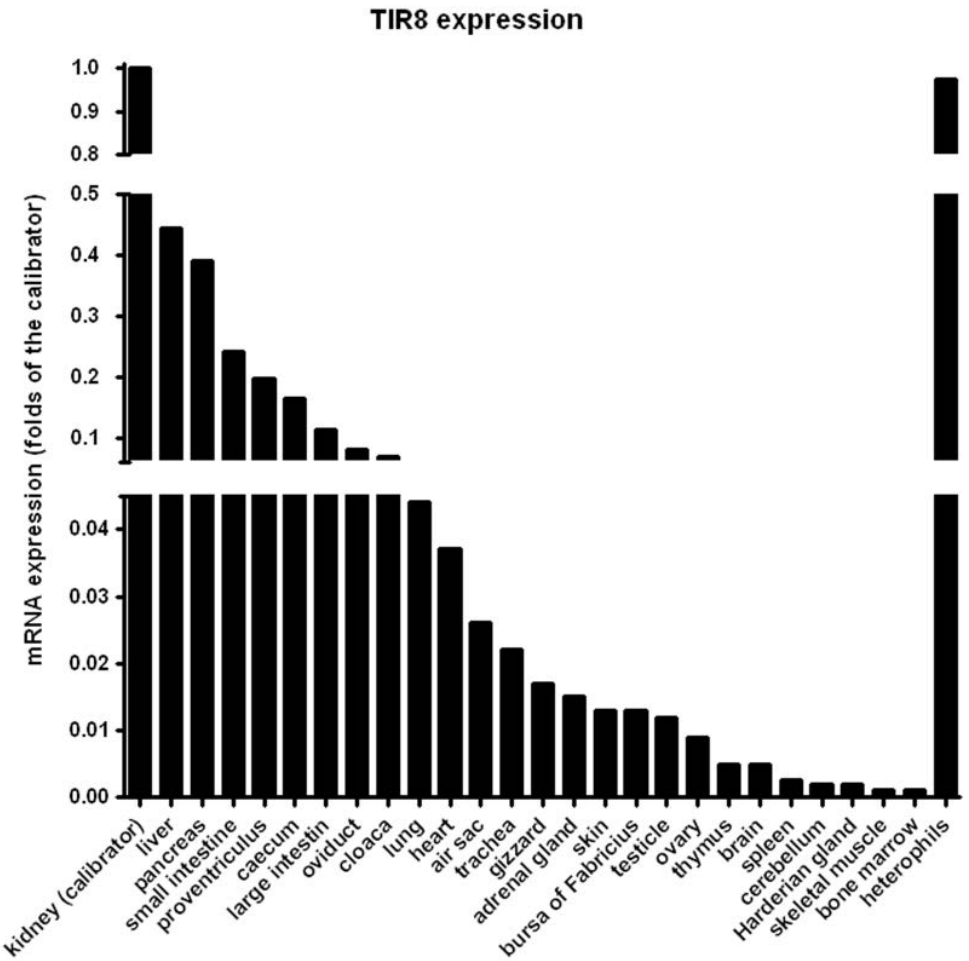

Fig. 1. *TIR8 mRNA expression in chicken organs and tissues (Real-Time PCR). The TIR8 expression level of each sample is quantified as folds of the expression of the same gene in the chicken kidney (calibrator). Data were normalized to beta-actin gene expression in all the organs.*

presence of *Tir8* transcript, with different levels of expression. Kidney RNA was the organ showing the highest level of *Tir8* mRNA; therefore it was used as experimental calibrator and as positive control. The results of Real-Time PCR quantification, expressed as ratio between each specimen and the calibrator, are summarized in Fig. 1. Besides kidney, *Tir8* is highly expressed in heterophils, liver and in pancreas, followed by GI tract and oviduct; it is moderately expressed in respiratory tract, heart and gizzard. Low expression of *Tir8* was detected in adrenal gland, skin, bursa of Fabricius, testicle and ovary. All the other samples displayed very low levels of *Tir8* mRNA. Interestingly, a different expression of *Tir8* was found in proventriculus and gizzard with higher levels in the former.

TIR8 protein expression analysis by Western blot

The expression of TIR8 protein in different chicken organs as well as the presence of possible tissue-specific isoforms, was assessed by Western blot analysis. A polyclonal goat anti-human TIR8 was used as primary antibody, after preliminary validation on chicken samples.

Results from Western blot analysis, presented in Fig. 2, show the presence of TIR8 protein in all the organs examined. Moreover, Western blot analysis revealed few TIR8 forms with different molecular

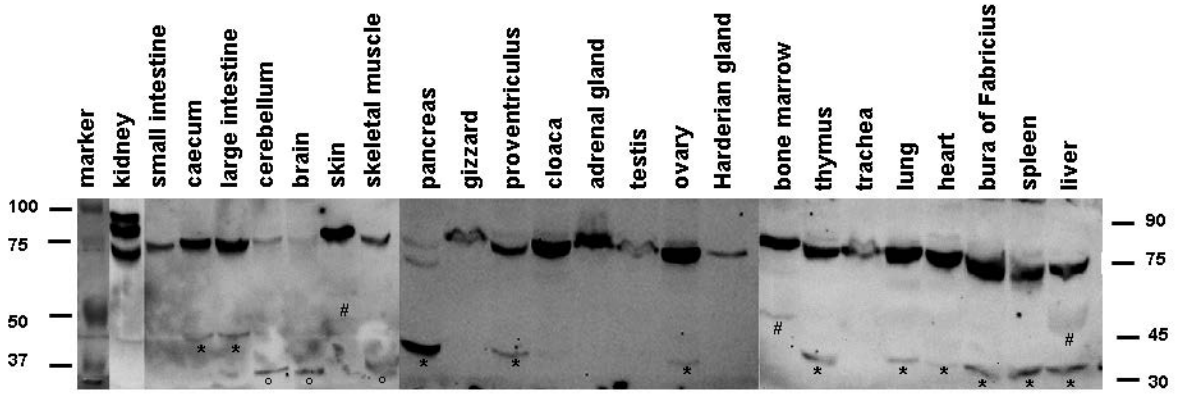

Fig. 2. *TIR8 protein expression in chicken organs and tissues (Western blot). Homogenates of 60 μg of total protein extracted from each sample were loaded. Target protein was detected on the blots by staining with polyclonal goat anti-human SIGIRR antibody. 45kDa bands are indicated with *, 50kDa bands are indicated with # and 35 kDa bands are indicated with °.*

weight in most of the examined samples.

A TIR8 form of about 75 kDa was observed in most of the tissues and organs. TIR8 bands corresponding to a molecular weight of approximately 45 kDa were detected only in caecum, large intestine, thymus, bursa of Fabricius, ovary, lung, heart, spleen, liver, pancreas and proventriculus. In other organs (cerebellum, brain, skeletal muscle) the anti-TIR8 antibody reacted with proteins showing a molecular weight around 35 kDa. Bone marrow, liver and skin presented a band with a molecular weight about 50 kDa.

The fraction with molecular weight of approximately 75 kDa, which corresponds to the expected molecular weight of the complete protein, appeared to be the major TIR8 component in all the samples except kidney, brain and pancreas. In kidney, three TIR8 forms were identified, ranging from 70 to 90 kDa; in pancreas the band at about 45 kDa appeared to be predominant.

TIR8 expression in Harderian gland were barely detectable by anti-TIR8 antibody.

Taken together, the results from this study showed that TIR8 receptor was widely expressed throughout all the digestive apparatus as well as in several other organs and tissues.

Immunohistochemistry

The expression of TIR8 protein was assayed by immunohistochemistry with the same polyclonal anti-human TIR8 antibody used for Western blot and validated for cross-reactivity with the chicken receptor. The expression of TIR8 protein was found only in scattered cells of the intestinal mucosa (Fig. 3) and in some thymus epithelial cells (data not shown), whereas all the other samples were negative.

DISCUSSION

The negative regulator of the immune response TIR8 has been gaining importance lately also in Veterinary Medicine as inflammatory diseases affecting farm animals have negative impacts on production, resulting in economic loss.

In this study, the expression of TIR8 was investigated in chicken at both transcriptional (mRNA) and translational (protein) levels. Messenger RNA was detected and quantified by Real-Time PCR, while TIR8 protein was revealed by both Western blot analysis and immunohistochemistry. The two sets of data are substantially in agreement. Few differences may be linked to different sensitivity of techniques, each one requiring a different protocol for sample preparation. In addition, different tissues may have a different presence of inhibitors of PCR reaction. Discrepancies between transcribed and translated products have been reported for TIR8 also in bovine species (24).

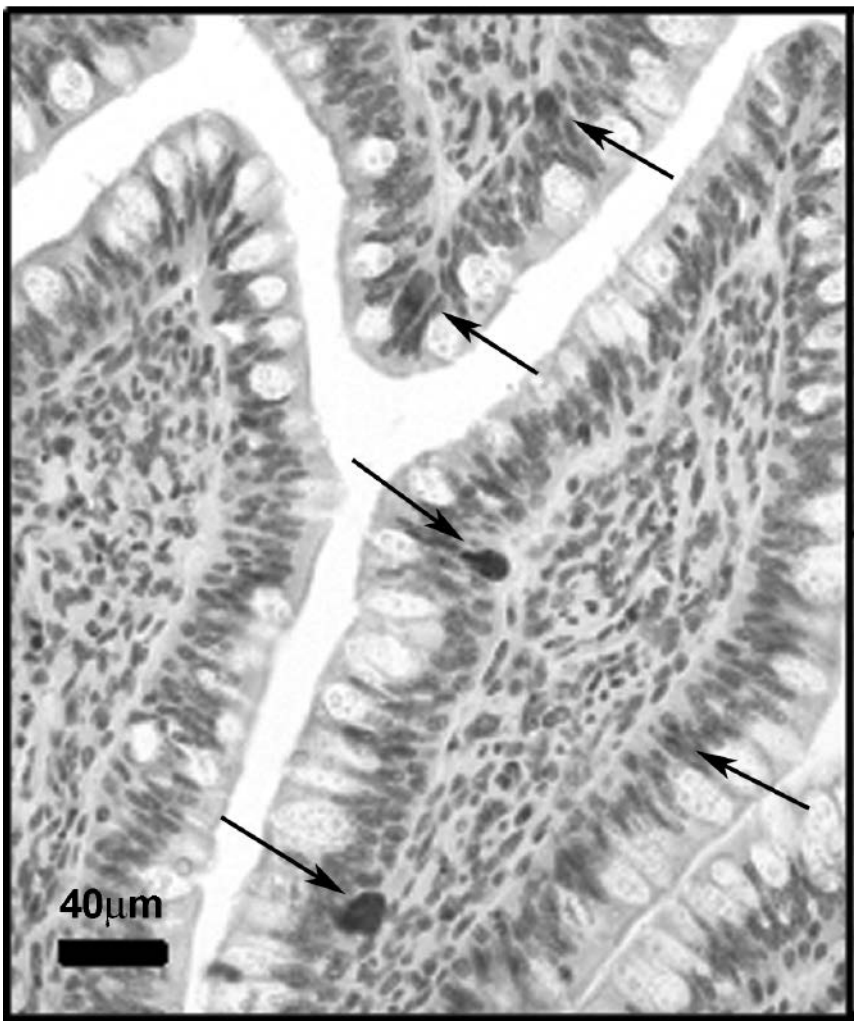

Fig. 3. *Expression of TIR8 protein in chicken gut (immunohistochemistry). In a section of intestine of chicken, few cells of intestinal villi (arrows) were positively immunolabelled for TIR8 (BAR: 40 μm). Anti-SIGRR immunohistochemistry, Mayer's Haematoxylin counterstain.*

The present findings confirm some conservation in the expression pattern of this receptor between chicken and the other species studied so far, i.e. mouse, humans and cattle (3, 9, 23, 24). The highest levels of *Tir8* expression were found in the kidney and in the GI; however, bird exhibited different expression levels in different organs, such as a high expression in liver and oviduct. These peculiar traits may be linked to a different evolutionary pressure by the environment and pathogens. Indeed, the rudimental lymphatic system of birds (lack of lymph nodes) and the presence of a renal portal system could account for the high *Tir8* expression in avian liver and kidney. It is well known that chicken ovary is a preferential site of microbial infections (for example due to *Salmonella enteritidis*) that can be subsequently transmitted to the eggs and embryos (28). Different levels of *Tir8* in different organs could suggest a complex regulatory mechanism for the receptor expression in response to microbial infections, particularly depending on their duration. Interestingly, the different *Tir8* expression in the

two chicken stomachs was possibly correlated with the different relevance of the epithelial component in the two stomachs, compared to the connective and muscular components. A similar observation was reported in other studies examining the cattle forestomachs (23, 24). Remarkably, the expression study of chicken *Tir8* mRNA by Real-Time PCR yielded results in agreement to those previously obtained by the same authors with Northern blot (23). Indeed, high levels of hybridization with the species-specific probe were observed for the kidney, the liver, the proventriculus and the cloaca; moderate levels were detected for the gizzard and for the bursa of Fabricius (23).

In order to study the effective presence of TIR8 protein and the possibility of different post-translational modifications occurring in the same tissues, SDS-PAGE and Western blots were carried out on tissue homogenates. Protein distribution was in agreement with mRNA analysis. Similarly to the results already shown in human and murine species, the high TIR8 expression observed in the whole digestive apparatus might support a role of local immunomodulator for chicken TIR8 (11). Indeed, the main activity attributed to TIR8 in the intestine was that of dampening the immune response in cells exposed to infections (17, 12, 16). Nevertheless, TIR8 expression pattern in chicken was not found homogeneous, due to the detection of several isoforms after Western blot analysis. Since the antibody used throughout these experiments was highly specific for TIR8, the possibility of a cross-reactivity with other proteins seemed very remote. It should not to be ruled out that *Tir8* mRNA could undergo alternative splicing and/or that the protein could host different post-translational modifications. The presence of *Tir8* mRNA with different lengths, presumably due to alternative splicing, was already reported in human and mouse species (3, 9) as well as by Northern blot analysis in chicken (23). The non-homogeneous pattern of TIR8 protein observed in electrophoresis (bands at 75, 45 and 35 kDa) could be also due to different post-translational modifications, such as tissue-specific glycosylation or proteolysis, which may result in different isoforms detectable by Western blot. This is not surprising, because TIR8 sequence displays seven glycosylation sites and the differences between predicted and actual molecular weight of TIR8 suggested an extensive glycosylation (3).

Immunohistochemistry displayed low sensitivity showing immunolabelling only in a few organs. This may be due to a lower reactivity of the commercial antibody with paraffin included tissues. Nevertheless, positivity of scattered cells of the intestinal mucosa further confirms the central role of TIR8 expression in chicken intestine. Noteworthy, the immunolabeling of scattered cells in chicken thymus reveals an unexpected presence of TIR8 in an organ showing only scarce *Tir8* mRNA expression.

In conclusion, an ubiquitous expression of TIR8 was demonstrated in chickens at both transcriptional (mRNA) and translational (protein) levels. This is a preliminary study of TIR8 in chicken, base for further investigation on the modulatory role of TIR8 during diseases of infectious and non-infectious origin, which are of particular relevance in chicken.

ACKNOWLEDGEMENTS

We wish to thank Prof. Gallazzi for providing us with the tissue samples, Prof. Tiziana Rampin for her precious advice and Dr. Silvia Russo for English editing. This work was supported by the FIRST and PUR Grants from the University of Milan (PN 121521500524).

REFERENCES

1. Gangloff M, Weber ANR, Gibbard RJ, Gay NJ. Evolutionary relationships, but functional differences, between the Drosophila and human Toll-like receptor families. Biochem Soc Trans 2003; 31:659-63.
2. Mantovani A, Locati M, Polentarutti N, Vecchi A, Garlanda C. Extracellular and intracellular decoys in the tuning of inflammatory cytokines and Toll-like receptors: the new entry TIR8/SIGIRR. J Leukoc Biol 2004; 75:738-42.
3. Thomassen E, Renshaw BR, Sims JE. Identification and characterization of SIGIRR, a molecule representing a novel subtype of the IL-1R superfamily. Cytokine 1999; 11:389-99.
4. Garlanda C, Riva F, Bonavita E, Mantovani A. Negative regulatory receptors of the IL-1 family. Semin Immunol 2013; 25:408-15.
5. Takeda K, Akira S. TLR signalling pathways. Semin

Immunol 2004; 16:3-9.
6. Henson PM. Dampening inflammation. Nat Immunol 2005; 6:1179-81.
7. Mantovani A, Garlanda C, Locati M, Rodriguez TV, Feo SG, Savino B, Vecchi A. Regulatory pathway in inflammation. Autoimmun Rev 2007; 7:8-11.
8. O'Neill LA. SIGIRR puts the brakes on Toll-like receptors. Nat Immunol 2003; 4:823-4.
9. Polentarutti N, Rol GP, Muzio M, et al. Unique pattern of expression and inhibition of IL-1 signaling by the IL-1 receptor family member TIR8/SIGIRR. Eur Cytokine Net 2003; 14:211-18.
10. Qin J, Qian Y, Yao J, Grace C, Li X. SIGIRR inhibits interleukin-1 receptor- and toll-like receptor 4-mediated signaling through different mechanisms. J Biol Chem 2005; 280:25233-41.
11. Wald D, Qin J, Zhao Z, et al. SIGIRR, a negative regulator of Toll-like receptor-interleukin 1 receptor signalling. Nat Immunol 2003; 4:920-7.
12. Garlanda C, Riva F, Polentarutti N, et al. Intestinal inflammation in mice deficient in Tir8, an inhibitory member of the IL-1 receptor family. Proc Natl Acad Sci USA 2004; 101:3522-6.
13. Lech M, Kulkarni OP, Pfeiffer S, et al. Tir8/Sigirr prevents murine lupus by suppressing the immunostimulatory effects of lupus autoantigens. J Exp Med 2008; 205:1879-88.
14. Garlanda C, Di Liberto D, Vecchi A, et al. Damping excessive inflammation and tissue damage in Mycobacterium tuberculosis infection by Toll IL-1 receptor 8/single Ig IL-1-related receptor, a negative regulator of IL-1/TLR signaling. J Immunol 2007a; 179:3119-25.
15. Huang X, Hazlett LD, Du W, Barrett RP. SIGIRR promotes resistance against *Pseudomonas aeruginosa* keratitis by down-regulating type-1 immunity and IL-1R1 and TLR4 signaling. J Immunol 2006; 177:548-56.
16. Xiao H, Gulen MF, Qin J, Yao J, Bulek K, Kish D, et al. The Toll–interleukin-1 receptor member SIGIRR regulates colonic epithelial homeostasis, inflammation, and tumorigenesis. Immunity 2007; 26:461-75.
17. Garlanda C, Riva F, Veliz T, et al. Increased susceptibility to colitis-associated cancer of mice lacking TIR8, an inhibitory member of the interleukin-1 receptor family. Canc Res 2007b; 67:6017-21.
18. Riva F, Bonavita E, Barbati E, Muzio M, Mantovani A, Garlanda C. TIR8/SIGIRR is an interleukin-1 receptor/Toll like receptor family member with regulatory functions in inflammation and immunity. Front Immunol 2012; 3:322. doi: 10.3389/fimmu.2012.00322.
19. Lech M, Skuginna V, Kulkarni OP, et al. SIGIRR/TIR8 aggravates hydrocarbon oil-induced lupus nephritis. J Pathol 2010; 220:596-607. doi:10.1002/path.2678.
20. Temperley ND, Berlin S, Paton IR, Griffin DK, Burt DW. Evolution of the chicken Toll-like receptor gene family: a story of gene gain and gene loss. BMC Genomics 2008; 9:62. doi: 10.1186/1471-2164-9-62.
21. Turin L, Riva F. Toll-like receptor family in domestic animal species. Crit Rev Immunol 2008; 28:513-38.
22. Wang R, Millam JR, Klasing KC. Distribution of interleukin-1 receptor in chicken quail brain. Comp Biochem Physiol Part A 2003; 136:663-71.
23. Riva F, Polentarutti N, Tribbioli G, Mantovani A, Garlanda C, Turin L. The expression pattern of TIR8 is conserved among vertebrates. Vet Immunol Immunopathol 2009; 131:44-9.
24. Riva F, Rahman MM, Turin L, et al. TIR8 receptor expression in bovine tissues. Vet Immunol Immunopathol 2010; 136:65-70.
25. Kogut MH, Genovese KJ, Lowry VK. Differential activation of signal transduction pathways mediating phagocytosis, oxidative burst and degranulation by chicken heterophils in response to stimulation with opsonized Salmonella enteritidis. Inflammation 2001; 25:7-15.
26. Turin L, Manarolla G, Rampin T, Riva F. The innate immunity receptor TIR8/SIGIRR is expressed in the early developmental stages of chicken embryos. J Biol Regul Homeost Agents 2014; 28:33-40.
27. Hsu SM, Raine L, Fanger H. Use of avidin-biotin peroxidase complex (ABC) in immunoperoxidase techniques: a comparison between ABC and unlabeled antibody (PAP) procedures. J Hictochem Cytochem 1981; 29:577-80.
28. Barua A, Yoshimura Y. Ovarian cell-mediated immune response to Salmonella enteritidis infection in laying hens (Gallus domesticus). Poult Sci 2004; 83:997-1002.

OSTEOPONTIN, OSTEOCALCIN AND OB-CADHERIN EXPRESSION IN SYNTHETIC NANOHYDROXYAPATITE *vs* BOVINE HYDROXYAPATITE CULTURED OSTEOBLASTIC-LIKE CELLS

A. SANTARELLI[1,2], M. MASCITTI[1], G. ORSINI[1], L. MEMÈ[1], R. ROCCHETTI[3], P. TIRIDUZZI[1], F. SAMPALMIERI[1], A. PUTIGNANO[1], M. PROCACCINI[1], L. LO MUZIO[4] and F. BAMBINI[1,2]

[1]Department of Clinical, Specialistic and Stomatological Sciences, Marche Polytechnic University, Ancona, Italy; [2]Odontostomatologic Clinic, National Institute of Care and Research on Ageing, Ancona, Italy; [3]Department of Pathologic Anatomy and Histopathology, Marche Polytechnic University, Ancona, Italy; [4]Department of Clinical and Experimental Medicine, Foggia University, Foggia, Italy

Received May 26, 2013 – Accepted July 14, 2014

Calcium phosphate ceramics have been applied in bone replacement for several decades due to their excellent biocompatibility, bioactivity, osteoconductivity and mechanical strength. Several studies have demonstrated that porous hydroxyapatite (HA) is an excellent scaffold for osteogenic proliferation and differentiation of the osteoprogenitor cells. However, different methods of synthesis and production of HA ceramic-based materials may have considerable effect on the physical and biological properties. In the present work, two hydroxyapatite-based materials, a natural hydroxyapatite ceramic of bovine origin and a synthetic nano-cristalline hydroxyapatite were tested *in vitro* with MG63 cell line. The results displayed that both the materials demonstrated a good biocompatibility. The immunocytochemical stain revealed a different positivity of the osteogenic markers between the cultures with the biomaterials, and the control culture. Western blot data confirmed the immunocytochemical stain. Both the materials tested in the present study demonstrated a good biocompatibility with the osteoblastic cells allowing, at the same time, the osteogenic differentiation, and they may be useful in clinical use.

For about 30 years the use of fixed prosthesis anchored to endosseous implant has been one of the most important treatments allowing rehabilitation of edentulous maxillary jaws with normal-levels of esthetics and function (1, 2). However, bone resorption in edentulous regions often results in an inadequate ridge for implant osseointegration (3). In order to overcome this problem, different bone-grafting procedures and materials have been used which allow to provide a proper implant placement.

For the reconstruction of bone defects of the jaws, many procedures have been developed, such as sinus lift technique or guide bone regeneration (GBR) (4), with autologous bone being the gold standard (5). However, there are several disadvantages, like infection, unpredictable graft resorption, the risk of

Key words: hydroxyapatite, synthetic nanocristalline hydroxyapatite, natural bovine hydroxyapatite, osteopontin, osteocalcin, OB-cadherin

Mailing address:
Prof. Lorenzo Lo Muzio,
Via Rovelli, 48
71122 Foggia, Italy
Tel.: +39 0881 588090
Fax: +39 0881 588081
e-mail: llomuzio@tin.it

0393-974X (2014)

postoperative pain, paresthesia or hypersensivity, the limited availability of bone in the oral site, and the necessity for an additional operation under general anesthesia with a prolonged stay in hospital, in the case of extra-oral donor sites (6, 7).

Thus, research focused on the use of biomaterials to facilitate bone repair processes (8). For this purpose, Hydroxyapatite (HA) and HA-based materials are widely used in the bone regeneration field as it has the same mineral phase as bone, with high biocompatibility results, and high potential to increase bone regeneration (9, 10). Other studies demonstrated that the porous HA is an excellent scaffold for the osteogenic proliferation and differentiation of the osteoprogenitor cells (11, 12). However, different methods of synthesis and production of HA ceramic-based materials, as well as addiction of composite materials like collagen or silica gel, may have considerable effect on the physical and biological properties (13). Moreover, a direct comparison between non-composite natural *vs* synthetic HA has still not been investigated in depth. Thus, the aim of this work is to test *in vitro* two HA-based materials, a natural HA ceramic of bovine origin (Endobon, Biomet, Florida, USA) and a synthetic nano-cristalline HA (Neo Active Apatite, Ghimas, Bologna, Italy). Thus, the two materials were co-cultured for 72 h with osteoblastic cell line and then differences in cell viability and differentiation were investigated.

MATERIALS AND METHODS

Cell culture

Osteoblast-like cells (MG63)(ATCC, Rockville, MD, USA) were cultured in sterile Falcon wells using Dulbecco's Modified Eagle's Medium (DMEM, Sigma-Aldrich, Milan, Italy) supplemented with 10% fetal bovine serum (FBS), 1% nonessential amino acids 2.0 mM L-glutamine, and 1% penicillin–streptomycin (all from GIBCO, Invitrogen, Milan, Italy). Cultures were maintained in a 5% CO_2 humidified atmosphere at 37°C. MG63 cells were collected and seeded at a density of $1x10^5$ cells/ml into 9 cm^2 (3 ml) wells. One set of wells contained the natural xenogenic HA, whereas another set contained the synthetic nano-HA covering the same area. The same concentration of cells was seeded into empty wells as a control (CTR). Plates were cultured under standard conditions up to 72 h. Every 24 h, the medium (3 ml of DMEM with 10% FBS) was changed.

MTT (3-dimethylthiazol-2,5-diphenyltetrazolium bromide) colorimetric assay

Detection of cytotoxicity effects was performed indirectly by quantification of mitochondrial dehydrogenase activity by MTT assay (Sigma, Milan, Italy). This viability test is based on the reduction of a tetrazolium salt to a soluble formazan salt by a reductase of the mitochondrial respiratory chain that is active only in viable cells. Cells were plated and treated as described above. After 72 h, the medium was removed; 200 µL of MTT (Sigma, Milan, Italy) solution (5 mg/mL in DMEM without phenol red) and 1.8 mL of DMEM were added to the cell monolayer; the multi-well plates were incubated at 37°C for further 4 h. After discarding the supernatants, the dark blue formazan crystals were dissolved by adding 2 mL of solvent (10% HCl 1N in isopropanol, Sigma, Milan, Italy) and quantified spectrophotometrically (Secomam, Anthelie light, version 3.8, Contardi, Italy) at 570 and 690 nm. Results of MTT are reported as optical density and can be directly correlated with the cell number. In the control cultures, the cells were placed directly into adherent polystyrene culture plates at the same culture density as placed onto the samples. The mean and the standard deviations were obtained from three different experiments of the same specimen.

Immunocytochemical stain of the cellular lines

Cells were cultured on glass slides coated with poly-L-lysine to enhance cell attachment. Cultured cells were rinsed with phosphate-buffered saline (PBS), fixed in cold acetone and air-dried. To improve the staining pattern, the slides were boiled three times for 3 min in 10 mM citrate buffer as antigen retrieval method. In order to prevent non-specific bindings of antibodies, sections were then pre-incubated with non-immune bovine serum (diluted 1:100 in PBS) for 25 min at room temperature (RT). After washing twice with Tris-HCl buffer, primary antibodies were applied. A negative control was performed in each run by substituting primary antibodies with non-immune reagent (DAKO Antibody Diluent, Dakopatts, Hamburg, Germany). All the slides were washed twice in Tris-HCl buffer between each step. Primary antibody was diluted using 0.05 M Tris-HCl buffer pH 7.2-7.6, containing 1% bovine serum albumin and incubated at optimal dilution and time: mouse monoclonal antibody against Osteopontin (American Research Products, Waltham, MA, USA) 1:100; Osteocalcin (Biogenex, Fremont, CA, USA) 1:100 and OB-Cadherin (Transduction Laboratories, Lexington, Kentucky, USA) 1:200. Sequential 20-min incubations with biotinylated anti-mouse immunoglobulins and streptavidin conjugated to alkaline phosphatase were performed. Finally, a new fast red substrate system (K0597, Dako, Glostrup, Denmark) was applied as a

chromogenic solution.

The number of markers expressing cells was estimated as a percentage of the final number of 100 cells of each slide, evaluating 5 random areas at high magnification.

Western blot

Cellular pellets were suspended in a lysis buffer (Phosphate-Buffered Saline (PBS), 1% Nonidet P40, 0.1% SDS, 1 mM phenylmethylsulfonylfluoride, 2 µg/mL aprotinin) and homogenized on ice using an Ultra-Turrax homogenizer (IKA, Staufen, Germany) at medium speed. The homogenate was centrifuged at 14,000 x 15 min at 4°C. Protein concentrations were estimated using Bradford assay (Sigma-Aldrich, St. Louis, Missouri, USA) using bovine serum albumin as the standard.

Subsequently, 50 µg of total protein extracts were heated to 95°C for 5 min and electrophoresed on 10% polyacrylamide gel (SDS-PAGE) under reducing conditions. Proteins were electrophoretically transferred to nitrocellulose membrane (Bio-Rad, Melville, NY, USA); complete transfer was assessed using prestained protein standards (Bio-Rad, Melville, NY, USA). Blots were placed in PBS, pH 7, containing 5% non-fat dried milk and 0.1% Tween-20 (blocking solution) and incubated for 60 min at 37°C. After washing in PBS containing 0.1% Tween-20, blots were incubated with Osteopontin monoclonal antibody (American Research Products, Waltham, MA, USA) 1:100 and OB-Cadherin (Transduction Laboratories, Lexington, Kentucky, USA) 1:200 in blocking solution for 60 min at room temperature. The membranes were then washed five times with PBS containing 0.1% Tween-20 before incubation with secondary antibody, horseradish peroxidase-conjugated goat anti-mouse IgG (Santa Cruz Biotechnology Inc., Santa Cruz, CA, USA) 1:10000 in blocking solution for 60 min at room temperature. Blots were finally washed five times in PBS containing 0.1% Tween-20, processed with Super Signal West Pico Chemiluminescent substrate (Pierce, Rockford, IL, USA) and autoradiographed. To confirm equal protein loading per lane, membranes were subsequently reacted with 1:5000 dilution of a mouse monoclonal antibody to β-actin (Sigma-Aldrich, St. Louis, Missouri, USA).

The relative signal intensity of proteins detected in blots of tissue samples was quantified using Quantity One 1-D Analysis software (Bio-Rad Laboratories).

Statistical analysis

To avoid variations, the experiment was carried out in triplicate. Differences were determined by one-way analysis of variance and considered statistically significant at $p < 0.05$.

RESULTS

Cellular viability

The analysis of the cellular viability conducted after 72 h of contact between the xenogenic biomaterial and the synthetic nano-hydroxyapatite did not show any significant difference in growth of the cellular population tested (MG63), compared to the control ($p > 0.05$). This demonstrates that both the hydroxyapatite-based materials are biocompatible and they do not block the normal osteoblastic-like cell proliferation.

Immunocytochemical stain of the cellular lines

The immunocytochemical stain revealed a

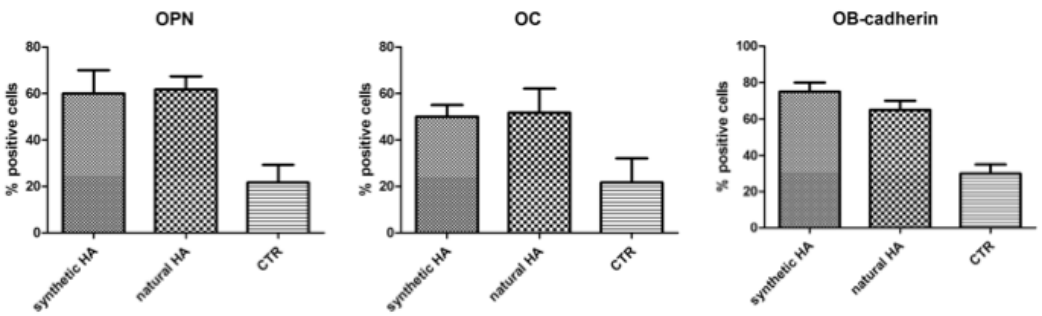

Fig. 1. *Immunocytochemical stain of positive cells for osteopontin, osteocalcin and OB-cadherin showing that the cells in contact with natural and synthetic hydroxyapatite displayed a higher marker expression compared to the control.*

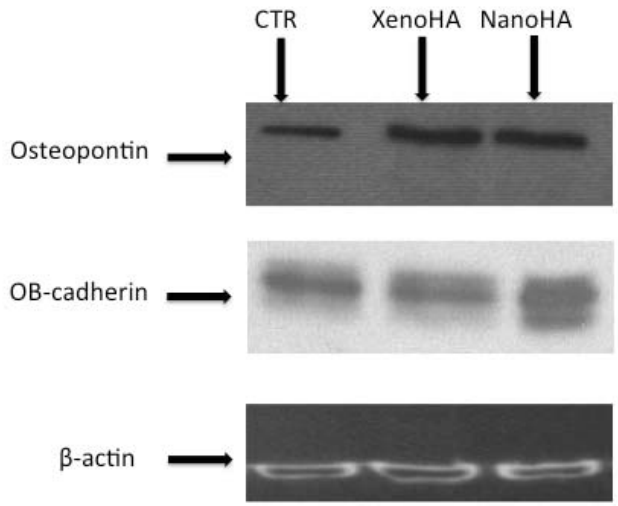

Fig. 2. *Western blot showing that the cells cultured with both the biomaterials have an increased marker expression compared to the control cells.*

different positivity of the osteopontin protein between the culture with the biomaterials, and the control culture (Fig. 1).

Therefore, 72 h later the cells in contact with natural and synthetic hydroxyapatite showed a superior osteopontin expression compared to the control ($p < 0.05$). The percentage of cells expressing the osteoblastic marker did not show statistically significant differences between the two materials tested ($p > 0.05$). Similar results were obtained for the other well-known markers of osteoblastic differentiation: osteocalcin and OB-cadherin. Indeed, cells cultured with both biomaterials showed a higher osteocalcin and OB-cadherin expression compared to control cells ($p < 0.05$).

Western blot

The Western blot analysis of the proteins extracted from the lyses of the MG63 cells, revealed that the osteoblastic cells normally express both osteopontin and ob-cadherin (Fig. 2). The analysis of the osteopontin expression, normalized for the actin expression, showed that the cells cultured with both the biomaterials, have an increased osteopontin expression compared to the control cells, without any statistical difference between the biomaterials used.

Regarding OB-cadherin, the band corresponding to this protein was slightly higher in the cells in contact with synthetic nano-HA compared to the cells in contact with natural bovine HA, even if differences were not statistically significant. Also for OB-cadherin control cells showed a low ammount of protein expression compared to cells in contact with both biomaterials.

DISCUSSION

Hydroxyapatite (HA) is widely used in the bone regeneration field due to it having the same mineral phase as bone. Multiple studies *in vivo* have demonstrated the high biocompatibility of the HA ceramics, and their high potential to increase bone regeneration (9, 10). Other studies demonstrated that the porous HA is an excellent scaffold for the osteogenic proliferation and differentiation of osteoprogenitor cells (11, 12). However, different methods of synthesis and production of HA ceramic-based materials, as well as other biomaterials, may have considerable effect on the physical and biological properties (13, 14).

Indeed, granule-shaped calcium phosphate-based biomaterials can be manufactured in different ways. One frequently applied approach is to remove proteins and other organic compounds from spongious bovine bone or calcareous algae or other natural sources using a high temperature treatment. The resulting porous structure from hydroxyapatite (HA) can be crushed into granules of different sizes (15).

Another strategy is the fabrication of synthetic calcium phosphate ceramics (such as HA, β-tricalciumphosphate or biphasic mixtures), recently mostly nano-HA (15). However, the microstructure and therefore also the solubility of the resulting calcium phosphate ceramic is not the same as the nanocrystalline structure of HA occurring in natural bone, nor the same between ceramics from natural sources and fully synthetic ceramics.

Therefore, in this study, two HA based materials, a natural HA ceramic of bovine origin (Endobon, Biomet, Florida, USA) and a synthetic nano-

cristalline HA (Neo Active Apatite, Ghimas, Bologna, Italy) were tested *in vitro*. These biomaterials were cultured with MG63 human osteoblastic-like cells, which are commonly used for the evaluation of the impact of an implant material on a microenvironment (16, 17). After 72 h the cells were analyzed for the expression of the osteoblastic differentiation markers (osteopontin, osteocalcin and OB-cadherin) by immunocytochemical and Western blotting techniques, and were compared to the control cells.

Osteocalcin (OC) is the most abundant non-collagenous protein of the Extracellular Matrix (ECM) representing approximately 15% of ECM non-collagenic proteins (18) and it is synthesized by the osteoblast before being secreted into the bone matrix. The role of this protein in osteogenesis and bone remodeling is still not clear, although it may regulate the mineral maturity and the ability to act as a chemotactic agent (19). Indeed, it is considered a marker of mature differentiated osteoblast that plays a role during bone mineralization (20).

Osteopontin (OPN), also known as bone sialoprotein (BSP-I), is another well-known marker of osteoblastic differentiation. The expression of this protein on the cell-matrix interface may suggest its role in the bone cell adhesion (21). This protein expression is increased by bone growth factors, such as TGF-β. This demonstrates the role of the sialoprotein in bone formation and its additional role in bone resorption (22).

OPN, as an early marker of osteogenic differentiation, is associated with the osteoblastic maturation during the matrix synthesis and before the mineralization (23).

Moreover, osteopontin expression occurs also in non-bone tissues in response to a stimulus such as inflammation and is associated with a wide array of cellular processes, including development, carcinogenesis, immunity, inflammation, and tissue repair (24).

OB-cadherin (also known as Cadherin-11) is a transmembrane glycoprotein, part of the cadherin super-family, produced by osteoblastic cells, that plays a pivotal role in their differentiation. Several lines of evidence have previously demonstrated that uncommitted mesenchymal embryonic cells express several cadherins, and that commitment and differentiation into osteogenic, myogenic or adipogenic lineages is associated with regulated expression of specific cadherins (25-27). Osteoblastic cells express both N-cadherin and OB-cadherin, where the latter was specifically associated to osteoblast differentiation (28).

Both the materials tested in the present study demonstrated a good biocompatibility with the osteoblastic cells, allowing, at the same time, osteogenic differentiation. Indeed, the assays of cell viability did not show any significant difference in growth of the cellular population tested (MG63), suggesting that both the HA materials did not retard the cell proliferation, which shows the ceramics are non-toxic. Based on the above results, it was taken for granted that both the HA materials had good cell biocompatibility *in vitro*.

The analysis of the marker's expression after 72 h of culture demonstrated with both the biomaterials that the cells had a greater positivity compared to the control.

However, when comparing the marker expression of osteogenic differentiation between the cell cultures with the two materials, there were no significant differences for any of the proteins considered. This demonstrates that both materials can act as a good scaffold, allowing osteoblast-like cell proliferation and differentiation.

It is also interesting to notice that *in vitro* performance of the synthesized nanocrystalline HA-based granular material is comparable to an already established natural HA material such as the xenogenic bovine HA.

The present results confirm previous findings about synthesized HA. Indeed, Panzavolta et al. showed how the presence of synthesized HA in the scaffold promoted the production of alkaline phosphatase (ALP) and OC in osteoblast culture, as well as the up-regulation of mRNA levels of ALP, OC, Runx2, and TGF- β1 after 3 days of culture (28). Moreover, gene expression of the osteogenic markers ALP, osteonectin, osteopontin and bone sialoprotein II was detected in osteoblatic-like cells cultivated on three different types of synthetic nanocrystalline hydroxyapatite granules (24).

Western blot confirmed immunocytochemistry results. Indeed, after 72 hours the OPN, normalized for the actin expression, is increased in the cultures with biomaterials compared to the control, irrelevant

of which biomaterial was used. OB-cadherin showed a similar result, even if the amount of this protein was slightly higher in the cells in contact with synthetic nano-HA compared to the cells in contact with natural bovine HA.

In vitro studies on biomaterial are useful to compare the biocompatibility data on new developed materials and give the possibility to quantify the cell differentiation. These also allow for a more objective control on the cell-material interaction, even if the results cannot be transferred directly to *in vivo* or clinical studies.

In the present experimental study, both the HA ceramics acted as good and biocompatible substrates, able to support the osteoblastic normal proliferation and osteogenic differentiation. The increased expression of the osteogenic markers osteocalcin, osteopontine and OB-cadherin compared to controls, may suggest the potential beneficial use of these ceramics also in clinical use. Indeed, osteocalcin is an important regulatory protein of bone remodeling and osteoblastic maturation (29); moreover, osteopontin plays an important role in matrix mineralization, and the expression is an index of *in vivo* new bone formation (30). Moreover, osteoblasts presenting a high expression of OB-cadherin, after sinus lift procedures in humans with allograft biomaterial, were considered as active forming bone cells (30).

In conclusion, the synthetic nanocrystalline granular material may be of clinical interest, especially for bone regeneration applications, since its *in vitro* performance is comparable to an already established bovine HA material.

ACKNOWLEDGEMENTS

This work was supported by the National Scientific Research Program PRIN 2008 number 20087BNE3K_003.

REFERENCES

1. Pjetursson BE, Tan WC, Zwahlen M, Lang NP. A systematic review of the success of sinus floor elevation and survival of implants inserted in combination with sinus floor elevation. J Clin Periodontol 2008; 35:216-40.
2. Bambini F, Greci L, Meme L, Santarelli A, Carinci F, Pezzetti F, Procaccini M, Lo Muzio L. Raloxifene covalently bonded to titanium implants by interfacing with (3-aminopropyl)-triethoxysilane affects osteoblast-like cell gene expression. Int J Immunopathol Pharmacol 2006; 19:905-14.
3. Pietrokovski J, Massler M. Alveolar ridge resorption following tooth extraction. J Prosthet Dent 1967; 17:21-7.
4. Wallace SS, Froum SJ. Effect of maxillary sinus augmentation on the survival of endosseous dental implants. A systematic review. Ann Periodontol 2003; 8:328-43.
5. Tessier P, Kawamoto H, Matthews D, Posnick J, Raulo Y, Tulasne JF, Wolfe SA. Autogenous bone grafts and bone substitutes--tools and techniques: I. A 20,000-case experience in maxillofacial and craniofacial surgery. Plast Reconstr Surg 2005; 116:6S-24S.
6. Iturriaga MT, Ruiz CC. Maxillary sinus reconstruction with calvarium bone grafts and endosseous implants. J Oral Maxillofac Surg 2004; 62:344-47.
7. Bambini F, Pellecchia M, Meme L, Santarelli A, Emanuelli M, Procaccini M, Lo Muzio L. Anti-inflammatory cytokines in peri-implant soft tissues: a preliminary study on humans using cDNA microarray technology. Eur J Inflamm 2007; 5:121-7.
8. Boccaccini AR, Blaker JJ. Bioactive composite materials for tissue engineering scaffolds. Expert Rev Med Devices 2005; 2:303-17.
9. Dong J, Kojima H, Uemura T, Kikuchi M, Tateishi T, Tanaka J. *In vivo* evaluation of a novel porous hydroxyapatite to sustain osteogenesis of transplanted bone marrow-derived osteoblastic cells. J Biomed Mater Res 2001; 57:208-16.
10. Huber FX, Berger I, McArthur N, Huber C, Kock HP, Hillmeier J, Meeder PJ. Evaluation of a novel nanocrystalline hydroxyapatite paste and a solid hydroxyapatite ceramic for the treatment of critical size bone defects (CSD) in rabbits. J Mater Sci Mater Med 2008; 19:33-8.
11. Okamoto M, Dohi Y, Ohgushi H, Shimaoka H, Ikeuchi M, Matsushima A, Yonemasu K, Hosoi H. Influence of the porosity of hydroxyapatite ceramics on in vitro and in vivo bone formation by cultured rat bone marrow stromal cells. J Mater Sci Mater Med 2006; 17:327-36.
12. Matsushima A, Kotobuki N, Tadokoro M, Kawate K, Yajima H, Takakura Y, Ohgushi H. *In vivo* osteogen-

ic capability of human mesenchymal cells cultured on hydroxyapatite and on beta-tricalcium phosphate. Artif Organs 2009; 33:474-81.
13. Weibrich G, Gnoth SH, Kunkel M, Trettin R, Werner HD, Wagner W. Roentgen spectrometry comparison of currently available bone substitutes. Mund Kiefer Gesichtschir 1999; 3:92-7.
14. Bambini F, Santarelli A, Marzo G, Rubini C, Orsini G, Di Iorio D, Lo Russo L, Lo Muzio L. CD3 and CD20 expression in titanium *vs* zirconia peri-implant soft tissues: a human study. Eur J Inflamm 2013; 11:305-10.
15. Bernhardt A, Dittrich R, Lode A, Despang F, Gelinsky M. Nanocrystalline spherical hydroxyapatite granules for bone repair: *in vitro* evaluation with osteoblast-like cells and osteoclasts. J Mater Sci Mater Med; Doi 10.1007/s10856-013-4933-2
16. Muzio L, Santarelli A, Orsini G, Meme L, Mattioli-Belmonte M, De Florio I, Gatto R, Bambini F. MG63 and MC3T3-E1 osteoblastic cell lines response to raloxifene. Eur J Inflamm 2013; 11:797-804.
17. Lepore S, Milillo L, Trotta T, et al. Adhesion and growth of osteoblast-like cells on laser-engineered porous titanium surface: Expression and localization of N-cadherin and β-catenin. J Biol Regul Homeost Agents 2013; 27:531-41.
18. Bronckers AL, Farach-Carson MC, Van Waveren E, Butler WT. Immunolocalization of osteopontin, osteocalcin, and dentin sialoprotein during dental root formation and early cementogenesis in the rat. J Bone Miner Res 1994; 9:833-41.
19. Ducy P, Desbois C, Boyce B, et al. Increased bone formation in osteocalcin-deficient mice. Nature 1996; 382:448-52.
20. Panzavolta S, Torricelli P, Amadori S, Parrilli A, Rubini K, della Bella E, Fini M, Bigi A. 3D interconnected porous biomimetic scaffolds: *In vitro* cell response. J Biomed Mater Res Part A 2013; 101(12):3560-70.
21. Standal T, Borset M, Sundan A. Role of osteopontin in adhesion, migration, cell survival and bone remodeling. Exp Oncol 2004; 26:179-84.
22. Sodek J, Chen J, Nagata T, Kasugai S, Todescan R Jr, Li IW, Kim RH. Regulation of osteopontin expression in osteoblasts. Ann N Y Acad Sci 1995; 760:223-41.
23. Beck GR Jr, Zerler B, Moran E. Phosphate is a specific signal for induction of osteopontin gene expression. Proc Natl Acad Sci U S A 2000; 97:8352-57.
24. Junaid A, Moon MC, Harding GEJ, Zahradka P. Osteopontin localizes to the nucleus of 293 cells and associates with polo-like kinase-1. Am J Physiol Cell Physiol 2007; 292:919-26.
25. Lo Muzio L, Sartini D, Santarelli A, Rocchetti R, Morganti S, Pozzi V, Rubini C, Emanuelli M. Expression and prognostic significance of apoptotic genes in oral squamous cell carcinoma. Mol Carcinogen 2014; 53(4):264-71.
26. Re M, Magliulo G, Ferrante L, et al. p63 expression in laryngeal squamous cell carcinoma is related to tumor extension, histologic grade, lymph node involvement and clinical stage. J Biol Regul Homeost Agents 2013; 27:121-9.
27. Di Benedetto A, Watkins M, Grimston S, Salazar V, Donsante C, Mbalaviele G, Radice GL, Civitelli R. N-cadherin and cadherin 11 modulate postnatal bone growth and osteoblast differentiation by distinct mechanisms. J Cell Sci 2010; 123:2640-48
28. Kawaguchi J, Kii I, Sugiyama Y, Takeshita S, Kudo A. The transition of cadherin expression in osteoblast differentiation from mesenchymal cells: consistent expression of cadherin-11 in osteoblast lineage. J Bone Miner Res 2001; 16:260-69.
29. Wang B, Liu YY, Zheng JB, Yuan SX, Chen GX. Changes of osteocalcin and IGF-I during bone lengthening. Chin J Traumatol 2005; 8:151-55.
30. Annibali S, Cristalli MP, La Monaca G, Bignozzi I, Scarano A, Corrado R, Lo Muzio L. Human maxillary sinuses augmented with mineralized, solvent-dehydrated bone allograft: a longitudinal case series. Implant Dent 2011; 20:445-54.

JOURNAL OF BIOLOGICAL REGULATORS & HOMEOSTATIC AGENTS Vol. 28, no. 3, 531-535 (2014)

LETTER TO THE EDITOR

INFLUENCE OF CHRONIC CHROMIUM EXPOSITION ON THE PROCESSES OF LIPID PEROXIDATION INFLAMMATION AND PLATELET ACTIVATION IN RATS

D. MITROV[1], N. HADZI-PETRUSHEV[2], V. STOJKOVSKI[1], E. GJORGIEVSKA[3], H. GAGOV[4] and M. MLADENOV[2]

[1]Faculty of Veterinary Medicine, "Sts, Cyril and Methodius" University, Skopje, Macedonia; [2]Faculty of Natural Sciences and Mathematics, Institute of Biology, "Sts, Cyril and Methodius" University, Skopje, Macedonia; [3]Faculty of Dental Medicine, "Sts, Cyril and Methodius" University, Skopje, Macedonia; [4]Faculty of Biology, Sofia University "St. Kliment Ohridski", Sofia, Bulgaria

Received February 3, 2014 – Accepted July 24, 2014

The aim of this study was to investigate the effect of chronic treatment with chromium hexavalent (Cr VI) on the platelet activation, inflammation and lipid peroxidation in rats. Thirty male Wistar rats weighing 251±18 g were randomly assigned to one control and one Cr-exposed group. 8-iso-prostaglandin $F_{2\alpha}$ (8-iso-$PGF_{2\alpha}$), interleukin 1β (IL-1β), tumor necrosis factor α (TNF-α) and creatinine (Crt), were measured in plasma, while 11-dehydro thromboxane B_2 (11-dehydro-TXB_2) in plasma and urine. Plasma levels of IL-1β, TNF-α, 8-iso-$PGF_{2\alpha}$ and Crt were significantly increased in the Cr (VI)-treated in comparison to the control group. Also, in the urine of Cr (VI)-treated rats, 11-dehydro-TXB_2 was significantly increased in comparison to control rats. From the obtained data it is evident that chronic treatment with Cr (VI), accelerates arachidonic acid peroxidation in rats, which peroxidation further probably induces enhanced 11-dehydro-TXB_2 excretion rate.

Chromium (Cr), a naturally occurring heavy metal, exists in many states, but the trivalent [Cr (III)] and hexavalent [Cr (VI)] forms are the most common types in the environment (1). The toxic effects of Cr are attributed to an overproduction of reactive oxygen species (ROS) during reduction of Cr intermediates [Cr (V) and Cr (IV)] (2). Potassium dichromate ($K_2Cr_2O_7$), a Cr (VI), is the most toxic form of Cr and has been demonstrated to induce nephrotoxicity and is recognized as a human carcinogen (3). The kidney is the main route of the Cr excretion, and it has been reported that acute treatment with Cr (VI) induces an increase in the kidney's Cr content in rats (4). A large body of experimental evidence suggests that oxidative stress is a prominent feature in the acceleration of pathogenesis of renal damage during treatment with Cr (VI) (3, 4). In fact, it was recently reported that lipid peroxidation induced as a result of toxicity by different metals can be estimated by arachidonic acid (AA) oxidation product 8-iso-prostaglandine $F_{2\alpha}$ (8-iso-$PGF_{2\alpha}$), and increased expression of proinflammatory cytokines (IL-1β and TNF-α) (5). However, the relative contribution of the proinflammatory cytokines in the enhanced 8-iso-$PGF_{2\alpha}$ biosynthesis, as a complementary onset during the chronic exposition to Cr (VI) has not yet been demonstrated. Furthermore, besides such a non-enzymatic AA degradation, we are of the opinion that Cr (VI) can also affect enzymatic AA degradation. A lot of reports concerning different metabolic

Key words:chromium, inflammation, lipid peroxidation, platelet activation

Mailing address: M. Mladenov, PhD, Assoc. Prof.
Faculty of Natural Sciences and Mathematics,
Institute of Biology,
"Sts, Cyril and Methodius" University,
P.O. Box 162, Skopje 1000, Macedonia
Tel.: +389 2 3249 605 Fax: +389 2 3228 141
e-mail: mitkom@pmf.ukim.mk

0393-974X (2014)

settings show that the enzymatic degradation of AA is always followed by increased urinary 11-dehydro-thromboxane B_2 (11-dehydro-TXB_2), as one of the most prominent imuno-tromboxanes present in the urine (6-8). Taking this, together with the reported ability of 11-dehydro-TXB_2 to induce platelet activity (9, 10), the expected logical outcome will be that: changes in the urinary 11-dehydro-TXB_2 as a consequence of the chronic treatment with Cr (VI) represent a direct reflection of the changes in platelet activity and nephrotoxicity.

To our knowledge, no studies have been carried out to examine the association of the platelet activation with AA peroxidation as a consequence of the Cr (VI) toxicity in rodents. Therefore, the present experiment was undertaken to evaluate lipid peroxidation associated platelet changes in male rats following chronic exposure to Cr (VI).

MATERIALS AND METHODS

Animals and experimental design

This study was carried out in accordance with the recommendations in the Guide for Care and Use of Laboratory Animals of the EC Directive 86/609/EEC. The protocol was approved by the Committee of the Ethics of Animal Experiments of the University "Sts. Cyril and Methodius" Skopje, R. Macedonia. All surgery was performed under sodium pentobarbital anesthesia, and all efforts were made to minimize suffering.

Animals were anesthetized with an intraperitoneal injection of (50 mg kg^{-1}b. wt. thiopentane sodium BP; Rhone-Poulenc Rorer Limited, Nenagh, Co-Tipperary, Ireland). Male Wistar rats (n = 30) were used for all protocols and were maintained on a 12:12, light:dark cycle and fed with standard rat chow.

In vivo treatment

Thirty male Wister rats were randomly divided into two groups of 15 each: group I served as controls and group II received 700 ppm of $K_2Cr_2O_7$ (Cr VI) (equivalent to 67 mg/kg) through the drinking water for 14 days (n = 15). Since the major route of Cr (VI) for the general population is the oral way (11), the present study is designed to investigate the toxicity of Cr (VI) given to rats via the oral route. The dose of Cr (VI) and the period of treatment were selected on the basis of previous studies (3, 4).

The levels of Cr (VI), used in the present study, are not usually found in the environment, but may be encountered in the workplace or in the vicinity of industrial establishments (11). Daily Cr (VI) intake by rats was determined after measuring drinking water consumption. So each treated rat ingested daily 39.31±5.72 mg of Cr (VI), (Table I).

Blood collection

Rat venous blood samples (from abdominal vein) were withdrawn into tubes containing 3.8% sodium citrate (0.9 mL of blood to 0.1 mL of sodium citrate). Plasma was prepared by centrifugation (2000*g* for 20 min), separated into aliquots, and stored at -80°C until analyses were performed.

Urine collection

Before sacrifice, urine samples were obtained from each animal housed in a specially designed metabolic cage, where fecal contamination was avoided. They were collected in bottles within 24 h cycles. The volume of each urine sample was centrifuged at 3000 g for 5 min, separated into aliquots, and stored at -80°C until analyses were performed.

IL-1β and TNF-α *immunoassay*

Plasma levels of IL-1β and TNF-α were determined using commercially available enzyme-linked immunosorbent assay kits (Rat IL-1β and TNF-α Platinum ELISA, Bender Med-Systems, Vienna, Austria). Results are expressed as pg mL^{-1}. All assays were performed as outlined in the protocols enclosed in each kit. Intra-assay and inter-assay coefficients of variation were < 9 %.

8-iso-$PGF_{2\alpha}$ and 11-dehydro-TXB_2 immunoassays

8-iso-$PGF_{2\alpha}$ and 11-dehydro-TXB_2 in the plasma were analyzed by a newly developed ELISA for quantitative analysis of 8-iso-$PGF_{2\alpha}$ and 11-dehydro-TXB_2 levels in biological fluids from Cayman Chemical Company (An Arbor, MI, USA). The total amounts of 8-iso-$PGF_{2\alpha}$ and 11-dehydro-TXB_2 were analyzed after hydrolysis and extraction. The limits of detection of the assays were about 2,7 pg mL^{-1} for 8-iso-$PGF_{2\alpha}$ and about 15,6 pg mL^{-1} for 11-dehydro-TXB_2. Intra-assay and inter-assay coefficients of variation were < 10 %.

Creatinine assay

The levels of creatinine (Crt) in the plasma and urine were estimated spectrophotometrically using the Jaffe reaction (12).

Statistical analysis

Data were analyzed by one-way ANOVA, followed by the Newman–Keulls multiple comparison test between all groups. The correlation between different parameters was assessed by Spearman's rank correlation analysis within-

subject of the tested variables. Only 2-tailed probabilities were used for testing statistical significance. Probability values < 0.05 were regarded as statistically significant. All analyses were performed with Graph Pad Prism 4.0 (San Diego, CA, USA).

RESULTS

In the present report, we performed a series of studies to test the hypothesis that Cr (VI)-induced platelet activation is related to biologically active products of arachidonic acid peroxidation. Increased plasma levels of Crt after treatment with Cr (VI) ($p < 0.05$; Fig. 1A), reflects the interaction of the Cr (VI) with the kidney cells. This interaction was additionally corroborated by the significant increase of plasma 8-iso-$PGF_{2\alpha}$, in the Cr (VI)-treated rats ($p < 0.05$; Fig. 1B). Our hypothesis that Cr (VI)-induced increase of lipid peroxidation is associated with inflammatory events was corroborated with the significant increasing of IL-1β and TNF-α levels ($p < 0.05$; Fig. 1 C and D, respectively). Treatment with Cr (VI) was without significant influence on plasma 11-dehydro-TXB_2 (Fig. 1E), while the urinary level was significantly increased ($p < 0.05$) (Fig. 1F). In order to define the relationship between the indexes of lipid peroxidation (8-iso-$PGF_{2\alpha}$) and inflammation (IL-1β and TNF-α), as a consequence of the treatment with Cr (VI), Spearman's rank correlation analysis was introduced. The obtained results are presented in Fig. 2A, and show that Cr (VI)-induced changes in plasma 8-iso-$PGF_{2\alpha}$ correlate positively with the changes in plasma IL-1β, (ρ=0.608; p<0.016). Also, by using the same Spearman's test we tested whether induced lipid peroxidation is associated with the platelet activation. In this direction our correlation test suggests positive linear correlation between the biosynthesis of 8-iso-$PGF_{2\alpha}$ and the excretion rate of 11-dehydro-TXB_2 (ρ=0.567, p<0.027, Fig. 2B).

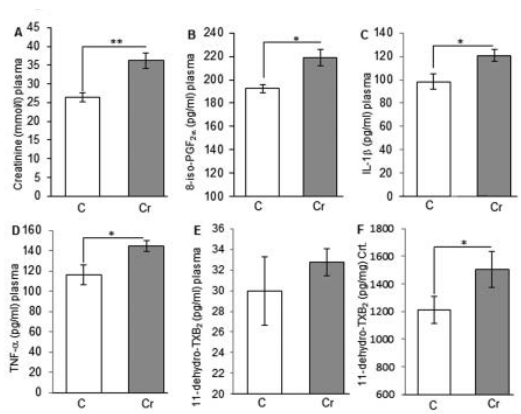

Fig. 1. ***A)*** *Creatinine in plasma (Crt, mean ± SD);* ***B)*** *8-iso-prostaglandin $F_{2\alpha}$ level in plasma (8-iso-$PGF_{2\alpha}$, mean ± SD);* ***C)*** *Interleukin-1β in plasma (IL-1β, mean ± SD);* ***D)*** *Tumor necrosis factor-α in plasma (TNF-α, mean ± SE);* ***E)*** *11-dehydro-TXB_2 level in plasma (11-DH-TXB_2, mean ± SD);* ***F)*** *11-dehydro-TXB_2 level in urine (11-dH-TXB_2, mean ± SD). Control (C), Chromium treated (Cr):*effect of Chromium: *$p < 0.05$.*

DISCUSSION

A Cr (VI) effect on the kidney function is evident through increased plasma Crt, as a marker of the kidney function. From the literature (13), it is evident that Cr (VI) interacts with the renal cell membranes and such interaction leads to altered membrane permeability and loss of functional integrity of the kidney. Similar mechanisms were determined in our study measured through increased 8-iso-$PGF_{2\alpha}$ biosynthesis. Our results for induced lipid peroxidation are in agreement with the studies of Franchini et al. and Shi et al. (13, 14), who reported that the Cr (VI)-induced lesions in the level of proximal tubular cells increase biosynthesis of the 8-iso-$PGF_{2\alpha}$ and inflammatory events. Also, the highest rates of the plasma IL-1β and TNF-α levels as a consequence of the treatment with Cr (VI),

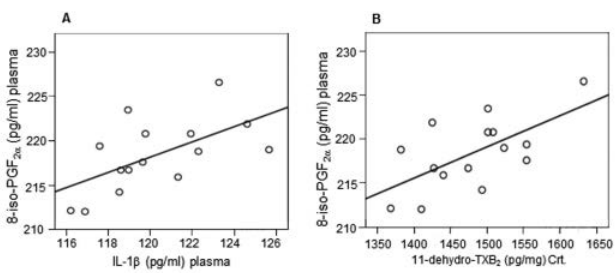

Fig. 2. ***A)*** *Spearman's rank correlation between 8-iso-$PGF_{2\alpha}$ formation and IL-1β in Cr (VI) treated rats (ρ=0.579, p<0.007);* ***B)*** *Spearman's rank correlation between 8-iso-$PGF_{2\alpha}$ formation and urinary 11-dehydro-TXB_2 excretion rate in Cr (VI) treated rats (ρ=0.579, p<0.007).*

Table I. *Quantities of ingested $K_2Cr_2O_7$. Rats were treated with 700 parts per million (ppm) $K_2Cr_2O_7$ administered in their drinking water.*

Parameters and treatment	Controls	$K_2Cr_2O_7$ - treated rats
Water consumption (mL/day/rat)	60.96±6.98	56.17±6.64
Quantities of $K_2Cr_2O_7$ ingested (mg/day/rat)	/	39.31±5.72

Data are shown as means + SD.

are relevant to the prediction that Cr (VI) induces inflammation at the circulatory level (5). The obtained significant correlation between the plasma 8-iso-$PGF_{2\alpha}$ and inflammatory IL-1β (ρ=0,608; p<0.016), after the treatment with Cr (VI), was additional support to our hypothesis. This finding is consistent with the *in vitro* results of Wuyts et al. (15), who reported four-fold enhanced production of 8-iso-$PGF_{2\alpha}$, by human airway vascular smooth muscle cells cultured in the presence of IL-1β. Furthermore, we also showed that enhanced formation of 8-iso-$PGF_{2\alpha}$ exerted detectable influence on the platelet activity in the Cr (VI)-treated rats, suggesting a positive linear correlation between its biosynthesis and 11-dehydro-TXB_2 excretion (ρ=0,567, p<0.027, Fig. 2B). This finding is consistent with the reported ability of 8-iso-$PGF_{2\alpha}$ to increase platelet activity (16). Although the systemic concentration of the 8-iso-$PGF_{2\alpha}$ may be too low to trigger platelet activation, this autacoid can synergize with subthreshold concentrations of other agonists in inducing platelet adhesion and aggregation (17). Moreover, it is likely that the enhanced formation of 8-iso-$PGF_{2\alpha}$, as a consequence of treatment with Cr (VI), is associated with the release of other bioactive isoeicosanoids formed through the same mechanism of oxygen radical catalyzed peroxidation of the AA.

On the other hand, differences in the kinetics of formation of the 11-dehydro-TXB_2 between plasma and urine in the Cr (VI)-treated rats (18) can be explained by significantly greater excretion of 11-dehydro-TXB_2 in comparison with its biosynthesis. Taking that reduction of the Cr (VI) at the level of proximal tubular cells in the kidney induces endothelial damage (3, 4), we assume that increased urinary excretion of the 11-dehydro-TXB_2 is the result of intrarenal platelet and macrophage activation, triggered probably as a consequence of the described endothelial damage. Consequently, we are of the opinion that platelets (or other blood-derived cells) are probably activated during their passage through the kidney with Cr (VI)-induced endothelial damage. This explanation is in agreement with the findings of Benigni et al. (19), who reported marked infiltration of blood-borne cells, mainly of monocyte-macrophage type, in the glomerular tuft of Cyclosporin A treated animals. On the basis of these results, we assume that increased urinary 11-dehydro-TXB_2 excretion rate can be taken as an indicator for increased platelet activity during Cr (VI)-induced nephrotoxcity.

Future studies addressing the metabolism of 11-dehydro-TXB_2 in rat kidney have to be carried out to make a distinction between renal and extrarenal production of the urinary 11-dehydro-TXB_2 as a consequence of the Cr (VI) metabolism. As far as the relevance of these findings in rodents with regard to humans, this could be another important area for future comparative investigation.

ACKNOWLEDGEMENTS

Our thanks to, K.L. Hristov, PhD, for statistical analysis. The authors gratefully acknowledge the financial support from the University ''Sts. Cyril and Methodius'' in Skopje. The Biological Institute at the Faculty of Natural Sciences also supported this research.

REFERENCES

1. Cohen MD, Kargacin B, Klein CB, Costa M. Mechanisms of chromium carcinogenicity and toxicity. Crit Rev Toxicol 1993; 23:255-81.
2. Stohs SJ, Bagchi D, Hassoun E, Bagchi M. Oxidative mechanisms in the toxicity of chromium and

cadmium ions. J Environ Pathol Toxicol Oncol 2000; 19:201-13.

3. Soudani N, Sefi M, Bouaziz H, Chtourou Y, Boudawara T, Zeghal N. Nephrotoxicity induced by chromium (VI) in adult rats and their progeny. Hum Exp Toxicol 2010; 30:1233-45.
4. Pedraza-Chaverri JD, Barrera ON, Medina-Campos RC, et al. Time course study of oxidative and nitrosative stress and antioxidant enzymes in $K_2Cr_2O_7$ induced nephrotoxicity. BMC Nephrol 2005; 6:4.
5. Rebecca T, Christina AG, Narayanan KH, Dominick LN, Narayanan NR, Narayanan AB. Hexavalent chromium activates mediators of inflammation in human lung cells. Fifth AACR International Conference on Frontiers in Cancer Prevention Research 2006; 12-15.
6. Morrow JD, Hill KE, Burk RF, Nammour TM, Badr KF, Roberts LJ. A series of prostaglandin F_2 like compounds are produced *in vivo* in humans by a non-cyclooxygenase, free radical-catalysed mechanism. Proc Natl Acad Sci USA 1990; 87:9383-87.
7. Takahashi K, Nammour TM, Fukunaga M, Ebert J, Morrow JD, Roberts LJ II, Hoover RL, Badr KF. Glomerular actions of a free radical generated novel prostaglandin, 8-iso-prostaglandin $F_{2\alpha}$ in the rat: evidence for interaction with thromboxane A_2 receptors. J Clin Invest 1992; 90:136-41.
8. Minuz P, Andrioli G, Degan M. The F_2-isoprostane 8-epi-prostaglandin $F_{2\alpha}$ increases platelet adhesion and reduces the antiadhesive and antiaggregatory effects of NO. Arterioscler Thromb Vasc Biol 1998; 18:1248-56.
9. Ciabattoni G, Maclouf J, Catella F, Fitzgerald GA, Patrono C. Radio imunoassay of 11-dehydro-TXB_2 in human plasma and urine. Biochim Biophys Acta 1987; 918:293-97.
10. Ciabattoni G, Pugliese F, Davı G, Pierucci A, Simonetti BM, Patrono C. Fractional conversion of thromboxane B_2 to urinary 11-dehydro-thromboxane B_2 in man. Biochim Biophys Acta 1989; 992:66-70.
11. Junaid M, Murthy RC, Saxena DK. Embryo-toxicity of orally administered chromium in mice: exposure during the period of organogenesis. Toxicol Lett 1996; 84:143-48.
12. Jaffe M. Uber den niederschlag, welchenpikrinsaure in normalenhrnerzeugt und ubereineneue reaction des kreatinins. Z Physiol Chem 1886; 10:391-400.
13. Franchini I, Mutti A, Cavatorta A, Corradi A, Cosi A, Olivetti G, Borghetti A. Nephrotoxicity of chromium. Remarks on an experimental and epidemiological investigation. Contrib Nephrol 1978; 10:98-110.
14. Shi X, Chiu A, Chen CT, Halliwell B, Castranova V Vallyathan V. Reduction of chromium (VI) and its relationship to carcinogenesis. J Toxicol Environ Health 1999; 2:87-104.
15. Wuyts WA, Pype JL, Verleden GM. Modulation of IL-1β induced MCP-1, MCP-3 and eotaxin expression in human airway smooth muscle cells. Am J Respir Crit Care Med 2001; 161:A594.
16. Morrow JD, Minton TA, Roberts LJ. The F 2-isoprostane, 8-epi-$PGF_{2\alpha}$, a potent agonist of the vascular thromboxane/endoperoxide receptor, is a platelet thromboxane /endoperoxide receptor antagonist. Prostaglandins 1992; 44:155-63.
17. Pratico D, Smyth EM, Violi F, FitzGerald GA. Local amplification of platelet function by 8-epi-prostaglandin $F_{2\alpha}$ is not mediated by thromboxane receptor isoforms. J Biol Chem 1996; 271:14916-24.
18. Funk CD. Platelet eicosanoids. In: Colman RW, Hirsh J, Marder VJ, Clowes AW, George JN editors. Hemostasis and thrombosis. Basic principles and clinical practice: Philadelphia PA: Lippincott Williams & Wilkins 2001; 30:533-39.
19. Benigni A, Chiabrando C, Piccinelli A, Perico N, Gavinelli M, Furci L, Patino O, Abbate M, Bertani T, Remuzzi G. Increased urinary excretion of thromboxane B_2 and 2,3-dinor-TxB_2 in cyclosporin A nephrotoxicity. Kidney Int 1988; 34:164-74.

JOURNAL OF BIOLOGICAL REGULATORS & HOMEOSTATIC AGENTS Vol. 28, no. 3, 537-543 (2014)

LETTER TO THE EDITOR

INHALED HYALURONIC ACID AS ANCILLARY TREATMENT IN CHILDREN WITH BACTERIAL ACUTE RHINOPHARYNGITIS

A. VARRICCHIO, M. CAPASSO, F. AVVISATI, A.M. VARRICCHIO, A. DE LUCIA, F.P. BRUNESE and G. CIPRANDI

Associazione Italiana Vie Aeree Superiori (AIVAS) - Study Group on respiratory infections, Italy

Received March 18, 2014 - Accepted June 27, 2014

Acute rhinopharyngitis (ARP) is the most common upper respiratory infection in children and represents a social problem for both the pharmaco-economic impact and a burden for the family. Topical antibiotic therapy is usually effective in bacterial ARP, but ancillary treatment might improve its efficacy. Hyaluronic acid (HA) is a promising molecule that has been recently proposed in upper respiratory disorders. Therefore, the purpose of this study was to evaluate the effects of ancillary HA treatment in children with bacterial ARP. Globally, 51 children (27 males, mean age 5.9±2.1 years) with bacterial ARP were enrolled in the study. At baseline, children were randomly assigned to the treatment with: 125 mg of thiamphenicol diluted in 4 mL of saline isotonic solution twice daily (group A) or with 125 mg of thiamphenicol plus 4 ml of sodium hyaluronate 0.2% plus xylitol 5% (Aluneb, Sakura Italia) twice daily (group B) administered by the nasal device Rinowash (Airliquide Medical System, Italy) and connected to an aerosol nebulizer with pneumatic compressor (1.5 bar per 5 L/min) Nebula (Airliquide Medical System, Italy), for 10 days. sVAS, nasopharyngeal spotting, neutrophils and bacteria were assessed at baseline and after the treatment. Both treatments induced significant reduction of symptom perception, spotting, neutrophil and bacteria count. However, thiamphenicol plus HA was able to significantly induce a greater effect on sVAS (p=0.006), neutrophil count (p=0.01), and bacteria count (p=0.0003) than thiamphenicol alone. In conclusion, this study provides the first evidence that intranasal HA, as ancillary treatment, may be able to improve topical antibiotic efficacy in children with bacterial ARP.

Acute rhinopharyngitis (ARP) is a very frequent respiratory infection in childhood and may commonly cause complications, such as otitis media, rhinosinusitis, and lower respiratory tract infections (1). Upper respiratory infections (URI) represent a social problem for both the pharmaco-economic impact and a burden for the family. Many factors may be involved as promoting and/or causing URI, such as age (for a relative immaturity of the immune response), social and community attendance, air and pollution in the home, atopic status, passive smoking, and low socio-economic level (2). Even though most URI are sustained by viral infections, bacterial superimposition may occur. In this regard, it has been currently estimated that biofilm formation is involved in at least 60% of chronic and/or recurrent infections (3). Biofilms are microbial communities consisting of bacteria that are self-reproducing on biological surfaces (4). Biofilms are thought to be frequently involved in the antibiotic

Key words: hyaluronic acid, children, bacterial acute rhinopharyngitis, topical antibiotic

Mailing address:
Giorgio Ciprandi, M.D.
Viale Benedetto XV 6,
16132 Genoa, Italy
Tel.: +39 10 35331820
Fax: +39 10 3538664
e-mail: gio.cip@libero.it

0393-974X (2014)

DISCLOSURE: ALL AUTHORS REPORT NO CONFLICTS OF INTEREST RELEVANT TO THIS ARTICLE.

resistance occurring in recent years. Resistance observed in biofilms is due to multicellular strategies and/or to the ability of individual cells contained in the biofilm, to differentiate into a protected state that tolerates antibiotic effects. Biofilms may be detected by nasal cytology, showing the presence of particular spots, specific for the polysaccharide nature of the biofilm envelope (5).

Intranasal inhaling treatment represents a crucial strategy in the management of ARP, as it allows to: i) achieve higher local medication concentration using lower drug dosage; ii) exert prompt activity; iii) remove secretions by the watery solution; iv) increase tolerability; and v) reduce the occurrence of antibiotic resistance. In this regard, we previously reported that inhaled thiamphenicol was effective and safe in treating children with bacterial ARP (6) as well as inhaled tobramycin (7).

Recent studies demonstrated that hyaluronic acid (HA) could be able to reduce inflammatory damage during UR disorders by exerting several interesting mechanisms of action (8-11). HA has immune-modulatory, repairing, lubricating, and anti-inflammatory activities. Therefore, the purpose of this study was to evaluate the effects of inhaled HA as ancillary therapy in children with bacterial ARP.

MATERIALS AND METHODS

Population and eligibility criteria

Children were enrolled in the trial according to inclusion and exclusion criteria. Inclusion criteria were based on: i) documented diagnosis of ARP by bacterial infection; ii) age ranging between 3-10 years; and iii) at least 5 of these parameters: nasal obstruction, muco-purulent discharge, post-nasal drip, cough, sore throat, fever, and positive culture, as previously stated (6, 7). Exclusion criteria were: i) primary or acquired immunodeficiency; ii) previous (last month) or current administration of drugs capable of interfering with the study (eg, immune-modulatory, homeopathic therapy, or systemic corticosteroids for at least 2 consecutive weeks); iii) history of chronic disease (including cystic fibrosis, cancer, or congenital malformation of the airways, allergic rhinitis); and iv) negative culture.

Study design

A randomized, single-blind, two arm parallel-group protocol was designed. The study was approved by the Ethics Committee of ASL Napoli 1-Centro, Italy. All parents of the enrolled children provided written informed consent.

Study treatment

At baseline, children were randomly assigned to the aerosol-therapy treatment with 125 mg of thiamphenicol (Glitisol, Zambon Italia, Vicenza, Italy) diluted in 4 mL of saline isotonic solution twice daily (group A) or with 125 mg of thiamphenicol plus 4 ml of sodium hyaluronate (high molecular weight) at 0.2% plus 5% xylitol (Aluneb, Sakura Italia, Lonato del Garda, Italy) twice daily (group B) for 10 days. Inhaled therapy was performed using the nasal device Rinowash (Airliquide Medical System, Italy) that was connected to an aerosol nebulizer with pneumatic compressor (1.5 bar per 5 L/min) Nebula (Airliquide Medical System, Italy). This nasal device allows the nebulization of particles with a median aerodynamic diameter > 10 micron over a nebulization time of 60-90 seconds for any application.

Study procedures

The entire study was carried out between November 2013 and February 2014.

The children were examined at the beginning of the study (T0) and after the 10-day treatment (T1). For each patient, clinical examination, including assessing of complaints perception, rhino-pharyngoscopic examination, and nasal cytology were performed.

Simplified Visual Analogue Scale (sVAS) is one of the most commonly used measures of assessing the perception of symptoms and was used in a previous study investigating nasal obstruction perception in children (12). The sVAS is a 4-point scale, from 1 to 4, such as 1 (no respiratory symptom), 2 (mild symptom), 3 (moderate symptom), and 4 (severe symptom).

Nasal cytology was performed by scraping the middle part of the inferior turbinate, using the Rhino-Probe device. The sample was stratified on a slide, fixed with methanol for 4 minutes, and colored using the May-Grunwald-Giemsa staining method. Microscopic observation was performed at 400x magnification to check coloration quality and cell distribution, and at 1000x magnification in immersion to discriminate different cell types and to study the intracellular components.

A semi-quantitative grading was used as previously defined by Gelardi (13). Neutrophil number was calculated as mean of 10 fields and categorized (13). They were graded as follows: Grade 0= not visible; Grade 1= less than 10% of total cell recovered; Grade 2= 11-30%; Grade 3= 31-50%; Grade 4= >50%.

Bacteria were assessed during the nasal cytology reading and were categorized as previously defined (13). They were graded as follows: Grade 0= not visible; Grade

1= occasional groups; Grade 2= moderate number; Grade 3= easily visible; Grade 4= covering the entire field.

Nasopharyngeal spotting: typical cyan-color patches corresponding to a wave-length of 480 nm were considered as an infectious spot as surrogate marker for bacterial biofilm (5).

Endoscopy was carried out with a pediatric rigid endoscope diameter 2.7 mm with 30° angle of vision (Karl Storz), and was video-recorded by a micro-camera connected to a digital recorder set (Karl Storz Tele Pack). A flexible endoscope (1.9 mm diameter) was used in restless children and in those with narrow nasal fossa due to anatomical abnormalities.

Statistical analysis

Descriptive statistics were firstly performed and quantitative parameters were reported as median and interquartile range [IQR] or mean and standard deviation (SD), when appropriate. Qualitative data were reported as frequencies and percentages. The test was used as a nonparametric counterpart.

Comparison of quantitative data between the two groups of patients, in case of two independent variables, was made by the U-Mann-Whitney test; the paired data were compared using the Wilcoxon test. Comparison of non-paired qualitative data for was made by the *chi*-squared test, or by the Fisher's Exact test in case of expected frequencies less than five; for paired data McNemar *chi*-squared test was used.

All statistical tests were two sided; a p value of less than 0.05 was considered as statistically significant. A statistical software program (StatSoft Italia s.r.l. 2005. Statistica 7.1) was used for all analyses.

RESULTS

Globally, 51 children (27 males, mean age 5.9±2.1 years) with bacterial ARP were enrolled in the study. All completed the study. No clinically relevant adverse events were reported in either group. Table I shows the baseline demographic and clinical characteristics of the patients in the two groups.

Of 51 patients screened, 24 patients received thiamphenicol alone (Group A) and 27 thiamphenicol + hyaluronic acid (Group B). The two groups were well-matched for all considered parameters (p= N.S.), thus the two groups were statistically homogeneous.

Group A showed a statistically significant reduction of median sVAS after treatment (from 3 [2-3] to 1.5 [1-2]; p = 0.0005, Wilcoxon test), as shown in Table II and Fig. 1. The treatment with thiamphenicol + hyaluronic acid (Group B) was also capable of significantly reducing sVAS median (from 3 [2-3] to 1 [0-1]; p = 0.0001, Wilcoxon test), as shown in Table II and Fig. 1. The intergroup analysis showed that Group B had lower sVAS values than Group A (1 [0-1] *vs* 1.5 [1-2]; p< 0.006, U-Mann-Whitney test), as shown in Table III and Fig. 1.

Table I. *Baseline demographic and clinical characteristic of the 51 patients evaluated.*

Characteristic	Group A (24 pts)	Group B (27 pts)	P value
Gender- males, N (%)	13 (54)	14 (52)	N.S.ǂ
Age (years), mean ±S.D.	6±2.4	5.8±1.9	N.S. *
sVAS, median [IQR]	3 [2-3]	3[2-3]	N.S. *
Spotting nasopharyngeal, N (%)	11 (45.8)	14 (51.8)	N.S. ǂ
Nasal cytology			
Neutrophils, median [IQR]	2 [2-3]	2 [1-2.5]	N.S. *
Bacteria, median [IQR]	2 [1-2]	2 [1-2]	N.S. *

The percentages in round brackets are calculated over the total number of subjects reported at the top of column.
ǂ: Chi-squared test.
**: Mann-Whitney U test*

Table II. *Clinical and cytological parameters assessed at baseline (Visit 1) and at the end of the study (Visit 2) in Group A and B.*

Group A			
Characteristic	Visit 1	Visit 2	P value
sVAS, median [IQR]	3 [2-3]	1.5 [1-2]	0.0005 **
Spotting nasopharyngeal, N (%)	11 (45.8)	3 (12.5)	0.002 ‡‡
Nasal cytology			
Neutrophils, median [IQR]	2 [2-3]	1.5 [1-2]	0.03**
Bacteria, median [IQR]	2 [1-2]	1 [1-2]	0.001**

Group B			
Characteristic	Visit 1	Visit 2	P value
sVAS, median [IQR]	3 [2-3]	1 [1-1]	0.0001 **
Spotting nasopharyngeal, N (%)	14 (51.8)	4(14.8)	0.004 ‡‡
Nasal cytology			
Neutrophils, median [IQR]	2 [1-2.5]	1 [0-1]	0.003 **
Bacteria, median [IQR]	2 [1-2]	0.5 [0-1]	0.00001 **

‡‡ *: Chi-squared McNemar test*
** *: Wilcoxon test*

Table III. *Clinical and cytological parameters assessed at Visit 2 in Group A compared to Group B.*

Characteristic	Group A (24 pts)	Group B (27 pts)	P value
sVAS, median [IQR]	1.5 [1-2]	1 [1-1]	0.006*
Spotting nasopharyngeal, N (%)	3 (12.5)	4(14.8)	N.S. ‡
Nasal cytology			
Neutrophils, median [IQR]	1.5[1-2]	1[0-1]	0.01*
Bacteria, median [IQR]	1[1-2]	0.5[0-1]	0.0003 *

*: *Mann-Whitney U test*
‡: *Chi-squared test.*

Both treatments reduced bacteria median count (from 2 [1-2] to 1 [1-2]; p= 0.001, for Group A. From 2 [1-2] to 0.5 [0-1]; p=0.00001, for B Group), as shown in Table II and Fig. 2. Group B had a significantly major reduction of bacteria median count (1 [1-2] *vs* 0.5 [0-1]; p= 0.0003), as shown in Table III and Fig. 2.

Neutrophil median count diminished in both Groups (from 2 [2-3] to 1.5 [1-2] p=0.03, for Group A; from 2 [1-2.5] to 1 [0-1] p=0.003, for B group),

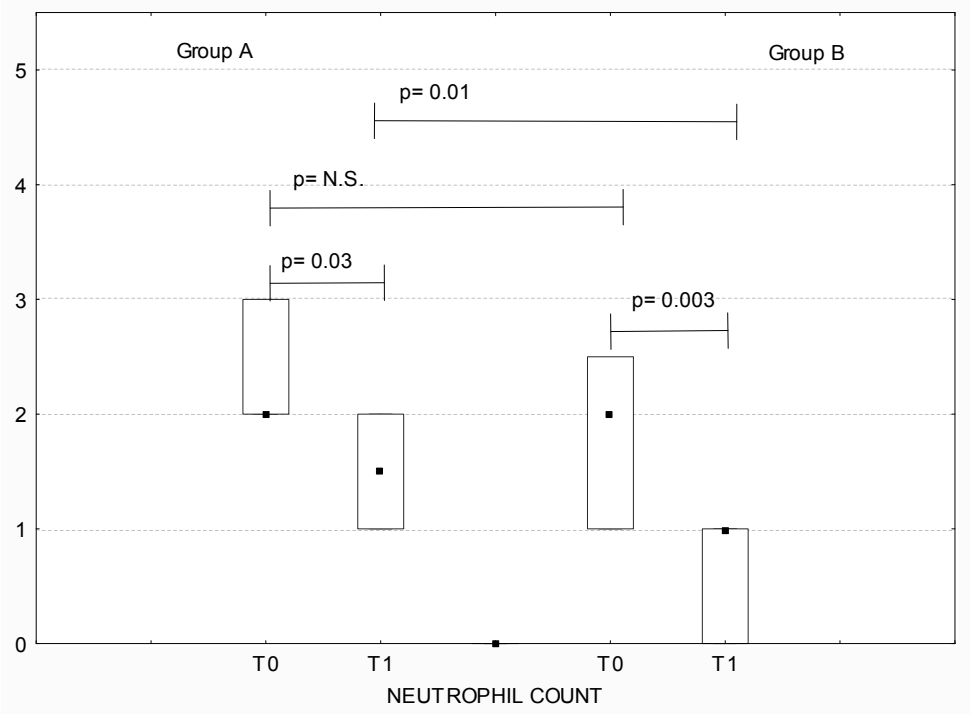

Fig. 1. *Simplified Visual Analogue Scale (sVAS) in Group A and B, at baseline and after treatment.*

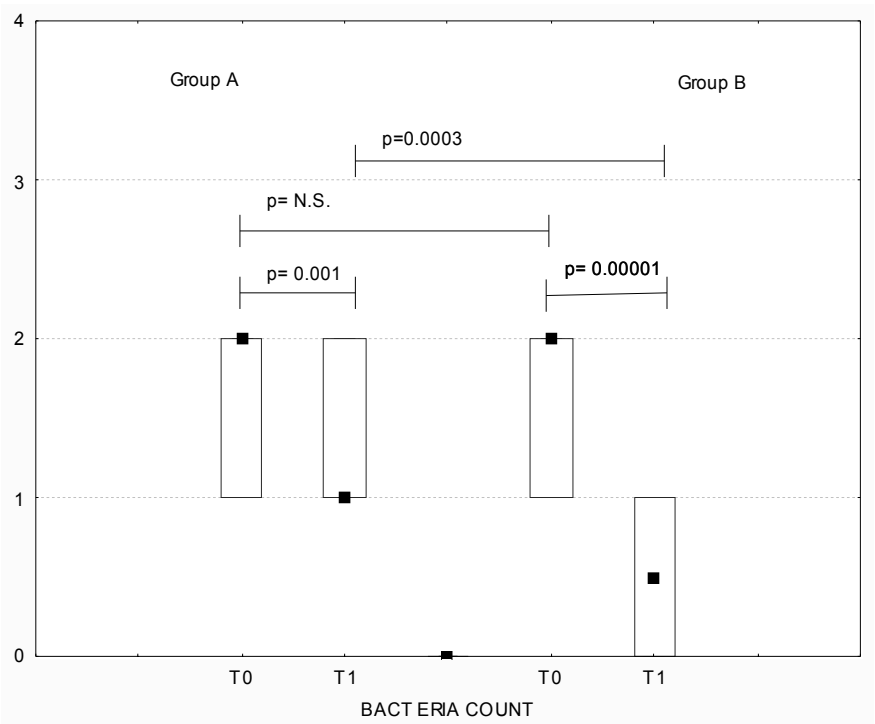

Fig. 2. *Bacteria count in Group A and B, at baseline and after treatment.*

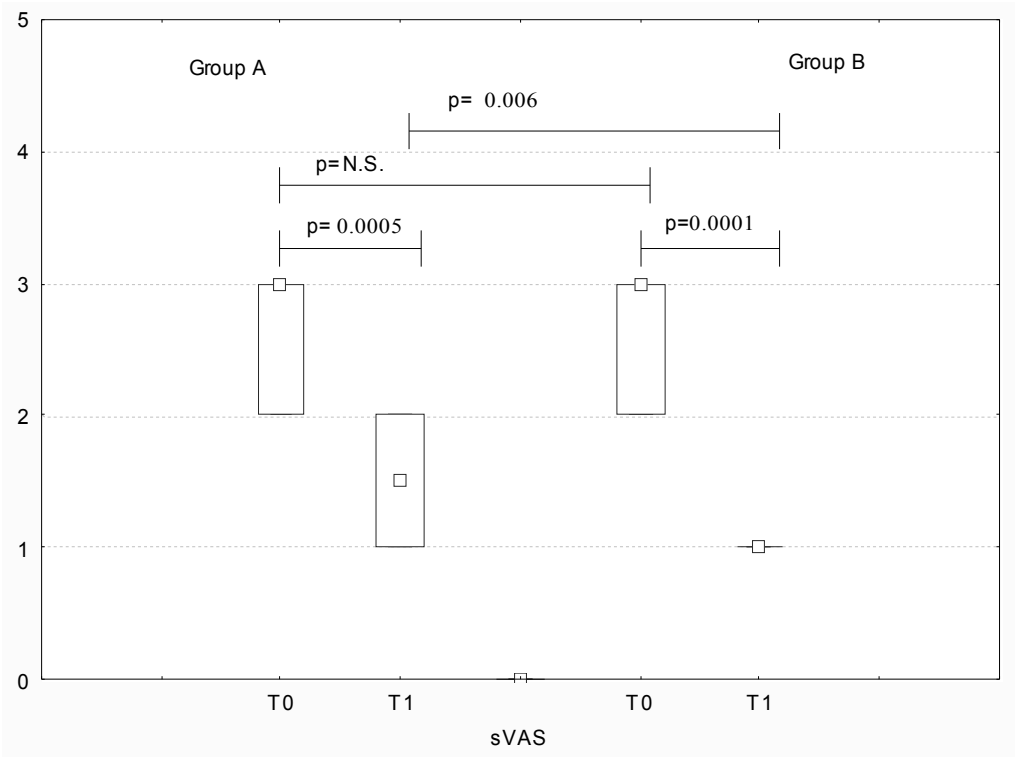

Fig. 3. *Neutrophil count in Group A and B, at baseline and after treatment.*

as shown in Table II and Fig. 3. The combination thiamphenicol plus HA induced a significantly more evident reduction of neutrophil median count (1.5 [1-2] *vs* 1 [0-1] p= 0.01), as shown in Table III and Fig. 3.

The number of subjects with spotting decreased significantly after treatment in both groups (from 45.8% to 12.5% for Group A, from 51.8% to 14.8% for Group B), as reported in Table II. However, there was no significant difference between groups at the end of treatment, as shown in Table III.

DISCUSSION

Aerosol therapy is very popular in the treatment of URI and should be preferred to systemic treatments, mainly in less severe clinical cases. There is evidence that topical intranasal administration of antibiotics is effective and safe in children with bacterial ARP (6, 7). However, bacterial biofilm represents a relevant issue in infection treatment, as it frequently causes antibiotic resistance. For this reason, ancillary therapy could support antibiotics. Many molecules have been proposed as adjunctive therapy, in this regard HA may be promising in the URI treatment.

HA is a glycosamino-glycan which is fundamental in the composition of the extra-cellular matrix of connective tissue. HA attracts active cations, such as Na, for matrix osmosis. More interestingly, HA regulates the innate immunity, promotes angiogenesis, and modulates proliferation, migration, and differentiation of the cells involved in injury repair (15). In particular, HA interacts with Toll Like Receptors 2 and 4, so stimulating innate immunity against bacteria and virus (16). Moreover, HA contributes to the integrity of epithelial barrier exerting a cyto-protective activity (17).

The present study provides evidence that HA, prescribed as ancillary therapy, may exert favorable effects in children with bacterial ARP.

Firstly, this study confirms previous findings demonstrating that thiamphenicol is effective and safe in treating children with bacterial ARP (6). In addition, the combination of thiamphenicol plus HA significantly affects the perception of respiratory complaints as well as reducing the biofilm, the

bacteria, and neutrophil count.

More interestingly, the comparison between thiamphenicol alone and the association tiamphenicol plus HA clearly shows that the latter is significantly superior in reducing symptom perception and infection parameters, such as bacteria and neutrophil count. These findings are surely clinically relevant as proof that HA may be useful in improving the effectiveness of aerosol antibiotic therapy in treating bacterial ARP.

Moreover, the present study confirms previous studies conducted on patients with upper airways disorders, such as recurrent URI (10) and sinus surgery (11). In addition, a possible indication could be the pre-treatment of children who have to undergo anesthesia in order to prevent asthma attacks (18).

The pleiotropic mechanisms of action provided by HA seem to exert a relevant anti-inflammatory and anti-infective activity in the management of bacterial ARP.

In conclusion, the present study provides evidence that HA associated with a topical antibiotic may induce a better control of respiratory symptoms and significantly affect inflammatory and infectious events.

REFERENCES

1. Ovchinnikov A. Rhinopharyngitis as one of clinical manifestations of acute respiratory tract infection. Modern view on the problem. Ter Arch 2006; 78:57-63.
2. Cazzola M, Anaupurapu S, Page CP. Polyvalent mechanical bacterial lysate for the prevention of recurrent respiratory infections: a meta-analysis. Pulm Pharmacol Ther 2011; 25:62-8.
3. Pintucci JP, Corno S, Garotta M. Biofilms and infections of the upper respiratory tract. Eur Rev Med Pharmacol Sci 2010; 14:683-90.
4. Palmer RJ Jr, Stoodley P. Biofilm: Broadened horizons and new emphases. J Bacteriol 2007; 189:7948-60.
5. Gelardi M, Passalacqua G, Fiorella ML, Mosca A, Quaranta N. Nasal cytology: the "infectious spot", an expression of a morphological-chromatic biofilm. Eur J Clin Microbiol Infect Dis 2011; 30:1105-9.
6. Varricchio A, Capasso M, Di Gioacchino M, Ciprandi G. Inhaled thiamphenicol and acetilcysteine in children with acute bacterial rhinopharyngitis. Int J Immunopathol Pharmacol 2008; 21:583-7.
7. Varricchio A, Tricarico D, De Lucia A, et al. Inhaled tobramycin in children with acute bacterial rhinopharyngitis. Int J Immunopathol Pharmacol 2006; 19:131-9.
8. Zahm JM, Milliot M, Bresin A, Coraux C, Birembaut P. The effect of hyaluronic on airway mucus transport and airway epithelial barrier integrity: potential application I the cytoprotection of airway tissue. Matrix Biol 2011; 30:389-95.
9. Forteza R, Lieb T, Aoki T, Savani RC, Conner GE, Salathe M. Hyaluronan serves a novel role in airway mucosal host defense. FASEB J 2001; 15:2179-86.
10. Macchi A, Castelnuovo P, Terranova P, Digilio E. Effects of sodium hyaluronate in children with recurrent upper respiratory tract infections. Int J Immunopathol Pharmacol 2013; 26:127-35.
11. Gelardi M, Guglielmi AVN, De Candia N, Maffezzoni E, Berardi P, Quaranta N. Effect of sodium hyaluronate on mucociliary clearance after functional endoscopic sinus surgery. Eur Ann Allergy Clin Immunol 2013; 45:103-8.
12. Ciprandi G, Tosca MA, Signori A, Ameli F. Comparison between symptoms and endoscopy in children with nasal obstruction. Int J Ped Otholaryngol 2010; 74:1405-8.
13. Gelardi M, Marseglia G, Licari A, Let al. Nasal cytology in children: recent advances. Ital J Pediatr 2012;38:51.
14. Ameli F, Brocchetti F, Tosca MA, Signori A, Ciprandi G. Adenoidal hypertrophy and allergic rhinitis: is there an inverse relationship? Am J Rhinol Allergy 2013; 27:e5-10.
15. Jiang D, Liang J, Noble PW. Hyaluronan in tissue injury and repair. Annu Rev Cell Dev Biol 2007; 23:435-61.
16. Jackson DG. Immunological functions of hyaluronan and its receptors in the lymphatics. Immunol Rev 2009; 230:216-31.
17. Tieu DD, Kern RC, Schleimer RP. Alterations in epithelial barrier function and host defense responses in chronic rhinosinusitis. J Allergy Clin Immunol 2009; 124:37-42
18. Franceschini F, De Benedictis FM, Peroni DG, et al. Anesthesia in children with asthma and rhinitis. Int J Immunopathol Pharmacol 2011; 24(3):S83-90.